ICE AND SNOW ALGAE

EDITED BY: Eric Marechal and Linda Nedbalová
PUBLISHED IN: Frontiers in Plant Science

frontiers Research Topics

ISSN 1664-8714
ISBN 978-2-88974-850-1
DOI 10.3389/978-2-88974-850-1

About Frontiers

Frontiers is more than just an open-access publisher of scholarly articles: it is a pioneering approach to the world of academia, radically improving the way scholarly research is managed. The grand vision of Frontiers is a world where all people have an equal opportunity to seek, share and generate knowledge. Frontiers provides immediate and permanent online open access to all its publications, but this alone is not enough to realize our grand goals.

Frontiers Journal Series

The Frontiers Journal Series is a multi-tier and interdisciplinary set of open-access, online journals, promising a paradigm shift from the current review, selection and dissemination processes in academic publishing. All Frontiers journals are driven by researchers for researchers; therefore, they constitute a service to the scholarly community. At the same time, the Frontiers Journal Series operates on a revolutionary invention, the tiered publishing system, initially addressing specific communities of scholars, and gradually climbing up to broader public understanding, thus serving the interests of the lay society, too.

Dedication to Quality

Each Frontiers article is a landmark of the highest quality, thanks to genuinely collaborative interactions between authors and review editors, who include some of the world's best academicians. Research must be certified by peers before entering a stream of knowledge that may eventually reach the public - and shape society; therefore, Frontiers only applies the most rigorous and unbiased reviews.
Frontiers revolutionizes research publishing by freely delivering the most outstanding research, evaluated with no bias from both the academic and social point of view. By applying the most advanced information technologies, Frontiers is catapulting scholarly publishing into a new generation.

What are Frontiers Research Topics?

Frontiers Research Topics are very popular trademarks of the Frontiers Journals Series: they are collections of at least ten articles, all centered on a particular subject. With their unique mix of varied contributions from Original Research to Review Articles, Frontiers Research Topics unify the most influential researchers, the latest key findings and historical advances in a hot research area! Find out more on how to host your own Frontiers Research Topic or contribute to one as an author by contacting the Frontiers Editorial Office: frontiersin.org/about/contact

ICE AND SNOW ALGAE

Topic Editors:
Eric Marechal, UMR5168 Laboratoire de Physiologie Cellulaire Vegetale (LPCV), France
Linda Nedbalová, Charles University, Czechia

Citation: Marechal, E., Nedbalová, L., eds. (2022). Ice and Snow Algae. Lausanne: Frontiers Media SA. doi: 10.3389/978-2-88974-850-1

Table of Contents

frontiers in Plant Science

EDITORIAL
published: 14 March 2022
doi: 10.3389/fpls.2022.868467

Editorial: Ice and Snow Algae

Eric Maréchal[1]* *and Linda Nedbalová*[2]*

[1] *Laboratoire de Physiologie Cellulaire et Végétale, Centre National de la Recherche Scientifique, Commissariat à l'Energie Atomique et aux Energies Alternatives, Institut National de Recherche pour l'Agriculture, l'Alimentation et l'Environnement, Université Grenoble Alpes, Institut de Recherche Interdisciplinaire de Grenoble, CEA Grenoble, Grenoble, France,*
[2] *Department of Ecology, Faculty of Science, Charles University, Prague, Czechia*

Keywords: snow alga, ice alga, *Sanguina*, red snow, bioalbedo, glacier, mountain

Editorial on the Research Topic

Ice and Snow Algae

Natural environments covered with snow or ice are home to still poorly characterized microbial life. Photosynthetic organisms play a key role in colonizing these thermally labile habitats and creating conditions for complex communities to develop. The duration of these cold-adapted microbial communities can range from a few months to permanent settlements depending on the complete or partial melting of the snow and ice cover. In such habitats, algae do not only cope with low temperatures (psychrotolerance and psychrophily), but they can also be subjected to high and variable light levels, UV irradiance, low levels of nutrients (oligotrophy), and a variety of other abiotic stresses. In some cases, bloom-forming algae cause the formation of "green snow." More often, they accumulate pigments, such as the carotenoid astaxanthin, leading to the development of "orange," "pink," or "red snow." The abundance of pigmented microalgae lowers the albedo and accelerates melting. Algae are therefore both "markers" (positively impacted by current environmental changes) and "actors" (positively acting on ice and snowmelt) of climate change. Research on ice and snow algae is thus essential to better address the impact of climate change in polar and mountain environments.

Our knowledge of snow and ice algae is fragmented and relies on studies concentrated in some high latitude and high-elevation sites. Some algae are supposed to specifically propagate in the snow ("snow algae") but we still have limited knowledge on the way they do. Their ecophysiological preferences and genetic diversity are still open questions. Some taxa seem to be dominant worldwide, in particular, the red snow alga *Sanguina* spp., detected in most high mountain ranges and polar areas, as in multiple studies reported in this Research Topic. An increasing number of algal species are being documented from the snow environment. Some are cultivable. In snow and glacier environments, green algae seem to be prominent, whereas diatoms, dinoflagellates, etc., are commonly encountered in sea ice. The present Research Topic compiles key contributions on the biodiversity, life cycles, (eco)physiology, developmental stages, and critical roles played by algae in ice (sea ice, glaciers, etc.) and snow, in high latitude polar and in high elevation mountain regions, in the context of climate change.

The determination of spatio-temporal distribution of taxa and the structure of communities rely on field sampling for the analysis of environmental DNA (eDNA), combined with other parameters, most notably chlorophyll and carotenoid pigments. Stewart et al. developed specific DNA-barcoding primers for Chlorophyta and Chlorophyceae, to analyze green algae biodiversity in top-soil along elevational gradients in five locations of the French Alps. They highlighted for the first time an altitudinal zonation of green algal taxa, some down to the genus level. The genus *Sanguina* was detected above the treeline, further assessing that this taxon is specific to alpine sites covered with snow for long periods and cannot be encountered at lower elevations in temperate regions. Environmental parameters and bioclimatic factors such as pH, C/N ratio, or intensity of freezing events proved determinant in algal distribution. Consistently, Williamson et al. analyzed

OPEN ACCESS

Edited and reviewed by:
Miroslav Obornik, Academy of Sciences of the Czech (ASCR), Czechia

***Correspondence:**
Eric Maréchal
eric.marechal@cea.fr
Linda Nedbalová
lindane@natur.cuni.cz

Specialty section:
This article was submitted to Marine and Freshwater Plants, a section of the journal Frontiers in Plant Science

Received: *02 February 2022*
Accepted: *07 February 2022*
Published: *14 March 2022*

Citation:
Maréchal E and Nedbalová L (2022) Editorial: Ice and Snow Algae. Front. Plant Sci. 13:868467. doi: 10.3389/fpls.2022.868467

the stoichiometry of macro-nutrients in the Southwestern margin of the Greenland Ice Sheet, revealing a low cellular macro-nutrient content and low C/N and C/P ratios, possibly reflecting adaptation of glacial algae assemblages to their specific oligotrophic surface ice environment. In Japan, Nakashima et al. addressed the structure of snow algal communities on Mt. Tateyama, combining eDNA with analyses of pigments. They could detect four general types of communities, some being dominated by *Sanguina* spp., whereas others were dominated by *Chlainomonas* and *Chloromonas* algae, causing different pigment compositions. Taking advantage of the relationship between pigment levels and snow algal biomass, Gray et al. used for the first time high-resolution WorldView multispectral satellite imagery to expand the scale of analysis of green and red snow blooms on Anchorage Island in the Antarctic. Future challenges rely therefore on the improvement of more specific eDNA markers for snow microbial communities, their use to unravel the spatiotemporal structure and dynamics of populations and communities in some study sites and correlation with satellite imagery-based approaches for more global characterizations.

Using strains isolated from sampling campaigns, refined taxonomic assessments can be achieved based on reconstructions of molecular phylogenies and analyses of cell morphological traits. If cultivable, ecophysiological studies can reveal some possible adaptation mechanisms. Galvez et al. thus identified a new Antarctic genus, named *Chlorominima*, with a species isolated in colored snow from the Collins glacier, therefore named *Chlorominima collina*. Together with other unidentified Antarctic and Arctic strains, a new polar subclade in the *Stephanosphaerinia* phylogroup within Chlamydomonadales is proposed. A partial transcriptome highlights the expression of genes coding for possible ice-binding proteins and enzymes involved in the synthesis of triacylglycerols and carotenoids, which could play a role in the adaptation to a cold environment. By contrast, Morales-Sanchez et al. showed that the polar alga *Chlamydomonas malina* RCC2488 did not accumulate triacylglycerol at low temperature (4°C) but rather at higher temperatures (8°C and above), suggesting that for this species, triacylglycerol may not be an adaptation to low temperature but a response to a high-temperature stress. Raymond et al. showed that two psychrophilic *Chlamydomonas* species isolated from Lake Bonney, a saline lake in the Antarctic, synthesize glycerol, an osmoprotectant, in a NaCl-dependent manner. Glycerol is synthesized by an unusual bidomain enzyme previously characterized in *Chlamydomonas reinhardtii*. In one of the Antarctic strains, they could identify an isoform of this enzyme, which expression is controlled by NaCl level. Eventually, Procházková et al. isolated a strain causing orange snow in the High Tatra Mountains in Poland and identified it as *Chloromonas krienitzii*, a species previously described from Japan. They characterized a unique mechanism shielding its algal cysts from a substantial part of UV irradiance and high visible light, by the presence of short wavelength-absorbing compounds in the cell wall. These articles illustrate the diversity of adaptation mechanisms that snow and ice algae may develop to live in their peculiar habitats. Factors determining the capacity to form blooms are still unknown. Future studies are therefore needed to evaluate which of these mechanisms are generic, shared by multiple species distant in the evolution, which are more specific to some taxa, and how these mechanisms may be related to the capacity to form blooms.

Eventually, considering that for tens of millions of years (720-635 Ma before present), the terrestrial habitats of the so-called "Snowball Earth" were likely dominated by snow and ice, Žárský et al. develops a scenario for the Zygnematophyceae–Embryophyta split, possibly stimulated by this long glacial period.

Altogether, the contributions to this Research Topic illustrate the dynamic international efforts to fill gaps in knowledge on algae living in the snow and ice. The efforts to characterize populations and communities in high elevations above treeline and polar areas, their dynamics, functioning, connectivity with other habitats such as soil, rivers, lakes, and oceans, together with genomic, ecophysiology, and multi-omics studies are likely to help us unravel adaptation mechanisms and to understand what it really means to live in the snow and the ice. Fascinating studies are expected in the near future.

AUTHOR CONTRIBUTIONS

Both authors listed have made a substantial, direct, and intellectual contribution to the work and approved it for publication.

FUNDING

EM is supported by the French National Research Agency (BLinK ANR-18-CE92-0015, Alpalga ANR-20-CE02-0020, GlycoAlps ANR-15-IDEX-02, GRAL Labex ANR-10-LABEX-04, and EUR CBS ANR-17-EURE-0003), Institut Carnot 3BCAR and the Kilian Jornet Foundation.

Conflict of Interest: The authors declare that the research was conducted in the absence of any commercial or financial relationships that could be construed as a potential conflict of interest.

Publisher's Note: All claims expressed in this article are solely those of the authors and do not necessarily represent those of their affiliated organizations, or those of the publisher, the editors and the reviewers. Any product that may be evaluated in this article, or claim that may be made by its manufacturer, is not guaranteed or endorsed by the publisher.

frontiers in Plant Science

ORIGINAL RESEARCH
published: 20 August 2020
doi: 10.3389/fpls.2020.01259

Glycerol Is an Osmoprotectant in Two Antarctic *Chlamydomonas* Species From an Ice-Covered Saline Lake and Is Synthesized by an Unusual Bidomain Enzyme

James A. Raymond[1]*, *Rachael Morgan-Kiss*[2] and *Sarah Stahl-Rommel*[2†]

[1] School of Life Sciences, University of Nevada Las Vegas, Las Vegas, NV, United States, [2] Department of Microbiology, Miami University, Oxford, OH, United States

OPEN ACCESS

Edited by:
Linda Nedbalová,
Charles University, Czechia

Reviewed by:
Aharon Oren,
Hebrew University of Jerusalem, Israel
David Dewez,
Université du Québec à Montréal, Canada

***Correspondence:**
James A. Raymond
raymond@unlv.nevada.edu

†Present address:
Sarah Stahl-Rommel
JES Tech, Houston, TX, United States

Specialty section:
This article was submitted to Marine and Freshwater Plants, a section of the journal Frontiers in Plant Science

Received: 18 June 2020
Accepted: 30 July 2020
Published: 20 August 2020

Citation:
Raymond JA, Morgan-Kiss R and Stahl-Rommel S (2020) Glycerol Is an Osmoprotectant in Two Antarctic Chlamydomonas Species From an Ice-Covered Saline Lake and Is Synthesized by an Unusual Bidomain Enzyme. Front. Plant Sci. 11:1259. doi: 10.3389/fpls.2020.01259

Glycerol, a compatible solute, has previously been found to act as an osmoprotectant in some marine *Chlamydomonas* species and several species of *Dunaliella* from hypersaline ponds. Recently, *Chlamydomonas reinhardtii* and *Dunaliella salina* were shown to make glycerol with an unusual bidomain enzyme, which appears to be unique to algae, that contains a phosphoserine phosphatase and glycerol-3-phosphate dehydrogenase. Here we report that two psychrophilic species of *Chlamydomonas* (*C*. spp. UWO241 and ICE-MDV) from Lake Bonney, Antarctica also produce high levels of glycerol to survive in the lake's saline waters. Glycerol concentration increased linearly with salinity and at 1.3 M NaCl, exceeded 400 mM in *C*. sp. UWO241, the more salt-tolerant strain. We also show that both species expressed several isoforms of the bidomain enzyme. An analysis of one of the isoforms of *C*. sp. UWO241 showed that it was strongly upregulated by NaCl and is thus the likely source of glycerol. These results reveal another adaptation of the Lake Bonney *Chlamydomonas* species that allow them to survive in an extreme polar environment.

Keywords: *Chlamydomonas*, glycerol synthesis, phosphoserine phosphatase, glycerol-3-phosphate dehydrogenase, Antarctica, Lake Bonney

INTRODUCTION

Glycerol is well-known for its ability to mitigate environmental stresses such as freezing and hyperosmotic conditions in a wide variety of organisms, including yeast (Wang et al., 2001), insects (Bentz and Mullins, 1999; Bennett et al., 2005), and vertebrates (Raymond, 1992; Layne, 1999). It is also well-known as an osmoprotectant in some algae, including salt pond isolates of *Dunaliella* (Ben-Amotz and Avron, 1973; Sussman and Avron, 1981) and several marine isolates of *Chlamydomonas* (Ahmad and Hellebust, 1986; Miyasaka and Ikeda, 1997; Miyasaka et al., 1998). As a compatible solute, glycerol prevents osmotic water loss and thus a build-up of intracellular salt concentrations. Two psychrophilic *Chlamydomonas* species, *Chlamydomonas* sp. UWO241 (Neale and Priscu, 1995) (hereafter Chlamy-UWO) and *Chlamydomonas* sp. ICE-MDV (Li et al., 2016)

(hereafter Chlamy-ICE) were isolated from Lake Bonney, a permanently ice-covered lake in Antarctica. The lake has a steep halocline, in which the salinity reaches about 150 PSU (equivalent to about 2.1 M NaCl, or 4.3 x the salinity of seawater) at a depth of 40 m (Spigel et al., 2018). Chlamy-UWO's ability to survive in this environment has been intensively studied for over two decades. Among its adaptation are a photochemical apparatus well-suited for a cold, saline and low light environment (Morgan et al., 1998), more fluid membranes (Morgan-Kiss et al., 2002) and ice-binding proteins (IBPs) to prevent freeze-thaw injury (Raymond and Morgan-Kiss, 2013). Less is known about Chlamy-ICE which was isolated more recently: it also possesses IBPs (Raymond and Morgan-Kiss, 2017) but appears to have differences in acclimatory ability compared to Chlamy-UWO (Cook et al., 2019). Much more is known about the cold adaptations of a closely-related Antarctic pyschrophile *Chlamydomonas* sp. ICE-L (Cvetkovska et al., 2017). Because both Chlamy-UWO and Chlamy-ICE are adapted to a saline environment, we wished to know whether they also produce glycerol as an osmoprotectant or cryoprotectant.

Until recently, the pathways used by algae to produce glycerol have been a matter of speculation. Glycogen, or one of its products, dihydroxyacetone phosphate (DHAP), has been identified as the source of glycerol in a number of organisms, including yeast, (Modig et al., 2007), *Arabidopsis* (Caparros-Martin et al., 2007), a bacterium (Larrouy-Maumus et al., 2013), mountain pine beetle (Fraser et al., 2017), and rainbow smelt (Raymond, 1995). In the DHAP pathway, DHAP is converted to glycerol-3-phosphatate (G3P) by a nicotinamide-adenine dinucleotide (NAD^+)-dependent glycerol-3 phosphate dehydrogenase (GPDH), which is then converted to glycerol by a phosphoserine phosphatase (PSP). The problem is that algae typically have several GPDHs and phosphatases, and attempts to identify the enzymes involved have been until recently unsuccessful.

Dunaliella salina has a bidomain enzyme that includes an N-terminal PSP and a C-terminal NAD^+-dependent GPDH (He et al., 2007). It was proposed as a candidate for glycerol production directly from DHAP (He et al., 2007), but initial attempts to confirm its activity were unsuccessful (He et al., 2009). However, this enzyme still seemed like the most likely source of glycerol. During our study of IBPs in Chlamy-UWO (Raymond and Morgan-Kiss, 2013), we noticed that it produced glycerol as an osmoprotectant, i.e., glycerol production increased with increasing salinity. We searched the Chlamy-UWO genome for a *Dunaliella*-like bidomain enzyme and found at least two homologs. We then examined the expression of one of the homologs and found that it strongly increased with increasing salinity, as reported in a master's thesis (Stahl, 2014). This suggested that this enzyme alone was capable of producing glycerol from DHAP

Recently, Morales-Sanchez et al. (2017) showed that a similar bidomain enzyme in *Chlamydomonas reinhardtii* was sufficient to produce glycerol directly from DHAP, and He Q. H. et al. (2020) finally confirmed that the *Dunaliella salina* bidomain protein was sufficient to produce glycerol. Here, we report our test of the hypothesis that Chlamy-UWO uses a similar bidomain enzyme to produce glycerol. We also show that Chlamy-ICE is capable of producing high levels of glycerol under saline conditions and has similar bidomain enzymes.

METHODS

Cells

Chlamydomonas sp. UWO241 [Chlamy-UWO, also referred to as *C. raudensis* in some earlier studies, e.g., (Dolhi et al., 2013)] and *Chlamydomonas* sp. ICE-MDV (Chlamy-ICE) were previously isolated from the east lobe of Lake Bonney, Antarctica. Chlamy-UWO was isolated from below the permanent chemocline in the deep photic zone (17 m) where the salinity is similar to the salinity of seawater but rapidly increases with increasing depth (Spigel et al., 2018). Its natural depth range is not known. Chlamy-ICE was recovered from a depth of 13 m, where the salinity is markedly lower (Li et al., 2016). Both strains were maintained in Bold's basal medium (BBM) supplemented with the indicated amounts of NaCl in a temperature/light regime of 8°C/50 $\mu mol \cdot m^{-2} \cdot s^{-1}$ at Miami University. *Chlamydomonas* sp. UWO241 is deposited in the Bigelow Algal collection (CCMP1619). *Chlamydomonas* sp. ICE-MDV is available upon request to RMK.

Glycerol Measurement

Fresh cells were shipped overnight to the University of Nevada Las Vegas (UNLV) with ice packs. The temperature varied by less than 2°C during shipment. For each sample, 1.50 ml of cell culture was centrifuged in pre-weighed tubes. The supernatant was removed and the remaining medium was removed with a fine, drawn-out pipet. The tubes were reweighed to obtain the pellet weights (about 3 mg), sealed, and stored at -25°C. For glycerol measurement, the tubes were thawed, and the bottoms of the tubes were subjected to two freeze-thaw cycles in liquid nitrogen to break the cells. The pellets were suspended in 1.00 ml DI water, vortexed to release glycerol and centrifuged at 16,000 x g for 2 min at 4°C to yield a clear supernatant. Subsequent testing of the pellet showed that virtually all of the glycerol was released from the cells. Glycerol was quantified enzymatically with Free glycerol reagent (Sigma no. F6428), which develops a 540 nm (purple) color in the presence of glycerol. Intracellular glycerol concentration (mM) in a cell pellet was calculated as M_g x 1,000/ (MW x M_p x f), where M_g is the mass of glycerol released from the pellet, MW is the molecular weight of glycerol (92 g mol^{-1}), M_p is the mass of the pellet, and f is fraction of the cell mass that is water. The latter was estimated as 0.7 based on measurements of *Chlamydomonas pulsatilla* (Ahmad and Hellebust, 1986). This calculation assumed that the extracellular water content in the pellets was zero. If extracelular water were present in the pellets, the actual glycerol concentrations would be higher than those reported.

Gene Sequences

Sequences of the enzymes described in this study were assembled from transcriptome and genome data obtained from Chlamy-

UWO (Raymond and Morgan-Kiss, 2013) and Chlamy-ICE (Raymond and Morgan-Kiss, 2017). The transcriptomes were obtained with 454 and Illumina sequencing, respectively. Additional DNA and mRNA reads needed to complete assembly of Chlamy-UWO isoform 3 were kindly provided by David Smith (University of Western Ontario). Gene expression levels were expressed as FPKM (fragments per kilobase per million reads) values: FPKM = r/R/L, where r is the number of unique reads for a given isoform with e-values less than $1e^{-20}$ (each read was assigned only to the isoform that it most closely matched), R is the number of millions of reads in the transcriptome, and L is the length of the gene in kb. The transcriptomes were searched for genes similar to the bidomain enzyme in *Dunaliella salina* (AAX56341). Several isoforms of the gene were found and assembled. Introns were identified by comparing these sequences with the genomic data. Sequences for the qPCR reference genes were obtained from the Chlamy-UWO transcriptome.

Chloroplast signals were predicted with ChloroP 1.1 (http://www.cbs.dtu.dk/services/ChloroP/) (Emanuelsson et al., 1999). PSP and GPDH domains were identified with NCBI's conserved domain database https://www.ncbi.nlm.nih.gov/Structure/cdd/wrpsb.cgi. A Neighbor-Joining phylogenetic tree was constructed with Mega X (Tamura et al., 2011), using two non-chlorophyte bidomain proteins to root the tree. We thank Armin Hallmann (University of Bielefeld, Germany) for correcting the bidomain sequence of *Volvox carteri* used in the tree.

Quantitative PCR

Cultures of Chlamy-UWO were grown at 8°C and 50 µmol m^{-2} s^{-1} in BBM supplemented with a range of salt concentrations (10, 300, 700, and 1,300 mM NaCl) until samples reached the mid exponential phase. Total RNA was extracted with a Qiagen RNeasy mini kit (No. 74104) as per manufacturer's instructions. Residual genomic DNA was removed by Ambion DNase (Thermo Fisher Scientific, Waltham, MA). RNA was reverse transcribed with an iScript cDNA synthesis kit (Bio-Rad, Hercules, CA) as specified by the manufacturer. Expression of the Chlamy-UWO PSP-GPDH isoform 2 was quantified by real-time quantitative PCR using the ΔΔCq method (Liu et al., 2012) and a Bio-Rad CFX Connect Real-time thermal cycler. Histone H2B (histh2b) and 40S ribosomal protein S10 (rps10) (GenBank accessions MT362546 and MT362547, respectively) were used as reference genes, as their expressions were fairly stable over the conditions used. Primers are shown in **Table S1**.

Structure Prediction

A 3D model of Chlamy-UWO isoform 1 was predicted with Swiss Model (Waterhouse et al., 2018) (https://swissmodel.expasy.org/) using the structure of the *Dunaliella salina* bidomain protein (6iuy.1.A) (He Q. H. et al., 2020) as template. In the 580-a.a. region of overlap, the two proteins had an identity of 54%. The free energy of the model was then minimized (from -22.8 to -30.9 MJ/mol) with the Yasara energy minimization server (Krieger et al., 2009) (http://www.yasara.org/minimizationserver.htm) and displayed with the Yasara viewer (Waterhouse et al., 2018) (http://www.yasara.org/). Stereo views were obtained by rotating the molecules 3° around the vertical axis.

RESULTS

Intracellular glycerol levels in Chlamy-UWO and Chlamy-ICE increased with increasing NaCl concentration. Both species maintained glycerol levels of about 150 mM at 700 mM NaCl (**Figure 1A**). At 1,300 mM NaCl, Chlamy-UWO cells reached over 400 mM glycerol while Chlamy-ICE cells were unable to grow. In contrast, glycerol levels in the supernatant of centrifuged dense cultures of Chlamy-UWO were very low (0.4 mM at 700 m NaCl and 1.1 mM at 1,300 mM NaCl), indicating that the cells were maintaining a strong gradient between the intracellular and extracellular environments.

We thus searched the Chlamy-UWO transcriptome for enzymes similar to the proposed PSP/GPDH that had been found in *Dunaliella* (He et al., 2007). Three complete isoforms could be assembled. We selected one of the isoforms to see if it could account for the increased glycerol production at increased salinity. The mRNA expression of Chlamy-UWO isoform 2 increased about four-fold as the NaCl concentration increased to 1,300 mM, regardless of the reference gene (**Figure 1B**). For the reference gene combination Rps10+Histone, whose points were more linear than those of the single reference genes, the increase was significant at the $p < 0.01$ level (linear regression). This increase closely paralleled the increase in glycerol concentration. This, together with the recent findings in *C. reinhardtii* and *D. salina*, strongly supports the idea that the bidomain enzymes are a major source (and possibly the main source) of glycerol in Chlamy-UWO.

When the Chlamy-ICE transcriptome became available in 2016, it was also examined for homologs of the bidomain proteins. It appeared to have seven such homologs, but only five of them could be completely assembled (**Table 1**). For each of the Lake Bonney species, the expression levels of the different isoforms varied considerably (**Table 1**). In the approximately 600-a.a. conserved region that includes both enzyme domains, the identities of the Chlamy-UWO and Chlamy-ICE isoforms to *C. reinhardtii* GPD3 are about 60% (**Table 1**). To gain insights into the relationships of the enzymes in the three *Chlamydomonas* species, their exon/intron structures were compared. The numbers of introns (and their locations) differed considerably among the three *Chlamydomonas* species (**Table 1**), suggesting that their divergence occurred long ago.

The eight complete isoforms of Chlamy-UWO and Chlamy-ICE consist of an N-terminal chloroplast-targeting signal, a PSP domain and a C-terminal NAD^+-dependent GDPH domain (**Figure 2A**), similar to the structure in *Dunaliella* (He Q. H. et al., 2020). A 3D model of isoform 1 of the Chlamy-UWO enzyme predicted from the structure of the *D. salina* enzyme is shown in **Figure 2B**. The region that could be modeled ranged from Thr60 at the start of the PSP domain (lower part of molecule in **Figure 2B**) to Phe639 near the end of the GPDH

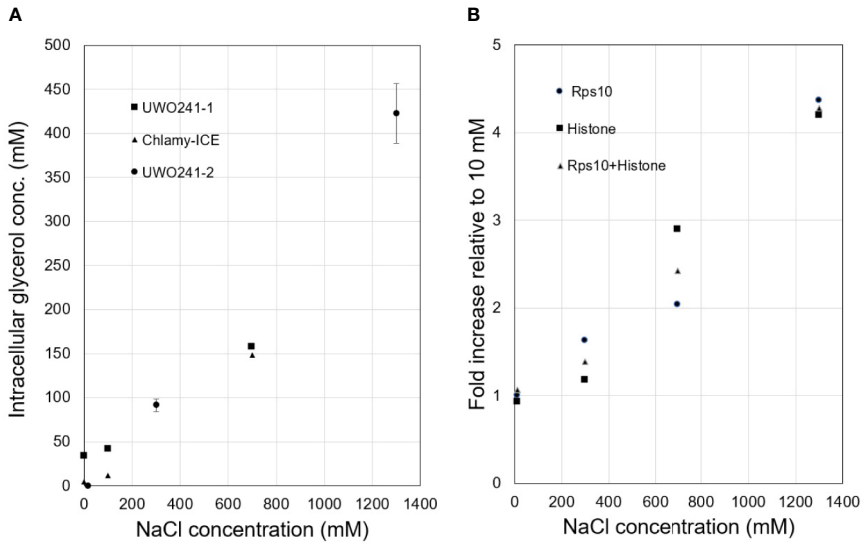

FIGURE 1 | Responses of Lake Bonney *Chlamydomonas* species to increasing salinity. **(A)**, Glycerol production in Chlamy-UWO and Chlamy-ICE. Two independent measurements were made for Chlamy-UWO. For UWO-2, three measurements were made for each sample. **(B)**, Expression of PSP/GPDH isoform 2 of Chlamy-UWO using different reference genes.

domain (upper part). The model is similar to the structure of the *Dunaliella* protein, with two nearly independent domains connected by a short link. The key residues forming the binding sites of DHAP, NAD^+, and glycerol-3-P in *Dunaliella* (He Q. H. et al., 2020) are conserved in the Chlamy-UWO isoform (**Figure S1**). As a test of the accuracy of the model, the predicted binding sites of DHAP and NAD^+ on the GPDH domain of the *Chlamydomonas* protein were compared to those in *Dunaliella*. The residues that form the binding sites in the two structures as well as their locations are nearly the same (**Figure S2**), supporting the accuracy of the model.

To better understand the evolution of the *Chlamydomonas* bidomain proteins, a phylogenetic tree of the conserved PSP/GPDH domains was constructed by the neighbor-joining method (**Figure 3**). The tree was rooted on homologous proteins from two non-chlorophytes, a rhodophyte (*Porphyridium purpureum*) and a primitive relative of the fungi (*Sphaeroforma arctica*) that were recently submitted to GenBank. Within each *Chlamydomonas* species, the isoforms clustered with high bootstrap values, suggesting that within each species, the isoforms diverged from a single gene. *C. reinhardtii*, Chlamy-UWO and Chlamy-ICE formed a group that clusters separately from *Dunaliella*, but otherwise the three *Chlamydomonas* clusters appear weakly related, in agreement with the considerable differences in exon structures of the three species. These findings, together with the finding of the *P. purpureum* protein, raise the possibility that the chlorophyte bidomain proteins have an ancient origin, possibly dating back to a common ancestor of the chlorophytes and rhodophytes.

DISCUSSION

In view of the importance of glycerol as a compatible solute in animal and plant physiology, it is surprising that so little was

TABLE 1 | Bidomain PSP/GPDH proteins in three species of *Chlamydomonas*.

Species/isoform	GenBank acc. no.	Relative Expression level[1]	Length (a.a.)	No. exons	% ID (% similarity)[2]
Chlamy-UWO-1	MT362548	13.7	745	18	61 (75)
Chlamy-UWO-2	MT362549	38.4	710	18	62 (77)
Chlamy-UWO-3	MT362550	1.0	741	18	60 (76)
Chlamy-ICE-1	MT362551	1.0	697	11	59 (77)
Chlamy-ICE-2	MT362552	1.7	693	13	56 (75)
Chlamy-ICE-3	MT362553	8.2	665	12	58 (74)
Chlamy-ICE-4	MT362554	6.3	710	7	58 (76)
Chlamy-ICE-5	MT362555	9.0	689	3	62 (77)
C. reinhardtii GPD3	AJG44150	N/A	725	15	100 (100)
C. reinhardtii GPD2	AJG44149	N/A	723	15	99.8 (99.1)

[1]*Reads (transcripts) per kilobase per million mapped reads relative to expression of the most weakly expressed isoform in each species. Culture conditions were 8°C and 700 mM NaCl (Chlamy-UWO) and 500 mM NaCl (Chlamy-ICE). N/A, data not available.*
[2]*Percent identity (% similarity) to PSP+GPDH region of C. reinhardtii GPD3.*

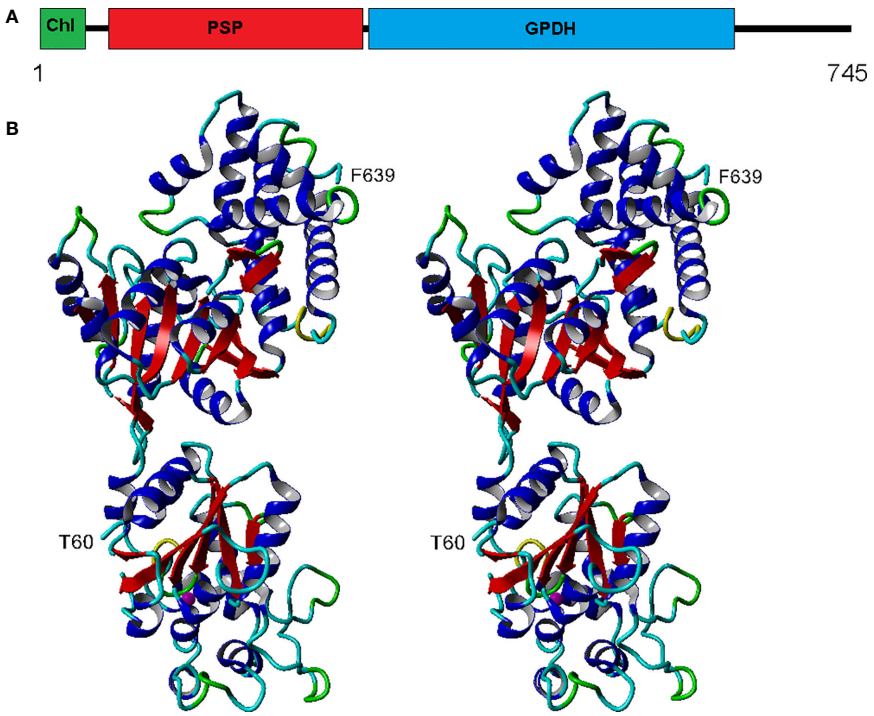

FIGURE 2 | Structure of Chlamy-UWO PSP/GPDH isoform 1. **(A)**, Domain structure, consisting of an N-terminal chloroplast-targeting signal, a phosphoserine phosphatase domain and a glycerol-3-phosphate dehydrogenase domain. **(B)**, Stereoview of the molecule generated by Swiss-Model using the PSP/GPDH of *D. salina* as template. The lower portion, beginning at Thr60, shows the PSP domain with an embedded magnesium ion (olive). The upper portion, ending at Phe639, shows the GPDH domain. Color codes: red, beta sheet; blue, alpha helix; cyan, coil; green, turn; yellow, 3_{10} helix.

known about how it was synthesized until recently. Previous studies referred to the enzymes involved only generically without identifying specific genes, and thus not really "nailing down" the pathway. Recently, the specific enzymes involved in glycerol synthesis have been identified in a bacterium (Larrouy-Maumus et al., 2013), a fish (Raymond, 2015), and, as highlighted here, two species of algae (Morales-Sanchez et al., 2017; He Q. H. et al., 2020). The algal enzymes are especially interesting because of their novel form in which the two enzymes needed to convert DHAP into glycerol are fused into a single enzyme. Although these double enzymes are largely limited to chlorophytes, the recent finding of homologous genes in two unicellular organisms (*P. purpureum* and *S. arctica*) that have links to some of the earliest eukaryotes (Mendoza et al., 2002; Bhattacharya et al., 2013) suggests that the fused gene may have evolved early in the history of eukaryotes.

The present results show that multiple copies of similar enzymes are found in two glycerol-producing *Chlamydomonas* species from Antarctica. Furthermore, the expression of a representative isoform from Chlamy-UWO was strongly upregulated by high salinity and the upregulation was associated with an increase in glycerol production. This result was supported by a recent proteomic study of Chlamy-UWO in which enzymes classified as NAD^+-dependent GPDHs showed a six-fold increase when NaCl concentration was increased from near zero to 700 mM (Kalra et al., 2020). These results indicate that the bidomain enzyme is a major source of glycerol in Chlamy-UWO, and most likely in Chlamy-ICE as well. Using glycerol as an osmoprotectant, Chlamy-UWO and Chlamy-ICE can survive in salinities greater than the salinity of seawater (at least 700 and 1300 mM NaCl for Chlamy-ICE and Chlamy-UWO, respectively; equivalent to about 1.4x and 2.5x the salinity of seawater, respectively). The highest glycerol levels observed in Chlamy-ICE and Chlamy-UWO were 150 and 420 mM, respectively (**Figure 1A**). (Chlamy-ICE may not need higher levels of glycerol since it appears to live in shallower and thus less saline waters than Chlamy-UWO). For comparison, *C. reinhardtii*, a non-halotolerant species, can tolerate a maximum salinity of 200 mM NaCl (León and Galván, 1994) (but no more than 100 mM NaCl in our laboratory) and accumulates only about 26 mM glycerol in medium containing 100 mM KCl. (Husic and Tolbert, 1986). On the other hand, the marine coastal *C. pulsatilla* can produce much higher levels of glycerol, 1,450 mM when grown in double-strength seawater (Ahmad and Hellebust, 1986).

It should be noted that the glycerol levels in the Lake Bonney species are not enough to balance the osmolarity of the external medium. For example, at 1,300 mM NaCl (~2.6 Osm), the glycerol level in Chlamy-UWO was only about 0.4 Osm. Thus, the cells appear to be increasing the concentrations of additional osmolytes to maintain osmotic equilibrium. In addition to glycerol, proline and sucrose were found to accumulate at high

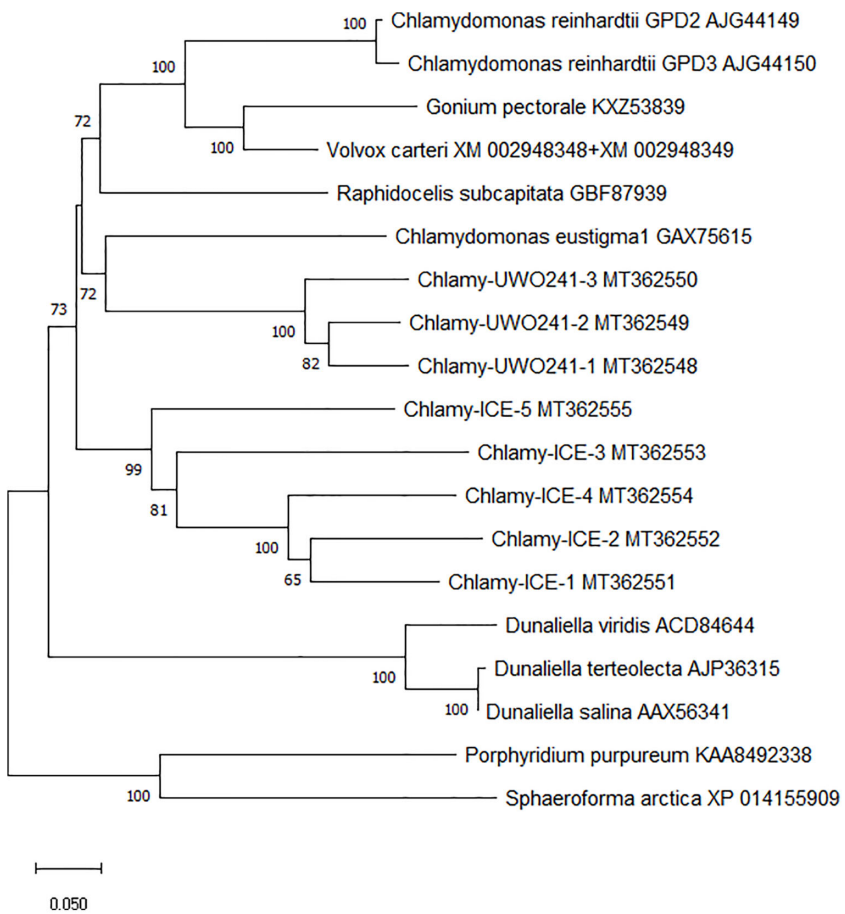

FIGURE 3 | Neighbor-joining phylogenetic tree of the ~600 a.a. region containing the PSP and GPDH domains of PSP/GPDH bidomain enzymes of 10 chlorophytes. Bootstrap values less than 65% are not shown.

levels in high-salt-grown Chlamy-UWO cultures (Kalra et al., 2020). In *C. pulsatilla*, in which glycerol contributed only about 57% to the intracellular osmolality, large increases in sodium and chloride ions made important contributions to maintaining osmotic equilibrium, but sugars and amino acids did not appear to have a significant role (Ahmad and Hellebust, 1986).

C. reinhardtii has four other GPDHs designated GPD1, GPD4, GPD5, and the mitochondrial mtGPD (Morales-Sanchez et al., 2017). tBlastn analyses of contigs assembled from the Chlamy-UWO and Chlamy-ICE transcriptomes indicate that both species have close homologs of each of these proteins (data not shown). We cannot rule out the possibility that these GPDHs also have a role in glycerol production, although GPD4 in *C. reinhardtii* was not upregulated by 125 mM NaCl (Morales-Sanchez et al., 2017).

That all the Lake Bonney PSP/GPDH isoforms have a chloroplast targeting signal suggests that they function in the chloroplast, as was concluded for the bidomain enzymes in *C. reinhardtii* (Morales-Sanchez et al., 2017) and *D. salina* (He Q. H. et al., 2020). This seems reasonable in view of the fact that the enzymes could act directly on DHAP produced by the Calvin cycle in the chloroplast. However, several chlorophyte bidomain proteins in the databank do not appear to have chloroplast signals as judged by ChloroP, which suggests they function in the cytoplasm.

Because Chlamy-UWO and Chlamy-ICE are living in an environment that is constantly exposed to freezing, as demonstrated by their expression of numerous ice-binding proteins (Raymond and Morgan-Kiss, 2013; Raymond and Morgan-Kiss, 2017), glycerol, by lowering the freezing point of the intracellular medium, could also act as a cryoprotectant. These might be the only organisms to use glycerol as both an osmoprotectant and a cryoprotectant.

Most of the known bidomain glycerol enzymes belong to chlorophytes, which in addition to *Chlamydomonas* and *Dunaliella*, include *Gonium*, *Raphidocelis*, *Micractinium*, *Chlorella*, *Chloropicon*, *Volvox*, and *Tetrabaena*. Many of these species are freshwater species and so it remains to be seen whether these species also produce glycerol and for what purpose. It also remains to be seen whether other marine *Chlamydomonas* species that make glycerol (Ahmad and Hellebust, 1986; Miyasaka et al., 1998) also have these

enzymes. Finally, little is known about how *Chlamydomonas* spp. sense changes in salinity. Recent studies on osmosensing in microalgae (Suescún-Bolívar and Thomé, 2015; Charneco et al., 2018; He Q. et al., 2020) have implicated the possible involvement of mitogen-activated protein (MAP) kinases. The behavior of these genes in response to increases in salinity should thus be interesting.

In summary, we show that two Antarctic extremophiles, in addition to having several adaptations to low light and low temperature, also have adapted to high salinity by producing glycerol as an osmoprotectant (and possibly a cryoprotectant), and at least one of them (Chlamy-UWO) achieves this by using an unusual bidomain enzyme that can make glycerol directly from DHAP.

DATA AVAILABILITY STATEMENT

Publicly available datasets were analyzed in this study. The Chlamydomonas sp. UWO241 transcriptome is available under GenBank accession PRJNA575885.

AUTHOR CONTRIBUTIONS

All authors contributed equally to this study.

FUNDING

This study was partially funded by NSF grant 1637708 and DOE Grant DE-SC0019138 to RM-K.

ACKNOWLEDGMENTS

We thank David Smith, Marina Cvetkovska, Xi Zhang, and Norm Hüner (University of Western Ontario) for providing additional sequence data for Chlamy-ICE. JR thanks the School of Life Sciences, UNLV for providing laboratory facilities for this study.

SUPPLEMENTARY MATERIAL

The Supplementary Material for this article can be found online at: https://www.frontiersin.org/articles/10.3389/fpls.2020.01259/full#supplementary-material

TABLE S1 | qPCR primers used in this study.

FIGURE S1 | Alignment of PSP/GPDH domains of Chlamy-ICE and *Dunaliella salina* showing conservation of ligand binding sites. The binding sites in *Dunaliella* are from He Q. H. et al. (2020). Red underline, PSP domain; blue underline, GPDH domain. Blue asterisks, glycerol-3 phosphate; green asterisks, NAD; red asterisks, DHAP. Black background, identical a.a.s; gray background, similar a.a.s. Numbering refers to position in the Chlamy-ICE protein. The region shown (from T60 to F639) is the same region shown in **Figure 2B**.

FIGURE S2 | Stereo views comparing the ligand binding sites in the GPDH domain of the PSP/GPDH protein in *Dunaliella salina* (top) and Chlamy-UWO isoform 2 (bottom). The *Dunaliella* structure was determined by X-ray crystallography. The Chlamy-UWO structure is predicted by SwissModel based on the *Dunaliella* structure. The binding sites for *Dunaliella* were obtained from He Q. H. et al. (2020). The amino acid residues forming the binding sites are shown. Red, DHAP binding site; green, NAD binding site. These amino acid residues correspond to the red and green asterisks, respectively, in **Figure S1**.

REFERENCES

Ahmad, I., and Hellebust, J. A. (1986). The role of glycerol and inorganic-ions in osmoregulatory responses of the euryhaline flagellate *Chlamydomonas-pulsatilla* wollenweber. *Plant Physiol.* 82, 406–410. doi: 10.1104/pp.82.2.406

Bhattacharya, D., Price, D. C., Chan, C. X., Qiu, H., Rose, N., Ball, S., et al. (2013). Genome of the red alga Porphyridium purpureum. *Nature Commun.* 4, 1941.

Ben-Amotz, A., and Avron, M. (1973). The role of glycerol in the osmotic regulation of the halophilic alga *Dunaliella parva*. *Plant Physiol.* 51, 875–878. doi: 10.1104/pp.51.5.875

Bennett, V. A., Sformo, T., Walters, K., Toien, O., Jeannet, K., Hochstrasser, R., et al. (2005). Comparative overwintering physiology of Alaska and Indiana populations of the beetle *Cucujus clavipes* (Fabricius): roles of antifreeze proteins, polyols, dehydration and diapause. *J. Exp. Biol.* 208, 4467–4477. doi: 10.1242/jeb.01892

Bentz, B. J., and Mullins, D. E. (1999). Ecology of mountain pine beetle (Coleoptera: Scolytidae) cold hardening in the intermountain west. *Environ. Entomol.* 28, 577–587. doi: 10.1093/ee/28.4.577

Caparros-Martin, J. A., Reiland, S., Kochert, K., Cutanda, M. C., and Culianez-Macia, F. A. (2007). *Arabidopsis thaliana* AtGpp1 and AtGpp2: two novel low molecular weight phosphatases involved in plant glycerol metabolism. *Plant Mol. Biol.* 63, 505–517. doi: 10.1007/s11103-006-9104-0

Charneco, G. O., Parages, M. L., Camarena-Gómez, M. T., and Jiménez, C. (2018). Phosphorylation of MAP Kinases crucially controls the response to environmental stress in *Dunaliella viridis*. *Environ. Exp. Bot.* 156, 203–213. doi: 10.1016/j.envexpbot.2018.08.030

Cook, G., Teufel, A., Kalra, I., Li, W., Wang, X., Priscu, J., et al. (2019). The Antarctic psychrophiles *Chlamydomonas* spp. UWO241 and ICE-MDV exhibit differential restructuring of photosystem I in response to iron. *Photosynthesis Res.* 141, 209–228. doi: 10.1007/s11120-019-00621-0

Cvetkovska, M., Hüner, N. P. A., and Smith, D. R. (2017). Chilling out: the evolution and diversification of psychrophilic algae with a focus on Chlamydomonadales. *Polar Biol.* 40, 1169–1184. doi: 10.1007/s00300-016-2045-4

Dolhi, J. M., Maxwell, D. P., and Morgan-Kiss, R. M. (2013). Review: the Antarctic *Chlamydomonas raudensis*: an emerging model for cold adaptation of photosynthesis. *Extremophiles* 17, 711–722. doi: 10.1007/s00792-013-0571-3

Emanuelsson, O., Nielsen, H., and Von Heijne, G. (1999). ChloroP, a neural network-based method for predicting chloroplast transit peptides and their cleavage sites. *Protein Sci.* 8, 978–984. doi: 10.1110/ps.8.5.978

Fraser, J. D., Bonnett, T. R., Keeling, C. I., and Huber, D. P. W. (2017). Seasonal shifts in accumulation of glycerol biosynthetic gene transcripts in mountain pine beetle, *Dendroctonus ponderosae* Hopkins (Coleoptera: Curculionidae), larvae. *Peerj* 5, e3284. doi: 10.7717/peerj.3284

He, Q., Qiao, D., Bai, L., Zhang, Q., Yang, W., Li, Q., et al. (2007). Cloning and characterization of a plastidic glycerol 3-phosphate dehydrogenase cDNA from *Dunaliella salina*. *J. Plant Physiol.* 164, 214–220. doi: 10.1016/j.jplph.2006.04.004

He, Y., Meng, X., Fan, Q., Sun, X., Xu, Z., and Song, R. (2009). Cloning and characterization of two novel chloroplastic glycerol-3-phosphate dehydrogenases from *Dunaliella viridis*. *Plant Mol. Biol.* 71, 193–205. doi: 10.1007/s11103-009-9517-7

He, Q. H., Toh, J. D., Ero, R., Qiao, Z., Kumar, V., Serra, A., et al. (2020). The unusual di-domain structure of *Dunaliella salina* glycerol-3-phosphate dehydrogenase enables direct conversion of dihydroxyacetone phosphate to glycerol. *Plant J.* 102, 153–164. doi: 10.1111/tpj.14619

He, Q., Lin, Y., Tan, H., Zhou, Y., Wen, Y., Gan, J., et al. (2020). Transcriptomic profiles of *Dunaliella salina* in response to hypersaline stress. *BMC Genomics* 21, 115. doi: 10.1186/s12864-020-6507-2

Husic, H. D., and Tolbert, N. E. (1986). Effect of Osmotic Stress on Carbon Metabolism in *Chlamydomonas reinhardtii*. *Accumulation Glycerol. as an Osmoregul. Solute* 82, 594–596. doi: 10.1104/pp.82.2.594

Kalra, I., Wang, X., Cvetkovska, M., Jeong, J., Mchargue, W., Zhang, R., et al. (2020). *Chlamydomonas* sp. UWO 241 exhibits high cyclic electron flow and rewired metabolism under high salinity. *Plant Physiol.* 183, 588–601. doi: 10.1104/pp.19.01280

Krieger, E., Joo, K., Lee, J., Lee, J., Raman, S., Thompson, J., et al. (2009). Improving physical realism, stereochemistry, and side-chain accuracy in homology modeling: four approaches that performed well in CASP8. *Proteins-Structure Funct. Bioinf.* 77, 114–122. doi: 10.1002/prot.22570

Larrouy-Maumus, G., Biswas, T., Hunt, D. M., Kelly, G., Tsodikov, O. V., and De Carvalho, L. P. S. (2013). Discovery of a glycerol 3-phosphate phosphatase reveals glycerophospholipid polar head recycling in *Mycobacterium tuberculosis*. *Proc. Natl. Acad. Sci. U.S.A.* 110, 11320–11325. doi: 10.1073/pnas.1221597110

Layne, J. R. (1999). Freeze tolerance and cryoprotectant mobilization in the gray treefrog (*Hyla versicolor*). *J. Exp. Zool.* 283, 221–225. doi: 10.1002/(SICI)1097-010X(19990215)283:3<221::AID-JEZ1>3.0.CO;2-Q

León, R., and Galván, F. (1994). Halotolerance studies on *Chlamydomonas reinhardtii*: glycerol excretion by free and immobilized cells. *J. Appl. Phycol.* 6, 13–20. doi: 10.1007/BF02185898

Li, W., Podar, M., and Morgan-Kiss, R. M. (2016). Ultrastructural and single-cell-level characterization reveals metabolic versatility in a microbial eukaryote community from an ice-covered Antarctic lake. *Appl. Environ. Microbiol.* 82, 3659–3670. doi: 10.1128/AEM.00478-16

Liu, C. L., Wu, G. T., Huang, X. H., Liu, S. H., and Cong, B. L. (2012). Validation of housekeeping genes for gene expression studies in an ice alga *Chlamydomonas* during freezing acclimation. *Extremophiles* 16, 419–425. doi: 10.1007/s00792-012-0441-4

Mendoza, L., Taylor, J. W., and Ajello, L. (2002). The class Mesomycetozoea: a heterogeneous group of microorganisms at the animal-fungal boundary. *Ann. Rev. Microbiol.* 56, 315–344.

Miyasaka, H., and Ikeda, K. (1997). Osmoregulating mechanism of the halotolerant green alga Chlamydomonas, strain HS-5. *Plant Sci.* 127, 91–96. doi: 10.1016/S0168-9452(97)00125-8

Miyasaka, H., Ohnishi, Y., Akano, T., Fukatsu, K., Mizoguchi, T., Yagi, K., et al. (1998). Excretion of glycerol by the marine *Chlamydomonas* sp. strain W-80 in high CO2 cultures. *J. Ferment. Bioeng.* 85, 122–124. doi: 10.1016/S0922-338X(97)80367-4

Modig, T., Granath, K., Adler, L., and Liden, G. (2007). Anaerobic glycerol production by *Saccharomyces cerevisiae* strains under hyperosmotic stress. *Appl. Microbiol. Biotechnol.* 75, 289–296. doi: 10.1007/s00253-006-0821-8

Morales-Sanchez, D., Kim, Y., Terng, E. L., Peterson, L., and Cerutti, H. (2017). A multidomain enzyme, with glycerol-3-phosphate dehydrogenase and phosphatase activities, is involved in a chloroplastic pathway for glycerol synthesis in *Chlamydomonas reinhardtii*. *Plant J.* 90, 1079–1092. doi: 10.1111/tpj.13530

Morgan, R. M., Ivanov, A. G., Priscu, J. C., Maxwell, D. P., and Huner, N. P. A. (1998). Structure and composition of the photochemical apparatus of the antarctic green alga, *Chlamydomonas subcaudata*. *Photosynthesis Res.* 56, 303–314. doi: 10.1023/A:1006048519302

Morgan-Kiss, R., Ivanov, A. G., Williams, J., Mobashsher, K., and Huner, N. P. A. (2002). Differential thermal effects on the energy distribution between photosystem II and photosystem I in thylakoid membranes of a psychrophilic and a mesophilic alga. *Biochim. Biophys. Acta* 1561, 251–265. doi: 10.1016/S0005-2736(02)00352-8

Neale, P. J., and Priscu, J. C. (1995). The photosynthetic apparatus of phytoplankton from a perennially ice-covered Antarctic lake: acclimation to an extreme shade environment. *Plant Cell Physiol.* 36, 253–263. doi: 10.1093/oxfordjournals.pcp.a078757

Raymond, J. A., and Morgan-Kiss, R. (2013). Separate Origins of Ice-Binding Proteins in Antarctic Chlamydomonas Species. *PloS One* 8 (3), e59186. doi: 10.1371/journal.pone.0059186

Raymond, J. A., and Morgan-Kiss, R. (2017). Multiple ice-binding proteins of probable prokaryotic origin in an antarctic lake alga, *Chlamydomonas* sp. ICE-MDV (Chlorophyceae). *J. Phycol.* 53, 848–854. doi: 10.1111/jpy.12550

Raymond, J. A. (1992). Glycerol is a colligative antifreeze in some northern fishes. *J. Exp. Zool.* 262, 347–352. doi: 10.1002/jez.1402620316

Raymond, J. (1995). Glycerol synthesis in the rainbow smelt *Osmerus mordax*. *J. Exp. Biol.* 198, 2569–2573.

Raymond, J. A. (2015). Two potential fish glycerol-3-phosphate phosphatases. *Fish Physiol. Biochem.* 41, 811–818. doi: 10.1007/s10695-015-0048-7

Spigel, R. H., Priscu, J. C., Obryk, M. K., Stone, W., and Doran, P. T. (2018). The physical limnology of a permanently ice-covered and chemically stratified Antarctic lake using high resolution spatial data from an autonomous underwater vehicle. *Limnol. Oceanogr.* 63, 1234–1252. doi: 10.1002/lno.10768

Stahl, S. E. (2014). *Photooxidative stress response in mesophilic and psychrophilic strains of Chlamydomonas raudensis: a comparative study*. Thesis (Miami, OH: Miami University).

Suescún-Bolívar, L. P., and Thomé, P. E. (2015). Osmosensing and osmoregulation in unicellular eukaryotes. *World J. Microbiol. Biotechnol.* 31, 435–443. doi: 10.1007/s11274-015-1811-8

Sussman, I., and Avron, M. (1981). Characterization and partial-purification of DL-glycerol-1-phosphatase from *Dunaliella salina*. *Biochim. Biophys. Acta* 661, 199–204. doi: 10.1016/0005-2744(81)90004-8

Tamura, K., Peterson, D., Peterson, N., Stecher, G., Nei, M., and Kumar, S. (2011). MEGA5: Molecular evolutionary genetics analysis using maximum likelihood, evolutionary distance, and maximum parsimony methods. *Mol. Biol. Evol.* 28, 2731–2739. doi: 10.1093/molbev/msr121

Wang, Z. X., Zhuge, J., Fang, H. Y., and Prior, B. A. (2001). Glycerol production by microbial fermentation: A review. *Biotechnol. Adv.* 19, 201–223. doi: 10.1016/S0734-9750(01)00060-X

Waterhouse, A., Bertoni, M., Bienert, S., Studer, G., Tauriello, G., Gumienny, R., et al. (2018). SWISS-MODEL: homology modelling of protein structures and complexes. *Nucleic Acids Res.* 46, W296–W303. doi: 10.1093/nar/gky427

Conflict of Interest: The authors declare that the research was conducted in the absence of any commercial or financial relationships that could be construed as a potential conflict of interest.

frontiers in Plant Science

ORIGINAL RESEARCH
published: 17 December 2020
doi: 10.3389/fpls.2020.617250

Cysts of the Snow Alga *Chloromonas krienitzii* (Chlorophyceae) Show Increased Tolerance to Ultraviolet Radiation and Elevated Visible Light

Lenka Procházková[1], Daniel Remias[2], Wolfgang Bilger[3], Heda Křížková[1], Tomáš Řezanka[4] and Linda Nedbalová[1]*

[1] Faculty of Science, Charles University, Prague, Czechia, [2] School of Engineering, University of Applied Sciences Upper Austria, Wels, Austria, [3] Botanical Institute, Christian-Albrechts-University Kiel, Kiel, Germany, [4] Institute of Microbiology, The Czech Academy of Sciences, Prague, Czechia

OPEN ACCESS

Edited by:
Koichiro Awai, Shizuoka University, Japan

Reviewed by:
Eric Marechal, UMR5168 Laboratoire de Physiologie Cellulaire Vegetale (LPCV), France
Alexei E. Solovchenko, Lomonosov Moscow State University, Russia
Rei Narikawa, Shizuoka University, Japan

***Correspondence:**
Lenka Procházková
lenkacerven@gmail.com

Specialty section:
This article was submitted to Marine and Freshwater Plants, a section of the journal Frontiers in Plant Science

Received: *14 October 2020*
Accepted: *30 November 2020*
Published: *17 December 2020*

Citation:
Procházková L, Remias D, Bilger W, Křížková H, Řezanka T and Nedbalová L (2020) Cysts of the Snow Alga Chloromonas krienitzii (Chlorophyceae) Show Increased Tolerance to Ultraviolet Radiation and Elevated Visible Light. Front. Plant Sci. 11:617250. doi: 10.3389/fpls.2020.617250

Melting mountainous snowfields are populated by extremophilic microorganisms. An alga causing orange snow above timberline in the High Tatra Mountains (Poland) was characterised using multiple methods examining its ultrastructure, genetics, life cycle, photosynthesis and ecophysiology. Based on light and electron microscopy and ITS2 rDNA, the species was identified as *Chloromonas krienitzii* (Chlorophyceae). Recently, the taxon was described from Japan. However, cellular adaptations to its harsh environment and details about the life cycle were so far unknown. In this study, the snow surface population consisted of egg-shaped cysts containing large numbers of lipid bodies filled presumably with the secondary carotenoid astaxanthin. The outer, spiked cell wall was shed during cell maturation. Before this developmental step, the cysts resembled a different snow alga, *Chloromonas brevispina*. The remaining, long-lasting smooth cell wall showed a striking UV-induced blue autofluorescence, indicating the presence of short wavelengths absorbing, protective compounds, potentially sporopollenin containing polyphenolic components. Applying a chlorophyll fluorescence assay on intact cells, a significant UV-A and UV-B screening capability of about 30 and 50%, respectively, was measured. Moreover, intracellular secondary carotenoids were responsible for a reduction of blue-green light absorbed by chloroplasts by about 50%. These results revealed the high capacity of cysts to reduce the impact of harmful UV and high visible irradiation to the chloroplast and nucleus when exposed at alpine snow surfaces during melting. Consistently, the observed photosynthetic performance of photosystem II (evaluated by fluorometry) showed no decline up to 2100 μmol photons m^{-2} s^{-1}. Cysts accumulated high contents of polyunsaturated fatty acids (about 60% of fatty acids), which are advantageous at low temperatures. In the course of this study, *C. krienitzii* was found also in Slovakia, Italy, Greece and the United States, indicating a widespread distribution in the Northern Hemisphere.

Keywords: snow algae, cysts, polyunsaturated fatty acids, photosynthesis, astaxanthin, chlorophyll fluorescence, UV-B radiation, UV-A radiation

INTRODUCTION

Long-lasting, melting snow is an extremophilic habitat for specialised phototrophic eukaryotes (Hoham and Remias, 2020). Cryoflora represents the primary producers in an ecosystem containing heterotrophic members like bacteria, ciliates, mites, rotifers, tardigrades, springtails in combination with fungi like chytrids (Yakimovich et al., 2020). During the melting period, snow algae cause the macroscopic phenomenon of coloured snow. Such blooms frequently occur in combination with abundant intracellular secondary carotenoids, altering the snow colour from green to red. This has an impact on snowmelt due to a significant albedo reduction, as shown in Polar (Onuma et al., 2016; Gray et al., 2020; Khan et al., 2020) and Alpine regions (Di Mauro et al., 2020).

Using state of the art morphological and molecular protocols, the number of recognised species causing snow blooms has increased during the last decade (e.g., Matsuzaki et al., 2019). The majority belongs to the green algal genus *Chloromonas*, and its ability of snow colonisation is based on a life cycle including sensitive, migrating flagellates deeper in the snow and a transformation into robust, immotile cyst stages that prevail at the surface (Hoham and Remias, 2020). Generally, knowledge about the geographic distribution or the ecophysiological preferences of these cryoflora microbes is limited. Some have been studied more extensively, such as the red snow causing *Chlainomonas* sp. (Remias et al., 2016; Procházková et al., 2018a; the first record from Antarctica in Luo et al., 2020) or *Sanguina nivaloides* (formerly assigned to *Chlamydomonas nivalis*) (Procházková et al., 2019a). There are not many works about snow dwelling *Chloromonas* that cause colours other than red (Hoham et al., 2006; Remias et al., 2010; Procházková et al., 2019b).

In this study, the ecophysiology of *Chloromonas krienitzii* (Chlorophyceae) was investigated. Specimens were collected in several alpine sites of Europe and North America, where cyst stages were responsible for orange blooms during summer. Historically, this species was one of several lineages formerly assigned to *Chloromonas brevispina*, which comprised characteristic cysts with cells possessing uniformly distributed spiky surface structures (Hoham et al., 1979). With samples from Japan, Matsuzaki et al. (2015) described an independent taxon out of this group based on morphological data and the multigene phylogeny of the vegetative strain. Although this species was recently detected by environmental sequencing in British Columbia (Canada) (Engstrom et al., 2020), its overall geographic distribution is still unexplored.

Cells of *C. krienitzii* were characterised using multiple approaches to understand strategies of adaptation to the harsh habitat. In a first step, the field collected cells were determined to the species level using the hypervariable ITS2 rDNA marker (barcoding). Second, since several details of the life cycle including cleavage of cysts into flagellates for this alga were unknown, thus hampering determination efforts by light microscopy of environmental samples, the putative life cycle was reconstructed. Third, since cysts are subject to high irradiation at the snow surface, the light-dependent photobiology was evaluated. Fatty acid and pigment profiles of the cysts complement the dataset, as these compounds are regarded as important players for low temperature and high irradiation adaptation (Leya, 2013, 2020). Finally, by applying a chlorophyll fluorescence assay to intact cells, the capacity for screening the chloroplast in the cysts against harmful radiation by UV absorbing carotenoids was measured to reveal the capability to reduce the impact of this irradiation.

MATERIALS AND METHODS

Field Sampling

Table 1 shows the snow sampling sites in the Rocky Mts. (Colorado, United States), the Sarntal Alps (South Tyrol, Italy), High Tatra Mts. (Slovakia, Poland) and North Pindus (Greece) (**Supplementary Figure 1**). With a field microscope, virtually monospecific blooms (LP05, WP191, Pind19) were harvested according to Procházková et al. (2019a). The unialgal spot of 1SAR was collected without previous light microscopy in the field. Additionally, three mixed algal snow communities (Saddle2, WP189, WP190) were included in this study to track the geographical distribution of the target species. Harvested snow was placed in 5 L buckets (LP05) or in 50 mL centrifugation tubes (all the other samples). Supplementary, a 10 mL subsample of LP05 was fixed immediately after harvest by a drop of acidic lugol solution (acetic acid). Samples LP05 and WP191 were used for cultivation assay. Samples LP05, WP191 and 1SAR were a subject of Sanger sequencing. Furthermore, sample LP05 was also used in other subsequent analysis (electron microscopy, photosynthesis measurements, UV and blue light transmittance protocol, analyses of pigment and fatty acid profiles). Prior to photosynthesis measurements, snow with live cells was melted gently in darkness overnight at 4–5°C. Electrical conductivity (EC) and pH of the meltwater were obtained with WTW Instruments (Cond 340i and Inolab, Germany) or with HANNA (Combo EC, ftb Romania). The snow water equivalent at the sampling site (SWE; referred to as "snow water content" in the following reference) was carried out as described previously (Procházková et al., 2018b).

Cultivation Assay

A feature of very low electrical conductivities recorded in the field was reproduced at laboratory conditions for cultivation. As long as the field cysts did not start to cleave, they were incubated in deionised water. In detail, for gaining unialgal strains out of field blooms to study the life cycle, subsamples of LP05 and WP191 containing sedimented cysts were put into sterile 2 mL cryotubes and the meltwater replaced with deionised water. For induction of germination of the cysts, the cells were kept at 1°C during the day (14 h) resp. −1°C during the night (10 h) in a Percival LT-36VL (CLF Plant Climatics, Wertingen, Germany). The light intensity generated by fluorescent tubes was approximately 40–70 μmol PAR m^{-2} s^{-1}. Subsequently, flagellates were transferred from the supernatant into liquid 0.6 N Bold's Basal Medium (BBM) (Bischoff and Bold, 1963) and irradiance was kept at 20–30 μmol PAR m^{-2} s^{-1}.

Light and Electron Microscopy

Light microscopy was performed with an Olympus BX43 at 1000× magnification using oil immersion, equipped with an Olympus DP27 camera (Olympus Europe SE, Hamburg, Germany), or with a Nikon Eclipse 80i with Nikon DS-5M camera (Nikon Instruments Europe, BV). Scanning and transmission electron microscopy (SEM and TEM) were carried out with sample LP05 as described previously (Procházková et al., 2018b), with the minor exception that for TEM only cells previously fixed by acidic lugol solution (acetic acid) were used. The autofluorescence of cell walls was studied using Nikon Eclipse 80i (objective Plan Apo VC 100 × 1.40, camera DS 5 M; Nikon Instruments, Amsterdam, Netherlands) equipped with a DAPI-filter (excitation = 340–380 nm, emission = 435–485 nm). Chloroplast shapes were visualised, by exposing them to excitation = 460–500 nm and emission 600 nm.

Isolation of DNA, PCR, Sequencing, ITS2 rRNA Secondary Structure Prediction

DNA isolation (sample LP05) was carried out with a DNeasy Plant Mini Kit (Qiagen, Germany), as in Procházková et al. (2018b). If less than 20 mg wet biomass was available (samples WP191 and 1SAR), DNA was extracted using the Instagene Matrix Kit (Bio-Rad Laboratories, Hercules, CA, United States) according to Remias et al. (2016). The internal transcribed spacer region 2 (ITS2 rDNA) was amplified from DNA isolates by polymerase chain reaction (PCR) using existing primers of SSU (CTGCGGAAGGATCATTGATTC) and LSU (AGTTCAGCGGGTGGTCTTG) (Piercey-Normore and DePriest, 2001). Amplification reactions were described in Procházková et al. (2018b). PCR products were purified and sequenced using an Applied Biosystems automated sequencer (ABI 3730xl) at Macrogen Europe (Amsterdam, Netherlands). The obtained sequences of *C. krienitzii* were submitted to NCBI Nucleotide sequence database (accession numbers: MW136658 for LP05–partial 18S rDNA + ITS1 rDNA + ITS2 rDNA + partial 28S rDNA; MW139361 for WP191–ITS2 rDNA; MW139362 for 1SAR–ITS2 rDNA). Methods for annotation and prediction of the secondary structure of the nuclear rDNA ITS2 region follow those described in a previous study (Remias et al., 2020).

Photosynthesis

In vivo chlorophyll fluorescence parameters were measured with a pulse–amplitude modulated fluorometer (PAM 2500, Heinz Walz GmbH, Germany) in a 0.6 mL chamber and cooled in an ice bath to approximately 2°C. To obtain the relative electron transport rates (rETRs), the apparent quantum yield for electron transport (alpha) and the light saturation point I_k, cells were exposed to photon flux densities (PFD) of 5, 9, 34, 67, 104, 201, 366, 622, 984, 1389, 1666, and 2018 μmol photons m^{-2} s^{-1} for 30 s each. Four independent replicates were measured. The data points were fitted to the model, assuming no photoinhibition (Webb et al., 1974). For further details, see Procházková et al. (2018b).

Screening of UV Radiation and Blue-Green Light

Ultraviolet and blue light screening were assessed by chlorophyll fluorescence measurements (Bilger et al., 1997). Frozen and subsequently thawed cells of *Chlorella vulgaris* (SAG 211-11b) were used as a reference green alga from a non-exposed habitat. Algae (LP05) were sent frozen to University of Kiel, Germany, where they were stored at −20°C until measurement. The sample was thawed and applied onto a glass fibre pre-filter (Sartorius Stedim biotech, Göttingen, Germany). Chlorophyll fluorescence was excited from the sample using a Xe-PAM fluorometer (Walz, Effeltrich, Germany) with blue-green (half-bandwidth (HBW), 420–560 nm), UV-A (λ_{max}, 366 nm; HBW, 32 nm), UV-B (λ_{max}, 314; HBW, 18 nm) and red (λ_{max}, 650 nm; HBW, 9 nm) measuring beams according to Pescheck and Bilger (2018). Ratios of fluorescence excited with blue-green light [F(BG)], UV-A [F(UV-A)] or UV-B [F(UV-B)] to that excited with red light [F(red)] were calculated. The measurements were conducted in three replicates. For comparison, a dense suspension of *Chlorella vulgaris* cells was measured the same time. In order to provide the same pre-treatment for these cells as for *C. krienitzii*, *Chlorella* cells were frozen for 2 h at −20°C and afterward rapidly thawed. *Chlorella* was cultivated in liquid culture medium in 400 mL culture vessels placed in a modified Kniese apparatus (Senger et al., 1972) under continuous aeration with filtered air. 3N BBM + V medium (modified BBM) (Starr and Zeikus, 1993) was used for the cultivation. The culture was grown on a 14:10 h light/dark cycle at 135 μmol photons m^{-2} s^{-1} of white fluorescent light at room temperature. Values of fluorescence excitation ratios of *C. krienitzii* were compared with those of *Chlorella vulgaris* cells using Student's *t*-test with SigmaPlot (Systat Software, Erkrath, Germany).

Pigment Analysis

For characterisation of carotenoids and chlorophylls (sample LP05), lyophilised cells were broken with liquid nitrogen in a mortar with a pestle, extracted with organic solvents and analysed by HPLC (Agilent 1200 ChemStation) equipped with a YMC C30 column and a diode array detector set at 450 nm in the same manner as described in Procházková et al. (2019b). Pigment ratios (w/w) were used because dry mass of cells as a reference could not be obtained due to the presence of particles.

Lipid Extraction and Fatty Acid Methyl Esters Analysis (FAMEs)

The extraction procedure was based on the method of Bligh and Dyer (1959), and elution was done from a Sep-Pak Vac Silica cartridge 35cc (Waters; 10 g normal-phase silica) by chloroform (neutral lipids), acetone (glycolipids), and methanol (phospholipids) according to Saunders and Horrocks (1984). All classes of lipids were saponified overnight in 10% KOH in methanol at room temperature. The structures of fatty acid methyl esters analysis (FAMEs) were confirmed by comparison with Gas Chromatography/Mass Spectrometry retention times and fragmentation patterns with those of standard FAMEs (Supelco, Prague) (Dembitsky et al., 1993;

Řezanka and Dembitsky, 1999). Procedures were described in more detail in Procházková et al. (2018b).

RESULTS

Habitat Conditions

In the High Tatras, the Sarntal Alps and the Northern Pindus mountain range, spots of orange snow were found in June and July at elevation from 1862 to 2240 m a.s.l., all of them situated above timberline (**Table 1**). In the Rocky Mts., the orange spots appeared as insertions in a large red snowfield dominated by *S. nivaloides* at 3540 m a.s.l. In the Polish High Tatras, the virtually monospecific orange snow was present at the surface, but the most intense bloom was about 3 to 5 cm below (LP05 sample). At this site, the surface was dominated by "black snow" (caused by inorganic particles) typical for this region (Kol, 1966). Although this blackish snow was removed before harvest, impurities were still present in the sample collected in subsurface layers (**Figure 1**). In the moment of harvest of the field cysts, a slightly acidic pH and low electrical conductivities were typical for the meltwater at all localities (**Table 2**).

Cell Morphology and Autofluorescence

In the High Tatras, the maximal population density was 45,900 ± 4,600 orange cysts mL^{-1} meltwater was recorded (LP05). In the light microscope, blooms consisted of orange, egg-shaped cells with mean sizes of 25.1 ± 3.9 μm × 22.6 ± 3.1 μm (**Figures 2–4**). Cells still had their outer envelope (**Figures 2A**, **3A**), were in the process of shedding their outer envelope (a cell on the right in **Figure 4E**) or this envelope was just shed (**Figures 2C**, **3B**). This outermost ephemeral cell wall possessed many characteristic short protrusions (**Figures 3D,F**), in contrast to the persisting smooth cell wall surface (**Figures 2B**, **3C**). The cytoplasm contained large numbers of peripheral, orange lipid bodies (**Figures 1A**, **3E**, **4A,C**), presumably deposits of the

TABLE 1 | *Chloromonas krienitzii* sample codes, collection date, sampling site, elevation (metres a.s.l.) and geographic position (GPS).

Sample	Date	Location	Altitude	GPS	#
Saddle2	July 8, 2017	Niwot Ridge, Front Range, Rocky Mts, Colorado, United States	3540	N40° 3.326′ W105° 35.265′	1
1SAR	July 15, 2013	Wannser Joch, Sarntal Alps, South Tyrol (BZ), Italy	2244	N46° 47.867′ E11° 21.697′	2
LP05	June 14, 2017	Valley Za Mnichem, High Tatras, Poland	1862	N49° 11.654′ E20° 3.168′	3
WP189	June 17, 2018	Next to Modré Lake shore, High Tatras, Slovakia	2177	N49° 11.559′ E20° 11.165′	4
WP190	June 17, 2018	At the bottom of Dolinka pod Sedielkom, High Tatras, Slovakia	2114	N49° 11.41′ E20° 11.27′	5
WP191	June 17, 2018	On a shore of Prostredné Sivé Lake, High Tatras, Slovakia	2017	N49° 11.016′ E20° 10.483′	6
Pind19	July 1, 2019	Next to a hiking trail, North Pindus, Greece	2376	N40° 5.153′ E20° 55.302′	7

The numbers indicate sampling sites at the map of ***Supplementary Figure 1****.*

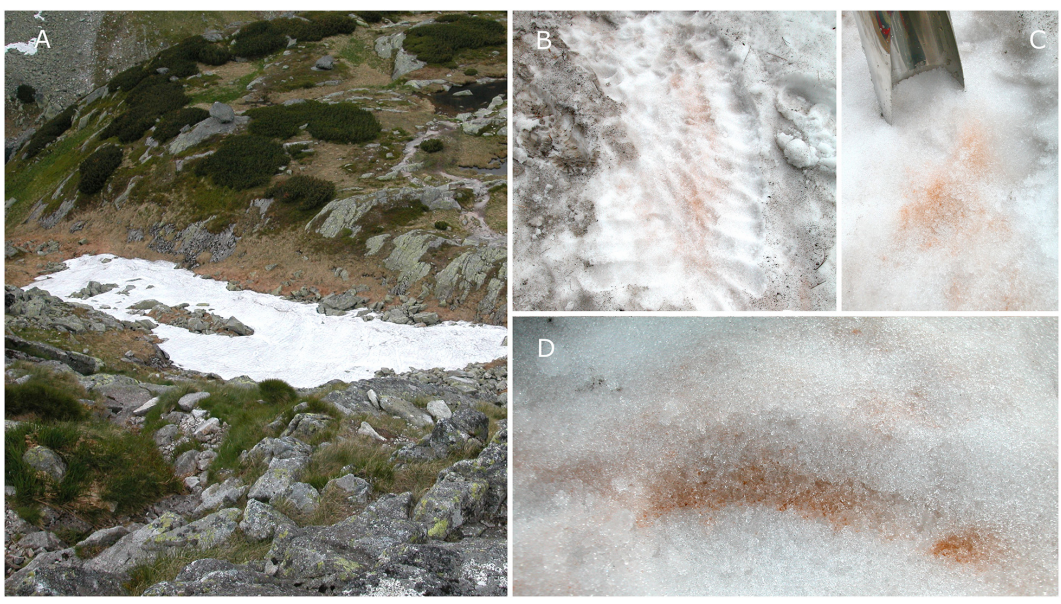

FIGURE 1 | Overview of a sampling site in the valley Za Mnichem, the High Tatras, Poland, with a bloom of *Chloromonas krienitzii*. The snow field was located on a modest slope in a field depression **(A)** and contained superficial "black snow" (likely airborne mineral dust) **(B)**. Before cell harvest, to avoid a high load of mineral particles in a sample, the surface snow was removed **(C)**. Orange spots were visible at the snow surface **(B)**, but the highest algal cell density was about 3–5 cm below **(D)**.

TABLE 2 | Abiotic habitat parameters and cyst sizes of *Chloromonas krienitzii* field samples.

Sample	Species	EC	pH	SWE	Cells per mL meltwater	Cell size (μm)
Saddle2	*S. nivaloides*, *C. krienitzii*	3	5.5	–	–	25.6–34.2 × 22.9–26.6 (2)
1SAR	*C. krienitzii*	–	–	–	–	22 ± 3; 15–27 (40)
LP05	*C. krienitzii*	6.8	5.2	53.8 ± 1.9	45 900 ± 4600	26 ± 1.8 × 21 ± 1.6; 22.9–29.4 × 18–24.3 (31)
WP189	*C.* cf. *nivalis*, *C. krienitzii*	8.1	6.2	–	(35 500); 850	21.6–25.7 × 22.3–24.4 (4)
WP190	*C. nivalis* subsp. *tatrae*, *C. krienitzii*	5.8	6.8	–	(15 250); 2050	23.9–30.4 × 23.3–28.1 (7)
WP191	*C. krienitzii*	–	–	–	–	24.9 ± 2.1 × 22 ± 1.7; 20.9–29.6 × 18.3–25.1 (33)
Pind19	*C. krienitzii*	–	–	–	–	33 ± 1.3 × 29.1 ± 1.5; 32.1–36.5 × 27.1–31.6 (10)

Electrical conductivities (EC) (μS cm^{-1}), pH of meltwater, the snow water equivalent (SWE) (%), maximum population density ± standard deviation (SD), average cell sizes [μm] and cell size ranges (with n = number of cells measured) are shown. In case C. krienitzii was a minor contribution in a bloom of other snow alga (e.g., Chloromonas cf. nivalis, Chloromonas nivalis subsp. tatrae), cell counts of the latter are shown in brackets.

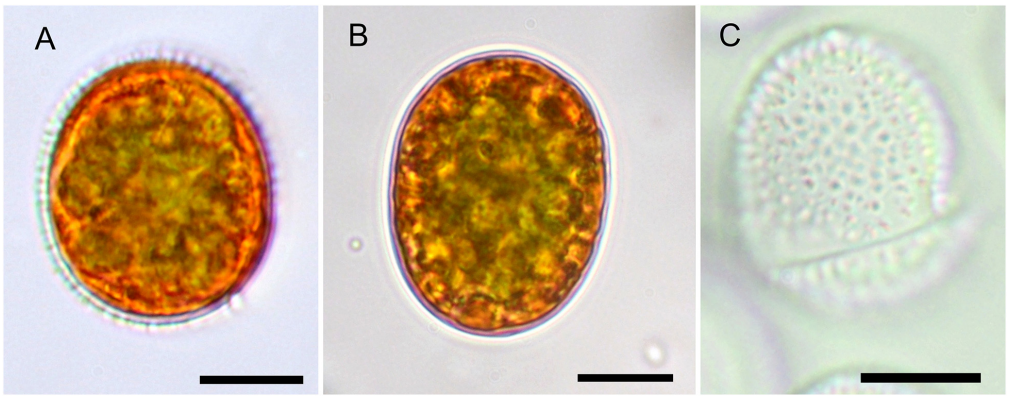

FIGURE 2 | The Light microscopy of *Chloromonas krienitzii* field cysts. **(A,B)** Median view, showing cytoplasm with peripheral, orange astaxanthin deposits and an axial, greenish chloroplast. **(A)** Prominent secondary cell wall spikes still present. **(B)** Smooth cell that had shed the outer envelope **(C)**, the latter possessed characteristic, short spikes (<1 μm). Scale bar 10 μm.

carotenoid astaxanthin which obscured the plastid morphology. Using chlorophyll autofluorescence, the chloroplast shape was revealed as axial and being sectioned into several discoid parts (**Figures 4B,D**). Remarkably, the remaining secondary cell wall exhibited a blue autofluorescence under UV-A exposure (**Figure 4F**). In contrast, vegetative flagellates of the strain (see below) had no wall UV-autofluorescence (data not shown).

Comparative Analysis of ITS2 rDNA

Regarding the variable marker ITS2 rDNA, cells of all blooms (LP05, 1SAR, WP191) were genetically identical with the type strain of *C. krienitzii* (GsCl-54) from Japan, except for one to four nucleotide positions (out of 288 bp). The different nucleotides were on a single strand only, thus no compensatory base change was found. The cysts in other samples collected in this study (**Table 2**) were used for the light microscopy observation only. Taking into an account these molecular findings together with the consistent morphology of the field sampled cysts and their identical type of habitat, all investigated samples were regarded to belong to this species (**Figure 5**).

Life Cycle Studies

The aim of life cycle observation was to reconstruct the fate of the bloom cysts. The shedding of the spiky, outermost cell wall was observed for cysts in the field (WP191, LP05) and later in the lab as well (**Figure 6A**). In course of this life cycle development, the remaining cells with smooth wall and orange pigmentation resembled a different snow alga, *Cryodactylon glaciale* (**Figure 6B**), instead of initial spiky cells traditionally identified as *Chloromonas* cf. *brevispina*. After 5 months of reproductive inactivity in original meltwater in the lab, these smooth cysts had cleaved into 4 to 16 daughter cells. Concurrently, the intracellular pigmentation of sporangia turned from orange to green (**Supplementary Figure 2A** and **Figures 6C,D**). Approximately 3 weeks later, the cysts germinated, i.e., vegetative green thickened cells (**Figures 6E–G**) or elongate bean to kidney shaped flagellates were released (**Figure 6H**). Two morphologic versions developed, either elongate (**Figures 6I–K**) or spherical stages (**Figures 6L–N**). No sexual reproduction was observed for this strain. Still, the formation of a new generation of cyst stages was occasionally observed at lab conditions (**Supplementary Figure 2H**).

UV and Blue Light Protection of the Cysts

In the fresh state, *Chlorella vulgaris* cells showed the same fluorescence excitation ratios as isolated chloroplasts from *Arabidopsis thaliana* (100% transmittance standard, data not

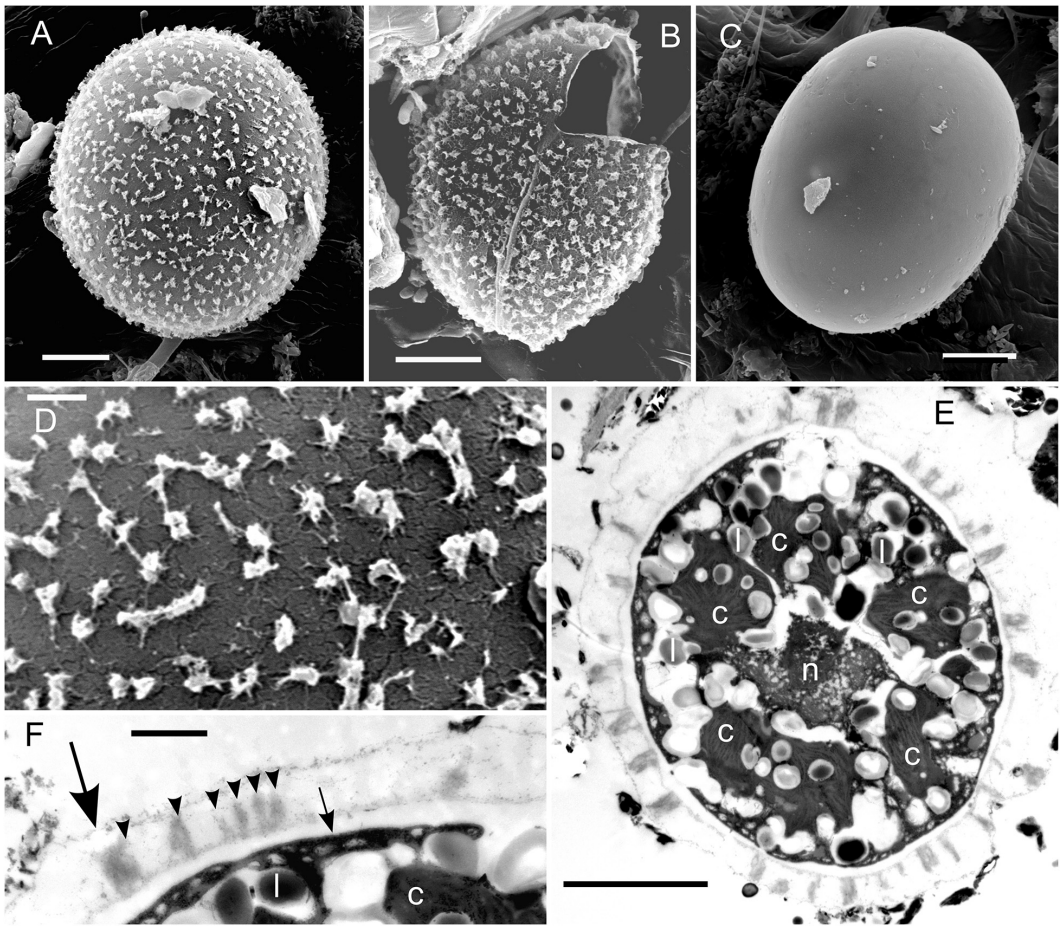

FIGURE 3 | EM of *Chloromonas krienitzii* field cysts from the High Tatras (LP05). **(A–D)** SEM. **(A)** A cyst with spiky surface structures. **(B)** Outer (putative secondary) cell wall with spines after shedding. **(C)** Remaining (putative tertiary) smooth cell wall. **(D)** Detail view of the spiky surface of the secondary cells wall. **(E,F)** TEM of cells fixed by acidic lugol solution. **(E)** The chloroplast, sectioned into several discs (c), surrounding the central nucleus (n) and abundant lipids bodies (l) **(F)** Detail view of cell wall layers, transient primary cell wall (large arrow), spikes as a part of the secondary cell wall (arrowheads), smooth tertiary cell wall (small arrow). Scale bars 5 μm for panels **(A–C,E)**; scale bars 1 mm for panels **(D,F)**.

shown). Since *C. krienitzii* cells were also frozen and thawed, its data may compare better to those of the frozen *Chlorella vulgaris* cells. Compared to *Chlorella vulgaris*, *C. krienitzii* showed a 25 to 35% higher UV-A screening ($p < 0.01$) while the screening of UV-B radiation was 40–50% higher ($p < 0.001$) (**Figure 7A**).

The astaxanthin of the snow alga shows strong absorption in the blue-green spectral region and should accordingly compete for light absorption with chlorophyll. Indeed, fluorescence excitation in the blue-green wavelength region (HBW 420–560 nm; Bilger et al., 1997) was reduced by about 50% as compared to astaxanthin-free *Chlorella* ($p < 0.001$) (**Figure 7B**).

Photosynthesis

The photosynthetic performance of *C. krienitzii* field samples was tested at different irradiance levels and rapid light curves were generated. The cysts were not dormant in terms of photosynthesis, as indicated by ETR (**Figure 8**). No decline of activity was noticed up to 2100 μmol PAR m^{-2} s^{-1}. Cells showed an alpha value of 0.17, a relative ETR_{max} of 22.9 ± 1.5, and an I_k value of 133 ± 8 μmol PAR m^{-2} s^{-1}.

Pigment and Fatty Acid Composition

The orange pigmentation of cysts of *C. krienitzii* was caused by astaxanthin. Its abundance and those of other pigments were calculated in reference to chlorophyll *a* (**Supplementary Table 1**). Astaxanthin comprised 28% of all pigments (LP05). In the chromatogram, it occurred as several peaks with identical absorption spectra, all of them likely ester derivatives (data not shown). Chlorophylls (a and b) comprised 61% of all pigments, primary (plastid) carotenoids represented 11%. The overall ratio of astaxanthin to chl-*a* was 0.4. In contrast, the laboratory strain stayed green (data not shown). The relative content of FAs (in percentage of total fatty acids) of *C. krienitzii* field cysts (LP05) is shown in **Figure 9**. FAs with C14 to C18 were found. Cells showed high levels of PUFAs (58.6% of total fatty acids), whereas the content of saturated acids (SAFAs) did not exceed 18.7% (mainly palmitic acid, 16:0, 17.1%). The main monounsaturated fatty

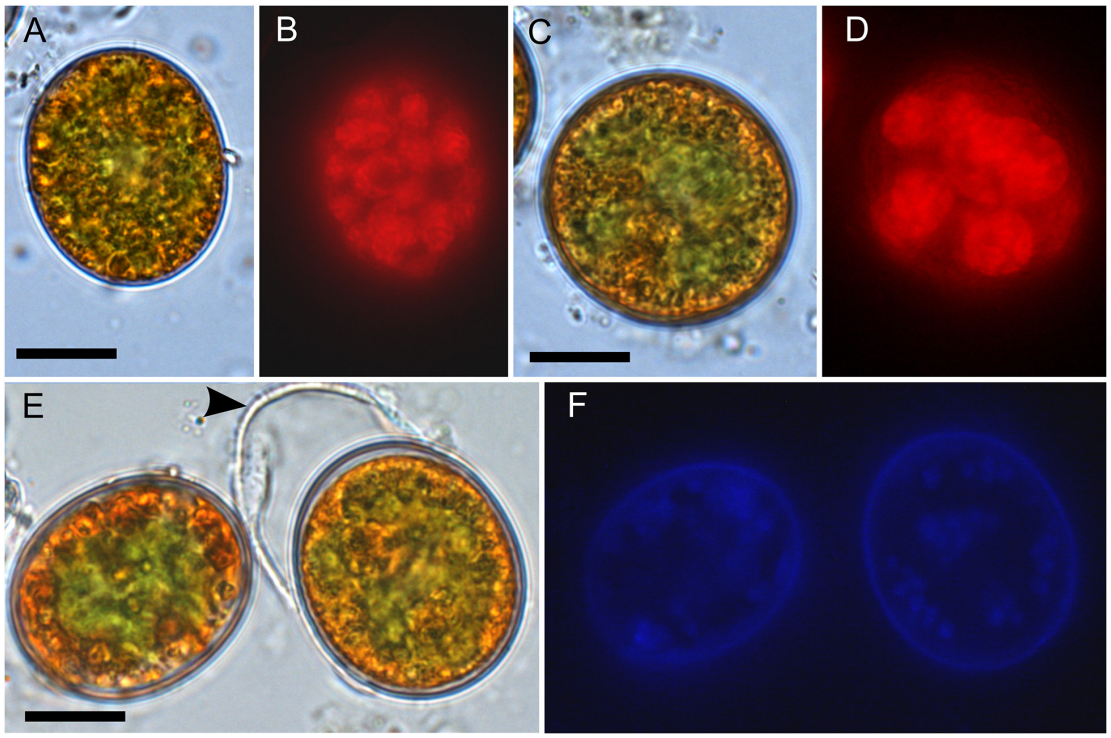

FIGURE 4 | Bright field vs. fluorescence LM comparison of *Chloromonas krienitzii* field cysts. Chlorophyll autofluorescence in red **(B,D)** showing the chloroplast sectioned into several discoid parts, with are otherwise partly obscured **(A,C)**. The tertiary cell wall exhibited blue, UV A-induced autofluorescence **(F)**, indicating the presence of putative UV-absorbing compounds. In contrast, the outer, secondary spiky wall (arrowhead) exhibited no autofluorescence (compare **E,F**). Scale: 10 μm.

acid (MUFA) was oleic acid (18:1 (9Z), 10.6%). The dominant PUFA was linolenic acid [18:3 (9Z, 12Z, 15Z), 27.8%], followed by hexadecatetraenoic acid [16:4 (4Z, 7Z, 11Z, 13Z), 11.6%].

DISCUSSION

Geographical Distribution of Snow Algae

Direct sequencing of monospecific algal blooms facilitates species-specific biogeographic conclusions (Procházková et al., 2019a). Individual species of snow algae can either show a cosmopolite distribution (e.g., *S. nivaloides*, Segawa et al., 2018; Procházková et al., 2019a) or their known occurrence is rather geographically limited (e.g., *Chloromonas polyptera*, Remias et al., 2013; *Sanguina aurantia*, Brown and Tucker, 2020). *C. krienitzii* seems to be in-between: It was initially described only from Japan (Matsuzaki et al., 2015) and subsequently found in Europe and North America as well (this study, Engstrom et al., 2020). Likely, the morphologically striking cysts have been observed many times elsewhere, but were determined as *Chloromonas* cf. *brevispina* due to the spiky wall surface, and molecular protocols were not available during older studies. For example, Hoham et al. (1979) described snow algal cysts similar to *C. krienitzii* in the United States. This work gives the first records of *C. krienitzii* for Europe, namely in the High Tatra Mts (Poland and Slovakia) and the Alps (Italy), which is based both on molecular and morphological data. Furthermore, cysts with the same morphology were found in Greece (this study) and previously reported from Sierra Nevada (Spain) (see Figures 23–25 in Cepák and Lukavský, 2012) and Stara Planina Mts. (Bulgaria) (see Figures 50–55 in Lukavský and Cepák, 2010). *C. krienitzii* has not been found in polar regions or the Southern hemisphere yet.

Species Distribution Along the Gradient of Elevations

The blooms occurred at open sites with elevation ranging from 1862 to 3500 m (this study), but earlier studies reported *C. krienitzii* to be predominant in clearings or sites with sparse trees around 1200 m (Engstrom et al., 2020) or at open sites in broad-leaf forest around 880 m elevation (R. Matsuzaki–pers. comm., Matsuzaki et al., 2015). Similarly, such a wide gradient of elevation was described for the occurrence of orange to pinkish snow caused by *Chloromonas hindakii* (Procházková et al., 2019b). Apparently, snow algae of the genus *Chloromonas* can thrive in a large range of irradiation levels (exposed to semi-shaded sites). In contrast, *S. nivaloides*, the probably most widespread cryoflora species (Procházková et al., 2019a), is restricted to exposed habitats (Remias et al., 2005). The slightly acidic pH and low meltwater conductivities where *C. krienitzii* was found correspond to similar values reported for many other chlorophycean snow algae (Hoham and Remias, 2020).

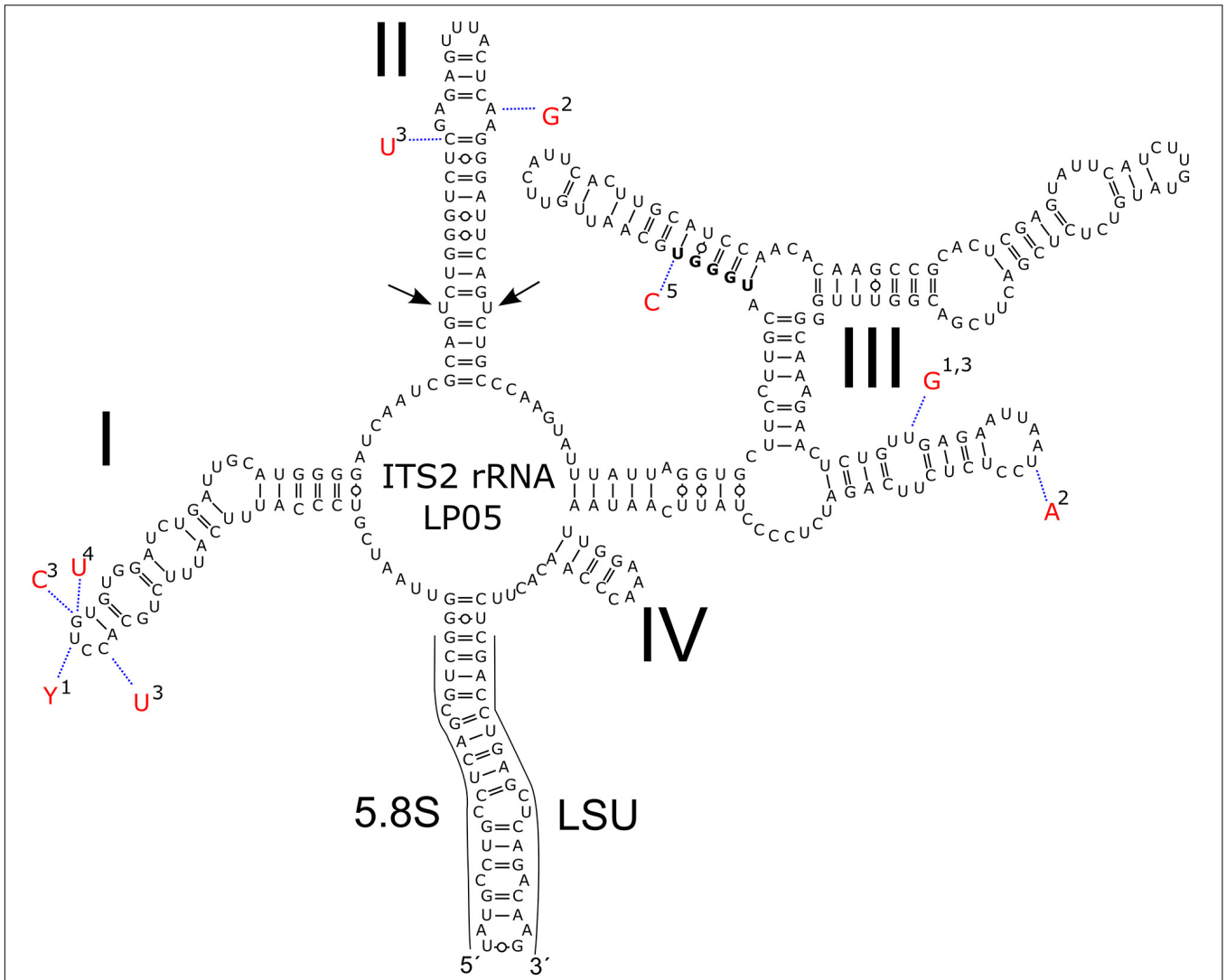

FIGURE 5 | Intraspecific variability in the secondary of ITS2 rDNA transcripts of *Chloromonas krienitzii*–comparison between field-cyst collected from different localities (LP05 [MW136658], 1-1SAR [MW139362], 2-WP191 [MW139361]; this study), the type strain (3-GsCl-54 [LC012756]; Matsuzaki et al., 2015) and published sequences of field cysts (4-Gassan-A [LC012753], 5-Hakkoda-2 [LC012755]; Matsuzaki et al., 2015). The marker sequence differed by 1–4 bp amongst the samples. Helices are labelled with Latin numbers: I–IV. Nucleotide differences of the field samples are described in red outside the structure and linked by dotted lines. No compensatory base change was found. Note the U–U mismatch in helix II (arrow).

Colours of Snow Bloom in the Context of *Chloromonas brevispina*-Like Species

Using molecular data, Matsuzaki et al. (2015) proved that cysts which were morphologically determined as *C. brevispina* are caused by several independent lineages, which are in several cases not taxonomically described yet. In Washington State (United States), mature zygotes *C. brevispina* were reported to develop yellow, orange or pink snow discolouration, or to remain green if found several centimetres below the snow surface (Hoham et al., 1979). In this study, solely orange cells were observed for *C. krienitzii* in the field samples. Different stages of pigmentation (reflecting the changing ratio astaxanthin to chlorophyll) were noticed for other representants of *Chloromonas* cf. *brevispina* (*C. brevispina* DL09 in the Austrian Alps, Lutz et al., 2019, usually causing green snow, while the pink version was observed in late summer, Remias–pers. obs.).

Different Morphological Stages in Course of Life Cycle

Combined field and lab observations have provided insights to the life cycle of several snow dwelling *Chloromonas* (e.g., Hoham, 1975; Hoham and Mullet, 1977; Hoham et al., 1983). For *C. krienitzii*, the transition from a cyst to vegetative stages was presented here for the first time. As for other *Chloromonas* species, the "gametic membrane," like in the case of *C. krienitzii*, may remain surrounding the developing zygote, later it is expanded, gelatinises and is eventually shed (Procházková et al., 2018a). Smooth-walled cyst stages with

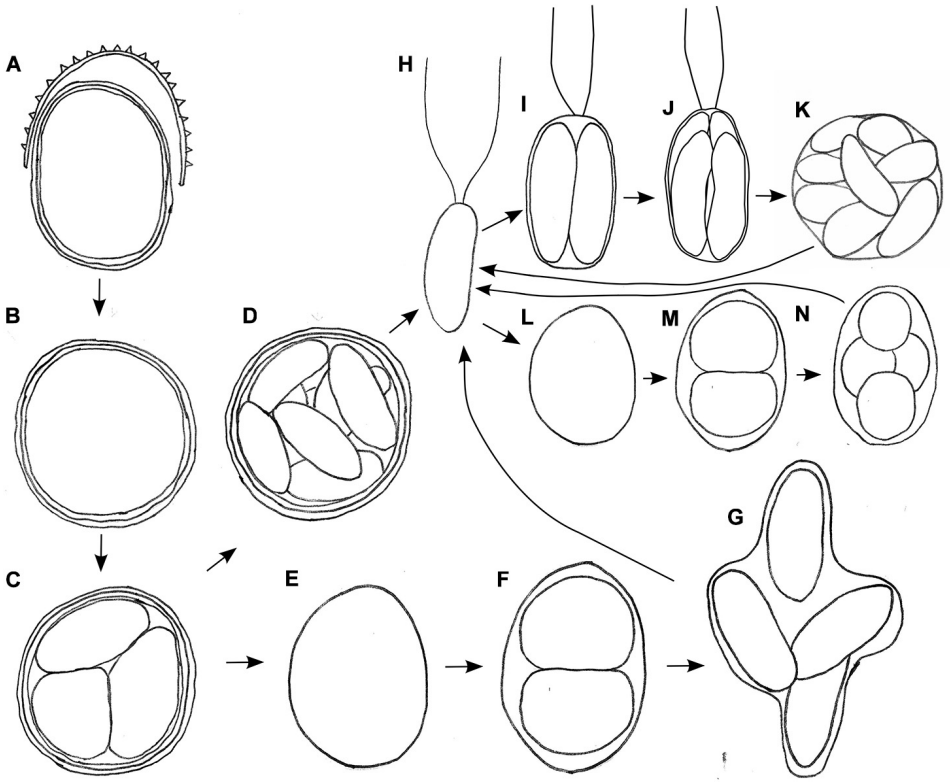

FIGURE 6 | Schematic, putative parts of the life cycle of *Chloromonas krienitzii*, based on combined observation of two field samples (LP05, WP191) kept in original meltwater **(A–H)** and vegetative flagellates **(H)** transferred into 0.6 N BBM medium **(H–L)** at laboratorial conditions. **(A)** Cyst from the field shedding outer, spiky wall. **(B)** Remaining cysts with smooth wall (resembling *Cryodactylon glaciale*). **(C)** Meiosis and cyst germination resulting in four daughter cells (three shown). Subsequently, two independent ways of development were observed: **(D)** Mitotic division (up to 16 cells per cyst). **(E)** Growth of released daughter cell and **(F,G)** mitotic divisions. **(H)** Vegetative flagellates are elongate- kidney or elongate-bean shaped. Then, two ways of asexual reproduction via zoospore formation were found, either via elongated **(I–K)** or spherical stages **(L–N)**, in both cases two to sixteen daughter cells were produced within the parental cell wall. Not shown: gamete fusion to form a new zygote, respectively a cysts.

partially orange cell compartments are difficult to be determined to the species level by light microscopy. Formerly, these cells were regarded as the independent species *Cryodactylon glaciale* (Chodat, 1921; Kol, 1968). We never observed shedding of secondary cell walls for other *Chloromonas* cf. *brevispina* species; in fact, they keep their spiky cell walls throughout the season (data not shown). During cyst germination, the number of daughter cells in *C. krienitzii* was always four, indicating that this process is probably meiotic. Concurrently, intracellular astaxanthin redistribution between daughter cells was noticed. It was followed by astaxanthin decomposition in these daughter cells (**Supplementary Figure 2A**). This can be interpreted as an adaptation to low-light conditions deep in the snow after germination during springtime, where secondary carotenoids would impair the photosynthetic performance by shading the chloroplast.

In the culture of *C. krienitzii*, the dominant vegetative stages were bean-shaped flagellates, however, spherical cells were regularly observed as well. This roundish shape is regarded as not being very common for *Chloromonas*, still it has been observed in several strains, and occasionally in the field (Hoham et al., 1979; Procházková, Remias–pers. obs.). The asexual reproduction of vegetative strain formed by flagellates for *C. krienitzii* was described previously (Matsuzaki et al., 2015). This corresponded with our finding that just before the first cell division, the protoplast rotated, and the parental contractile vacuoles moved to the equator of the parent cells (**Supplementary Figure 2C**, compare with Figure 11 in Matsuzaki et al., 2015). Without such observation, one may have a misleading impression that the strain contains two unrelated flagellates–thin elongate ones (i.e., not dividing at the given moment) and thickened ones (i.e., prepared for cell division). During this study, packages of two to four flagellates still inside the parental cells were occasionally observed (analogy can be seen in Figures 9, 10 in Hoham et al., 1979). The flagellates of *C. krienitzii* were "backward"-swimmers, meaning that during the cell movement the flagella are in the rear (**Supplementary Video 1**). In this study, sexual reproduction (e.g., Matsuzaki et al., 2020) was not observed.

Photosynthesis at Changing Light Conditions

Life at high alpine sites requires adaptation to extreme abiotic factors like temperature, visible and UV radiation and to

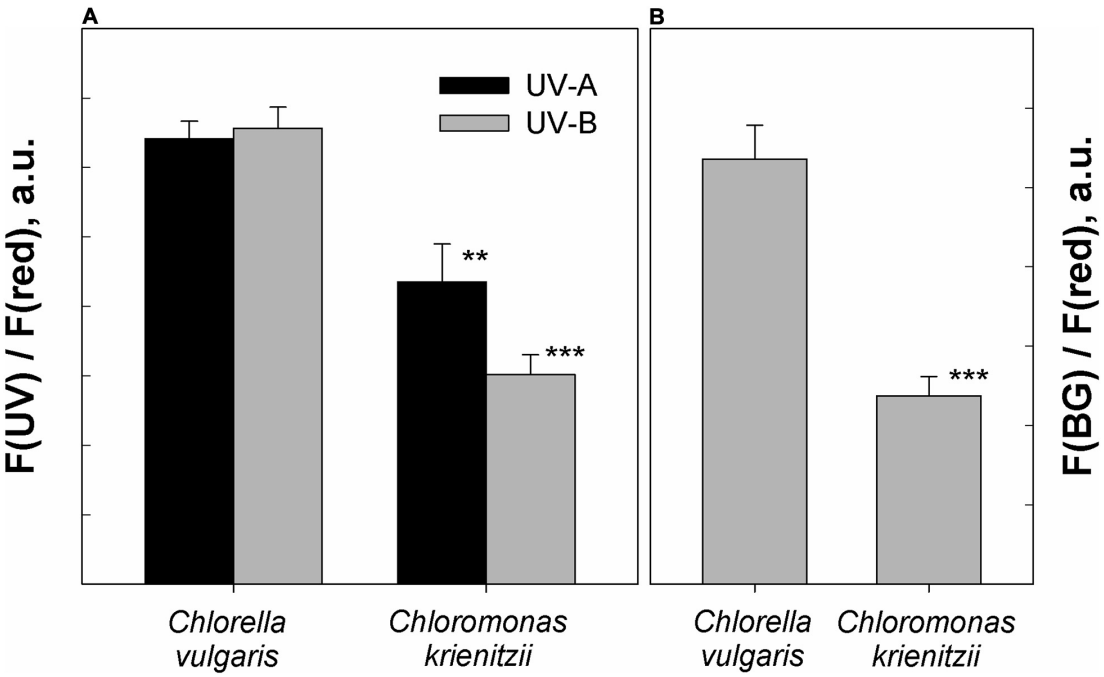

FIGURE 7 | Protection against UV and blue light as determined by chlorophyll fluorescence measurements. **(A)** UV-A and UV-B fluorescence excitation ratios (arbitrary units) of frozen and subsequently thawed *Chlorella vulgaris* cells and *Chloromonas krienitzii* cysts (LP05). **(B)** Blue-green to red fluorescence excitation ratios (arbitrary units), indicating competition for excitation light between chlorophyll and carotenoids. Error bars show standard deviation, $n = 3$. Significant differences were calculated using Student's *t*-test. $^{**}p < 0.01$; $^{***}p < 0.001$.

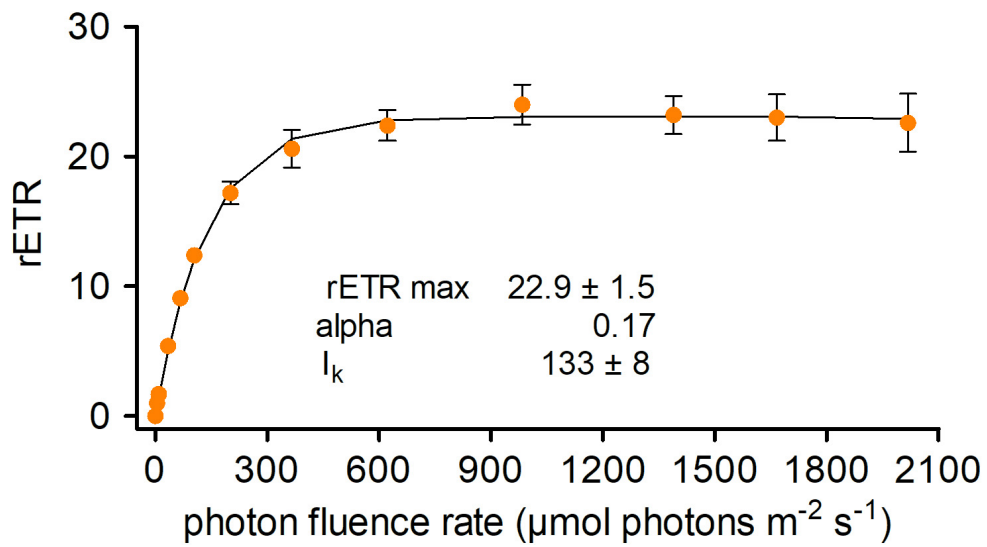

FIGURE 8 | Photosynthetic rapid light curves of *Chloromonas krienitzii*. The effect of increasing photon fluence rates (*x*-axis) on the relative electron transport rate (rETR) (*y*-axis) of chloroplasts was measured for field-collected cysts (sample LP05) ($n = 4$, ±SD). The data points were fitted to the model, assuming no photoinhibition (Webb et al., 1974).

their significant diurnal variations. Fluorometric measurements showed that the *C. krienitzii* cysts were not dormant in terms of photobiology similarly to other snow algal species (Remias et al., 2013; Procházková et al., 2018b). The photosystem II was well adapted to high levels of irradiation and showed no sign of photoinhibition up to 2100 µmol PAR m^{-2} s^{-1}. In mid-latitude regions, cells are subject to such irradiances at the snow surface on sunny days (Gorton and Vogelmann, 2003). Nonetheless, relatively high alpha value indicated that this species was shown to perform well also under low light conditions.

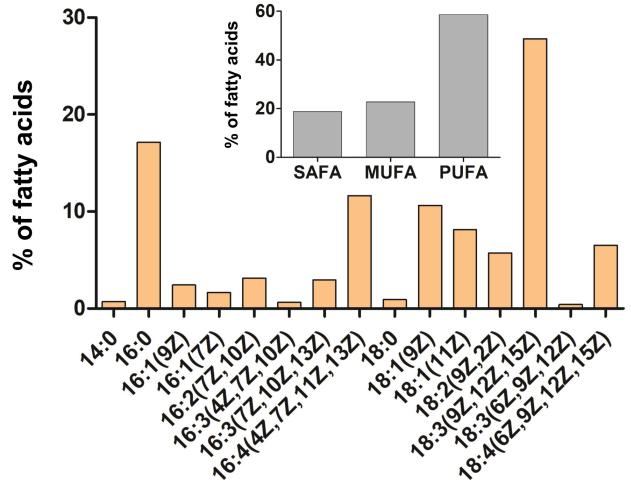

FIGURE 9 | Cellular fatty acid composition of *Chloromonas krienitzii* cysts (LP05) in [%] of total fatty acids. The relative proportion of saturated (SAFA), monounsaturated (MUFA), and polyunsaturated (PUFA) fatty acids is given in the inset. The figure shows only fatty acids that had abundances greater than 0.1% of total fatty acids.

This corresponds to the localisation of most cells 3 to 5 cm below snow surface.

Cellular Adaptation to Elevated Light Levels at Alpine Conditions

The apparent ability of the cysts to cope with high light conditions is a result of an interplay of several cellular adaptations. The fluorescence excitation ratio of blue-green light (BG, 420 to 560 nm; Bilger et al., 1997) to red light (R, 650 nm) was explored, which gives an indication on the competition between carotenoids and chlorophyll for excitation light (Nichelmann et al., 2016). In *C. krienitzii*, this ratio was significantly lower when compared with a non-cryoflora *Chlorella* reference. Spectral data provided evidence that carotenoids are the compounds which were responsible in *A. thaliana* for the observed changes in the fluorescence excitation efficiency between chloroplasts adapted to different light levels (Nichelmann et al., 2016). In *C. krienitzii* cysts, the significant reduction of the F(BG) to F(R) fluorescence excitation ratio may be attributed to intracellular deposits of carotenoids since the spectrum of the BG excitation beam covers roughly the visible absorption of astaxanthin. Light must pass through a layer of this pigment at the cell periphery before it reaches the centrally located chloroplast (**Figure 2B**). In addition, a high pool size of violaxanthin (V), antheraxanthin (A), and zeaxanthin (Z) (V-cycle) could have contributed to the reduction of this ratio. However, the carotenoids of the VAZ cycle were present only in a comparatively low concentration (**Supplementary Table 1**). Thus, a screening function of astaxanthin was much more probable than one of the V-cycle xanthophylls. If algae display a similar adjustment of the VAZ pool size to irradiance as higher plants (see e.g., Nichelmann et al. (2016) and citations therein), the comparatively low pool size observed here indicates that the photoprotective nature of the outer carotenoid layers was quite effective. The cellular concentration of astaxanthin varies depending on the individual species and stage within the life-cycle of chlamydomonadacean snow algae (Hoham and Remias, 2020). While vegetative cells of *C. krienitzii* produced no astaxanthin, cysts had an astaxanthin to chl-a ratio of 0.4. Similar levels were found for *Chloromonas nivalis* cysts from the Austrian Alps (Remias et al., 2010). In contrast, species causing red snow at exposed sites (*Chlainomonas* sp. and *S. nivaloides*) have significantly higher ratios (Remias et al., 2005; Procházková et al., 2018a).

Ultraviolet Radiation

High levels of short wavelength irradiation are typical for alpine environments. Harmful effects of UV on ultrastructure and metabolism in algae were reviewed by Holzinger and Lütz (2006). They include destruction of chloroplasts and mitochondria, and are probably mitigated by adaptive structures likely related to the UV stress (in the case of cryoflora: intracellular lipid bodies and vacuoles containing secondary pigments or partially crystallised content, respectively) (Holzinger and Lütz, 2006). Cells growing deeper in snow are less exposed to UV stress, since transmittance drops more rapidly for UV than for VIS with increasing snow depth (Gorton and Vogelmann, 2003). On the other hand, the localisation of a cell within the vertical snow profile may change throughout the day due to snow melt processes. The smooth tertiary cell wall of *C. krienitzii* exhibited a blue autofluorescence, which indicates the presence of UV-absorbing protective polyphenolic compounds. In contrast, the glacial algae *Mesotaenium berggrenii* and *Ancylonema nordenskioldii* do not exhibit such UV induced cell wall autofluorescence (Remias-own observation). On the other hand, this cell wall signal was observed for other close relatives of *C. krienitzii*, e.g., *C. hindakii* and "*Scotiella cryophila*-K1" cysts (Procházková-own observation) which indicates that this strategy may be common for cyst stages for *Chloromonas*. Furthermore, the measurements of fluorescence excitation ratios confirmed a significant UV-B and UV-A screening capability of *C. krienitzii* (**Figure 7**). Interestingly, the UV absorbance spectrum of isolated cell walls from snow alga *Chlamydomonas nivalis* cells (Gorton and Vogelmann, 2003) resembled that of sporopollenin (Xiong et al., 1997). In the latter study, the UV-B tolerant algal species contained substantial amounts of acetolysis-resistant residues of sporopollenin, while the sensitive species contained little or no sporopollenin. Still, for methodological reasons, the nature of the UV screening substances in the cell wall of *C. krienitzii* cysts has not been determined yet. Although only a very limited portion of the living and fossil algae have been studied for the presence and composition of resistant cell walls (Versteegh and Blokker, 2004), the existence of sporopollenin in *C. krienitzii* walls would not be surprising since zygospores of a related green alga is known to contain such resistant macromolecules (*Chlamydomonas monoica*; VanWinkle-Swift and Rickoll, 1997). An intracellular UV protectant may be represented by astaxanthin. Interestingly, in red pigmented cell

of *Chlamydomonas nivalis*, cytoplasmatic compounds absorbed UV more strongly than the cell walls (Gorton and Vogelmann, 2003). Indeed, astaxanthin has maximum absorbance in the visible region but still a significant capability in the UV-A region (Remias, 2012), which may become important at the high astaxanthin concentrations observed here.

Low Temperatures

A further challenge, for living in melting snow, represent low temperatures around the freezing point. At such conditions, a major role in avoiding membrane rigidity is played by unsaturation of the fatty acids in membrane lipids (Morgan-Kiss et al., 2006). This may correspond with the detected high level of PUFAs in *C. krienitzii* cysts. The level of PUFA likely relates to the presence of well-developed chloroplasts. In addition to galactolipids in chloroplasts, highly unsaturated phosphatidylcholine was identified in *Chlamydomonas reinhardtii* (Vieler et al., 2007), and phosphatidylglycerol in *C. reticulata* (Lukeš et al., 2014). In this study, α–linolenic acid as the dominant unsaturated FA in cells of *C. krienitzii* was consistent with profiles of other *Chloromonas* species harvested from snow (e.g., Řezanka et al., 2014) or from those kept in nitrogen deficient medium (Spijkerman et al., 2012). The previous analysis of three major lipid groups in related *Chloromonas* species dwelling in snow showed that PUFAs are present in phospholipids, glycolipids as well in neutral lipids (Procházková et al., 2018b, 2019b). In this study, a total fatty acid profile was performed for field-collected cysts of *C. krienitzii*, so the specific allocation of these compounds remains open. At the cyst stage, the proportion of PUFAs in *C. nivalis* subsp. *tatrae* was nearly 70% in lipid groups associated with membranes (glycolipids, phospholipids, etc.), and it was twice lower in neutral lipids (Procházková et al., 2018b) which are likely deposited in cytosolic lipid bodies as storage products (Thompson, 1996). When cultivated at 1°C, vegetative flagellates of snow alga *C. hindakii* had almost as high relative PUFAs contribution in all the three lipids classes; PUFAs accounted for ∼64% in neutral lipids, ∼65% in phospholipids and ∼75% in glycolipids (Procházková et al., 2019b).

CONCLUSION

To conclude, cyst stages of the snow alga *C. krienitzii* possess effective mechanisms for protection against harmful UV and excessive VIS radiation, because screening compounds are localised in both the remaining smooth cyst wall and in peripheral cytoplasmic compartments. The nature of the former compound is not known (sporopollenin?), the latter was shown to be astaxanthin. Absorbance spectra of cell wall extracts remain to be determined. Next, cells were photosynthetically active under ambient conditions and were not impaired at low or high irradiation levels. Furthermore, the results showed that the adaptation of this snow alga to low temperatures possibly included high levels of PUFAs, although future work should evaluate this hypothesis with more comprehensive analyses of distinguishing between membrane and storage lipids. The findings showed that *C. krienitzii* is more widespread than previously known, it occurs in the northern hemisphere without the Arctic region. Further cryoflora relatives in the *C. brevispina*-like complex are awaiting their characterisation once flagellate stages will be available (Nedbalová et al., 2008; Matsuzaki et al., 2015).

DATA AVAILABILITY STATEMENT

The datasets presented in this study can be found in online repositories. The names of the repository/repositories and accession number(s) can be found below: NCBI GenBank, accession nos: MW136658 (sample LP05), MW139361 (sample WP191), MW139362 (sample 1SAR).

AUTHOR CONTRIBUTIONS

LP and DR designed this study, conducted the independently light microscopy, prepared a draft of the manuscript, and collected the samples with independent assistance from HK. LP sequenced the field material with assistance of HK, wrote the manuscript with the edit and input of DR. LP was further responsible for PAM measurements and electron microscopy observations. DR performed the pigment analysis, fluorescence light microscopy, and cultivation assays. TŘ carried out fatty acid methyl esters analysis. WB carried out chlorophyll fluorescence assay and contributed with the relevant part. TŘ and LN edited the final manuscript. All authors discussed the results and contributed to the final manuscript.

FUNDING

This research was funded by the Czech Science Foundation (GACR) projects 18-02634S granted to LN and LP, and by the Austrian Science Fund (FWF) project P29959 granted to DR.

ACKNOWLEDGMENTS

We thank Petr Sklenář and Eva Hejduková (both Charles University, Czechia) for support at field sampling. We are grateful to Tomáš Hájek for his technical support in the field (University of South Bohemia in České Budějovice, Czechia). Opayi Mudimu (University of Kiel, Germany) is gratefully acknowledged for the gift of *Chlorella vulgaris* cells.

SUPPLEMENTARY MATERIAL

The Supplementary Material for this article can be found online at: https://www.frontiersin.org/articles/10.3389/fpls.2020.617250/full#supplementary-material

REFERENCES

Bilger, W., Veit, M., Schreiber, L., and Schreiber, U. (1997). Measurement of leaf epidermal transmittance of UV radiation by chlorophyll fluorescence. *Physiol. Plant.* 101, 754–763. doi: 10.1034/j.1399-3054.1997.1010411.x

Bischoff, H. W., and Bold, H. C. (1963). *Phycological Studies. IV. Some Soil Algae from Enchanted Rock and Related Algal Species*. Austin, TX: University of Texas.

Bligh, E. G., and Dyer, W. J. (1959). A rapid method of total lipid extraction and purification. *Can. J. Biochem. Phys.* 37, 911–917.

Brown, S. P., and Tucker, A. E. (2020). Distribution and biogeography of *Sanguina* snow algae: fine-scale sequence analyses reveal previously unknown population structure. *Ecol. Evol.* 10, 11352–11361. doi: 10.1017/CBO9781107415324.004

Cepák, V., and Lukavský, J. (2012). Cryoseston in the Sierra Nevada Mountains (Spain). *Nova Hedwigia* 94, 163–173. doi: 10.1127/0029-5035/2012/0094-0163

Chodat, R. (1921). Algues de la région du Grand St. Bernard. *Bull. Soc. Bot. Genève* 2, 293–305.

Dembitsky, V. M., Rezanka, T., and Rozentsvet, O. A. (1993). Lipid composition of three macrophytes from the Caspian Sea. *Phytochemistry* 33, 1015–1019. doi: 10.1016/0031-9422(93)85014-I

Di Mauro, B., Garzonio, R., Baccolo, G., Franzetti, A., Pittino, F., Leoni, B., et al. (2020). Glacier algae foster ice-albedo feedback in the European Alps. *Sci. Rep.* 10:4739. doi: 10.1038/s41598-020-61762-0

Engstrom, C. B., Yakimovich, K. M., and Quarmby, L. M. (2020). Variation in snow algae blooms in the coast mountains of British Columbia. *Front. Microbiol.* 11:569. doi: 10.3389/fmicb.2020.00569

Gorton, H. L., and Vogelmann, T. C. (2003). Ultraviolet radiation and the snow alga *Chlamydomonas nivalis* (Bauer) Wille. *Photochem. Photobiol.* 77, 608–615. doi: 10.1562/0031-8655(2003)0770608URATSA2.0.CO2

Gray, A., Krolikowski, M., Fretwell, P., Convey, P., Peck, L. S., Mendelova, M., et al. (2020). Remote sensing reveals Antarctic green snow algae as important terrestrial carbon sink. *Nat. Commun.* 11:2527. doi: 10.1038/s41467-020-16018-w

Hoham, R. W. (1975). The life history and ecology of the snow alga *Chloromonas pichinchae* (Chlorophyta, Volvocales). *Phycologia* 14, 213–226. doi: 10.2216/i0031-8884-14-4-213.1

Hoham, R. W., Berman, J. D., Rogers, H. S., Felio, J. H., Ryba, J. B., and Miller, P. R. (2006). Two new species of green snow algae from Upstate New York, *Chloromonas chenangoensis* sp. nov. and *Chloromonas tughillensis* sp. nov. (Volvocales, Chlorophyceae) and the effects of light on their life cycle development. *Phycologia* 45, 319–330. doi: 10.2216/04-103.1

Hoham, R. W., and Mullet, J. E. (1977). The life history and ecology of the snow alga *Chloromonas cryophila* sp. nov. (Chlorophyta, Volvocales). *Phycologia* 16, 53–68. doi: 10.2216/i0031-8884-16-1-53.1

Hoham, R. W., Mullet, J. E., and Roemer, S. C. (1983). The life history and ecology of the snow alga *Chloromonas polyptera* comb. nov. (Chlorophyta, Volvocales). *Phycologia* 61, 2416–2429. doi: 10.1139/b83-266

Hoham, R. W., and Remias, D. (2020). Snow and glacial algae: a review. *J. Phycol.* 56, 264–282. doi: 10.1111/jpy.12952

Hoham, R. W., Roemer, S. C., and Mullet, J. E. (1979). The life history and ecology of the snow alga *Chloromonas brevispina* comb. nov. (Chlorophyta, Volvocales). *Phycologia* 18, 55–70. doi: 10.2216/i0031-8884-18-1-55.1

Holzinger, A., and Lütz, C. (2006). Algae and UV irradiation: effects on ultrastructure and related metabolic functions. *Micron* 37, 190–207. doi: 10.1016/j.micron.2005.10.015

Khan, A. L., Dierssen, H., Scambos, T., Höfer, J., and Cordero, R. R. (2020). Spectral characterization, radiative forcing, and pigment content of coastal Antarctic snow algae: approaches to spectrally discriminate red and green communities and their impact on snowmelt. *Cryosphere Discussions* doi: 10.5194/tc-2020-170. [Epub ahead of print].

Kol, E. (1966). Snow algae from the valley of the Morskie Oko lake in the High Tatra. *Ann. Hist. Nat. Mus. Natl. Hung.* 58, 161–168.

Kol, E. (1968). "Kryobiologie; biologie und limnologie des schnees und eises. I. Kryovegetation," in *Die Binnengewässer, Band XXIV*, eds P. Elster and W. Ohle (Stuttgart: Schweizerbart'sche Verlagsbuchhandlung), 216.

Leya, T. (2013). "Snow algae: adaptation strategies to survive on snow and ice," in *Cellular Origin, Life in Extreme Habitats and Astrobiology, Volume 27, Polyextremophiles: Life Under Multiple Forms of Stress*, eds J. Seckbach, A. Oren, and H. Stan-Lotter (Dordrecht: Springer), 401–423. doi: 10.1007/978-94-007-6488-0_17

Leya, T. (2020). The CCCryo culture collection of cryophilic algae as a valuable bioresource for algal biodiversity and for novel, industrially marketable metabolites. *Appl. Phycol.* doi: 10.1080/26388081.2020.1753572. [Epub ahead of print].

Lukavský, J., and Cepák, V. (2010). Cryoseston in Stara Planina (Balkan) Mountains, Bulgaria. *Acta Bot. Croat.* 69, 163–171.

Lukeš, M., Procházková, L., Shmidt, V., Nedbalová, L., and Kaftan, D. (2014). Temperature dependence of photosynthesis and thylakoid lipid composition in the red snow alga *Chlamydomonas* cf. *nivalis* (Chlorophyceae). *FEMS Microbiol. Ecol.* 89, 303–315. doi: 10.1111/1574-6941.12299

Luo, W., Ding, H., Li, H., Ji, Z., Huang, K., Zhao, W., et al. (2020). Molecular diversity of the microbial community in coloured snow from the Fildes Peninsula (King George Island, Maritime Antarctica). *Polar Biol.* 43, 1391–1405. doi: 10.1007/s00300-020-02716-0

Lutz, S., Procházková, L., Benning, L. G., Nedbalová, L., and Remias, D. (2019). Evaluating amplicon high–throughput sequencing data of microalgae living in melting snow: improvements and limitations. *Fottea* 19, 115–131. doi: 10.5507/fot.2019.003

Matsuzaki, R., Kawachi, M., Nozaki, H., Nohara, S., and Suzuki, I. (2020). Sexual reproduction of the snow alga *Chloromonas fukushimae* (Volvocales, Chlorophyceae) induced using cultured materials. *PLoS One* 15:e0238265. doi: 10.1371/journal.pone.0238265

Matsuzaki, R., Kawai-Toyooka, H., Hara, Y., and Nozaki, H. (2015). Revisiting the taxonomic significance of aplanozygote morphologies of two cosmopolitan snow species of the genus *Chloromonas* (Volvocales, Chlorophyceae). *Phycologia* 54, 491–502. doi: 10.2216/15-33.1

Matsuzaki, R., Nozaki, H., Takeuchi, N., Hara, Y., and Kawachi, M. (2019). Taxonomic re-examination of "*Chloromonas nivalis* (Volvocales, Chlorophyceae) zygotes" from Japan and description of *C. muramotoi* sp. nov. *PLoS One* 14:e0210986. doi: 10.1371/journal.pone.0210986

Morgan-Kiss, R. M., Priscu, J. C., Pocock, T., Gudynaite-Savitch, L., and Huner, N. P. A. (2006). Adaptation and acclimation of photosynthetic microorganisms to permanently cold environments. *Microbiol. Mol. Biol. R.* 70, 222–252. doi: 10.1128/MMBR.70.1.222

Nedbalová, L., Kociánová, M., and Lukavský, J. (2008). Ecology of snow algae in the Giant Mts. *Opera Corcontica* 45, 59–68.

Nichelmann, L., Schulze, M., Herppich, W. B., and Bilger, W. (2016). A simple indicator for non-destructive estimation of the violaxanthin cycle pigment content in leaves. *Photosynthesis Res.* 128, 183–193. doi: 10.1007/s11120-016-0218-1

Onuma, Y., Takeuchi, N., and Takeuchi, Y. (2016). Temporal changes in snow algal abundance on surface snow in Tohkamachi, Japan. *Bul. Glac. Res.* 34, 21–31. doi: 10.5331/bgr.16A02

Pescheck, F., and Bilger, W. (2018). Compensation of lack of UV screening by cellular tolerance in green macroalgae (Ulvophyceae) from the upper eulittoral. *Mar. Biol.* 165:132. doi: 10.1007/s00227-018-3393-0

Piercey-Normore, M. D., and DePriest, P. T. (2001). Algal switching among lichen symbioses. *Am. J. Bot.* 88, 1490–1498. doi: 10.2307/3558457

Procházková, L., Leya, T., Křížková, H., and Nedbalová, L. (2019a). *Sanguina nivaloides* and *Sanguina aurantia* gen. et spp. nov. (Chlorophyta): the taxonomy, phylogeny, biogeography and ecology of two newly recognised algae causing red and orange snow. *FEMS Microbiol. Ecol.* 95:fiz064. doi: 10.1093/femsec/fiz064

Procházková, L., Remias, D., Holzinger, A., Řezanka, T., and Nedbalová, L. (2018a). Ecophysiological and morphological comparison of two populations of *Chlainomonas* sp. (Chlorophyta) causing red snow on ice-covered lakes in the High Tatras and Austrian Alps. *Eur. J. Phycol.* 53, 230–243. doi: 10.1080/09670262.2018.1426789

Procházková, L., Remias, D., Řezanka, T., and Nedbalová, L. (2018b). *Chloromonas nivalis* subsp. *tatrae*, subsp. nov. (Chlamydomonadales, Chlorophyta): re–examination of a snow alga from the High Tatra Mountains (Slovakia). *Fottea* 18, 1–18. doi: 10.5507/fot.2017.010

Procházková, L., Remias, D., Řezanka, T., and Nedbalová, L. (2019b). Ecophysiology of *Chloromonas hindakii* sp. nov. (Chlorophyceae), causing orange snow blooms at different light conditions. *Microorganisms* 7:434. doi: 10.3390/microorganisms7100434

Remias, D. (2012). "Cell structure and physiology of alpine snow and ice algae," in *Plants in Alpine Regions. Cell Physiology of Adaption and Survival Strategies*, ed. C. Lütz (Wien: Springer), 175–186. doi: 10.1007/978-3-7091-0136-0

Remias, D., Karsten, U., Lűtz, C., and Leya, T. (2010). Physiological and morphological processes in the Alpine snow alga *Chloromonas nivalis* (Chlorophyceae) during cyst formation. *Protoplasma* 243, 73–86. doi: 10.1007/s00709-010-0123-y

Remias, D., Lütz-Meindl, U., and Lütz, C. (2005). Photosynthesis, pigments and ultrastructure of the alpine snow alga *Chlamydomonas nivalis*. *Eur. J. Phycol.* 40, 259–268. doi: 10.1080/09670260500202148

Remias, D., Nicoletti, C., Krennhuber, K., Möderndorfer, B., Nedbalová, L., and Procházková, L. (2020). Growth, fatty, and amino acid profiles of the soil alga *Vischeria* sp. E71.10 (Eustigmatophyceae) under different cultivation conditions. *Folia Microbiol.* 65, 1017–1023. doi: 10.1007/s12223-020-00810-8

Remias, D., Pichrtová, M., Pangratz, M., Lütz, C., and Holzinger, A. (2016). Ecophysiology, secondary pigments and ultrastructure of *Chlainomonas* sp. (Chlorophyta) from the European Alps compared with *Chlamydomonas nivalis* forming red snow. *FEMS Microbiol. Ecol.* 92:fiw030. doi: 10.1093/femsec/fiw030

Remias, D., Wastian, H., Lütz, C., and Leya, T. (2013). Insights into the biology and phylogeny of *Chloromonas polyptera* (Chlorophyta), an alga causing orange snow in Maritime Antarctica. *Antarct. Sci.* 25, 648–656. doi: 10.1017/S0954102013000060

Řezanka, T., and Dembitsky, V. (1999). Novel brominated lipidic compounds from lichens of Central Asia. *Phytochemistry* 51, 963–968. doi: 10.1016/S0031-9422(99)00034-5

Řezanka, T., Nedbalová, L., Procházková, L., and Sigler, K. (2014). Lipidomic profiling of snow algae by ESI-MS and silver-LC/APCI-MS. *Phytochemistry* 100, 34–42. doi: 10.1016/j.phytochem.2014.01.017

Saunders, R. D., and Horrocks, L. A. (1984). Simultaneous extraction and preparation for high-performance liquid chromatography of prostaglandins and phospholipids. *Anal. Biochem.* 143, 71–75. doi: 10.1016/0003-2697(84)90559-1

Segawa, T., Matsuzaki, R., Takeuchi, N., Akiyoshi, A., Navarro, F., Sugiyama, S., et al. (2018). Bipolar dispersal of red-snow algae. *Nat. Commun.* 9:3094. doi: 10.1038/s41467-018-05521-w

Senger, H., Pfau, J., and Werthmueller, K. (1972). "Continuous automatic cultivation of homocontinuous and synchronized microalgae," in *Methods in Cell Physiology*, ed. D. M. Prescott (New York, NY: Academic Press), 301–321. doi: 10.1016/s0091-679x(08)60716-5

Spijkerman, E., Wacker, A., Weithoff, G., and Leya, T. (2012). Elemental and fatty acid composition of snow algae in Arctic habitats. *Front. Microbiol.* 3:380. doi: 10.3389/fmicb.2012.00380

Starr, R., and Zeikus, J. (1993). UTEX—the culture collection of algae at the University of Texas at Austin 1993 list of cultures. *J. Phycol.* 29, 1–106. doi: 10.1111/j.0022-3646.1993.00001.x

Thompson, G. A. (1996). Lipids and membrane function in green algae. *Biochim. Biophys. Acta* 1302, 17–45. doi: 10.1016/0005-2760(96)00045-8

VanWinkle-Swift, K. P., and Rickoll, W. L. (1997). The zygospore wall of *Chlamydomonas monoica* (Chlorophyceae): morphogenesis and evidence for the presence of sporopollenin. *J. Phycol.* 33, 655–665. doi: 10.1111/j.0022-3646.1997.00655.x

Versteegh, G. J. M., and Blokker, P. (2004). Resistant macromolecules of extant and fossil microalgae. *Phycol. Res.* 52, 325–339. doi: 10.1111/j.1440-1835.2004.tb00342.x

Vieler, A., Wilhelm, C., Goss, R., Süß, R., and Schiller, J. (2007). The lipid composition of the unicellular green alga *Chlamydomonas reinhardtii* and the diatom *Cyclotella meneghiniana* investigated by MALDI-TOF MS and TLC. *Chem. Phys. Lipids* 150, 143–155. doi: 10.1016/j.chemphyslip.2007.06.224

Webb, W. L., Newton, M., and Starr, D. (1974). Carbon dioxide exchange of *Alnus rubra*. A mathematical model. *Oecologia* 17, 281–291. doi: 10.1007/BF00345747

Xiong, F., Komenda, J., Kopecký, J., and Nedbal, L. (1997). Strategies of ultraviolet-B protection in microscopic algae. *Physiol. Plant.* 100, 378–388. doi: 10.1034/j.1399-3054.1997.1000221.x

Yakimovich, K. M., Engstrom, C. B., and Quarmby, L. M. (2020). Alpine snow algae microbiome diversity in the Coast Range of British Columbia. *Front. Microbiol.* 11:1721. doi: 10.3389/fmicb.2020.01721

Conflict of Interest: The authors declare that the research was conducted in the absence of any commercial or financial relationships that could be construed as a potential conflict of interest.

The reviewer EM is currently organising a Research Topic with one of the authors [LN]. The review process met the standards of a fair and objective review.

frontiers in Plant Science

ORIGINAL RESEARCH
published: 23 December 2020
doi: 10.3389/fpls.2020.619064

Temperature-Dependent Lipid Accumulation in the Polar Marine Microalga *Chlamydomonas malina* RCC2488

Daniela Morales-Sánchez[1,2], Peter S. C. Schulze[2,3], Viswanath Kiron[2] and Rene H. Wijffels[2,4]*

[1] The Norwegian College of Fishery Science, Faculty of Biosciences, Fisheries and Economics, UiT – The Arctic University of Norway, Tromsø, Norway, [2] Faculty of Biosciences and Aquaculture, Nord University, Bodø, Norway, [3] Green Colab – Associação Oceano Verde, University of Algarve, Faro, Portugal, [4] Bioprocess Engineering, AlgaePARC, Wageningen University, Wageningen, Netherlands

The exploration of cold-adapted microalgae offers a wide range of biotechnological applications that can be used for human, animal, and environmental benefits in colder climates. Previously, when the polar marine microalga *Chlamydomonas malina* RCC2488 was cultivated under both nitrogen replete and depleted conditions at 8°C, it accumulated lipids and carbohydrates (up to 32 and 49%, respectively), while protein synthesis decreased (up to 15%). We hypothesized that the cultivation temperature had a more significant impact on lipid accumulation than the nitrogen availability in *C. malina*. Lipid accumulation was tested at three different temperatures, 4, 8, and 15°C, under nitrogen replete and depleted conditions. At 4°C under the nitrogen replete condition *C. malina* had the maximal biomass productivity (701.6 mg L^{-1} day^{-1}). At this condition, protein content was higher than lipids and carbohydrates. The lipid fraction was mainly composed of polyunsaturated fatty acids (PUFA) in the polar lipid portion, achieving the highest PUFA productivity (122.5 mg L^{-1} day^{-1}). At this temperature, under nitrogen deficiency, the accumulation of carbohydrates and neutral lipids was stimulated. At 8 and 15°C, under both nitrogen replete and depleted conditions, the lipid and carbohydrate content were higher than at 4°C, and the nitrogen stress condition did not affect the algal biochemical composition. These results suggest that *C. malina* is a polar marine microalga with a favorable growth temperature at 4°C and is stressed at temperatures ≥8°C, which directs the metabolism to the synthesis of lipids and carbohydrates. Nevertheless, *C. malina* RCC2488 is a microalga suitable for PUFA production at low temperatures with biomass productivities comparable with mesophilic strains.

Keywords: psychrophilic microalgae, oleaginous, PUFA, TAG, temperature

OPEN ACCESS

Edited by:
Linda Nedbalová, Charles University, Czechia

Reviewed by:
Inna Khozin-Goldberg, Ben-Gurion University of the Negev, Israel
Alexei E. Solovchenko, Lomonosov Moscow State University, Russia

****Correspondence:***
Daniela Morales-Sánchez
daniela.morales-sanchez@uit.no

Specialty section:
This article was submitted to Marine and Freshwater Plants, a section of the journal Frontiers in Plant Science

Received: *19 October 2020*
Accepted: *30 November 2020*
Published: *23 December 2020*

Citation:
Morales-Sánchez D, Schulze PSC, Kiron V and Wijffels RH (2020) Temperature-Dependent Lipid Accumulation in the Polar Marine Microalga Chlamydomonas malina RCC2488. Front. Plant Sci. 11:619064. doi: 10.3389/fpls.2020.619064

INTRODUCTION

In recent years, it has been demonstrated that several microalgal species are efficient for lipid production (Guschina and Harwood, 2006; Da Silva et al., 2009; Harwood and Guschina, 2009; Li-Beisson et al., 2015). Products from microalgal lipids include polyunsaturated fatty acids (PUFA), pigments, antioxidants, and neutral lipids, among others (Grima et al., 1995; Spolaore et al., 2006; Chisti, 2008; Gong et al., 2011; Milledge, 2011; Andruleviciute et al., 2014; Tiwari and Kiran, 2018).

Consequently, the processes that have been developed to obtain these compounds usually involve the cultivation of high-lipid content microalgae, or the use of strategies to increase intracellular lipid content (Rodolfi et al., 2009; Pal et al., 2011; He et al., 2015; Hulatt et al., 2017b). Some of these strategies include the control of nutrient availability (carbon, nitrogen, phosphorous and silicate) (Xin et al., 2010; Msanne et al., 2012; Jiang et al., 2014), the manipulation of environmental conditions (pH, salinity, light intensity, and temperature) (Renaud et al., 2002; Converti et al., 2009; Pal et al., 2011; Liu et al., 2012; Draaisma et al., 2013), and genetic and metabolic engineering approaches (Courchesne et al., 2009; Radakovits et al., 2010; Liu and Benning, 2013; Li-Beisson et al., 2015). *Nannochloropsis gaditana* is a mesophilic microalga which is often used for lipid production and upon nitrogen stress conditions it is increasing the lipid content (Hulatt et al., 2017b). High light intensities (600 μmol photons m^{-2} s^{-1}) stimulated the lipid accumulation in *Chlorella sorokoniana, C. viscosa*, *C. emersoni*, and *C. vulgaris* (Takeshita et al., 2014). The cold-adapted microalga *Koliella antarctica* showed PUFA increase under phosphorous depletion (Suzuki et al., 2018). Low temperature cultivation stimulated PUFA synthesis in *Scenedesmus* sp. (Xin et al., 2011).

In our previous study, the polar microalga *Chlamydomonas malina* RCC2488 (*C. malina* hereafter) was tested for lipid accumulation using a nitrogen stress strategy. The growth temperature suggested was 8°C (Schulze et al., 2019) which yielded high biomass and lipid productivities. Interestingly, we observed that under both, nitrogen replete and deplete conditions, *C. malina* cells accumulated lipids and carbohydrates, while protein synthesis decreased (Morales-Sánchez et al., 2020). It is rather unique for microalgae to accumulate lipids and carbohydrates under nutrient replete conditions. At these conditions, most microalgae cells proliferate and duplicate, biosynthesizing mainly proteins (Guccione et al., 2014; Barka and Blecker, 2016; Bleakley and Hayes, 2017; Hulatt et al., 2017b). We hypothesize that *C. malina* was in a temperature stress condition at 8°C, since this strain is a polar microalga with an optimum temperature below 8°C (Balzano et al., 2012), which lead to lipids and carbohydrate accumulation. To address this hypothesis, *C. malina* was cultivated at three different temperatures (4, 8, and 15°C) under nitrogen replete and deplete conditions. Growth kinetics, biomass productivities and macromolecular composition are reported here. Non-polar lipid accumulation in *C. malina* was monitored in a fluorescence microscope by staining cells with the fluorophore Nile red.

MATERIALS AND METHODS

Strain and Culture Conditions

The *C. malina* RCC2488 (strain *Chlamydomonas* sp. MALINA FT89.6 PG5, Roscoff Culture Collection, henceforth referred to as *C. malina*) is a marine microalga isolated from the Beaufort Sea, within the Arctic Ocean (Balzano et al., 2012). The maintenance of the algal stock was made in agar plates containing f/2 medium (Guillard and Ryther, 1962). For all experiments, inocula were prepared in 250 mL shake-flaks containing 100 mL of f/2 medium as detailed earlier (Morales-Sánchez et al., 2020). The preparation of f/2 medium included the use of seawater from the North Atlantic shoreline of Bodø (Norway) with a salinity of approximately 35, which was adjusted to a salinity concentration of 17.5 using distilled water for optimal growth, according to a previous study (Morales-Sánchez et al., 2020). All experiments were conducted in bubble columns photobioreactors (Hulatt et al., 2017a; Morales-Sánchez et al., 2020). The reactors were inoculated with 0.2 g of dry cell weight (DCW) per L (g_{DCW} L^{-1}) and operated at three different temperatures (4, 8, and 15°C). Cells were cultured until mid-exponential phase (5 days) in f/2 medium and 120 μmol photons m^{-2} s^{-1} of light intensity. After this period, cells were collected by centrifugation, washed twice and resuspended in f/2 medium with (a) nitrogen replete or (b) nitrogen deplete (here abbreviated to as +N and −N, respectively) conditions for cultivation in the bubble columns. These experiments were maintained at 120 μmol photons m^{-2} s^{-1} of light intensity during 3 days. At the end of the experimental period, cells were harvested by centrifugation at 2,000 *g* for 5 min, washed with 0.5 M ammonium formate, centrifuged again as before and the pellets were stored at −70°C for further analyses. All experiments were carried out in triplicate.

Growth Measurements

The cellular growth was determined based on the dry cell weight (DCW) measurement. A correlation was made between the optical cell density and the dry weight using the equation:

$$W = (0.884 \times A_{750}) + 0.0117 \quad (1)$$

Where W is the DCW (g_{DCW} L^{-1}) and A_{750} is the absorbance measured at 750 nm. Culture samples (0.5–1 mL) were collected daily to measure the absorbance at 750 nm in a 1 cm micro-cuvette using a spectrophotometer (Hach-Lange DR3900, Hach, International). The algal DCW was evaluated gravimetrically by filtrating 5–10 mL of culture broth through a pre-dried and pre-weighed 0.45 μm pore size nitrocellulose membrane filter (Merck Milipore, MA, United States). The membrane containing the biomass was washed three times with 0.5 M ammonium formate prior drying in an oven at 60°C for 24 h or until constant weight.

Lipid, Protein, and Carbohydrate Analyses

Organic solvents, such as chloroform and methanol, were used to extract lipids from *C. malina*. Fatty acid methyl esters (FAMEs) from both, neutral and polar lipids were identified by gas chromatography (GC) following the methodology fully described previously (Breuer et al., 2013; Morales-Sánchez et al., 2020). Solid-phase extraction was used to separate neutral and polar lipids (Hulatt et al., 2017a). Briefly, total lipid extracts were dissolved in 0.5 mL hexane:diethyl ether (7:1 v/v) and loaded onto 6 mL (1 g) silica cartridges (Supelco®). Neutral lipids were first eluted with 10 mL of hexane:diethyl ether (7:1 v/v), then 10 mL of methanol:acetone:hexane (2:2:1 v/v/v) was added to elute the polar lipids. A stream of nitrogen gas was used to dry each lipid fractions. The fatty acyl chains contained in both lipid fractions were derivatized to FAMEs and identified by GC

using the methodology previously mentioned (Breuer et al., 2013; Hulatt et al., 2017a; Morales-Sánchez et al., 2020).

Neutral lipids content in *C. malina* was detected by fluorescence microscopy as previously described (Msanne et al., 2012; Morales-Sánchez et al., 2017). Briefly, *C. malina* cells were stained with the lipophilic fluorophore Nile Red, incubated at 20°C for 15 min and visualized in a fluorescence microscope (Biorad Zoe^{TM}, CA, United States).

Carbohydrate analysis was performed using the phenol-sulfuric acid method (Thompson, 1950) after hydrolysis of the biomass using 1 N HCl to produce reducing sugars.

Protein content was analyzed using the Lowry method (Lowry et al., 1951) after alkaline hydrolysis of the sample with 1 N NaOH.

Calculations

The cellular growth kinetics and productivities were calculated accordingly with a 4-parameter logistic function (Hulatt et al., 2017b), following the next equations:

$$C_x = \emptyset 1 + \frac{\emptyset 2 - \emptyset 1}{1 + \exp\left(\frac{\emptyset 3 - t}{\emptyset 4}\right)} \quad (2)$$

Where C_x is the DCW (g_{DCW} L^{-1}) at time t (days), φ1 is the lowest asymptote (minimum C_x), φ2 is the upper asymptote (maximum C_x), φ3 is t at 0.5φ2 (the inflection point) and φ4 is the scale parameter (Hulatt et al., 2017b). Consequently, the productivity was calculated between two time points, accordingly with the next equation (Eq. 3):

$$P_i = \frac{C_{x,i} - C_{x,i-1}}{t_i - t_{i-1}} \quad (3)$$

Where P_i is the productivity (g_{DCW} L^{-1} day^{-1}), $C_{x,i}$ and $C_{x,i-1}$ are the concentrations of the biomass (g_{DCW} L^{-1}) at two time points and t_i and t_{i-1} are the time of cultivation (days). The specific cellular growth rate k (d^{-1}) was therefore derived (Eq. 4):

$$k_i = \frac{P_i}{C_{X,1}} \quad (4)$$

The duplication time (t_D), which is the time to double the number of cells, was then calculated from the specific growth rate (Eq. 4):

$$t_D = \frac{ln2}{k_i} \quad (5)$$

Statistical Analysis

Shapiro-Wilk test was used to validate the normal distribution of the data, and Brown-Forsythe test was applied to confirm the homogeneity of the variance between treatments. One-way analysis of variance (ANOVA) and *post hoc* Tukey's multiple comparison test was applied to each set of experiments in order to determine statistical differences among treatments. *P* values smaller than 0.05 were considered statistically significant. Details of each test are described in **Supplementary Material** Statistical Procedures 1.

RESULTS

Effect of Temperature and Nitrogen Availability on the Growth and Productivity of *Chlamydomonas malina*

Maximal biomass concentration of 5.61 g_{DCW} L^{-1} and productivity of 701.6 mg_{DCW} L^{-1} day^{-1} were found at a temperature cultivation of 4°C, in the nitrogen replete condition (+N, **Figures 1A,C**, $p < 0.05$). *Chlamydomonas malina* cells grew at a duplication time (t_D) of 11 h at 4°C, which was 6 and 71 h faster, compared with 8 and 15°C, respectively ($p < 0.05$). At 15°C, cells showed a linear growth, the biomass productivity decreased significantly about 5 and 4-times compared with 4 and 8°C, respectively ($p < 0.05$).

Under nitrogen deprivation (−N), cell growth was arrested in all treatments compared with +N conditions. After a period of nutrient sufficiency during the first 5 days of cultivation, cells entered to a nitrogen starvation period in which cells grew slower in all temperature tested (**Figure 1B**). During the 8 days of cultivation at 4°C in the −N treatment, the total cell concentration reached 4.6 g_{DCW} L^{-1}, with an overall productivity of 570 mg_{DCW} L^{-1} day^{-1} (**Figure 1D**). These values represent about 20% decreased compared with the values obtained at +N conditions ($p < 0.05$). At these conditions, the analysis of the starvation period (3 days) showed that the cell concentration increased only 18% (DCW) in that time, which represents a biomass productivity of 24.5 mg_{DCW} L^{-1} day^{-1}. At 8°C, cells presented a linear biomass accumulation during the 8 days of cultivation in −N, the biomass concentration and productivity were reduced in about 30% compared to +N conditions (**Figures 1B,D**; $p < 0.05$). However, the productivity during the starvation period was 2.5-times higher (62.4 mg_{DCW} L^{-1}, $p < 0.05$) compared with the productivity at 4°C. At 15°C under −N, biomass concentration and productivity were the lowest of all temperature treatments (**Figures 1B,D**; $p < 0.05$). At these conditions (15°C, −N), the overall biomass concentration and productivity during 8 days were 2-times lower than cells maintained at same temperature and +N conditions ($p < 0.05$). During the starvation period, the biomass concentration increased 26% (DCW), and the productivity was 5.15 g_{DCW} L^{-1}, which was the lowest productivity obtained in this work.

Effect of Temperature and Nitrogen Availability on the Biochemical Composition of *Chlamydomonas malina*

Protein

Under +N conditions (**Figure 2A**), the analysis of protein content was made in the middle of the exponential phase (5th cultivation day). The highest protein content of 41% ($mg_{protein}$ $mg_{DCW}{}^{-1}$) was obtained in cells cultivated at 4°C ($p < 0.05$). The protein content in the treatments at 8 and 15°C were not significantly different ($p > 0.05$) between each other with an average of 26.5%.

Under −N conditions (**Figure 2B**), the protein determination was performed after 3 days of nitrogen starvation (8th cultivation day). The protein content among the temperature treatments

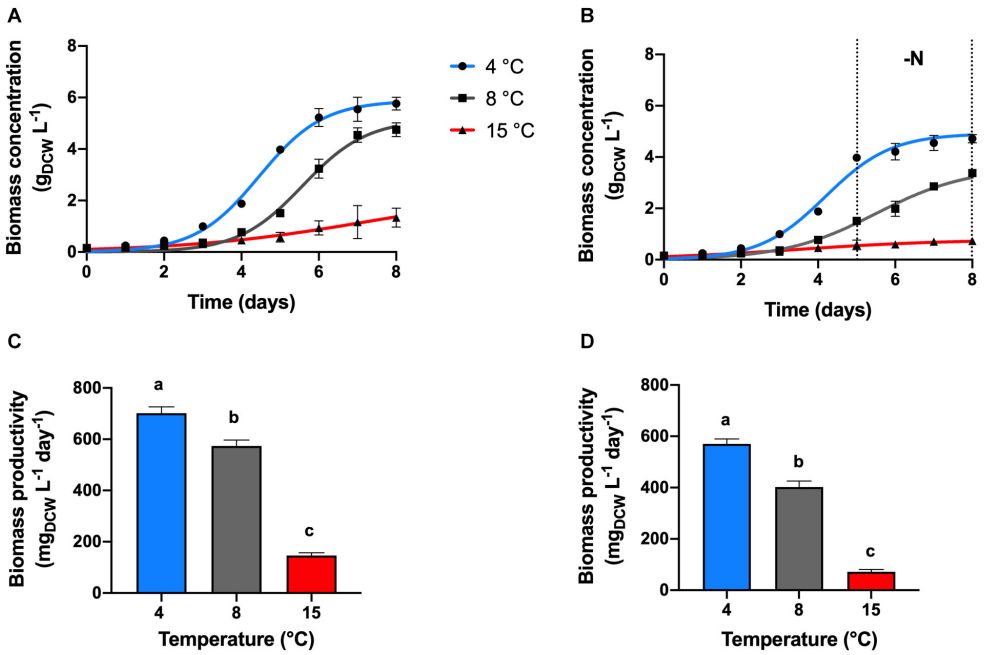

FIGURE 1 | Growth kinetics and productivity. Effect of temperature on the growth kinetics and productivities of *C. malina* under +N **(A,C)** and –N **(B,D)** conditions, after 8 days of batch cultivation in bubble-column photobioreactors. Data are presented as means ± SD of three independent experiments. Dotted black lines denote the nitrogen deprivation period. Different lowercase letters indicate a significant difference among means of groups (one-way ANOVA with *post hoc* Tukey HSD test, $p < 0.05$).

were not statistically different ($p > 0.05$), with an average of 16% of protein. However, at this condition, the protein content decreased in all treatments, compared with cells cultivated under +N conditions ($p < 0.05$). The reduction in protein content was significant at 4°C (25% reduction), and less at 8°C (12%), and at 15°C (8%).

Carbohydrates

Cells cultivated at +N conditions (**Figure 2C**), during exponential growth, had similar carbohydrate content ($p > 0.05$), obtaining in average 24.4% ($mg_{Carbohydrate}$ $mg_{DCW}{}^{-1}$). However, cells maintained at −N (3 days after mid-exponential growth; **Figure 2D**) presented higher carbohydrate content compared with cells cultivated in +N conditions ($p < 0.05$). Highest carbohydrate content was obtained in cells cultivated at 4 and 8°C, obtaining on average 42.3% with no significant differences among them ($p > 0.05$).

Lipids

Cells maintained at 4°C under +N conditions showed lipid content of 20% (mg_{LIPID} $mg_{DCW}{}^{-1}$), which was the lowest value reported in this study. Under these conditions, formation of lipid bodies was not detected by Nile Red fluorescence (**Figure 3**). However, lipid content in cells cultivated at 8 and 15°C in +N conditions presented an unusual behavior (**Figure 2E**). At these temperatures, the lipid content was extraordinarily high (30%), with no significant differences between these temperature treatments ($p > 0.05$). In addition, Nile Red fluorescence indicated high amounts of neutral lipids in cells exposed to 8 and 15°C (**Figure 3**). In all temperature treatments at +N condition, cells for lipid (as well as for protein and carbohydrate) analysis were taken in the mid-exponential growth phase, ensuring nutrient-sufficient conditions. The lipid content in cells cultivated under −N at 4 and 8°C showed no significant difference ($p > 0.05$), obtaining up to 31.8% in average (**Figure 2F**).

Under −N condition, maximum lipid content was found at 15°C, reaching 40%. At 4°C, the lipid content increased 12% in cells cultivated under −N, compared with cells maintained at +N conditions. At 8°C, the lipid content was not significantly different ($p > 0.05$) in cells cultivated at +N and −N conditions. The lipid content increased 10% in cells cultivated at 15°C under −N, related to cells grown in +N conditions. Nile Red fluorescence revealed high lipid body formation in cells under −N in all temperatures tested (**Figure 3**).

Fatty Acid Content and Profiles

Under +N conditions, the major lipid content was found in the polar lipid fraction for cells maintained at 4°C, and in the TAG fraction for cells at 8 and 15°C. The saturated fatty acid content (SFA) in the polar fraction was higher in cells at 15°C (34.4 mg g^{-1}; $p < 0.05$), but in the TAG fraction, the SFA content had no significant differences among all temperature treatments (**Figure 4A**). Cells at 4°C had increased monounsaturated fatty acid (MUFA) in the polar fraction (115.5 mg g^{-1}) but decreased in the TAG fraction (11.4 mg g^{-1}). Contrary to cells at 4°C, cells at higher temperatures had decreased MUFA content in the polar fraction and increased in the TAG fraction. Highest PUFA

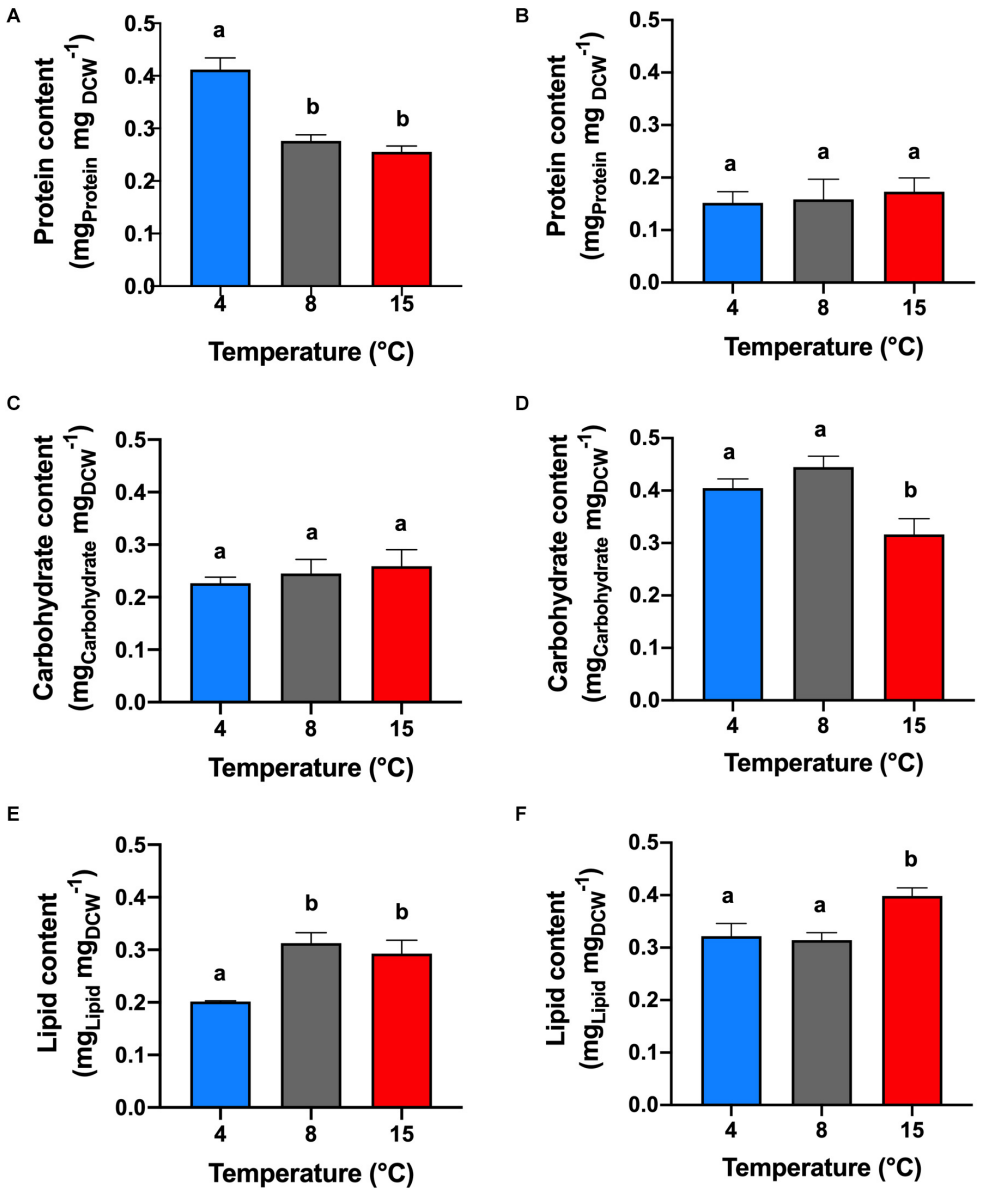

FIGURE 2 | Protein, carbohydrate and lipid contents. Effect of temperature on the protein **(A,B)**, carbohydrate **(C,D)**, and lipid **(E,F)** contents of *C. malina* under +N **(A,C,E)** and –N **(B,D,F)** conditions in bubble-column photobioreactors. Samples in the +N condition were taken in the middle exponential growth, and in the –N condition after 3 days of starvation. Data are presented as means ± SD of three independent experiments. Different lowercase letters indicate a significant difference among means of groups (one-way ANOVA with *post hoc* Tukey HSD test, $p < 0.05$).

content was found in cells cultivated at 4°C in the polar fraction (122.5 mg g^{-1}, $p < 0.05$) and cells cultivated at 8 and 15°C in the TAG fraction (122 and 80 mg g^{-1}, respectively).

Cells maintained under −N in all temperatures accumulated preferentially TAG as the major lipid content (**Figure 4B**). In the polar fraction, the SFA content was similar in all treatments. The MUFA content was significantly higher in cells cultivated at 15°C (4-times; $p < 0.05$) compared to cells maintained at lower temperatures. The opposite effect was observed for the PUFA content, cells at lower temperature had significantly higher content (3-times; $p < 0.05$) compared with cells at 15°C. In the TAG fraction, the SFA content was higher in cells at 15°C (3-times; $p < 0.05$). The same effect observed in the polar fraction was also noted in the TAG fraction for the MUFA and PUFA content. The MUFA content was higher in cells at 15°C (2-times; $p < 0.05$), but the PUFA content was higher in cells at 4 and 8°C (1.5-times; $p < 0.05$). The highest PUFA productivity under −N conditions was found at 4°C (79.7 mg L^{-1} day^{-1}; $p < 0.05$).

Under +N conditions at 4°C, cells mainly synthesized PUFA, such as hexadecatetraenoic acid (C16:4*n*-3) and α-linolenic acid (C18:3*n*-3), and the MUFA oleic acid (C18:1*n*-9) in the polar fraction (**Figure 4C**). Cells maintained at 8°C synthesized the

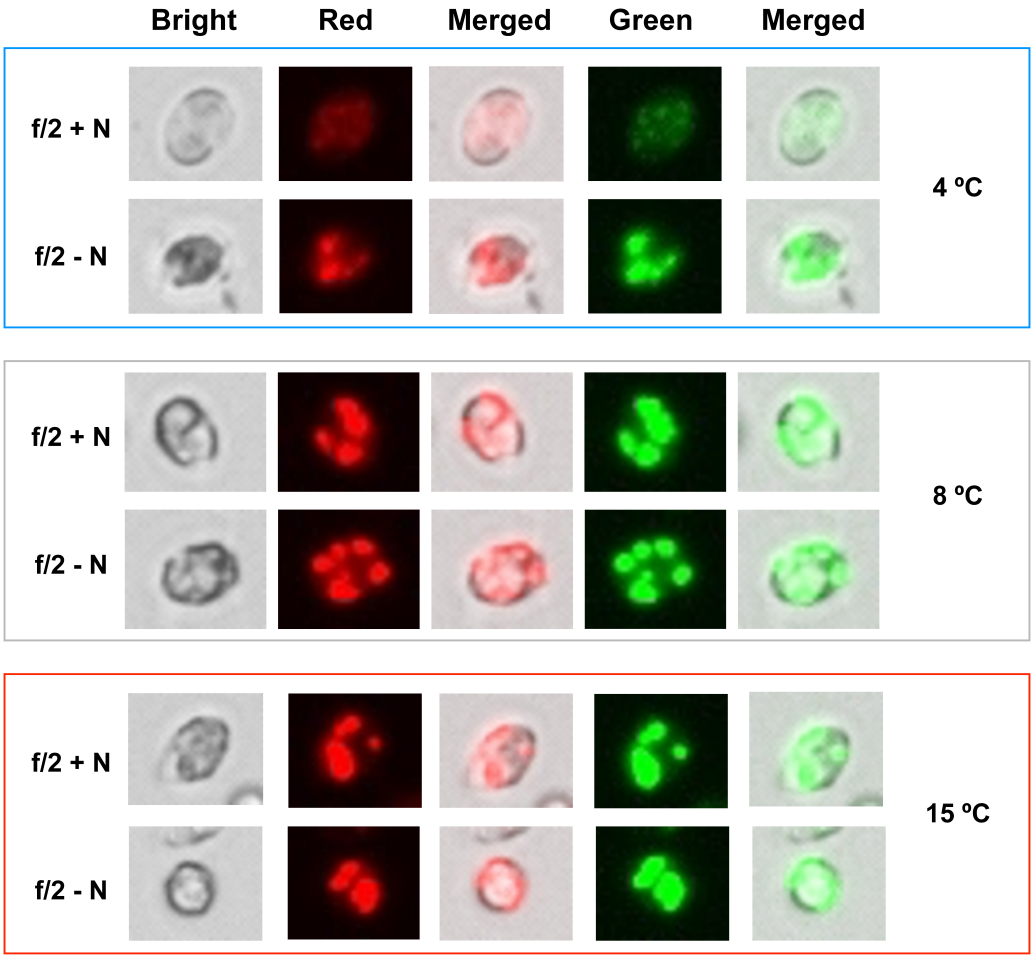

FIGURE 3 | Neutral lipid stained with Nile Red. Neutral lipid accumulation in *C. malina* cells cultivated at 4, 8, and 15°C subjected to +N and –N conditions. Cells at different temperatures were cultured for 2 days in f/2 medium at +N and –N conditions, harvested and stained with Nile Red. Lipid bodies were detected in a fluorescent microscopy in three different filters (bright, red and green). The images shown are representative of typical cells in the samples. Scale bar can be seen in **Supplementary Figure 1**.

same fatty acid classes than at 4°C, but they were found mainly in the TAG fraction. At 15°C, the major fatty acid types were MUFA in both fractions, like palmitoleic acid (C16:1*n*-7), C18:1*n*-9 and vaccenic acid (C18:1*n*-7). Saturated fatty acids such as palmitic acid (C16:0) and stearic acid (C18:0) were found in cells cultivated at 15°C in higher proportion ($p < 0.05$) than in cells at lower temperatures. Under −N conditions (**Figure 4D**), TAG fraction contained the majority of lipids in all treatments. In general, SFA such as C16:0 and C18:0, and MUFA like C18:1*n*-9 and C18:1*n-7* were found abundantly in cells cultivated at 15°C. At lower temperatures (4 and 8°C), C18:1*n*-9 and C18:3*n*-3 were mainly found.

DISCUSSION

Most microalgal species are able to grow and accomplish photosynthesis over a wide range of temperatures, with optimal conditions between 20 and 25°C (Li, 1980; Ras et al., 2013). These species are called mesophilics and their metabolism responds to the exponential (Q_{10}) or the Arrhenius equation, in which it is stated that below optimal growth temperatures, an increase in the temperature has a positive effect on photosynthesis and growth (Ahlgren, 1987; Ras et al., 2013).

On the other hand, there are some microalgae found in the polar and cold regions known as psychrophiles, which have optimum growth temperatures at or below 15°C (Morgan-Kiss et al., 2006). These microalgae have experienced a strong and persistent selection and have evolved to develop a wide range of physiological adaptations that allow them to thrive at temperatures close to or below freezing (Morgan-Kiss et al., 2006; Hulatt et al., 2017a). The strain *C. malina* RCC2488 is a psychrophilic alga isolated from the Beufourt Sea within the Arctic Ocean (Balzano et al., 2012). This microalga has its highest growth rate and biomass productivity at low temperatures (4°C). Microalgae should invariably reduce its metabolic rate at cold conditions (Hulatt et al., 2017a), but as demonstrated by *C. malina* in this study and other cold-adapted algal strains

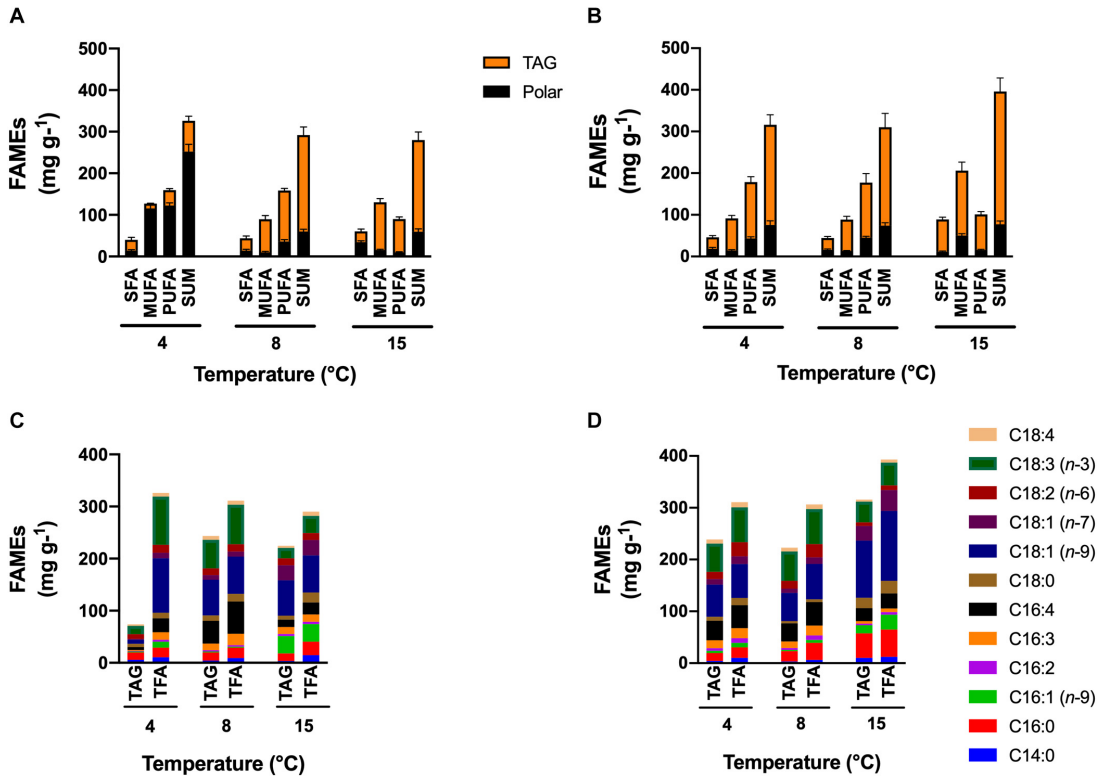

FIGURE 4 | FAMEs content and profile. Effect of temperature on the FAMEs content and profile of total fatty acids (TFA) and fatty acids in triacylglycerols (TAG) contained in *C. malina* under the +N **(A,C)** and the –N **(B,D)** conditions in tubular photobioreactors. Samples in the +N condition were taken in the middle exponential growth, and in the –N condition after 3 days of starvation. SFA, saturated fatty acids; MUFA, monounsaturated fatty acids; PUFA, polyunsaturated fatty acids; TAG, triacylglycerols. Data are presented as means ± SD of three independent experiments. Statistical comparison was performed individually for each component and each class of fatty acid (polar, TAGs, SFA, MUFA, PUFA, and sum) among the treatments.

TABLE 1 | Analysis of biomass productivities.

Microalgal strain	Productivity (mg L^{-1} day^{-1})	Temperature (°C)	References
Chlamydomonas malina	701	8	This study
Chlamydomonas pulsatilla	580	6	Hulatt et al., 2017a
Chloromonas platystigma	250	6	Hulatt et al., 2017a
Chlamydomonas klinobasis	215	6	Hulatt et al., 2017a
Raphidonema sempervirens	133	6	Hulatt et al., 2017a
Koliella antarctica	480	15	Suzuki et al., 2018
Koliella antarctica	2,370	15	Suzuki et al., 2018
Nannochloropsis gaditana	(best condition)	25	
	510		Hulatt et al., 2017b
Chlorella sp. F&M-M49	640	25	Chen et al., 2017
Chlorella sp. CCAP 211-11b	590	25	Chen et al., 2017
Chlorella sp. IAM C-212	710	25	Chen et al., 2017
Chlorella sp. PROD1	730	25	Chen et al., 2017

Comparison of biomass productivities of C. malina cultivated at 4°C, 17.5 salinity, nitrogen replete conditions and 120 μmol m^{-2} s^{-1} of light intensity with other polar and cold-adapted microalgae strains cultivated at similar conditions and mesophilic microalgae cultivated at optimum conditions (Chen et al., 2017; Hulatt et al., 2017a,b; Suzuki et al., 2018).

(Lyon and Mock, 2014; Cao et al., 2016; Hulatt et al., 2017a; Suzuki et al., 2018), this is not applicable to microalgae found living in polar or cold environments. At temperatures exceeding the optimum, a decrease in the microalgal growth rate can be observed as a response to heat stress, which can affect the metabolism thereby inhibiting growth (Ras et al., 2013).

Microalgae adapted to cold environments might be stressed at temperatures above the optimum. This stress may be reflected

on its macromolecular composition, as in the case of *C. malina* which synthesized high lipid and carbohydrate content at 8 and 15°C, even under nutrient replete conditions (+N). This phenomenon is unusual and remarkable since normally microalgal cells respond to nutrient sufficiency conditions by synthesizing the cellular building blocks proteins (Morales-Sánchez et al., 2013), as observed in *C. malina* cultivated at 4°C. However, at 8 and 15°C, in both +N and −N conditions, the protein content was lower compared to the high lipid and carbohydrate content, suggesting a stress condition caused by temperature. Therefore, nitrogen stress did not cause an effect on the biochemical composition of the cells at 8 and 15°C, but it caused the usual phenomenon of lipid accumulation at 4°C under nitrogen deprivation (−N), as observed in many mesophilic algae in nitrogen-deprived cultivations (Pruvost et al., 2009; Lv et al., 2010; Work et al., 2010; Msanne et al., 2012; Li-Beisson et al., 2013; Liu and Benning, 2013; Çakmak et al., 2014). Also, at higher temperatures (8 and 15°C), cells mainly synthesized neutral lipids (TAG), probably as a consequence of stress. However, cells cultivated at 4°C and +N conditions mainly synthesized PUFA in the polar fraction (cellular membrane). The reason is that PUFA are essential to keep the fluidity of the membrane at low temperatures (D'Amico et al., 2006; Morgan-Kiss et al., 2008). Especially, polyunsaturated and short-chain length fatty acids, such as C16:4*n*-3 which was found in high concentrations in *C. malina*. This C16:4*n*-3 acyl group is nearly exclusively present in monogalactosyldiacylglycerol (MGDG) –the most abundant membrane lipid in Chlamydomonas chloroplast– and is known to be a significant contributor in the transition from liquid-crystalline to gel phase (Dolhi et al., 2013; Li-Beisson et al., 2013; Liu and Benning, 2013). It is hypothesized that the availability of C16:4*n*-3 affects the total amount of the prevalent MGDG molecular species that contains C18:3*n*-3 in the *sn-1* and C16:4*n*-3 in the *sn-2* position of the glycerol backbone (Liu and Benning, 2013). It is still unknown why C16:4*n*-3 is primarily present in MGDG and how its abundance is regulated in this membrane galactolipid. Therefore, it has been suggested that loss-of-function studies with mutants entirely lacking (or decreased amounts) 16:4*n*-3 could be interesting to possibly answer what are the specific roles of this molecular species of MGDG in the photosynthetic membrane (Liu and Benning, 2013). Similar to our findings, the same classes of fatty acids were found in the polar microalga and closest *C. malina* relative, UWO 241 (Morgan-Kiss et al., 2002). Cells of *C. malina* cultivated at 4°C responded in a similar way to other algal species when they were cultivated at +N conditions by stimulating the synthesis of proteins, and to −N conditions by accumulating lipids and carbohydrates, and reducing nitrogen-rich compounds like proteins (Siaut et al., 2011; Msanne et al., 2012; Morales-Sánchez et al., 2013; Schmollinger et al., 2014; Zhu et al., 2016). Also, under −N, the lipid fraction was mainly composed of TAG.

Our results indicate that *C. malina* can be highly productive at low temperatures, making it a potential candidate for biomass, carbohydrate and polyunsaturated lipids production in cold environments. **Table 1** present a comparison of biomass productivity of several mesophilic and polar/cold-adapted microalgae, including *C. malina* at best growth conditions. As observed, *C. malina* productivity is comparable with mesophilic microalgae and high productive polar/cold-adapted microalgae.

CONCLUSION

Polar *C. malina* is a marine microalga that can be stressed at temperatures ≥8°C. As a consequence, high accumulation of carbohydrates and lipids can be stimulated. Particularly, the lipid fraction was predominantly composed of TAG with a high PUFA productivity of 122 mg L^{-1} day^{-1}. At these temperatures, nitrogen stress did not have an effect on the algal biochemical composition. At 4°C, under +N conditions, *C. malina* synthesized mainly proteins and the lipid portion was primarily found in the polar fraction with high PUFA content (122.5 mg L^{-1} day^{-1}). At this temperature, −N stimulated the synthesis of lipids but arresting the cell growth and protein synthesis. Nevertheless, the PUFA productivity was high as well, reaching up to 79.7 mg L^{-1} day^{-1}. Under −N, carbohydrate content increased between 32 and 44% in all temperature tested. Neutral lipids increased at 15°C, reaching the highest content of this study (44% DCW). The polar microalga *C. malina* has high potential for carbohydrates, lipids and PUFA production in cold climates, with biomass productivities comparable with mesophilic microalgae.

DATA AVAILABILITY STATEMENT

The original contributions presented in the study are included in the article/**Supplementary Material**, further inquiries can be directed to the corresponding author/s.

AUTHOR CONTRIBUTIONS

Within the work package in the A2F project, RW designed the research that resulted in this manuscript. DM-S designated the study, collected the data, and conducted the bioreactor experiments. PS performed the lipid and fatty acid analysis. DM-S, PS, VK, and RW contributed to manuscript drafting, discussion, and critical revision of the article for important intellectual content. All authors contributed to the article and approved the submitted version.

FUNDING

This work was funded by the Research Council of Norway's BIONÆR Program and it's part of the project Algae to Future (267872/E50).

SUPPLEMENTARY MATERIAL

The Supplementary Material for this article can be found online at: https://www.frontiersin.org/articles/10.3389/fpls.2020.619064/full#supplementary-material

REFERENCES

Ahlgren, G. (1987). Temperature Functions in Biology and Their Application to Algal Growth Constants. *Oikos* 49:177. doi: 10.2307/3566025

Andruleviciute, V., Makareviciene, V., Skorupskaite, V., and Gumbyte, M. (2014). Biomass and oil content of Chlorella sp., Haematococcus sp., Nannochloris sp. and Scenedesmus sp. under mixotrophic growth conditions in the presence of technical glycerol. *J. Appl. Phycol.* 26, 83–90. doi: 10.1007/s10811-013-0048-x

Balzano, S., Gourvil, P., Siano, R., Chanoine, M., Marie, D., Lessard, S., et al. (2012). Diversity of cultured photosynthetic flagellates in the northeast Pacific and Arctic Oceans in summer. *Biogeosciences* 9, 4553–4571. doi: 10.5194/bg-9-4553-2012

Barka, A., and Blecker, C. (2016). Microalgae as a potential source of single-cell proteins. *Biotechnol. Agron. Soc. Environ.* 20, 427–436.

Bleakley, S., and Hayes, M. (2017). Algal Proteins: Extraction, Application, and Challenges Concerning Production. *Foods* 6:33. doi: 10.3390/foods6050033

Breuer, G., Evers, W. A. C., de Vree, J. H., Kleinegris, D. M. M., Martens, D. E., Wijffels, R. H., et al. (2013). Analysis of fatty acid content and composition in microalgae. *J. Vis. Exp.* 2013:50628. doi: 10.3791/50628

Çakmak, Z. E., Ölmez, T. T., Çakmak, T., Menemen, Y., and Tekinay, T. (2014). Induction of triacylglycerol production in *Chlamydomonas reinhardtii*: Comparative analysis of different element regimes. *Bioresour. Technol.* 155, 379–387. doi: 10.1016/j.biortech.2013.12.093

Cao, K., He, M., Yang, W., Chen, B., Luo, W., Zou, S., et al. (2016). The eurythermal adaptivity and temperature tolerance of a newly isolated psychrotolerant Arctic *Chlorella* sp. *J. Appl. Phycol.* 28, 877–888. doi: 10.1007/s10811-015-0627-0

Chen, B., Wan, C., Mehmood, M. A., Chang, J.-S., Bai, F., and Zhao, X. (2017). Manipulating environmental stresses and stress tolerance of microalgae for enhanced production of lipids and value-added products–A review. *Bioresour. Technol.* 244, 1198–1206. doi: 10.1016/j.biortech.2017.05.170

Chisti, Y. (2008). Biodiesel from microalgae beats bioethanol. *Trends Biotechnol.* 26, 126–131. doi: 10.1016/j.tibtech.2007.12.002

Converti, A., Casazza, A. A., Ortiz, E. Y., Perego, P., and Del Borghi, M. (2009). Effect of temperature and nitrogen concentration on the growth and lipid content of *Nannochloropsis oculata* and *Chlorella vulgaris* for biodiesel production. *Chem. Eng. Process. Process Intensif.* 48, 1146–1151. doi: 10.1016/j.cep.2009.03.006

Courchesne, N. M. D., Parisien, A., Wang, B., and Lan, C. Q. (2009). Enhancement of lipid production using biochemical, genetic and transcription factor engineering approaches. *J. Biotechnol.* 141, 31–41. doi: 10.1016/j.jbiotec.2009.02.018

D'Amico, S., Collins, T., Marx, J.-C., Feller, G., and Gerday, C. (2006). Psychrophilic microorganisms: challenges for life. *EMBO Rep.* 7, 385–389. doi: 10.1038/sj.embor.7400662

Da Silva, T. L., Reis, A., Medeiros, R., Oliveira, A. C., and Gouveia, L. (2009). Oil production towards biofuel from autotrophic microalgae semicontinuous cultivations monitorized by flow cytometry. *Appl. Biochem. Biotechnol.* 159, 568–578. doi: 10.1007/s12010-008-8443-5

Dolhi, J. M., Maxwell, D. P., and Morgan-Kiss, R. M. (2013). The Antarctic *Chlamydomonas raudensis*: An emerging model for cold adaptation of photosynthesis. *Extremophiles* 17, 711–722. doi: 10.1007/s00792-013-0571-3

Draaisma, R. B., Wijffels, R. H., Breuer, G., Lamers, P. P., and Martens, D. E. (2013). Effect of light intensity, pH, and temperature on triacylglycerol (TAG) accumulation induced by nitrogen starvation in *Scenedesmus obliquus*. *Bioresour. Technol.* 143, 1–9. doi: 10.1016/j.biortech.2013.05.105

Gong, Y., Hu, H., Gao, Y., Xu, X., and Gao, H. (2011). Microalgae as platforms for production of recombinant proteins and valuable compounds: Progress and prospects. *J. Ind. Microbiol. Biotechnol.* 38, 1879–1890. doi: 10.1007/s10295-011-1032-6

Grima, E. M., Pérez, J. A. S., Camacho, F. G., Medina, A. R., Giménez, A. G., and López Alonso, D. (1995). The production of polyunsaturated fatty acids by microalgae: from strain selection to product purification. *Process Biochem.* 30, 711–719. doi: 10.1016/0032-9592(94)00047-6

Guccione, A., Biondi, N., Sampietro, G., Rodolfi, L., Bassi, N., and Tredici, M. R. (2014). *Chlorella* for protein and biofuels: From strain selection to outdoor cultivation in a Green Wall Panel photobioreactor. *Biotechnol. Biofuels* 7:84. doi: 10.1186/1754-6834-7-84

Guillard, R. R., and Ryther, J. H. (1962). Studies of marine planktonic diatoms. I. Cyclotella nana Hustedt, and Detonula confervacea (cleve) Gran. *Can. J. Microbiol.* 8, 229–239. doi: 10.1139/m62-029

Guschina, I. A., and Harwood, J. L. (2006). Lipids and lipid metabolism in eukaryotic algae. *Prog. Lipid Res.* 45, 160–186. doi: 10.1016/j.plipres.2006.01.001

Harwood, J. L., and Guschina, I. A. (2009). The versatility of algae and their lipid metabolism. *Biochimie* 91, 679–684. doi: 10.1016/j.biochi.2008.11.004

He, Q., Yang, H., Wu, L., and Hu, C. (2015). Effect of light intensity on physiological changes, carbon allocation and neutral lipid accumulation in oleaginous microalgae. *Bioresour. Technol.* 191, 219–228. doi: 10.1016/J.BIORTECH.2015.05.021

Hulatt, C. J., Berecz, O., Egeland, E. S., Wijffels, R. H., and Kiron, V. (2017a). Polar snow algae as a valuable source of lipids? *Bioresour. Technol.* 235, 338–347. doi: 10.1016/j.biortech.2017.03.130

Hulatt, C. J., Wijffels, R. H., Bolla, S., and Kiron, V. (2017b). Production of fatty acids and protein by *Nannochloropsis* in flat-plate photobioreactors. *PLoS One* 12:1–17. doi: 10.1371/journal.pone.0170440

Jiang, Y., Laverty, K. S., Brown, J., Nunez, M., Brown, L., Chagoya, J., et al. (2014). Effects of fluctuating temperature and silicate supply on the growth, biochemical composition and lipid accumulation of *Nitzschia* sp. *Bioresour. Technol.* 154, 336–344. doi: 10.1016/j.biortech.2013.12.068

Li, W. K. W. (1980). "Temperature Adaptation in Phytoplankton: Cellular and Photosynthetic Characteristics," in *Primary Productivity in the Sea*, ed. P. Falkowski (Boston: Springer), 259–279. doi: 10.1007/978-1-4684-3890-1_15

Li-Beisson, Y., Beisson, F., and Riekhof, W. (2015). Metabolism of acyl-lipids in *Chlamydomonas reinhardtii*. *Plant J.* 82, 504–522. doi: 10.1111/tpj.12787

Li-Beisson, Y., Shorrosh, B., Beisson, F., Andersson, M. X., Arondel, V., Bates, P. D., et al. (2013). Acyl-Lipid Metabolism. *Arabidopsis Book* 11:e0161. doi: 10.1199/tab.0161

Liu, B., and Benning, C. (2013). Lipid metabolism in microalgae distinguishes itself. *Curr. Opin. Biotechnol.* 24, 300–309. doi: 10.1016/j.copbio.2012.08.008

Liu, J., Yuan, C., Hu, G., and Li, F. (2012). Effects of light intensity on the growth and lipid accumulation of microalga *Scenedesmus* sp. 11-1 under nitrogen limitation. *Appl. Biochem. Biotechnol.* 166, 2127–2137. doi: 10.1007/s12010-012-9639-2

Lowry, O. H., Rosebrough, N. J., Farr, A. L., and Randall, R. J. (1951). Protein measurement with the Folin phenol reagent. *J. Biol. Chem.* 193, 265–275.

Lv, J. M., Cheng, L. H., Xu, X. H., Zhang, L., and Chen, H. L. (2010). Enhanced lipid production of Chlorella vulgaris by adjustment of cultivation conditions. *Bioresour. Technol.* 101, 6797–6804. doi: 10.1016/j.biortech.2010.03.120

Lyon, B., and Mock, T. (2014). Polar Microalgae: New Approaches towards Understanding Adaptations to an Extreme and Changing Environment. *Biology* 3, 56–80. doi: 10.3390/biology3010056

Milledge, J. J. (2011). Commercial application of microalgae other than as biofuels: A brief review. *Rev. Environ. Sci. Biotechnol.* 10, 31–41. doi: 10.1007/s11157-010-9214-7

Morales-Sánchez, D., Kim, Y., Terng, E. L., Peterson, L., and Cerutti, H. (2017). A multidomain enzyme, with glycerol-3-phosphate dehydrogenase and phosphatase activities, is involved in a chloroplastic pathway for glycerol synthesis in *Chlamydomonas reinhardtii*. *Plant J.* 90, 1079–1092. doi: 10.1111/tpj.13530

Morales-Sánchez, D., Schulze, P. S. C., Kiron, V., and Wijffels, R. H. (2020). Production of carbohydrates, lipids and polyunsaturated fatty acids (PUFA) by the polar marine microalga Chlamydomonas malina RCC2488. *Algal Res.* 50:102016. doi: 10.1016/j.algal.2020.102016

Morales-Sánchez, D., Tinoco-Valencia, R., Kyndt, J., and Martinez, A. (2013). Heterotrophic growth of *Neochloris oleoabundans* using glucose as a carbon source. *Biotechnol. Biofuels* 6:100. doi: 10.1186/1754-6834-6-100

Morgan-Kiss, R. M., Ivanov, A. G., Modla, S., Czymmek, K., Hüner, N. P. A., Priscu, J. C., et al. (2008). Identity and physiology of a new psychrophilic eukaryotic green alga, *Chlorella* sp., strain BI, isolated from a transitory pond near Bratina Island, Antarctica. *Extremophiles* 12, 701–711. doi: 10.1007/s00792-008-0176-4

Morgan-Kiss, R. M., Priscu, J. C., Pocock, T., Gudynaite-Savitch, L., and Huner, N. P. A. (2006). Adaptation and acclimation of photosynthetic microorganisms to permanently cold environments. *Microbiol. Mol. Biol. Rev.* 70, 222–252. doi: 10.1128/MMBR.70.1.222-252.2006

Morgan-Kiss, R., Ivanov, A. G., Williams, J., Khan, M., and Huner, N. P. A. (2002). Differential thermal effects on the energy distribution between photosystem

II and photosystem I in thylakoid membranes of a psychrophilic and a mesophilic alga. *Biochim. Biophys. Acta* 1561, 251–265. doi: 10.1016/S0005-2736(02)00352-8

Msanne, J., Xu, D., Konda, A. R., Casas-Mollano, J. A., Awada, T., Cahoon, E. B., et al. (2012). Metabolic and gene expression changes triggered by nitrogen deprivation in the photoautotrophically grown microalgae *Chlamydomonas reinhardtii* and *Coccomyxa* sp. C-169. *Phytochemistry* 75, 50–59. doi: 10.1016/j.phytochem.2011.12.007

Pal, D., Khozin-Goldberg, I., Cohen, Z., and Boussiba, S. (2011). The effect of light, salinity, and nitrogen availability on lipid production by *Nannochloropsis* sp. *Appl. Microbiol. Biotechnol.* 90, 1429–1441. doi: 10.1007/s00253-011-3170-1

Pruvost, J., Van Vooren, G., Cogne, G., and Legrand, J. (2009). Investigation of biomass and lipids production with Neochloris oleoabundans in photobioreactor. *Bioresour. Technol.* 100, 5988–5995. doi: 10.1016/j.biortech.2009.06.004

Radakovits, R., Jinkerson, R. E., Darzins, A., and Posewitz, M. C. (2010). Genetic engineering of algae for enhanced biofuel production. *Eukaryot. Cell* 9, 486–501. doi: 10.1128/EC.00364-09

Ras, M., Steyer, J.-P., and Bernard, O. (2013). Temperature effect on microalgae: a crucial factor for outdoor production. *Rev. Environ. Sci. Bio/Technol.* 12, 153–164. doi: 10.1007/s11157-013-9310-6

Renaud, S. M., Thinh, L., Van, Lambrinidis, G., and Parry, D. L. (2002). Effect of temperature on growth, chemical composition and fatty acid composition of tropical Australian microalgae grown in batch cultures. *Aquaculture* 211, 195–214. doi: 10.1016/S0044-8486(01)00875-4

Rodolfi, L., Zittelli, G. C., Bassi, N., Padovani, G., Biondi, N., Bonini, G., et al. (2009). Microalgae for oil: Strain selection, induction of lipid synthesis and outdoor mass cultivation in a low-cost photobioreactor. *Biotechnol. Bioeng.* 102, 100–112. doi: 10.1002/bit.22033

Schmollinger, S., Muhlhaus, T., Boyle, N. R., Blaby, I. K., Casero, D., Mettler, T., et al. (2014). Nitrogen-Sparing Mechanisms in *Chlamydomonas* Affect the Transcriptome, the Proteome, and Photosynthetic Metabolism. *Plant Cell* 26, 1410–1435. doi: 10.1105/tpc.113.122523

Schulze, S. C. P., Hulatt, C., Morales-Sánchez, D., Wijffels, R., and Kiron, V. (2019). Fatty acids and proteins from cold adapted microalgae for biotechnology. *Algal Res.* 42:101604. doi: 10.1016/j.algal.2019.101604

Siaut, M., Cuiné, S., Cagnon, C., Fessler, B., Nguyen, M., Carrier, P., et al. (2011). Oil accumulation in the model green alga *Chlamydomonas reinhardtii*: Characterization, variability between common laboratory strains and relationship with starch reserves. *BMC Biotechnol.* 11:7. doi: 10.1186/1472-6750-11-7

Spolaore, P., Joannis-Cassan, C., Duran, E., and Isambert, A. (2006). Commercial applications of microalgae. *J. Biosci. Bioeng.* 101, 87–96. doi: 10.1263/JBB.101.87

Suzuki, H., Hulatt, C. J., Wijffels, R. H., and Kiron, V. (2018). Growth and LC-PUFA production of the cold-adapted microalga *Koliella antarctica* in photobioreactors. *J. Appl. Phycol.* 31, 981–997. doi: 10.1007/s10811-018-1606-z

Takeshita, T., Ota, S., Yamazaki, T., Hirata, A., Zachleder, V., and Kawano, S. (2014). Starch and lipid accumulation in eight strains of six *Chlorella* species under comparatively high light intensity and aeration culture conditions. *Bioresour. Technol.* 158, 127–134. doi: 10.1016/j.biortech.2014.01.135

Thompson, A. R. (1950). A colorimetric method for the determination of esters. *Aust. J. Chem.* 3, 128–135. doi: 10.1071/CH9500128

Tiwari, A., and Kiran, T. (2018). Biofuels from Microalgae. *Adv. Biofuels Bioenergy* 2018:73012. doi: 10.5772/intechopen.73012

Work, V. H., Radakovits, R., Jinkerson, R. E., Meuser, J. E., Elliott, L. G., Vinyard, D. J., et al. (2010). Increased lipid accumulation in the Chlamydomonas reinhardtii sta7-10 starchless isoamylase mutant and increased carbohydrate synthesis in complemented strains. *Eukaryot. Cell* 9, 1251–1261. doi: 10.1128/EC.00075-10

Xin, L., Hong-ying, H., and Yu-ping, Z. (2011). Growth and lipid accumulation properties of a freshwater microalga *Scenedesmus* sp. under different cultivation temperature. *Bioresour. Technol.* 102, 3098–3102. doi: 10.1016/j.biortech.2010.10.055

Xin, L., Hong-ying, H., Ke, G., and Ying-xue, S. (2010). Effects of different nitrogen and phosphorus concentrations on the growth, nutrient uptake, and lipid accumulation of a freshwater microalga *Scenedesmus* sp. *Bioresour. Technol.* 101, 5494–5500. doi: 10.1016/j.biortech.2010.02.016

Zhu, L. D., Li, Z. H., and Hiltunen, E. (2016). Strategies for Lipid Production Improvement in Microalgae as a Biodiesel Feedstock. *Biomed Res. Int.* 2016:8792548. doi: 10.1155/2016/8792548

Conflict of Interest: The authors declare that the research was conducted in the absence of any commercial or financial relationships that could be construed as a potential conflict of interest.

frontiers in Plant Science

ORIGINAL RESEARCH
published: 07 June 2021
doi: 10.3389/fpls.2021.679428

Altitudinal Zonation of Green Algae Biodiversity in the French Alps

Adeline Stewart[1,2,3], Delphine Rioux[3], Fréderic Boyer[3], Ludovic Gielly[3], François Pompanon[3], Amélie Saillard[3], Wilfried Thuiller[3], Jean-Gabriel Valay[2], Eric Maréchal[1] and Eric Coissac[3]* on behalf of The ORCHAMP Consortium*

[1] Laboratoire de Physiologie Cellulaire et Végétale, CEA, CNRS, INRAE, IRIG, Université Grenoble Alpes, Grenoble, France, [2] Jardin du Lautaret, CNRS, Université Grenoble Alpes, Grenoble, France, [3] Université Grenoble Alpes, Université Savoie Mont Blanc, CNRS, LECA, Grenoble, France

Mountain environments are marked by an altitudinal zonation of habitat types. They are home to a multitude of terrestrial green algae, who have to cope with abiotic conditions specific to high elevation, e.g., high UV irradiance, alternating desiccation, rain and snow precipitations, extreme diurnal variations in temperature and chronic scarceness of nutrients. Even though photosynthetic green algae are primary producers colonizing open areas and potential markers of climate change, their overall biodiversity in the Alps has been poorly studied so far, in particular in soil, where algae have been shown to be key components of microbial communities. Here, we investigated whether the spatial distribution of green algae followed the altitudinal zonation of the Alps, based on the assumption that algae settle in their preferred habitats under the pressure of parameters correlated with elevation. We did so by focusing on selected representative elevational gradients at distant locations in the French Alps, where soil samples were collected at different depths. Soil was considered as either a potential natural habitat or temporary reservoir of algae. We showed that algal DNA represented a relatively low proportion of the overall eukaryotic diversity as measured by a universal Eukaryote marker. We designed two novel green algae metabarcoding markers to amplify the *Chlorophyta* phylum and its *Chlorophyceae* class, respectively. Using our newly developed markers, we showed that elevation was a strong correlate of species and genus level distribution. Altitudinal zonation was thus determined for about fifty species, with proposed accessions in reference databases. In particular, *Planophila laetevirens* and *Bracteococcus ruber* related species as well as the snow alga *Sanguina* genus were only found in soil starting at 2,000 m above sea level. Analysis of environmental and bioclimatic factors highlighted the importance of pH and nitrogen/carbon ratios in the vertical distribution in soil. Capacity to grow heterotrophically may determine the *Trebouxiophyceae* over *Chlorophyceae* ratio. The intensity of freezing events (freezing degree days), proved also determinant in *Chlorophyceae* distribution. Guidelines are discussed for future, more robust and precise analyses of environmental algal DNA in mountain ecosystems and address green algae species distribution and dynamics in response to environmental changes.

Keywords: *Chlorophyta*, metabarcoding, mountain environment, soil, biodiversity, high elevation, *Sanguina*, snow algae

OPEN ACCESS

Edited by:
Tomas Morosinotto, University of Padua, Italy

Reviewed by:
Nozomu Takeuchi, Chiba University, Japan
Marco Cantonati, Museo delle Scienze, Italy

***Correspondence:**
Eric Maréchal
eric.marechal@cea.fr
Eric Coissac
eric.coissac@metabarcoding.org

Specialty section:
This article was submitted to Marine and Freshwater Plants, a section of the journal Frontiers in Plant Science

Received: *11 March 2021*
Accepted: *11 May 2021*
Published: *07 June 2021*

Citation:
Stewart A, Rioux D, Boyer F, Gielly L, Pompanon F, Saillard A, Thuiller W, Valay J-G, Maréchal E and Coissac E (2021) Altitudinal Zonation of Green Algae Biodiversity in the French Alps. Front. Plant Sci. 12:679428. doi: 10.3389/fpls.2021.679428

INTRODUCTION

Green algae are unicellular, colonial or multicellular photosynthetic organisms that are ubiquitous in almost all ecosystems. They have evolved in two major lineages, one referred to as *Chlorophyta*, what has been traditionally called green algae, another referred to as *Charophyta*, containing a smaller but often geographically widespread number of taxa (Lewis and Mccourt, 2004; Domozych et al., 2016). Recently, a third lineage was introduced, covering marine *Prasinodermophyta*, which diverged before the split of *Chlorophyta* and *Streptophyta* (Li et al., 2020), and that was not considered in the present work.

The majority of green algae species are found in aero-terrestrial habitats, living either freely or in lichens in association with fungi (Rindi et al., 2010), from wet to dry areas (Lewis and Mccourt, 2004; Holzinger et al., 2017). Although algae are often considered to live primarily in "free" water, soil surface is known for long to host an important algal biodiversity (Tchan, 1952; Reisigl, 1969; Koelewijn et al., 2001; John et al., 2011; Foets et al., 2020). Numerous green algae can grow heterotrophically in the dark, using an external source of organic carbon, and often much faster compared to pure autotrophic conditions (Fan et al., 2012; Bell, 2013). Soil can therefore be colonized from its surface to its depth by the combined photosynthetic and heterotrophic capacity of algal communities. In soil, algae contribute actively to the global cycles of carbon and nitrogen (Elbert et al., 2012). In addition, soil may also contain resting algal cysts or non-motile spores (aplanospores), thus acting as a reservoir for species needing more appropriate conditions to grow. This latter context is difficult to assess, since most microbial species are non-cultivable (Schmeisser et al., 2007) and the determination of life cycles are therefore extremely challenging. Some algae species can also occupy non-liquid water systems, most notably snow and ice (Remias, 2012; Lukes et al., 2014; Hisakawa et al., 2015; Holzinger et al., 2016; Lu et al., 2016; Hoham and Remias, 2019).

Mountain environments are marked by the tight apposition of contrasted habitats, structured by the topography, elevation, temperature, exposure to sunlight, wind, precipitations, etc., with abiotic conditions considered as "extreme" such as high light intensity, extreme negative temperatures, high UV irradiance, strong winds, desiccation, extreme diurnal variations in temperatures and chronic scarceness of nutrients (Geremia et al., 2016). Knowledge on the biodiversity and distribution of green algae in mountain environments is fragmented and overall poor. Some habitats have attracted more attention, such as lakes (Jacquemin et al., 2019) or snowpack at high elevation (Hoham and Remias, 2019). Soil was barely explored, although it represents a much more extended and permanent surface, with a strong potential for spatiotemporal studies of species distribution, interfaced with hydrologic networks and seasonal snow covers. A first survey of aero-terrestrial algae in alpine soils was based on the morphological study of cells sampled in the Tyrolean Alps above 3,000 m a.s.l., with about 90 species described, counting a majority of *Chlorophyta* (Reisigl, 1964). A recent review on algae populating soil surface in the Alps (Karsten and Holzinger, 2014), reported that eukaryotic algae of mountains were mainly represented by monadoid and coccoid *Chlorophyta*, and to a lower extent *Charophyta* and a few *Ochrophyta* (Gartner, 2004; Tschaikner et al., 2007). This review highlighted the potential role of UV light and desiccation as drivers of soil algal communities in the Alps (Karsten and Holzinger, 2014), but other environmental factors may be determinant as well.

In environments undergoing rapid evolutions, photosynthetic algae can act as pioneering organisms, able to develop autotrophically on empty surfaces, and being the primary producers allowing the subsequent foundation of trophic networks. As an example, green algae have been shown to be primary colonizers after glacier's retreat (Kastovska et al., 2005; Hotaling et al., 2017). Atmospheric CO_2 proved to influence microbial communities in a pH-dependent manner (Gulliver et al., 2016; Yu and Chen, 2019). It is also expected, although not demonstrated yet, that the current increase in atmospheric CO_2 could be beneficial to the development of photosynthetic algae and as such, act positively on the efficiency of colonization. Green algae are therefore expected to be "markers" of climate change. In mature ecosystems, once established in their habitat, green algae can proliferate to such an extent that they form so called blooms, which can be determinant in further evolutions of their environment. For instance, at the surface of snowpack, green algae blooms are detected by the pigmentation of resistant cells (cysts), containing red carotenoids, such as astaxanthin (Holzinger et al., 2016). The "red snow" thus formed reduces the albedo, triggering an increase of superficial temperature and accelerating snow melting (Lutz et al., 2016; Di Mauro et al., 2020). In this aspect, green algae are therefore also expected to be "actors" of environmental changes. If we aim to comprehend the dynamics of ecosystems, data on microbial communities, and most notably on photosynthetic microorganisms, are critical. Spatiotemporal distribution of green algae is thus a major information we need to address changes in mountain areas exposed to drastic seasonal variations and to irreversible transformations triggered by climate evolution. These data are currently missing.

The distribution of plant species in mountain environment is generally assumed to be mostly constrained by abiotic factors (Benton, 2009; Martinez-Almoyna et al., 2019; Körner, 2021) and it could be the same for microalgae, as suggested by a microscopy-based study performed in the Himalayas along an elevational gradient (Rehakova et al., 2011). To study microalgae communities, some research groups have performed sampling, followed by microscopic observation of microalgae (e.g., Rehakova et al., 2011) or DNA-barcoding analyses (e.g., Hall et al., 2010). None of these studies has provided a comprehensive taxonomic assessment of sampled green algae. Cell morphology is not sufficient to identify species, and information on life cycles, biochemical traits or genomic sequences would be requested to refine characterizations. In addition, microscopy-based studies rely on the relative abundance of species at the time of sampling, and on the survival rate of species, when transferred from their environment to the laboratory. By contrast, environmental DNA allows detecting genomic fragments released by broken cells, by past and present communities, thus providing data on the spatial

distribution with a so called "soil memory effect," mitigating short term temporal variations (Foucher et al., 2020). DNA-based analysis is therefore currently the best compromise to obtain more exhaustive information on microalgae communities (Lutz et al., 2016; Groendahl et al., 2017; Foucher et al., 2020).

Metabarcoding is based on assigning amplified molecular operational taxonomic unit (MOTU) sequences from an environmental sample (eDNA) to a database of sequences. Its success depends on the effectiveness of the markers to amplify targeted taxa, the effectiveness of the PCRs and sequencing, the status of the reference database (Ficetola et al., 2010, 2016) and the quality of the bioinformatic pipeline (Calderòn-Sanou et al., 2020). Markers for green algae of the *Chlorophyta* phylum were designed in several studies (e.g., Vieira and Bagatini, 2016; Zou et al., 2016; Pfendler et al., 2018) but most previous works use more general eukaryotic markers like ITS (internal transcribed spacer, Heeger et al., 2018) or COX1 (cytochrome oxidase I, Ward et al., 2005). The use of general eukaryotic markers reflects the fact that databases contain more of these sequences available for assignments. None of these markers has proven ideal for the study of green algae. They have issues such as too high or too low variability, presence of introns, absence of data in the databases, or amplification of only a part of the community (Vieira and Bagatini, 2016).

Here, we evaluated green algae biodiversity, focusing on *Chlorophyta*, in selected elevational gradients in the French Alps from 1,250 to 3,000 m high, from forests at lowest levels, to a variety of other habitats such as heathlands, grasslands and rocky areas at high elevations (**Figure 1**). Presence of green algae was monitored at different depths in the soil. The sampling campaign was part of a large project aiming at understanding biodiversity and its drivers and dynamics over time in the Alps, called Orchamp, and which provided the samples[1]. To that purpose, we validated two new markers for metabarcoding studies, a *Chlorophyta* phylum marker "Chlo01" designed in the V7 region of the 18S ribosomal RNA, to cover most of the green algae and a *Chlorophyceae* marker "Chlo02" designed in the 23S ribosomal RNA chloroplast sequence. We then asked whether green algae could be detected with these markers and if we could point some possible environmental drivers of their distribution patterns and community structure.

MATERIALS AND METHODS

Soil Sampling

In late summer 2016, 158 soil samples were collected in the French Alps along elevation gradients covering elevations from 1,250 to 2,940 m at five different sites: Chamrousse (CHA) 45.098692°N, 5.885508°E, elevations from 1,250 to 2,180 m, sampled on September the 1st; Loriaz (LOR) 46.038079°N, 6.918759°E, from 1,370 to 2,330 m, sampled on September the 6th; Anterne (ANT) 46.009245°N, 6.805825°E from 1,400 to 2,370 m, sampled on September the 7th; Ristolas (RIS) 44.724622°N, 7.031392°E, from 1,900 to 2,890 m, sampled on September the 15th; and Vieux Chaillol (VCH) 44.721000°N, 6.187555°E, from 2,150 to 2,940 m, sampled on September the 14th (**Figure 1**). The four lowest sites include environments composed of forests at the lowest elevations, and grasslands and pastures at the highest elevations. At their highest elevations, only RIS and VCH reach the nival zone, and the latter has no forest at its base. The sampling was done along the elevational gradients approximatively every 200 m. For each level, sampling was performed in triplicate at two different soil horizons: the litter (soil not totally decomposed) between 0 and 10 cm depth, and the deep soil between 10 and 25 cm depth (soil totally decomposed).

Environmental Variables

In addition to the sampling site (*Site*), six environmental variables were measured for each sample: elevation above sea level in meters (*Elevation*); soil pH (*pH*) and organic matter content (*Organic Matter*) assessed using standard protocols (Robertson et al., 1999); total soil carbon (*Carbon*) and nitrogen (*Nitrogen*) measured using a Flash EA1112 (Thermo Scientific) elemental analyzer (Martinez-Almoyna et al., 2019); the *Carbon* over *Nitrogen* ratio (*C/N ratio*). Ten bioclimatic variables, estimated as averages over 1988–2018 were used: the mean of the annual temperature (TG), the growing degree days (GDD), the freezing degree days (FDD), these three variables were estimated at 1 and 10 cm below ground, the climatic water stress (CWD), the solar radiation, the total snow depth (DSN_T_ISBA) and the diurnal temperature range (DRT.air). Details on these variables are available in Martinez-Almoyna et al. (2019) and Martinez-Almoyna et al. (2020) Finally, two categorical variables: the type of environment (*Environment*) with two modalities, forest or open-area, and the soil horizon (*Horizon*) with two modalities, litter or deep soil, complete this description. It is common for environmental variables to be multi-colinear with respect to each other. To overcome this problem, a subset of continuous environmental variables was selected using the variance and inflation factor (VIF) criterion: $VIF = 1/(1–R^2)$ where R^2 is the coefficient of determination of the multiple linear model of one of the explanatory variables explained by the others. Variables with a VIF greater than 5 (Sheather, 2009) were iteratively removed. At the end of the selection process, *Elevation*, *pH*, *Nitrogen*, *C/N ratio*, *FDD* at 1 cm, *CWD*, and *DTR* were retained, while *other variables* were removed because of there colinearity with the selected variables (**Supplementary Figure 1**).

DNA Metabarcoding Markers

Two new DNA metabarcodes were designed for this analysis. The first one targets *Chlorophyta* (Chlo01), the second targets Chlorophyceae (Chlo02). To design these new metabarcodes, 1,628 complete chloroplast sequences were downloaded from the NCBI database[2] (November 2017) comprising 74 Chlorophyta plastid genomes, including 23 Chlorophyceae genomes. The ecoPCR software[3] and the ROBIBarcodes R package[4] were used to refine the corresponding primer sequences, assess

[1]https://orchamp.osug.fr/home

[2]https://www.ncbi.nlm.nih.gov

[3]http://metabarcoding.org/ecopcr

[4]https://git.metabarcoding.org/obitools/ROBIBarcodes

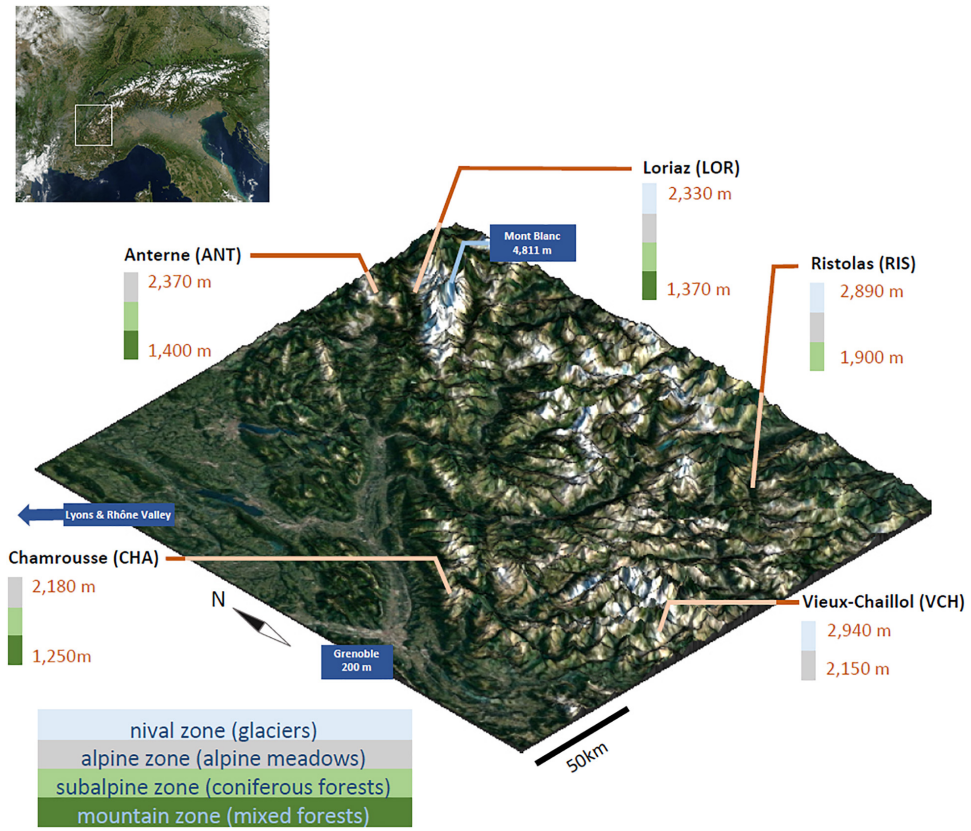

FIGURE 1 | Aerial view of the five sampled elevational gradients and their topography (1,250–2,940 m). Selected sites cover the full range of environments and habitats found in the Alpine altitudinal zonation and a representative geographical distribution. DNA was extracted from soil collected at each sampling location and used for an evaluation of *Chlorophyta* communities by DNA metabarcoding. Satellite images from Nasa.

the conservation of the priming sites using sequence logos (Schneider and Stephens, 1990), and estimate *in silico* the taxonomic resolution as proposed in Ficetola et al., 2010. The sequence library used to realize those tests was the entire EMBL sequence database (release 139, Amid et al., 2020). The hybridization temperature was empirically determined using OligoCalc[5] following recommendations in Taberlet et al. (2018). Chlo01 was adapted from the eukaryotic marker Euka02 and corresponds to the V7 variable region of nuclear 18S rRNA gene (Taberlet et al., 2018). Corresponding primers were modified to make them specific of Chlorophyta. Chlo02 was designed using the ecoPrimers software[6] (Riaz et al., 2011). A third marker, Euka03 (Euka03F: CCCTTTGTACACACCGCC, Euka03R: CTTCYGCAGGTTCACCTAC) targeting all eukaryota, was used to assess relative proportion of algal eDNA within the eukaryota super kingdom (Taberlet et al., 2018).

Algae Mock Community for Positive Controls

A mock community constituted by 13 green unicellular marine algae species from the Roscoff Culture Collection (RCC)[7] were used as template for the PCR positive controls. According to the order presented in **Supplementary Table 1**, the DNA concentration for each species was adjusted to half of the previous one. The community was expected to be similar in concentration and complexity to our samples. If the thirteen species could theoretically be amplified by Euka03 and Chlo01, only 3 species were expected to be amplified by Chlo02. The DNA of each species constituting the mock community was extracted using the Macherey Nagel NucleoSpin Plant II extraction kit according to the instruction manual[8].

Soil DNA Extraction, PCR Amplification and Sequencing

Extracellular DNA was extracted from 15 g of soil or litter as described previously (Taberlet et al., 2012). PCRs were then performed in triplicates for each sample, in parallel with extraction blanks, with no template soil and PCR blanks, with no template DNA (negative controls) and positive control. After an initial denaturation at 95°C for 10 min, 40 cycles (38 for Chlo01) of amplification were run: denaturation 95°C, 30 s; hybridization 30 s; elongation 72°C 1 min. Hybridization temperature was respectively 55°C, 50°C, and 55°C for Chlo01, Chlo02, and

[5]http://biotools.nubic.northwestern.edu/OligoCalc.html
[6]http://metabarcoding.org/ecoprimers
[7]http://www.roscoff-culture-collection.org
[8]https://www.mn-net.com/

Euka03. Each PCR product was individually tagged according to Taberlet et al. (2018). This enabled the pooling of up to 1,052 PCRs per sequencing libraries. Pooled PCRs were purified using the Qiagen MinElute PCR Purification Kit for Chlo01 and Euka03 and the Qiagen QIAquick PCR Purification Kit for Chlo02[9]. Sequencing libraries were prepared and sequenced (2 × 125 bp paired-end reads) by Fasteris (Geneva, Switzerland), using their MetaFast protocol.

Design of a Reference Database of Green Algae Sequences

The reference sequence databases used for taxonomic assignment were extracted using ecoPCR (Ficetola et al., 2010; Boyer et al., 2016) from the EMBL database (version 140, 2019; Amid et al., 2020), using Chlo01, Chlo02 or Euka03 primers as queries. EcoPCR results were filtered using OBITools (Boyer et al., 2016) to keep only the sequences annotated with an unambiguous family and genus. Strictly identical sequences were merged and their taxonomic annotations summarized at the lowest common ancestor. Sequences containing ambiguous nucleotides were also discarded. The cleaned reference databases for Chlo01, Chlo02, and Euka03 are constituted respectively by 1444, 744, and 17207 sequences. The Chlo01 database represents 295 genera and 62 families belonging the *Chlorophyta*. The Chlo02 database represents 42 genera and 19 families belonging the *Chlorophyceae*. The Euka03 database represents 5179 genera and 2488 families belonging the *Eukaryota*.

Read Filtering and Processing

The reading pairs were assembled, and demultiplexed to be separated by sample. The sequences were then de-replicated to obtain the number of reads of each sequence variant in each PCR. These steps and the following were realized using the OBITools software (Boyer et al., 2016) following the protocol by Taberlet et al. (2018). According to the amplicon lengths estimated from our reference databases for each marker, sequences shorter than 65 bp and longer than 200 bp for Chlo01 and Euka03, and 130 bp for Chlo02 were discarded. Rare sequence variants never represented by more than 10 reads in a PCR were discarded. Punctual errors generated during PCR cycles were discarded using the obiclean (Boyer et al., 2016). Sequence variants were taxonomically annotated using the ecotag and the reference database described above. Only MOTUs annotated in the target clade of its marker were conserved. At this stage, any MOTU that was more abundant in the negative PCR controls than in any of the samples was annotated as a contaminant and discarded.

Removing of Unsuccessful PCRs

Of all the PCRs analyzed, some provided unreliable results. They were detected according to two criteria, the number of reads associated with a PCR, and considering a sample, the similarity between PCR replicates. Based on the distribution of the number of reads per PCR observed for each marker, PCRs with more than 200 reads for the markers Chlo01 and Chlo02, and 1,000 reads for Euka03 were considered unsuccessful and rejected. The reproducibility of PCR replicates was estimated by the distance between a replicate and the barycenter of the replicates for that sample. Distances were estimated using Euclidean distances computed on the Hellinger transformed data (square roots of the relative frequencies), which corresponds to a correlation distance. Distribution of these distances is used to detect potential outliers.

Data Analyses and Statistics

Further filtering and data analysis were run using R (v.3.6.2, R Development Core Team, 2019) using the ROBItools package[10] for managing OBITools data files, ggplot2 (Wickham, 2011) for graphics, the ade4 package (Dray and Dufour, 2007) for every multidimensional scaling and the Vegan package (Oksanen et al., 2020) for computing Hellinger transformation (square rooted relative frequencies), relative frequencies, and *Permutational multivariate analyses of variance* (PERMANOVA). The iteratively reweighted least squares (IRLS) procedure for estimating outlier robust linear models was computed with the robustRegBS function of the robustreg package, implementing the methods presented in Hubert (1981).

Taxonomic Diversity

The diversity of algal communities was estimated for metabarcoding data using Hill numbers, with $q = 1$ here (the exponential of the Shannon entropy index). A Hill number is the effective number of species composing a theoretical community, which would be perfectly even, and having the same diversity as the community studied. A taxonomic diversity measured by a Hill number (^{q}D) takes less and less account of rare species when the q parameter increases. In the case of metabarcoding data, using $q = 1$ penalizes not only the rarest species, but also the many false taxa generated during PCR amplification that occur at low read frequencies. As a result, the taxonomic diversity ^{1}D values estimated from DNA metabarcoding data are relatively congruent with those estimated from conventional inventories (Calderòn-Sanou et al., 2020). The relationships between diversity and environmental parameters were measured by discretizing the gradients into seven levels. The strength of the relationship was estimated with a one-factor ANOVA and its significance was tested with the Kruskal–Wallis method.

Community Turnover

The composition turnover between communities was estimated using Euclidean distances calculated on the Hellinger transformed contingency table of sequence reads, per MOTU and samples. We then projected those pairwise distances using principal coordinate analysis (PCOA). The strength of the correlations between community changes and environmental variables was estimated using Redundancy Analysis (RDA) using the Vegan R package. The environmental variables were centered and scaled for the analysis. The optimal model was selected using a forward-backward selection procedure implemented in the ordistep function. Partitioning of the community changes variance was performed using the varpart

[9]https://www.qiagen.com/

[10]https://git.metabarcoding.org/obitools/ROBITools

function. Permutation-based estimate of *p*-values relied on 999 permutations.

Niche Inference

Niches of the MOTUs identified at the species or genus levels were estimated using the Outlying Mean Index (OMI) method (Doledec et al., 2000) as implemented in the niche function of the ADE4 R package. This method describes the niche according to three terms: its marginality, its marginal tolerance and its residual tolerance. Marginality measures the distance of the center of a taxon's niche from the center of the environmental space, which would represent a ubiquitous species. Marginal tolerance measures the width of the niche along its the marginality axis, defined by the vector connecting the center of the environmental space and the center of the taxon's niche. The marginal tolerance measures the width of the niche in the orthogonal plan to the marginality axis. Doledec et al. (2000) measured the specialization of a taxon by the non-zero marginality of its niche. In our case a taxon could also be considered as specialized, if its marginality was null but its marginal tolerance was lower than that expected for a taxon uniformly distributed in the environmental space. Therefore, a taxon was defined as specialized if its marginality was not null or if its marginal tolerance is smaller than expected under uniform distributions. Both conditions were tested by permutation (n = 999) following the procedure implemented in the *r*-test function.

RESULTS

Design and Validation of *Chlorophyta* and *Chlorophyceae* DNA Markers

There are three main lineages of green algae: *Chlorophyta*, *Prasinophyta*, and *Charophyta*, the latter of which also is close to land plants (Kapraun, 2007). We focused on the *Chlorophyta* phylum, an important and diverse lineage of green algae, and were particularly interested in the *Chlorophyceae* class, which we expected to yield the greatest diversity of algae. The developed markers were termed Chlo01 and Chlo02.

Similarly to Euka02 (Taberlet et al., 2018), the Chlo01 marker corresponds to the V7 region of the 18S nuclear rRNA gene. Its length ranges from 80 to 180 bp. The primer pair Chlo01F: AGTTGGTGGGTTGCCTTGT, Chlo01R: CACAGACCTGTTATTGCCTC has an estimated hybridization temperature of 55°C. The Chlo01 marker theoretically discriminates 24% of the sequences at the species level, 43% at the genus level, 53% at the family level, 62% at the order level and 74% at the class level (**Supplementary Figure 2**).

The Chlo02 marker corresponds to a sequence included in the 23S chloroplastic rRNA gene. Its length ranges from 91 to 94 bp. The primer pair Chlo02F: RCTTAGTCCCGGCCATT, Chlo02R: CTAAGTGGWAAAGGATGTG has an estimated hybridization temperature of 50°C. The Chlo02 marker discriminates 47% of the sequences at the species level, 65% at the genus level, and 73% at the family level (**Supplementary Figure 2**).

Sequencing Results

We used the three markers to amplify DNA extracted from soil samples collected along the five elevation gradients. After filtering, the Chlo01 marker amplified 4,080 MOTUs represented by ∼5.8 million reads, including 566 Chlorophyta MOTUs corresponding to 3.3 million reads (see **Table 1**). The Chlo02 marker amplified 8,580 MOTUs, corresponding to 6.3 million reads; among them, 61 MOTUs belonged to Chlorophyceae, represented by less than 0.2 million reads. The Euka03 marker amplified 8,743 MOTUs, represented by 5.7 million reads, including 4,108 *Eukaryota* MOTUs corresponding to 4.1 million reads and 37 *Chlorophyta* MOTUs representing only 14,829 reads.

Chlorophyta DNA Represents a Minor Fraction of Soil DNA

To evaluate the relative part of algal eDNA present in soil samples, data obtained with the Euka03 marker were analyzed. **Figure 2** shows the fraction of fungi, *Streptophyta* (mostly vascular plants) or *Chlorophyta* reads amplified by the Euka03 marker. While fungi and vascular plants occupy on average a high fraction of the reads, 59% (sd = 19%) and 21% (sd = 17%), respectively, *Chlorophyta* represent less than 3.3% of the reads in every PCR and 0.6% on average. In fact, only 18.6% of the PCRs with the Euka03 marker had some *Chlorophyta* reads (**Figure 2**). That trend is the same at every sampling site, even if the abundance of algae seems to increase at sites that cover higher elevations. Due to this low abundance of reads, which could result in under-sampling of diversity, and due to the low taxonomic resolution of Euka03, only 37 MOTU of *Chlorophyta* were identified. Of these, 7 belong to *Chlorophyceae* and 16 to *Trebouxiophyceae*. That low abundance of *Chlorophyta* eDNA is also confirmed by the marker Chlo01. Despite the fact that this marker is supposed to be highly specific to that clade (**Supplementary Figure 2**), we observed that many sequences were not annotated as *Chlorophyta*. Such high artifactual amplifications are commonly observed when target DNA concentration is very low in PCRs. Using an IRLS procedure, a linear model explaining 25% of the variance can be established on a logarithmic scale between the relative frequencies of *Chlorophyta* reads estimated by Euka03 and Chlo01 (**Figure 3**).

TABLE 1 | Amplified MOTU and read counts by each marker for all samples.

Marker	Number of MOTU and reads in raw data	Number of MOTU and reads after filtering	Number of green algae MOTU and reads
Chlo01	1,280,988 MOTUs 12,849,650 reads	4,080 MOTUs 5,763,181 reads	566 MOTUs 3,305,241 reads
Chlo02	2,392,669 MOTUs 32,640,026 reads	8,580 MOTUs 6,210,043 reads	61 MOTUs 186,616 reads
Euka03	1,902,234 MOTUs 13,604,341 reads	8,743 MOTUs 5,700,798 reads	37 MOTUs 14,829 reads

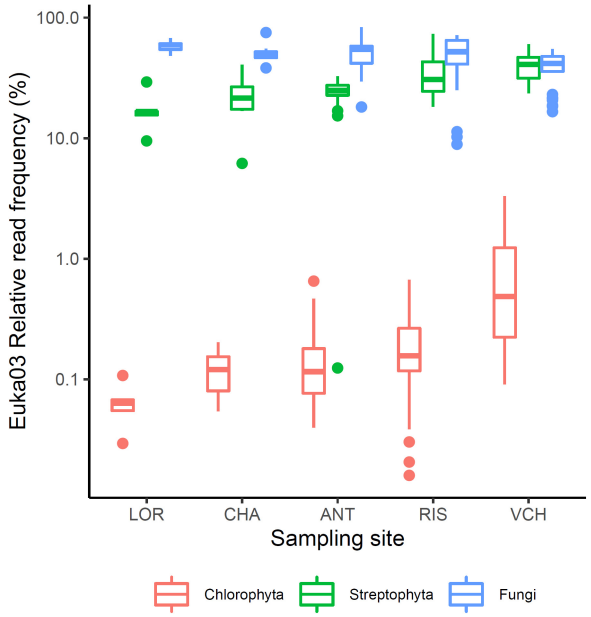

FIGURE 2 | Relative frequencies of three eukaryotic clades; *Fungi*, *Streptophyta*, and *Chlorophyta*, among the sampling sites. The lower and upper limits of the boxes correspond to the first and third quartile, respectively, while the bold center line marks the median. The whiskers delineate the confidence interval defined as 1.5 times the difference between the first and third quartile. Outlier PCRs ranging outside of that interval are marked with dots.

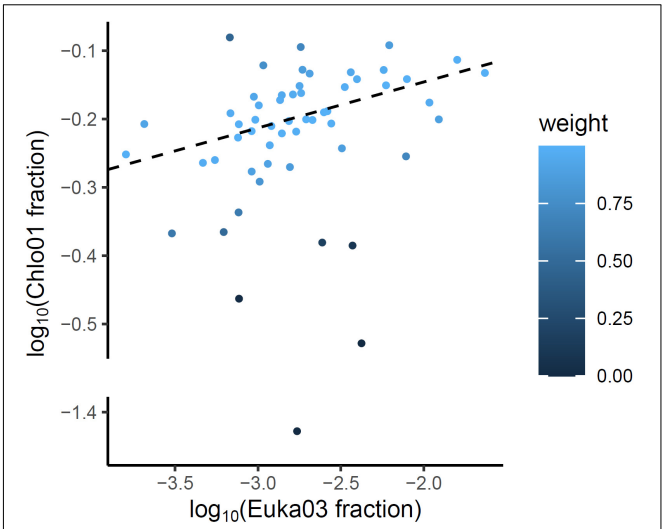

FIGURE 3 | On a logarithmic scale, the relative frequencies of *Chlorophyta* reads estimated by the two markers Chlo01 and Euka03 are correlated. The linear model (dotted line) was estimated using an iteratively reweighted least squares procedure (IRLS) to underweight the influence of the few outliers PCRs. The blue scale indicates the weight associated to each PCR after the convergence of the algorithm.

Diversity of the *Chlorophyta* Communities

The scarcity of *Chlorophyta* eDNA, confirmed by both Euka03 and Chlo01, can be explained either by a low biomass of algae in Alpine terrestrial environments or by our poor ability to extract algal eDNA from soil samples. Whatever the reason, this rarity limits the completeness of our sampling. Therefore, we certainly sampled only the most abundant taxa. This must be kept in mind when analyzing the data. For checking at minima, the quality of the ^{1}D estimation for algae and considering our data filtering stringency, we estimated ^{1}D for positive controls carried out on the mock community of 10 marine species of *Chlorophyta*. According to its composition, the theoretical diversity of the mock community was ^1D = 4.0 using the marker Chlo01 and 1.8 using the marker Chlo02 since only three of the ten species are *Chlorophyceae*. For Chlo01 the 72 replicates of the positive control gave a mean diversity ^1D = 3.83 species (sd = 0.016), which is slightly underestimated. For Chlo02, the same positive controls gave a mean diversity ^1D = 1.330 species (sd = 0.0016) instead of the theoretical 1.8. Over all five elevation gradients, the mean diversity observed for a sample for *Chlorophyta* (Chlo01) was ^1D = 9.58 (sd = 0.018 for 321 PCRs), and for *Chlorophyceae* (Chlo02) ^1D = 2.224 (sd = 0.0075 for 187 PCRs). A rough estimate of regional diversity (γ), by cumulating the results of the five elevational gradients, gave ^1D = 49.03 for *Chlorophyta* and ^1D = 13.40 for *Chlorophyceae*. The β diversity estimated as γ/α can be evaluated to 5.11 sites for Chlo01 and 6.02 sites for Chlo02. These two values have to be related to the number of studied gradients, i.e., five, and indicate that most of the MOTUs are site specific. Among the 566 MOTUs identified by Chlo01, 367 are present on only one gradient, 76 on two, the remaining 123 being observable on at least three gradients. For Chlo02, among the 61 MOTUs detected, 35, 9 and 17 MOTUs appear respectively in one, two, or three or more gradients (**Figure 4**). There is a strong link in that dataset between the endemism of a MOTU and its rarity, the MOTUs occurring in one or two sites only are also those having the lowest frequencies of occurrences at these sites (**Figure 4**). Therefore, the high endemism observed was probably related to the low coverage of the sampling. With the exception of the CHA gradient, which shows atypical results, among the seven non-collinear environmental and bioclimatic variables, pH, elevation, nitrogen, CWD and FDD (**Figure 5**) are significantly related to diversity. They explained 22, 9, 22, 21, and 11% of the variance of ^{1}D, respectively.

At the 5% threshold, the C/N ratio and DRT have no detectable effect on algal community diversity. The litter, which was richer in nitrogen, carbon and organic matter had a mean algal diversity ^1D = 11.8 (sd = 0.43) significantly higher (Mann–Whitney p-value = 10^{-15}) than that of the deep soil layer ^1D = 6.7 (sd = 0.43). On the other hand, forest environments did not present a significantly different diversity from open environments (Mann–Whitney p-value = 0.54), although the former were also richer than the latter in Nitrogen, Carbon and Organic Matter.

Main Components of *Chlorophyta* Communities

The *Chlorophyta* taxa identified with Chlo01 belong to four classes: *Trebouxiophyceae*, *Chlorophyceae*, *Ulvophyceae*, and

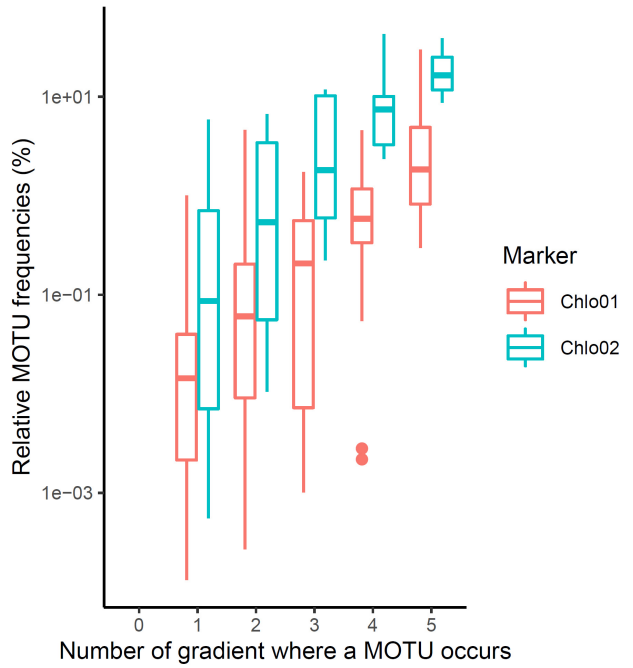

FIGURE 4 | Endemism of the MOTUs according to their maximum frequency of occurrence in one of the gradients. The higher a MOTU has a high frequency of reads on at least one gradient, the more likely it will be present in many gradients.

Pedinophyceae. They corresponded respectively to 82.3, 11.1, 1.6, and 0.02% of the reads of this marker. *Pedinophyceae*, the rarest clade, was detected only on the RIS gradient in only two PCRs (**Figure 6**). *Trebouxiophyceae*, and *Chlorophyceae*, the two most abundant classes see their relative abundance evolving as a function of soil pH, elevation, CWD, and FDD (**Figure 7**). Because of their large dominance and the relative measure of their abundance, the decrease of one class mechanically increased the other. It was therefore not possible from these results to decide between the different hypotheses of substitution of one class by the other, the rarefaction of one class, or the increase of the other. As for the variation in diversity presented below, environmental factors had a significant effect, with here, again, a higher variance explained by pH (R^2 = 0.22) than that explained by elevation (R^2 = 0.026). On the other hand, no effect of nitrogen or C/N ratio was detected on this variation in abundance between the two classes.

The Impact of Environmental and Bioclimatic Variables Was Significant but Small

The impact of environmental variables on *Chlorophyta* community variation was assessed using a RDA on non-scaled Hellinger transformed community data (**Figure 8**). Sites were used as a covariate. Algae species may use various sources of organic carbon available in soil (Pintaldi et al., 2021), as part of their heterotrophic and/or mixotrophic life styles, and nitrogen, including soluble nitrate, nitrite and/or ammonium, as well as colloid-bound ammonium (Lee et al., 2006). In addition, the bioavailability of inorganic nitrogen is influenced by soil pH (Lee et al., 2006). The model selection retained the seven variables considered as significant. However, the explanatory power of these variables on the variance of the communities is very low (global adjusted R^2 = 0.116). In decreasing order of influence, the variables Elevation, CWD, Nitrogen, PH, C/N ratio, FDD, and DRT have respectively an adjusted partial R^2 of 0.026, 0.025, 0.009, 0.007, 0.004, and 0.003.

Niche Description of the MOTUs Identified at the Species and Genus Levels

Fifty-one and forty-five MOTUs were assigned to a species or genus respectively. For each of these 96 taxa, the optimal range for each of the seven environmental and bioclimatic variables was determined. For each of the variables, it was possible to identify taxa with optimal ranges spanning the entire environmental gradient (**Figure 9** and **Supplementary Figures 3–15**). **Figure 9** shows the optimal elevational range of all identified genera, from lowest to highest altitude. While *Symbiochloris*, *Desmococcus*, *Chloroidium*, *Apatococcus*, *Trentepohlia* were associated with low elevation, *Actinochloris*, *Sanguina*, *Scotinosphaera*, and *Spongiochloris* were preferentially found at high elevations (**Figure 9**). Forty-three of the 96 taxa tested (18 species and 25 genera) had a niche significantly specialized compared to the tested span of environmental variables. The niche of these taxa was compared by performing a Principal Component Analysis (PCA) where each of these taxa was defined by the center of its optimum interval for each of the variables (**Figure 10**). The two first axes of the PCA carried most of the variance (66.1 and 16.6%, respectively). *Chlorophyceae* were significantly more localized to the left on this axis than *Trebouxiophyceae* (Mann–Whitney p-value = 2.5×10^{-6}). This position corresponded to a preference for higher pH and elevations, whereas *Trebouxiophyceae* prefer a higher C/N ratio and higher nitrogen. This was consistent with the impact of pH and elevation on the relative abundance of these two classes of *Chlorophyta* (**Figure 7**). The second axis, mainly related to FDD, segregates *Chlorophyceae* taxa, when *Trebouxophyceae* are closer to its center.

DISCUSSION

This work addressed the potential altitudinal zonation of green algae in mountain areas in temperate regions in the Northern hemisphere, focusing on algae populating soil, either as their natural habitat or as a transient reservoir for dormant cysts, taking the French Alps as study case. Analysis of eDNA allowed the detection of DNA fragments released by broken cells over long periods, mitigating short term temporal variations, and providing access to a "soil memory effect" (Foucher et al., 2020), of interest for such a preliminary study of the spatial distribution of algal communities. To date, and to our knowledge, no such systematic investigation has been attempted. We benefitted from the availability of soil eDNA samples, obtained by the

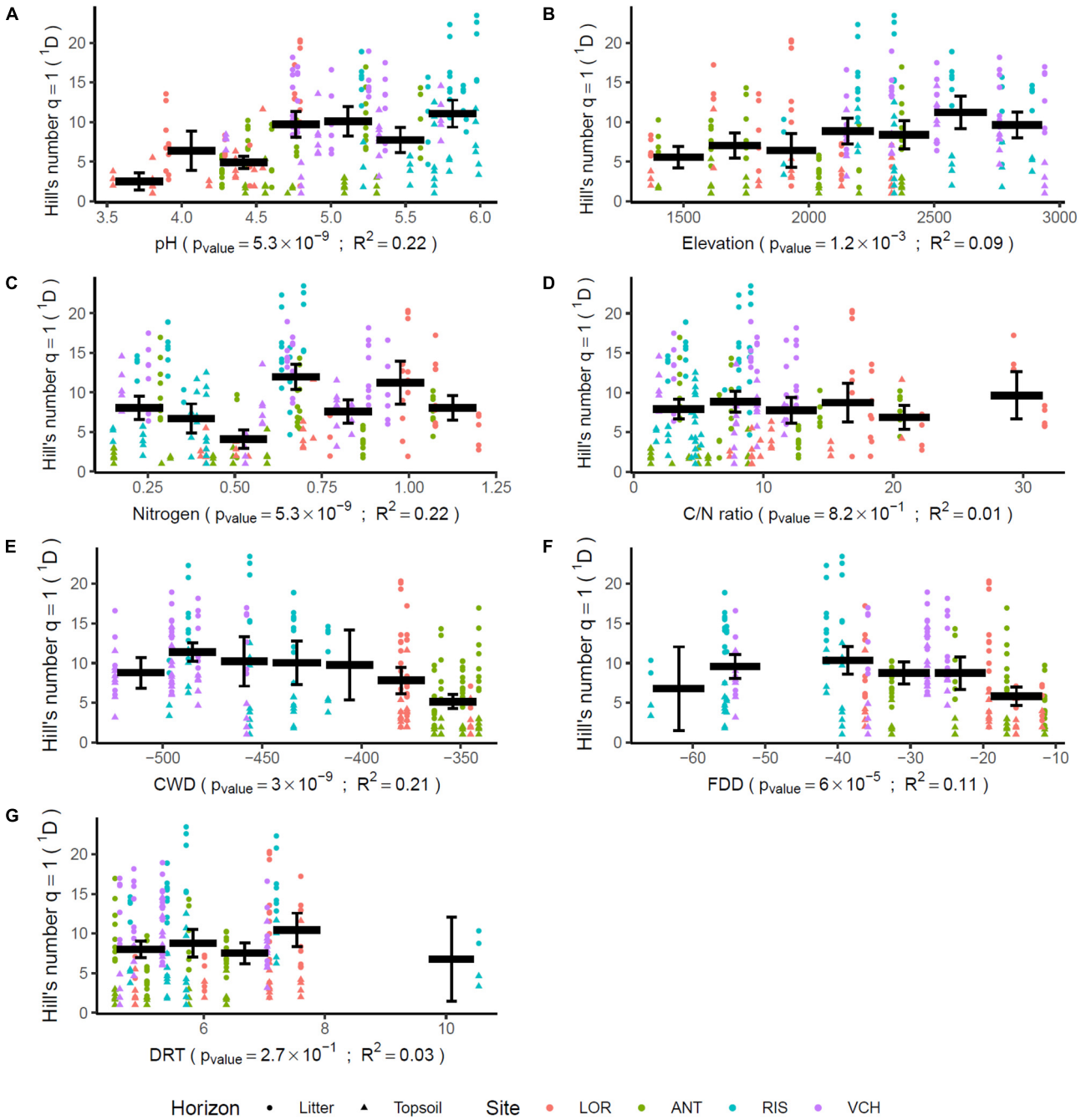

FIGURE 5 | Impact of environmental parameters on algae community diversity. Each gradient is divided in seven parts. This division allows for mixing in a single part, samples from several sites. The bold horizontal bars indicate the mean of the diversity for the covered interval. The whiskers delimitate the 95% confidence interval of that mean. The *p*-values are adjusted for multiple tests using the false discovery rate method (Benjamini and Hochberg, 1995). The determination coefficients R^2 measure the part of the variance explained by the sliced gradients using one way ANOVA.

Orchamp consortium. Five gradients have been sampled at distant locations, covering elevations from about 1,250 to 3,000 m (**Figure 1**). It must be noted that only two of the five gradients reached the niveal zone, nevertheless, they provide information on *Chlorophyta* clades present at the highest elevations. We based our study on several assumptions. The first one is that soil samples could provide information on the presence of species regardless of seasonal variations, based on the above-mentioned "soil memory effect," which may alter relative abundance, and even determine the absence or presence of some species at the time of sampling. The second assumption was that elevation gradients could be compared, and that an elevation

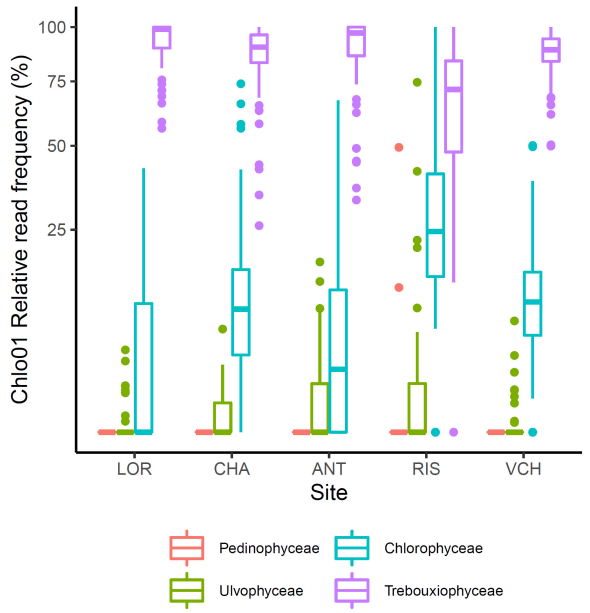

FIGURE 6 | Distribution of the four taxonomic classes of *Chlorophyta*. *Trebouxiophyceae* and *Chlorophyceae* are the two main clades. *Pedinophyceae* just occurs sporadically in two PCRs on the RIS gradient.

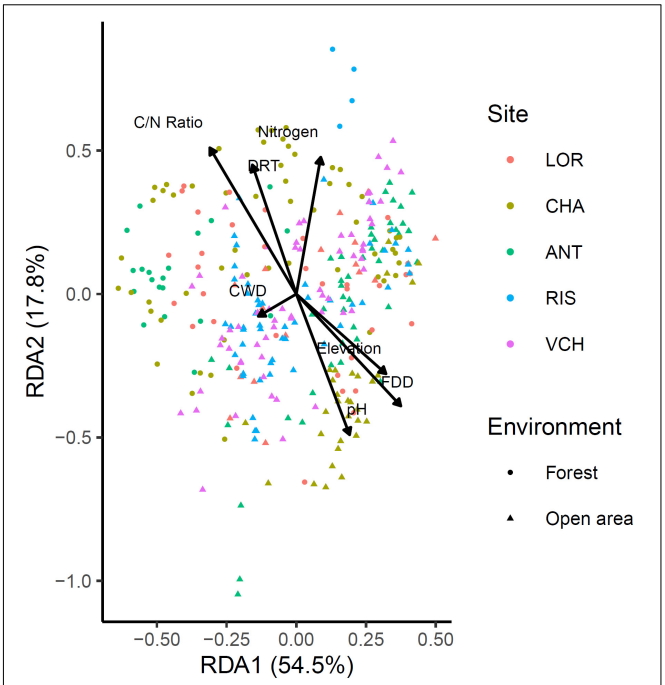

FIGURE 8 | Redundancy analysis (RDA) of the *Chlorophyta* community against seven environmental (Nitrogen, Elevation, C/N ratio, pH) and bioclimatic (DRT, CWD, FDD) variables.

in one site may correspond, approximately, to an elevation in another site.

We hypothesized that, due to their role as primary producers and as pioneer species in open areas, algal DNA could be detected in most sites. The presence of *Chlorophyta* was indeed confirmed in the five elevational gradients, and in most of the soil samples. However, based on a first evaluation using the Euka03 eukaryotic marker, it was clear that *Chlorophyta* DNA occurred in an extremely low proportion (**Figure 2** and **Table 1**). We designed, and validated, two new markers for metabarcoding studies, the *Chlorophyta* phylum marker Chlo01 in the V7 region of the 18S ribosomal RNA, to cover most of the green algae, and the *Chlorophyceae* marker Chlo02 in the

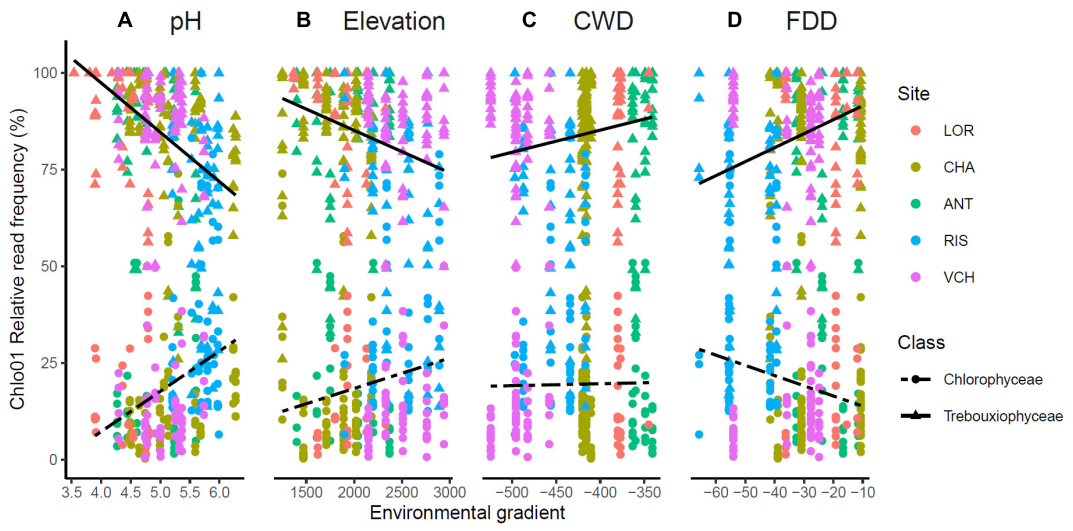

FIGURE 7 | *Trebouxiophyceae* and *Chlorophyceae* relative abundance was impacted by soil pH **(A)**, elevation **(B)**, CWD **(C)**, and FDD **(D)**. The upper lines indicate the tendency of *Trebouxiophyceae* relative abundance when the environmental (pH, elevation) or bioclimatic (CWD, FDD) values increase. The opposite trend is materialized for the *Chlorophyceae* by the bottom dashed lines.

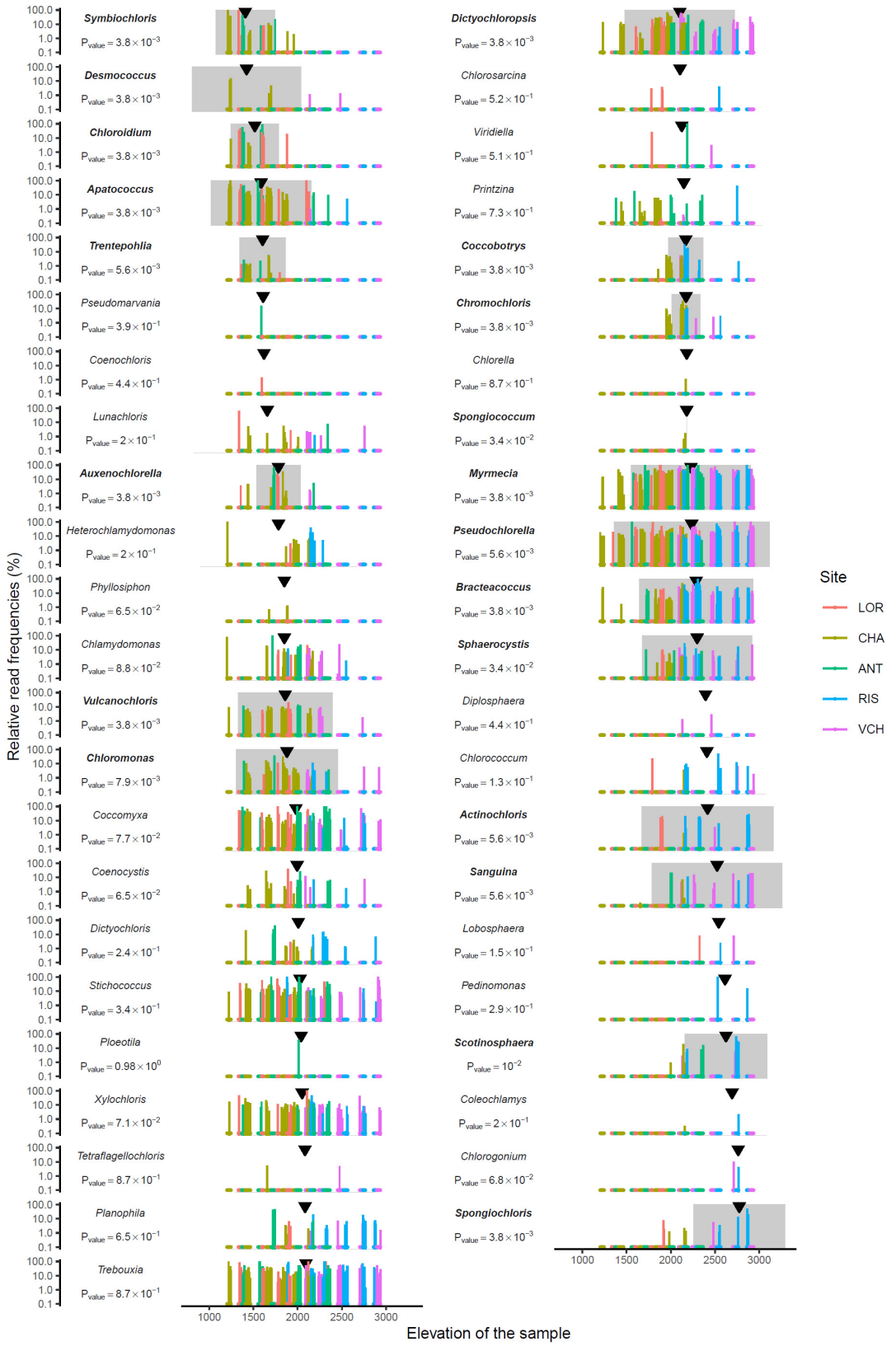

FIGURE 9 | Read relative frequency along elevation for each genus identified. Arrows indicate the median. The range in grey centered on the pic of density is where the MOTU is the most abundant. *P*-values were evaluated using the Mann–Whitney test. Bold taxon names indicate a significant *p*-value at 0.05.

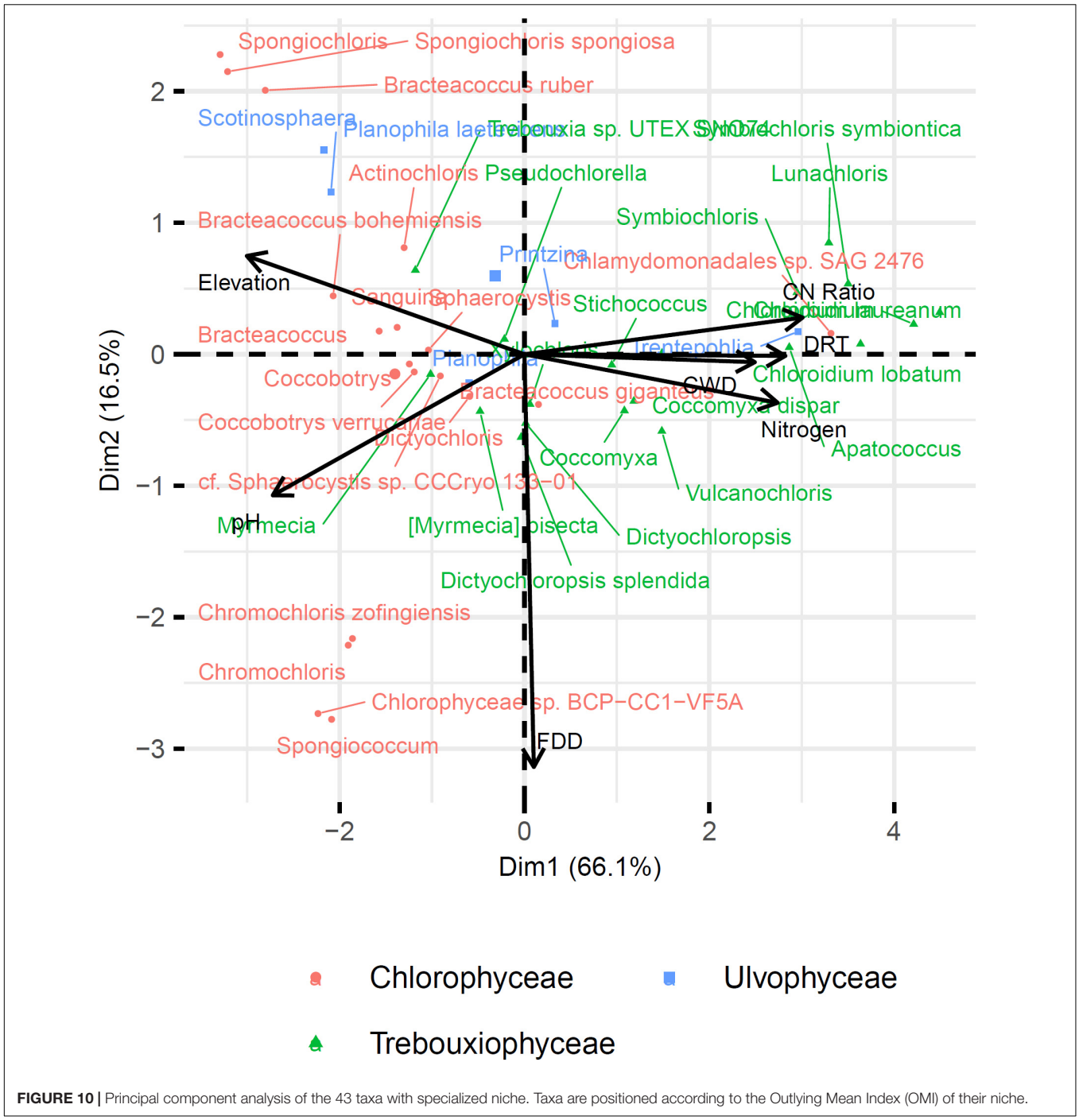

FIGURE 10 | Principal component analysis of the 43 taxa with specialized niche. Taxa are positioned according to the Outlying Mean Index (OMI) of their niche.

23S ribosomal RNA chloroplast sequence. Both improved our detection of algal DNA and the identification of algal MOTUs, still highlighting an extremely low proportion of *Chlorophyta* DNA in soil samples (**Table 1**).

The low coverage of green algae might be attributed to the higher proportion of DNA from other organisms, which present a higher biomass. Microbial communities develop in soil away from light exposure, and are therefore expected to be dominated by heterotrophic species feeding off of available organic carbon and other nutrients. Multicellular eukaryotes are also present with substantial levels in biomass, like fungi, animals or plant roots. The low proportion of algal DNA may explain why most of the MOTUs we detected appeared site-specific (**Figure 4**). This limitation should be taken into account, and hopefully corrected in future, more comprehensive analyses. Here, we therefore considered that the detected clades were probably the most abundant ones in algal communities, and that the distribution patterns we detected reflected strong trends.

Since numerous green algae have the capacity to form airborne spores (Tesson et al., 2016), allowing them to be transported by ascending winds, and since many stressful environmental parameters such as extreme temperatures and high UV light exposure are correlated with elevation, we wondered whether altitudinal zonation may be a major determinant of spatial occupancy and of biodiversity, regardless of the sampling sites. Among the seven non-collinear environmental and bioclimatic variables we monitored, pH, elevation, nitrogen content, FDD, and CWD (**Figure 5**) were significantly related to diversity. Thus, our prior assumption that elevation could be compared between sites proved to be acceptable, as this parameter appeared as one of the plausible determinants of algal distribution. Nevertheless, it was not sufficient, not even prominent, since pH and nitrogen appeared as likely more important. It must be noted that the CHA gradient showed some atypical results compared to other sites, which may be due to the location of this site, facing a highly dense urban area and likely influenced by winds streaming from the Rhône valley (**Figure 1**).

When focusing on *Chlorophyta* classes, *Trebouxiophyceae*, and *Chlorophyceae* appeared as the two most abundant ones in all our samples, consistent with their prominence in aero-terrestrial habitats. Their relative abundance was strikingly correlated with soil pH and elevation (**Figure 7**), highlighting again these two parameters as determinant. We refined our analysis on the 51 and 45 MOTUs we could assign to a species or genus, respectively, attempting to determine the optimal range for each of the four environmental variables.

The distribution at the genus level is not simple to analyze, as genera encompass a number of species, which can be distinct between samples, and/or having overlapping niches hiding more specific distributions at the species levels. Some genera, like *Stichococcus*, *Coccomyxa*, *Xylochlorus*, *Trebouxia*, *Dictiochloropsis*, *Myrmecia*, *Pseudochloroella*, or *Bracteacoccus* were detected at nearly all elevations, and the pattern of their distribution rather suggest that they correspond to cosmopolitan genera (**Figure 9**). This does not exclude that, within these genera, some species may have emerged as highly specific of certain niches. Further studies, at the species and/or ecotype levels are therefore needed for these large clades. *Desmococcus*, known to comprise species that are tolerant to desiccation (Lüttge and Büdel, 2010) or covering artificial hard surfaces in urban areas in central Europe (Hallmann et al., 2016), are associated with low elevations (**Figure 9**), possibly connected to a broader geographic distribution in valleys. *Symbiochloris*, comprising free-living and/or lichenized algae (Škaloud et al., 2016) are also associated with low elevation, but data do not allow determining whether corresponding species are lichen photobionts or not. Interestingly, the *Sanguina* genus corresponding to species causing red snow blooms, i.e., *Sanguina nivaloides* and *Sanguina aurantia* (Procházková et al., 2019), is found at elevations higher than ∼2,000 m, with an optimal occurrence at ∼2,400 m. This finding is consistent with the proliferation of *S. nivaloides* and *S. aurantia* in the snow cover encountered at these elevations. It also highlights that the soil can possibly be a long-term reservoir for these snow algae in the summer season. Surprisingly, *Sanguina* distribution did not highlight any significant correlation with the intensity of freezing events, as measured by FDD (**Figure 10** and **Supplementary Figure 12**), which may relate to the specific habitat of this genus, developing in the snow (and underneath soil), at temperatures close to 0°C, regardless of air above, which could reach much lower temperature levels. Eventually, the two genera preferentially found at high elevations were *Scotinosphaera*, described previously in various habitats in low elevations as well (Škaloud et al., 2013) and *Spongiochloris*, based on a small number of occurrence in two sites (**Figure 9**). The airborne spreading of *Spongiochloris* has been described in previous reports (Tesson et al., 2016), which may explain a transport of this taxon reported in various locations in desertic or mountain sites to such high elevation.

When focusing on species-level MOTUs (**Supplementary Figure 3**), obtained patterns needs to be considered with caution due to the lack of reference genomes of *Chlorophyta* in existing databases, and possible misannotations. Still, the number of accessions previously recorded in mountain areas or in polar regions is striking, including *Chloromonas nivalis* (optimal elevation at ∼1,800 m; Procházková et al., 2018); *Ploeotila* sp. CCCryo 086-99 (which is closely related to *Sanguina* species; Procházková et al., 2019), detected here in one sample at ∼2,000 m; *Trebouxiophyceae* sp. SC2-2 (first described in glacial refugia in Antarctica; De Wever et al., 2009), here quite cosmopolitan, with an optimal elevation at ∼2,100 m; *Sphaerocystis* sp. CCCryo 133-01 (described in moss fields along snow melt in the Spitzberg, in the CCCryo collection; Leya, 2020), here with an optimal elevation at ∼2,150 m; *Trebouxia* sp. UTEX SNO74 (previously recorded as *Chlamydomonas nivalis*, based on a collection in the snow; Matsuzaki et al., 2018), here with an optimal elevation at ∼2,500 m. In the latter case, the distribution of *Trebouxia* sp. UTEX SNO74 is broad, including occurrence at lower elevation, suggesting that species associated to this accession might be tolerant, but not specific, to the conditions found in high elevations. With optimal elevation higher than 2,500, species include *Planophila laetevirens* (previously detected in various locations in the Alps as well as high latitudes; Schmidt and Darcy, 2015), *Bracteococcus ruber* (recently detected in alpine mountains in New Zealand; Novis and Visnovsky, 2012) and *Spongiochloris spongiosa*. Taxa known to accumulate high levels of carotenoids, such as *Chromochloris zofingiensis* (Ye and Huang, 2020), *Sanguina* (Procházková et al., 2019), or *Bracteacoccus* (Chekanov et al., 2020) species were also found at high altitudes. Interestingly, in one occurrence at ∼3,000 m, *Bracteacoccus aerius* was detected. This species known to stick to dust in air suspension, may have reached the top of this mountain site via ascending winds.

Altogether, obtained data support that species-level MOTUs are likely associated with an altitudinal zonation. Other environmental factors may be also important, in combination, as shown by the distribution patterns we also obtained with pH, nitrogen and C/N (**Supplementary Figures 3–9**). We do not exclude that the taxonomic assessments presented in this study may be biased, first by a high level of similarity between the amplified DNA with that of a close but different species/accession

in the reference database, and secondly by an overrepresentation of psychrophile species in the reference database.

Our search for significant correlations highlighted that clades belonging to the *Chlorophyceae* were distinct from *Trebouxiophycea* by their preference for higher pH and elevations. By contrast, *Trebouxiophyceae* appeared to prefer a higher C/N ratio and higher nitrogen (**Figure 10**), suggesting that soil nutrients were determinant as well. When we considered all sites, the algal diversity was actually significantly higher in the litter (soil not totally decomposed) compared to the deep soil layer underneath. The litter is richer in nitrogen, carbon and organic matter and is only partially exposed to light. Based on their compositions, soils may therefore favor species being both phototroph and heterotroph, which has been known for a long time to comprise numerous *Chlorophyta* species (Parker et al., 1961). The capacity to combine phototrophy and heterotrophy, and in the case of synergies between these two energetic metabolisms, mixotrophy, seems therefore a possible strategy for algae to spread in the soil, compared to algae from lakes and rivers, which may simply rely on strict phototrophy. This metabolic capacity may therefore also be determinant at the level of genera and/or species.

CONCLUDING REMARKS

Metabarcoding is a tool of choice to study algae communities in such large areas and territories as the different mountain massifs that make up the French Alps. The main difficulty compared to other microbial phyla lies in the lack of molecular markers and the lack of reference genomes in databases. The Chlo01 and Chlo02 green algae markers developed here successfully amplified green algae from Alpine soil samples. They also amplified DNA from marine green algae strains from the RCC public collection used as positive controls. They will be extremely useful for future studies.

The amount of microalgae DNA is very small in the soil. To get a solid overview of the biodiversity of microalgae in the Alpine soil, the sampling effort should be increased as well as the number of PCR technical replicates, resembling the type of effort used for ancient or freshwater DNA (Valentini et al., 2016). Despite this technical limit, we assumed that detected DNA corresponded to the most abundant species, and we were therefore still able to draw some conclusions from this preliminary work. Firstly, our sampling sites allowed us to test whether elevation was a major, if not the most prominent, determinant of spatial distribution, based on the assumption that algae would mainly spread via airborne spores (Tesson et al., 2016) and sit in their preferred habitats under the pressure of parameters correlated with elevation, such as decreasing temperature levels and exposure to increasing UV light. A putative decline of biodiversity due to the extreme conditions in highest elevations was not evidenced. This indicates that photosynthetic eukaryotic algae are present in all niches, and that their diversity can be a source of pioneering species colonizing open areas, such as those opened by the retreat of glaciers. Comparison of read frequency along elevational gradients suggested that elevation, but also pH and soil N in combination contribute to the spatial distribution of green algae. This may be related to the role of pH in the bioavailability of soluble nitrogen (Lee et al., 2006), but one cannot exclude that some species may have optimal pH *preferenda*. Future works will therefore be needed to investigate the impact of the geological context, since all sites investigated here were crystalline and acidic. Different distribution patterns might therefore be encountered in soils covering calcareous and alkaline rocks in pre-alpine massifs. More refine analyses regarding inorganic nitrogen (nitrate, nitrite, and ammonium) are also requested. Vertical differences in green algae biodiversity supported the fact that factors other than light were determinant in the presence of species in soil, possibly acting as essential local reservoirs for a long-term occupancy of this habitat. In particular, the C/N ratios seems determinant in the case of *Trebouxiophyceae*, and future work will be needed to refine the role of this parameter in relation with the energetic metabolism of species, being not only phototrophic, but also heterotrophic and/or mixotrophic. Eventually, since atmospheric CO_2 proved to influence microbial communities in a pH-dependent manner (Gulliver et al., 2016; Yu and Chen, 2019), a relation with CO_2 solubility, bioavailability and the presence of carbon concentration mechanisms (CCM) in algal plastids need to be investigated.

At the species/accession level, an altitudinal zonation was evidenced, again with pH being determinant in the distribution pattern in a more refined manner. Some species seem cosmopolitan whereas others appear specific to some elevations and corresponding habitats; it is possible that there is an altitudinal zonation of microbial communities in a broader sense, and that there is a relationship with multicellular organisms who are also specific to certain elevations. Based on this work, some of the accessions we highlighted need to be assigned taxonomically with greater precision, to be considered as potential markers of ecosystems' evolution. *Sanguina* distribution has also attracted our attention, as it was consistently correlated with elevation, with an occurrence at altitudes higher than 2,000 m a.s.l. It is noteworthy to mention that *Sanguina* distribution pattern was not significantly correlated with the intensity of freezing events (FDD), likely related to its snow habitat which temperature is more constant, at 0°C, protected from strong temperature variations of the air above. In this matter, other taxa appear more correlated with the intensity of freezing events, possibly reflecting different adaptation strategies. Altogether, this study will help drawing up guidelines for future, more robust and precise analyses of environmental green algal DNA, from the analysis of more local patterns in some habitats such as forests, meadows, lakes, streams, glaciers, etc., to larger scale comparisons of remote sites in Alpine massifs. In addition to organic carbon, that seems essential for heterotrophic/mixotrophic species over obligate photoautotrophs, light, N, or pH, other factors like temperature, other nutrients including iron, phosphorus, etc., or the availability of water streaming from the network of rivers, lakes and/or runoff from snow/ice melting, etc., need to be considered as well. Future analyses of this group of primary producers, integrating various spatial and temporal scales could therefore help addressing the evolution of mountain habitats and ecosystems, strongly affected by the effects of climate change.

DATA AVAILABILITY STATEMENT

The original contributions presented in the study are included in the article/**Supplementary Material**. The data presented in the study and the complete details of the analysis are available on the GitHub webpage (https://alpalga.github.io/Zonation/). All the scripts used for the data analysis and the production of every figure are available on GitHub in the Alpalga/Zonation repository (https://github.com/Alpalga/Zonation).

AUTHOR CONTRIBUTIONS

AM-S and WT collected the samples along the Orchamp gradients. LG, AM-S, and DR performed DNA extractions and dilutions. AD-S and DR performed PCRs. FB, AD-S, and EC performed data filtering. AD-S and EC performed data analyses. FP provided expertise in environmental DNA analyses. J-GV, EM, and EC conceived the project. AD-S, EM, and EC contributed to the writing of the manuscript. All authors contributed to the article and approved the submitted version.

FUNDING

This work was supported by CNRS (Mission pour l'Interdisciplinarité) and National Research Agency (Alpalga ANR-20-CE02-0020, Oceanomics ANR-11-BTBR-0008, GlycoAlps ANR-15-IDEX-02, GRAL Labex ANR-10-LABEX-04, EUR CBS ANR-17-EURE-0003, GlobNets ANR−16−CE02−0009, and AnaEE-France ANR-11-INBS-0001AnaEE-Services) and from "Investissement d'Avenir" grants managed by the ANR (Montane, OSUG@2020 ANR−10−LAB−56).

ACKNOWLEDGMENTS

The authors wish to thank Ian Probert (Roscoff Culture Collection, Station Biologique de Roscoff, France) who provided marine green algae strains used as a control in this study, Isabelle Domaizon (INRAE, Thonon, France) for fruitful discussions and the consortium in charge of the Orchamp program for guidance throughout the project, DNA samples and soil analyses data (https://orchamp.osug.fr).

SUPPLEMENTARY MATERIAL

The Supplementary Material for this article can be found online at: https://www.frontiersin.org/articles/10.3389/fpls.2021.679428/full#supplementary-material

REFERENCES

Amid, C., Alako, B. T. F., Kadhirvelu, B. V., Burdett, T., Burgin, J., Fan, J., et al. (2020). The European Nucleotide Archive in 2019. *Nucleic Acids Res.* 48, D70–D76. doi: 10.1093/nar/gkz1063

Bell, G. (2013). Experimental evolution of heterotrophy in a green alga. *Evolution* 67, 468–476. doi: 10.1111/j.1558-5646.2012.01782.x

Benjamini, Y., and Hochberg, Y. (1995). Controlling the False Discovery Rate - a Practical and Powerful Approach to Multiple Testing. *J. R. Statis. Soc. B-Statis. Methodol.* 57, 289–300. doi: 10.1111/j.2517-6161.1995.tb02031.x

Benton, M. J. (2009). The Red Queen and the Court Jester: species diversity and the role of biotic and abiotic factors through time. *Science* 323, 728–732. doi: 10.1126/science.1157719

Boyer, F., Mercier, C., Bonin, A., Le Bras, Y., Taberlet, P., and Coissac, E. (2016). OBITools: a unix-inspired software package for DNA metabarcoding. *Mol. Ecol. Resour.* 16, 176–182. doi: 10.1111/1755-0998.12428

Calderòn-Sanou, I., Munkemuller, T., Boyer, F., Zinger, L., and Thuiller, W. (2020). From environmental DNA sequences to ecological conclusions: How strong is the influence of methodological choices? *J. Biogeogr.* 47, 193–206. doi: 10.1111/jbi.13681

Chekanov, K., Fedorenko, T., Kublanovskaya, A., Litvinov, D., and Lobakova, E. (2020). Diversity of carotenogenic microalgae in the White Sea polar region. *FEMS Microbiol. Ecol.* 2020:96.

De Wever, A., Leliaert, F., Verleyen, E., Vanormelingen, P., Van Der Gucht, K., Hodgson, D. A., et al. (2009). Hidden levels of phylodiversity in Antarctic green algae: further evidence for the existence of glacial refugia. *Proc. Biol. Sci.* 276, 3591–3599.

Di Mauro, B., Garzonio, R., Baccolo, G., Franzetti, A., Pittino, F., Leoni, B., et al. (2020). Glacier algae foster ice-albedo feedback in the European Alps. *Sci. Rep.* 2020, 0–9. doi: 10.1038/s41598-020-61762-0

Doledec, S., Chessel, D., and Gimaret-Carpentier, C. (2000). Niche separation in community analysis: A new method. *Ecology* 81, 2914–2927. doi: 10.1890/0012-9658(2000)081[2914:nsicaa]2.0.co;2

Domozych, D. S., Popper, Z. A., and Sorensen, I. (2016). Charophytes: Evolutionary Giants and Emerging Model Organisms. *Front. Plant Sci.* 7:1470.

Dray, S., and Dufour, A. B. (2007). The ade4 package: Implementing the duality diagram for ecologists. *J. Statist. Soft.* 22, 1–20.

Elbert, W., Weber, B., Burrows, S., Steinkamp, J., Budel, B., Andreae, M. O., et al. (2012). Contribution of cryptogamic covers to the global cycles of carbon and nitrogen. *Nat. Geosci.* 5, 459–462. doi: 10.1038/ngeo1486

Fan, J., Huang, J., Li, Y., Han, F., Wang, J., Li, X., et al. (2012). Sequential heterotrophy-dilution-photoinduction cultivation for efficient microalgal biomass and lipid production. *Bioresour. Technol.* 112, 206–211. doi: 10.1016/j.biortech.2012.02.046

Ficetola, G. F., Coissac, E., Zundel, S., Riaz, T., Shehzad, W., Bessiere, J., et al. (2010). An in silico approach for the evaluation of DNA barcodes. *BMC Genomics* 11:434. doi: 10.1186/1471-2164-11-434

Ficetola, G. F., Taberlet, P., and Coissac, E. (2016). How to limit false positives in environmental DNA and metabarcoding? *Mol. Ecol. Resour.* 16, 604–607. doi: 10.1111/1755-0998.12508

Foets, J., Wetzel, C. E., Teuling, A. J., and Pfister, L. (2020). Temporal and spatial variability of terrestrial diatoms at the catchment scale: controls on productivity and comparison with other soil algae. *PeerJ.* 8:e9198. doi: 10.7717/peerj.9198

Foucher, A., Evrard, O., Ficetola, G. F., Gielly, L., Poulain, J., Giguet-Covex, C., et al. (2020). Persistence of environmental DNA in cultivated soils: implication of this memory effect for reconstructing the dynamics of land use and cover changes. *Sci. Rep.* 10:10502.

Gartner, G. (2004). ASIB - The Culture Collection of Algae at the Botanical Institute, Innsbruck, Austria. *Nova Hedwigia* 79, 71–76. doi: 10.1127/0029-5035/2004/0079-0071

Geremia, R. A., Puscas, M., Zinger, L., Bonneville, J. M., and Choler, P. (2016). Contrasting microbial biogeographical patterns between anthropogenic subalpine grasslands and natural alpine grasslands. *N. Phytol.* 209, 1196–1207. doi: 10.1111/nph.13690

Groendahl, S., Kahlert, M., and Fink, P. (2017). The best of both worlds: A combined approach for analyzing microalgal diversity via metabarcoding and

morphology-based methods. *PLoS One* 12:e0172808. doi: 10.1371/journal.pone.0172808

Gulliver, D. M., Lowry, G. V., and Gregory, K. B. (2016). Comparative Study of Effects of CO2 Concentration and pH on Microbial Communities from a Saline Aquifer, a Depleted Oil Reservoir, and a Freshwater Aquifer. *Env. Eng. Sci.* 33, 806–816. doi: 10.1089/ees.2015.0368

Hall, J. D., Fucikova, K., Lo, C., Lewis, L. A., and Karol, K. G. (2010). An assessment of proposed DNA barcodes in freshwater green algae. *Criptogamie Algol.* 31, 529–555.

Hallmann, C., Hoppert, M., Mudimu, O., and Friedl, T. (2016). Biodiversity of green algae covering artificial hard substrate surfaces in a suburban environment: a case study using molecular approaches. *J. Phycol.* 52, 732–744. doi: 10.1111/jpy.12437

Heeger, F., Bourne, E. C., Baschien, C., Yurkov, A., Bunk, B., Sproer, C., et al. (2018). Long-read DNA metabarcoding of ribosomal RNA in the analysis of fungi from aquatic environments. *Mol. Ecol. Resour.* 18, 1500–1514. doi: 10.1111/1755-0998.12937

Hisakawa, N., Quistad, S. D., Hester, E. R., Martynova, D., Maughan, H., Sala, E., et al. (2015). Metagenomic and satellite analyses of red snow in the Russian Arctic. *PeerJ.* 3:e1491. doi: 10.7717/peerj.1491

Hoham, R. W., and Remias, D. (2019). Snow and Glacial Algae: A Review. *J. Phycol.* 56, 264–282. doi: 10.1111/jpy.12952

Holzinger, A., Allen, M. C., and Deheyn, D. D. (2016). Hyperspectral imaging of snow algae and green algae from aeroterrestrial habitats. *J. Photochem. Photobiol. B* 162, 412–420. doi: 10.1016/j.jphotobiol.2016.07.001

Holzinger, A., Herburger, K., Blaas, K., Lewis, L. A., and Karsten, U. (2017). The terrestrial green macroalga Prasiola calophylla (Trebouxiophyceae, Chlorophyta): ecophysiological performance under water-limiting conditions. *Protoplasma* 254, 1755–1767. doi: 10.1007/s00709-016-1068-6

Hotaling, S., Hood, E., and Hamilton, T. L. (2017). Microbial ecology of mountain glacier ecosystems: biodiversity, ecological connections and implications of a warming climate. *Environ. Microbiol.* 19, 2935–2948. doi: 10.1111/1462-2920.13766

Hubert, P. (1981). *Robust statistics*. New York,NY: John Wiley & Sons.

Jacquemin, C., Bertrand, C., Franquet, E., Mounier, S., Misson, B., Oursel, B., et al. (2019). Effects of catchment area and nutrient deposition regime on phytoplankton functionality in alpine lakes. *Sci. Total Environ.* 674, 114–127. doi: 10.1016/j.scitotenv.2019.04.117

John, D., Whitton, B., and Brook, A. (2011). *The Freshwater Algal Flora of the British Isles An Identification Guide to Freshwater and Terrestrial Algae Second Edition*. Cambridge,MA: Cambridge University Press.

Kapraun, D. F. (2007). Nuclear DNA Content Estimates in Green Algal Lineages : Chlorophyta and Streptophyta. *Ann. Bot.* 99, 677–701. doi: 10.1093/aob/mcl294

Karsten, U., and Holzinger, A. (2014). Green algae in alpine biological soil crust communities: acclimation strategies against ultraviolet radiation and dehydration. *Biodiv. Conserv.* 23, 1845–1858. doi: 10.1007/s10531-014-0653-2

Kastovska, K., Elster, J., Stibal, M., and Santruckova, H. (2005). Microbial assemblages in soil microbial succession after glacial retreat in Svalbard (high arctic). *Microb. Ecol.* 50, 396–407. doi: 10.1007/s00248-005-0246-4

Koelewijn, H. P., De La Guerie, P., and Bell, G. (2001). Variation in growth rate in a natural assemblage of unicellular green soil algae. *Heredity* 87, 162–171. doi: 10.1046/j.1365-2540.2001.00887.x

Körner, C. (2021). *Alpine Plant Life: Functional Plant Ecology of High Mountain Ecosystems*. Berlin: Springer.

Lee, M. S., Lee, K. K., Hyun, Y. J., Clement, T. P., and Hamilton, D. (2006). Nitrogen transformation and transport modeling in groundwater aquifers. *Ecol. Model.* 192, 143–159. doi: 10.1016/j.ecolmodel.2005.07.013

Lewis, L. A., and Mccourt, R. M. (2004). Green algae and the origin of land plants. *Am. J. Bot.* 91, 1535–1556. doi: 10.3732/ajb.91.10.1535

Leya, T. (2020). The CCCryo Culture Collection of Cryophilic Algae as a valuable bioresource for algal biodiversity and for novel, industrially marketable metabolites. *Appl. Phycol.* 2020, 1–22. doi: 10.1080/26388081.2020.1753572

Li, L., Wang, S., Wang, H., Sahu, S. K., Marin, B., Li, H., et al. (2020). The genome of Prasinoderma coloniale unveils the existence of a third phylum within green plants. *Nat. Ecol. Evol.* 2020:7. doi: 10.1038/s41559-020-1221-7

Lu, N., Chen, J. H., Wei, D., Chen, F., and Chen, G. (2016). Global Metabolic Regulation of the Snow Alga Chlamydomonas nivalis in Response to Nitrate or Phosphate Deprivation by a Metabolome Profile Analysis. *Int. J. Mol. Sci.* 2016:17.

Lukes, M., Prochazkova, L., Shmidt, V., Nedbalova, L., and Kaftan, D. (2014). Temperature dependence of photosynthesis and thylakoid lipid composition in the red snow alga Chlamydomonas cf. nivalis (Chlorophyceae). *FEMS Microbiol. Ecol.* 89, 303–315. doi: 10.1111/1574-6941.12299

Lüttge, U., and Büdel, B. (2010). Resurrection kinetics of photosynthesis in desiccation−tolerant terrestrial green algae (Chlorophyta) on tree bark. *Plant Biol.* 12, 437–444. doi: 10.1111/j.1438-8677.2009.00249.x

Lutz, S., Anesio, A. M., Raiswell, R., Edwards, A., Newton, R. J., Gill, F., et al. (2016). The biogeography of red snow microbiomes and their role in melting arctic glaciers. *Nat. Commun.* 7:11968.

Martinez-Almoyna, C., Thuiller, W., Chalmandrier, L., Ohlmann, M., Foulquier, A., Clément, J.-C., et al. (2019). Multi-trophic β-diversity mediates the effect of environmental gradients on the turnover of multiple ecosystem functions. *Funct. Ecol.* 33, 2053–2064. doi: 10.1111/1365-2435.13393

Martinez-Almoyna, C., Piton, G., Abdulhak, S., Boulangeat, L., Choler, P., Delahaye, T., et al. (2020). Climate, soil resources and microbial activity shape the distributions of mountain plants based on their functional traits. *Ecography* 43, 1–11. doi: 10.1111/ecog.05269

Matsuzaki, R., Nozaki, H., and Kawachi, M. (2018). Taxonomic revision of Chloromonas nivalis (Volvocales, Chlorophyceae) strains, with the new description of two snow-inhabiting Chloromonas species. *PLoS One* 13:e0193603. doi: 10.1371/journal.pone.0193603

Novis, P. M., and Visnovsky, G. (2012). Novel alpine algae from New Zealand: Chlorophyta. *Phytotaxa* 39, 1–30. doi: 10.11646/phytotaxa.39.1.1

Oksanen, A. J., Blanchet, F. G., Friendly, M., Kindt, R., Legendre, P., Mcglinn, D., et al. (2020). Vegan: Community Ecology Package. R package version 2.5-7. Available online at: https://CRAN.R-project.org/package=vegan ISSN.

Parker, B. C., Bold, H. C., and Deason, T. R. (1961). Facultative heterotrophy in some chlorococcacean algae. *Science* 133, 761–763. doi: 10.1126/science.133.3455.761

Pfendler, S., Karimi, B., Maron, P. A., Ciadamidaro, L., Valot, B., Bousta, F., et al. (2018). Biofilm biodiversity in French and Swiss show caves using the metabarcoding approach: First data. *Sci. Total Environ.* 615, 1207–1217. doi: 10.1016/j.scitotenv.2017.10.054

Pintaldi, E., D'amico, M. E., Colombo, N., Colombero, C., Sambuelli, L., De Regibus, C., et al. (2021). Hidden soils and their carbon stocks at high-elevation in the European Alps (North-West Italy). *Catena* 2021:198.

Procházková, L., Remias, D., Øezanka, T., and Nedbalová, L. (2018). Chloromonas nivalis subsp. tatrae, subsp. nov. (Chlamydomonadales, Chlorophyta): re–examination of a snow alga from the High Tatra Mountains (Slovakia). *Fottea* 18:1. doi: 10.5507/fot.2017.010

Procházková, L., Leya, T., Køížková, H., and Nedbalová, L. (2019). Sanguina nivaloides and Sanguina aurantia gen. et spp. nov. (Chlorophyta): the taxonomy, phylogeny, biogeography and ecology of two newly recognised algae causing red and orange snow. *FEMS Microb. Ecol.* 95:fiz064.

R Development Core Team (2019). *R: A Language and Environment for Statistical Computing*. Vienna: R Foundation for Statistical Computing.

Rehakova, K., Chlumska, Z., and Dolezal, J. (2011). Soil cyanobacterial and microalgal diversity in dry mountains of Ladakh, NW Himalaya, as related to site, altitude, and vegetation. *Microb. Ecol.* 62, 337–346. doi: 10.1007/s00248-011-9878-8

Reisigl, H. (1964). Zur Systematik und Okologie alpiner Bodenalgen. *Osterr. Bot. Z.* 116, 492–506.

Reisigl, H. (1969). Bodenalgen-Studien II. *Osterreichische Botanische Zeitschrift* 116, 492–506. doi: 10.1007/bf01379645

Remias, D. (2012). "Cell Structure and Physiology of Alpine Snow and Ice Algae," in *Plants in Alpine Regions*, ed. C. Lütz (Vienna: Springer), 175–186. doi: 10.1007/978-3-7091-0136-0_13

Riaz, T., Shehzad, W., Viari, A., Pompanon, F., Taberlet, P., and Coissac, E. (2011). ecoPrimers: inference of new DNA barcode markers from whole genome sequence analysis. *Nucleic Acids Res.* 39, e145. doi: 10.1093/nar/gkr732

Rindi, F., Allali, H. A., Lam, D. W., and López-Bautista, J.-M. (2010). "An overview of the biodiversity and biogeography of terrestrial green algae," in *Biodiversity Hotspots*, eds V. Rescigno and S. Maletta (New York, NY: Nova Science), 105–122.

Robertson, G. P., Coleman, D. C., Sollins, P., and Bledsoe, C. S. (1999). *Standard soil methods for long−term ecological research*, Vol. 2. New York, NY: Oxford University Press.

Schneider, T. D., and Stephens, R. M. (1990). Sequence Logos: A New Way to Display Consensus Sequences. *Nucleic Acids Res.* 18, 6097–6100. doi: 10.1093/nar/18.20.6097

Sheather, S. A. (2009). Modern Approach to Regression with R. *Sci. Business Media* 2009, 9780387096087.

Schmidt, S. K., and Darcy, J. L. (2015). Phylogeny of ulotrichalean algae from extreme high-altitude and high-latitude ecosystems. *Polar Biol.* 38, 689–697. doi: 10.1007/s00300-014-1631-6

Schmeisser, C., Steele, H., and Streit, W. R. (2007). Metagenomics, biotechnology with non-culturable microbes. *Appl. Microbiol. Biotechnol.* 75, 955–962. doi: 10.1007/s00253-007-0945-5

Škaloud, P., Kalina, T., Nemjová, K., De Clerck, O., and Leliaert, F. (2013). Morphology and phylogenetic position of the freshwater green microalgae Chlorochytrium (Chlorophyceae) and Scotinosphaera (Scotinosphaerales, ord. nov., Ulvophyceae). *J. Phycol.* 49, 115–129. doi: 10.1111/jpy.12021

Škaloud, P., Friedl, T., Hallmann, C., Beck, A., and Dal Grande, F. (2016). Taxonomic revision and species delimitation of coccoid green algae currently assigned to the genus Dictyochloropsis (Trebouxiophyceae, Chlorophyta). *J. Phycol.* 52, 599–617. doi: 10.1111/jpy.12422

Taberlet, P., Prud'Homme, S. M., Campione, E., Roy, J., Miquel, C., Shehzad, W., et al. (2012). Soil sampling and isolation of extracellular DNA from large amount of starting material suitable for metabarcoding studies. *Mol. Ecol.* 21, 1816–1820. doi: 10.1111/j.1365-294x.2011.05317.x

Taberlet, P., Bonin, A., Zinger, L., and Coissac, E. (2018). *Environmental DNA: For Biodiversity Research and Monitoring*. Oxford: Oxford University Press.

Tchan, Y. T. (1952). Counting soil algae by direct fluorescence microscopy. *Nature* 170, 328–329. doi: 10.1038/170328b0

Tesson, S. V. M., Skjoth, C. A., Santl-Temkiv, T., and Londahl, J. (2016). Airborne Microalgae: Insights, Opportunities, and Challenges. *Appl. Environ. Microbiol.* 82, 1978–1991. doi: 10.1128/aem.03333-15

Tschaikner, A., Ingolic, E., and Gartner, G. (2007). Observations in a new isolate of Coelastrella terrestris (REISIGL) HEGEWALD & HANAGATA (Chlorophyta, Scenedesmaceae) from alpine soil (Tyrol, Austria). *Phyton-Annales Rei Botanicae* 46, 237–245.

Valentini, A., Taberlet, P., Miaud, C., Civade, R., Herder, J., Thomsen, P. F., et al. (2016). Next-generation monitoring of aquatic biodiversity using environmental DNA metabarcoding. *Mole. Ecol.* 25, 929–942. doi: 10.1111/mec.13428

Vieira, H. H., and Bagatini, I. L. (2016). tufA gene as molecular marker for freshwater Chlorophyceae. *Algae* 31, 155–165. doi: 10.4490/algae.2016.31.4.14

Ward, R. D., Zemlak, T. S., Innes, B. H., Last, P. R., and Hebert, P. D. (2005). DNA barcoding Australia's fish species. *Philos. Trans. R. Soc. Lond. B Biol. Sci.* 360, 1847–1857.

Wickham, H. (2011). *ggplot2*, Vol. 3. Hoboken, NJ: WIREs Computational Statistics, 180–185. doi: 10.1002/wics.147

Ye, Y., and Huang, J. C. (2020). Defining the biosynthesis of ketocarotenoids in Chromochloris zofingiensis. *Plant Divers* 42, 61–66. doi: 10.1016/j.pld.2019.11.001

Yu, T., and Chen, Y. G. (2019). Effects of elevated carbon dioxide on environmental microbes and its mechanisms: A review. *Sci. Total Env.* 655, 865–879. doi: 10.1016/j.scitotenv.2018.11.301

Zou, S., Fei, C., Wang, C., Gao, Z., Bao, Y., He, M., et al. (2016). How DNA barcoding can be more effective in microalgae identification: a case of cryptic diversity revelation in Scenedesmus (Chlorophyceae). *Sci. Rep.* 6:36822.

Conflict of Interest: The authors declare that the research was conducted in the absence of any commercial or financial relationships that could be construed as a potential conflict of interest.

frontiers in Plant Science

ORIGINAL RESEARCH
published: 07 June 2021
doi: 10.3389/fpls.2021.662298

Revealing the Characteristics of the Antarctic Snow Alga *Chlorominima collina* gen. et sp. nov. Through Taxonomy, Physiology, and Transcriptomics

Francisca E. Gálvez[1,2], Mónica Saldarriaga-Córdoba[3], Pirjo Huovinen[1,2], Andrea X. Silva[4,5] and Iván Gómez[1,2]*

[1] Instituto de Ciencias Marinas y Limnológicas, Facultad de Ciencias, Universidad Austral de Chile, Valdivia, Chile, [2] Centro FONDAP de Investigación en Dinámica de Ecosistemas Marinos de Altas Latitudes (IDEAL), Valdivia, Chile, [3] Centro de Investigación en Recursos Naturales y Sustentabilidad (CIRENYS), Universidad Bernardo O'Higgins, Santiago, Chile, [4] Instituto de Ciencias Ambientales y Evolutivas, Facultad de Ciencias, Universidad Austral de Chile, Valdivia, Chile, [5] AUSTRAL-omics, Vicerrectoría de Investigación, Desarrollo y Creación Artística, Universidad Austral de Chile, Valdivia, Chile

OPEN ACCESS

Edited by:
Linda Nedbalová, Faculty of Science, Charles University, Czechia

Reviewed by:
Thomas Leya, Branch Bioanalytics and Bioprocesses (IZI-BB), Potsdam-Golm, Germany
Claire Remacle, University of Liège, Belgium

***Correspondence:**
Francisca E. Gálvez
franciscaelibethgalvez@gmail.com

Specialty section:
This article was submitted to Marine and Freshwater Plants, a section of the journal Frontiers in Plant Science

Received: *01 February 2021*
Accepted: *10 May 2021*
Published: *07 June 2021*

Citation:
Gálvez FE, Saldarriaga-Córdoba M, Huovinen P, Silva AX and Gómez I (2021) Revealing the Characteristics of the Antarctic Snow Alga Chlorominima collina gen. et sp. nov. Through Taxonomy, Physiology, and Transcriptomics. Front. Plant Sci. 12:662298. doi: 10.3389/fpls.2021.662298

Snow algae play crucial roles in cold ecosystems, however, many aspects related to their biology, adaptations and especially their diversity are not well known. To improve the identification of snow algae from colored snow, in the present study we used a polyphasic approach to describe a new Antarctic genus, *Chlorominima* with the species type *Chlorominima collina*. This new taxon was isolated of colored snow collected from the Collins Glacier (King George Island) in the Maritime Antarctic region. Microscopy revealed biflagellated ellipsoidal cells with a rounded posterior end, a C-shaped parietal chloroplast without a pyrenoid, eyespot, and discrete papillae. Several of these characteristics are typical of the genus *Chloromonas*, but the new isolate differs from the described species of this genus by the unusual small size of the cells, the presence of several vacuoles, the position of the nucleus and the shape of the chloroplast. Molecular analyzes confirm that the isolated alga does not belong to *Chloromonas* and therefore forms an independent lineage, which is closely related to other unidentified Antarctic and Arctic strains, forming a polar subclade in the *Stephanosphaerinia* phylogroup within the Chlamydomonadales. Secondary structure comparisons of the ITS2 rDNA marker support the idea that new strain is a distinct taxon within of *Caudivolvoxa*. Physiological experiments revealed psychrophilic characteristics, which are typical of true snow algae. This status was confirmed by the partial transcriptome obtained at 2°C, in which various cold-responsive and cryoprotective genes were identified. This study explores the systematics, cold acclimatization strategies and their implications for the Antarctic snow flora.

Keywords: Antarctic, *Chlorominima*, polyphasic approach, psychrophilic, snow algae, cysts, transcriptome

INTRODUCTION

The cryospheric biome is dominated by highly specialized microorganisms that thrive under extreme low temperatures at the interface between snow/ice and liquid water (Anesio and Laybourn-Parry, 2012). The basis of these microbial communities, and hence the precursors of inorganic carbon fixation and primary source of macromolecules, are snow and ice algae, and cyanobacteria (Boetius et al., 2015; Anesio et al., 2017). Especially during the thaw season, these algae actively fix carbon (Yallop et al., 2012; Lutz et al., 2014). In fact, daily measurements of gas exchange in dense patches of snow algae have shown values of CO_2 uptake close to 2,300 μmol m^{-2} day^{-1}, indicating that summer snowfields can be surprisingly productive and even in some circumstances can be a significant CO_2 sink (Williams et al., 2003; Hamilton and Havig, 2017). Snow algae play crucial ecological roles as foundation organisms sustaining a high diversity of heterotrophic micro-eukaryotes, bacteria, and archaea (Lutz et al., 2015; Havig and Hamilton, 2019). The biological interactions within these communities, especially mutualism, have enhanced resilience to changes in the snow environment (Krug et al., 2020). In fact, it has been suggested that such biological processes can promote horizontal exchange and recombination of genetic material, which enables the acquisition of new genes, enhancing diversity (Lyon and Mock, 2014; Liu et al., 2018).

The identification of snow algae had previously been limited to morphological observations of cysts of red snow that were recognized as zygotes of the algae *Chlamydomonas nivalis* (Bauer) Wille and *Chloromonas nivalis* (Chodat) Hoham and Mullet. Therefore, these species were recurrently associated with the global distribution of cysts, resulting in cosmopolitan species (Marchant, 1982; Gradinger and Nürnberg, 1996; Müller et al., 1998). In the case of green snow, the identification of vegetative cells, also was normally based only on microscopic observations (Kol, 1968; Ettl, 1970). This has probably challenged the comprehensive identification of cryosestic algae in the past. However, the use of polyphasic approaches that include the combined use of multi-gene analyses, light and electron microscopy, biochemical and physiological approaches (Pröschold and Leliaert, 2007), strain designations by culture collections, as well as a better access to samples from previously inaccessible regions, has allowed both the re-examination of many strains of snow algae and the description of novel lineages (Muramoto et al., 2010; Demchenko et al., 2012; Matsuzaki et al., 2014; Hoham and Remias, 2020). To the date, polyphasic analyses show that field-collected cysts identified as *Chloromonas nivalis* zygotes consist actually of multiple species (Matsuzaki et al., 2018, 2019). Extensive phylogenetic analyses performed on the *Chlamydomonas–Chloromonas* complex have shown that 21 taxa from cold environments occur in four clades (Hoham et al., 2002; Remias et al., 2010) being most of the snow algae included in the phylogroup *Chloromonadinia* (Nakada et al., 2008). Another clade composed of algae that cause reddish coloration includes the new genus *Sanguina* (Procházková et al., 2019a). Thus, it is possible to argue that diversity of snow algae has been underestimated and is just being revealed.

For Antarctica, since the first microscopic surveys (Fogg, 1967; Kol, 1971; Broady, 1996; Ling, 1996) it has been recognized that snow fields from continental and insular regions host abundant and diverse communities of snow algae. However, only few of these snow algae have been identified with certainty (Ling, 1996). In the case of the Maritime Antarctic region, especially the South Shetland Islands, the snow algae communities were dominated by species of the Trebouxiophyceae and Chlorophyceae classes, whose structure and functional traits are set basically by the marine influence, sources of eutrophication and color of bloom (Komárek and Komárek, 1999, 2001; Soto et al., 2020).

Considering that regional warming has become an important environmental threat in the Maritime Antarctic (Vaughan et al., 2003), the biological processes, and fate of snow microbial communities will be strongly impacted by melting (Boetius et al., 2015; Garcia-Lopez and Cid, 2017). For example, the Collins Glacier in King George Island, has lost 8.42% of its mass between 1,983 and 2,012, mostly in the north and central-west sectors (Cook, 2005; Simoes et al., 2015). In a first stage, snow algae could be favored in ablation zones as melting provides suitable environments for their development, thus reducing albedo and exacerbating melting (Huovinen et al., 2018). As a contribution to the knowledge of the Antarctic cryoflora, we isolated a new alga (*Chlorominima*) from the red snow of this glacier that is in close proximity to the coast. Snowfields close to marine bird and seal colonies are typical sites for the development of snow algae in Antarctica due to a high nutrient input (Kol and Flint, 1968; Komárek and Komárek, 1999; Remias et al., 2013). To continue monitoring the consequences of melting of the glaciers on the microbial diversity it is relevant not only to perform accurate taxonomic identifications, but also to characterize physiological responses and perform gene profiling to gain insight into the dynamic and functions of snow algae under changing environmental scenarios (Cvetkovska et al., 2017; Garcia-Lopez and Cid, 2017).

The present study aimed (i) to propose a new genus, with the species type *Chlorominima collina* identified through an integrative approach of cultures obtained from samples collected from the Collins Glacier, King George Island; and (ii) to combine physiological and transcriptional approaches to describe some key adaptive traits that allow this organism thriving under permanently low temperatures. Thus, this report connects systematics aspects with the ecology and functionality of an Antarctic snow alga from a region that is being impacted by multiple environmental changes.

MATERIALS AND METHODS

Sample Collection, Isolation and Cultivation

Red snow samples were collected from the surface of the Collins Glacier, King George Island, South Shetland Islands (62°10′5.412″S, 58°51′18.216″W), in February 2018. Each sample (approximately 400 g) was excavated 5 cm deep with a sterile metal spatula, transferred to an 18 cm × 20 cm sterile plastic bag and transported to the laboratory in the station "Base Profesor

Julio Escudero." After melting at 4°C, aliquots of 40 ml were stored in culture bottles (TR6000, TrueLine, United States) with 10 ml of 1% Bold's basal medium (BBM, Bischoff and Bold, 1963). These bottles were transported in a cooling box at no more than 10°C to the Photobiology Laboratory of the Universidad Austral de Chile, in Valdivia, where they were kept in a cold room at 1°C. Samples were taken from one of the bottles in a 2.0-ml graduated microcentrifuge tube (Sorenson^{TM} BioScience, Inc., United States) under a laminar flow hood. Cysts were harvested and washed by centrifugation (3,500 rpm for 5 min at 4°C) four times with 1% BBM. Before cyst selection, the samples were examined under light microscopy to ensure that the cysts were free of other algae or microorganisms. Most of the observed cysts were in an early developing stage. Individual cysts were isolated manually under a microscope with a sterile glass micropipette (from Pasteur pipette) and then sown on agar plates with 1% BBM. The plates were kept in a cold room at 2°C with a photoperiod of 16:8 h light:dark (L:D) at photosynthetically active radiation (PAR) of 20–30 μmol m^{-2} s^{-1} provided by fluorescent tubes (T8, 36W-cold white, Westinghouse). The first green colonies were obtained after 8 weeks (**Figure 1**). A strain was isolated by means of serial dilutions in combination with differential centrifugation (Andersen, 2005). The isolated strain was transferred to Erlenmeyer flasks containing 1% BBM and cultivated in a cold room at 2°C. The isolate has been deposited and is available in the Culture Collection of Algae and Protozoa (CCAP), SAMS Limited, Scottish Marine institute, under strain number CCAP 6/1.

Light and Electron Microscopy

The isolate was studied under light microscopy with an Olympus BX51 (Tokyo, Japan). Photomicrographs were taken with a QImaging MicroPublisher 5.0 digital camera, with Real Time Viewing (RTV). The QCapture Pro-6.0 (Teledyne Photometrics, Tucson, AR, United States) microimaging software was used to process images and obtain morphometric measurements of the cells. For transmission electron microscopy (TEM) two samples were taken, one of the mother culture with fresh medium and other from an old culture, both kept at 2°C. These samples were fixed in 2.5% glutaraldehyde and 0.1 M sodium cacodylate buffer (pH 7.2) for 24 h. Samples were washed with the cacodylate buffer (3 × 15 min) and subsequently fixed in 1% OsO_4 at 4°C under shaking. After washing with deionized water (3 × 15 min) the fixed samples were dehydrated through a series of ethanol (35, 50, 70, 80, 96, and 100% for 10 min each), transferred to acetone (3 × 100% for 15 min) and finally embedded in epon resin: acetone-epon (1:1) from the EMBed-812 kit and then left in neat epon for polymerization at 60 °C during 24 h. Semi-fine sections (stained with toluidine blue) and ultra-fine sections were prepared with a Leica EM UC7 automatic ultramicrotome (Leica, Germany) and stained with 2% aqueous uranyl acetate and lead citrate for 5 min. The sections were examined using a Libra 120 Plus Transmission Electron Microscope, 80,000 KV acceleration voltage (Carl Zeiss, Germany). Photomicrographs were obtained using a Veleta CCD camera (EMSIS) equipped with Zemas V2.0 image analysis software. The images were tagged with Adobe Illustrator 2019 (version 23.03).

DNA Extraction, PCR and Sequencing

Total genomic DNA was extracted with the GenElute Plant Genomic DNA Miniprep Kit (Sigma-Aldrich). According to this protocol, cells were ground in a mortar and pestle with liquid nitrogen, until obtaining 100 mg of powder. PCRs were performed using KAPA Taq HotStart PCR Kit, in a total volume of 12.5 μl (6.25 μl of the mix, 2.5 μl of primers and 1.25 μl of DNA). The 18S rRNA gene was amplified using the universal eukaryotic primers NS1 (White et al., 1990) and 18L (Hamby et al., 1988), with the cycling program as described in a previous study (Barcytė et al., 2018a). The region was sequenced with primers NS1 (White et al., 1990), 891F, 1122F (T. Friedl, unpublished) 18L (Hamby et al., 1988), 895R (Remias et al., 2012), and 1122R (T Friedl, unpublished). The complete region of the ITS was amplified with the ITS1 and ITS4 primers (White et al., 1990), following the cycling program of Barcytė et al. (2018a). The region was sequenced with primers ITS1 (White et al., 1990), 1800F (Friedl, 1996), 5.8 SbF (Mikhailyuk et al., 2008) and ITS2, ITS4, and LR3 (Vilgalys and Hester, 1990). Finally, a part of the ribulose-1,5-biphosphate carboxylase oxygenase (Rubisco) large subunit (rbcL) gene was amplified and sequenced with the primers rbcL1F and rbcL23R and the cycling program detailed in a previous study (Hoham et al., 2002). The PCR products were purified using the E.Z.N.A gel extraction Kit (Omega Bio-tek) and sequenced at Austral-Omics core facility at Universidad Austral de Chile. New sequences are available in GenBank under accession numbers MW554521 and MW553075.

Phylogenetic Analysis

The BLAST algorithm (Altschul et al., 1990) from Geneious Prime (2019.2.1)[1], was used to search for sequence identifiers of the 18S rRNA genes, rbcL and ITS of species closely related to the isolated strain, in addition to other representatives of the order Chlamydomonadales used in previous studies (Hoham et al., 2002; Barcytė et al., 2018a). Sequence assembly, alignment and verification to detect possible misaligned positions were made in Geneious Prime (2019.2.1). The 18S rRNA alignment comprised 136 OTUs (operational taxonomic units)/1,758 positions, while rbcL included 77 OTUs/872 positions. To perform the phylogenies, in both markers, the substitution parameter-rich model, GTR + I + G was used (Abadi et al., 2019). The maximum-likelihood phylogenies were performed in IQ-TREE Web Server (Trifinopoulos et al., 2016) considering statistical support values of ultrafast bootstrapping (10,000 replicates). Additional support values based on Bayesian posterior probabilities were obtained in MrBayes 3.2.7a x 64 (Ronquist et al., 2012) with sequence data set divided by codon positions. Two runs of the Markov Monte Carlo chain (MCMC) were carried out for twenty million generations each with one single cold chain and three heated chains being used in the GTR + I + G evolutionary model. The trees were sampled every 100 generations. After 10^6 generations the mean standard deviation of the divided frequencies fell below 0.006 and the potential downscaling factor (PSRF) approached 1,000–1,001 for the diagnostic convergence parameters. The final trees of

[1]https://www.geneious.com

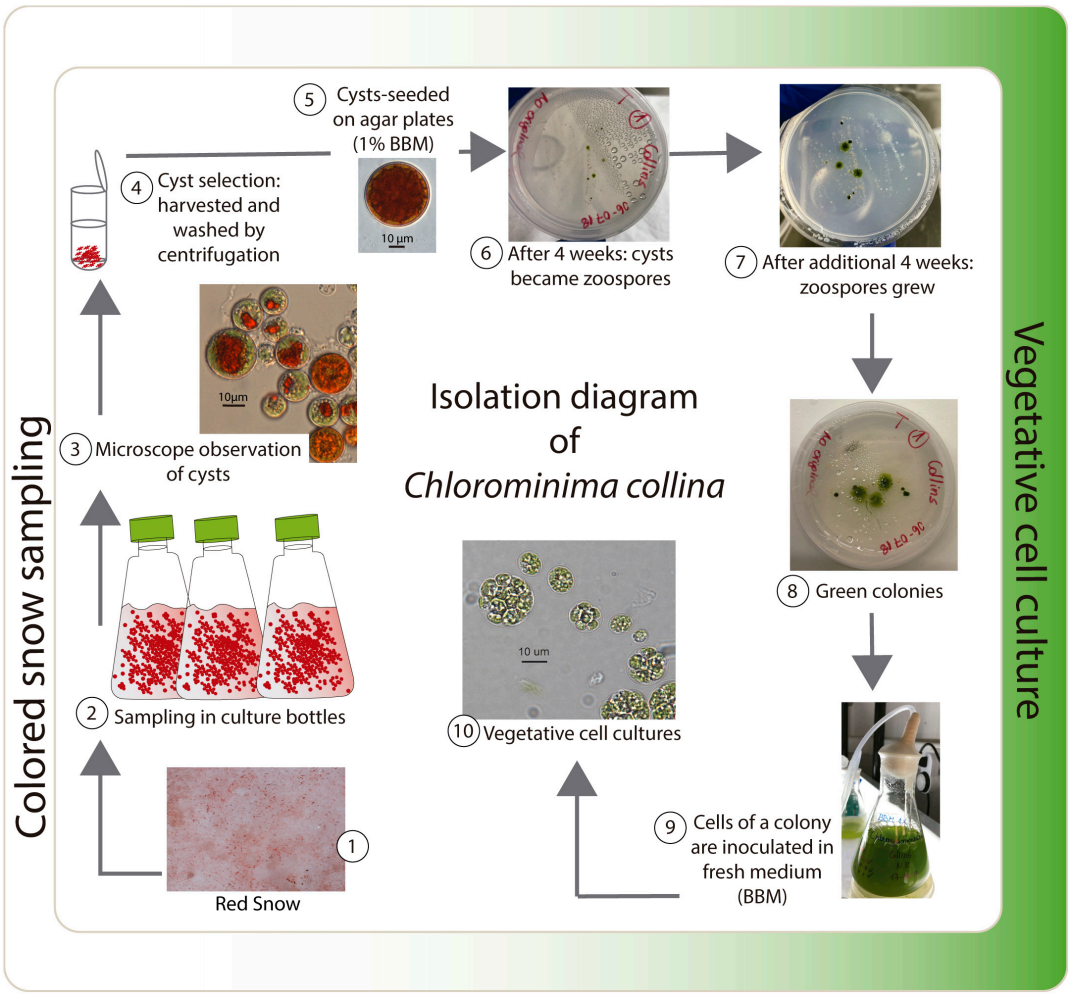

FIGURE 1 | Isolation diagram of *Chlorominima collina* CCAP 6/1.

IQ-TREE and MrBayes were observed in the FigTree v1.4.4 (Rambaut and Drummond, 2018).

Secondary Structure Analysis of ITS2 rDNA

The annotation of the secondary structure of the ITS2 rDNA nuclear region (including the 5.8 and 28S flanking regions) of the new strain and only a few sequences of ITS2 of strains closely related obtained by BLAST algorithm (Altschul et al., 1990) was performed through the web server[2] based on hidden Markov models (Keller et al., 2009), in conjunction with the ITS2 database (Schultz et al., 2006; Selig et al., 2008; Koetschan et al., 2010, 2012). Secondary structure of the annotated ITS2 sequences was predicted in RNAfold WebServer[3] considering the minimum energy secondary structure and centroid secondary structure model of ITS2 (Hofacker, 2003) and then visualized by VARNA 3.93 (Darty et al., 2009).

Finally, a sequences-structures alignment, including the five very close sequences [*Chloromonas* sp. CCCryo257-06 (HQ404888), *Chloromonas* sp. CCCryo244-06 (HQ404887), *Chloromonas* sp. CCCryo273-06 (HQ404890); *Chloromonas perforata* CCAP 11/43 (FR865585) and *Chlamydomonas applanata* CCAP 11/9 (FR865616)], was built with the ClustalW2 1.83 algorithm from 4SALE 1.7.1 (Seibel et al., 2006, 2008). This program was also used to detect compensatory base changes (CBCs) between the sequences-structures (Wolf et al., 2013). The alignment obtained in 4SALE was exported to build a neighbor-joining tree (Saitou and Nei, 1987) in MEGA X (Kumar et al., 2018). The evolutionary distances were computed using the Jukes-Cantor method (Jukes and Cantor, 1969). A matrix plot of CBCs was performed in PAST 4.03 software (Hammer et al., 2001).

Determination of Thermal Thresholds

To confirm the psychrophilic or psychrotrophic characteristics of the new strain, an experiment considering three temperatures (2, 10, and 20°C) was performed. After counting in a Neubauer

[2]http://its2.bioapps.biozentrum.uni-wuerzburg.de
[3]http://rna.tbi.univie.ac.at/cgi-bin/RNAWebSuite/RNAfold.cgi

chamber, suspensions of 400,000 cells/mL (2 ml) of culture were inoculated in 24-well cell culture plates (Thermo Fisher Scientific, United States). To avoid evaporation and contamination, the microplates were sealed with parafilm. The microplates (24 replicates) were left for 12 h at their control temperature (2°C). Subsequently they were transferred to acclimatization chambers for 19 days, under illumination conditions of 20–30 μmol m^{-2} s^{-1} and 16:8 h L:D regime. Growth was measured as changes in *in vivo* relative fluorescence units (RFU) in a microplate reader (Varioskan Flash, Thermo Fisher Scientific, United States). Fluorescence was measured at excitation (λex = 435 nm) and emission (λem = 685 nm) wavelengths. The specific growth rate (μ) was calculated using the equation:

$$\mu = \ln (N_2/N_1) / (t_2 - t_1)$$

where N_1 and N_2 are the growth (RFU) at time 1 (t_1) and time 2 (t_2), respectively.

The maximum quantum yield of chlorophyll fluorescence of dark-adapted photosystem II (F_v/F_m) was measured with an Imaging-PAM fluorometer (Walz, Effeltrich, Germany). The saturation pulse method was used to determine the basal (F_0) and maximum (F_m) fluorescence performance of dark-adapted samples (10 min is sufficient in dense microalgal mass cultures). Simultaneously, samples (100 μL) were taken for the qualitative detection of reactive oxygen species (ROS) on the third day of treatment when a decrease in F_v/F_m values was observed in the treatment at 20°C, indicating stress or photoinhibition. To compare ROS production, samples were examined at 2°C (control) and at 10°C. The *in vivo* production of ROS was examined using the CellROX® Green fluorogenic probe (Thermo Fisher Scientific, United States) according to a previously described protocol (Cornejo-Corona et al., 2016). For the visualization of intracellular ROS, the fluorescence was observed in an Olympus BX51 epifluorescent microscope (Olympus Corporation, Tokyo, Japan). Photographs were taken with a QImaging MicroPublisher 5.0 digital camera and the QCapture Pro-6.0 microimaging software was used for image processing.

Statistical Analysis

To examine how temperature and time influence RFU and F_v/F_m signals, generalized linear mixed models (GLMM) (Breslow and Clayton, 1993) were performed. Temperature was considered in the analysis as a fixed factor with three levels (2, 10, and 20°C, considering 2°C as a control). Time was also considered as a fixed factor. In all the models, ID of individual microalgae was incorporated as a random effect. The models that examine F_v/F_m were based on Beta distribution, using "logit" as the link function. In the case of the models that evaluate growth by *in vivo* fluorescence (RFU), a Gamma distribution was considered, using "log" as the link function. All the statistical modeling was carried out in the R program version 3.5.2 (R Core Team, 2018), using the glmmTMB (Brooks et al., 2017) and lm4 (Bates et al., 2015) packages. Model comparisons were made using Akaike Information Criterion (AIC) applied within the bbmle (Bolker and Team, 2017) and MuMIn (Barton, 2019) packages. To examine how much variation is explained by the models (R^2 coefficients), functions of the performance packages (Lüdecke et al., 2020) and MuMIn (Barton, 2019) were used. The assumptions of the fitted models were evaluated with DHARMa package (Hartig, 2020). Subsequently, a *post hoc* Tukey test was performed on the best models fitted with the multcomp package (Hothorn et al., 2008) and emmeans (Lenth, 2019). Multiple comparisons were applied to analyze differences between the temperature treatments, as a function of the mean time. Significance was examined at the 5% level.

RNA Isolation, Library Preparation and Sequencing

Samples of the isolated strain cultured at 2°C (total 30 ml) were centrifugated at 4,500 × *g* for 10 min at 4°C. The cell pellets were immediately frozen in liquid nitrogen and subsequently stored at −80°C until further RNA extraction. The total RNA of the frozen cells was extracted and purified from 100 mg of cell powder, according to the protocols of the SpectrumTM Plant Total RNA kit (Sigma-Aldrich). The RNA concentration was quantified by Qubit 3.0 Fluorometric Quantification (Thermo Fisher Scientific) and its integrity (RIN = 9.8) evaluated by Fragment Analyzer—Advanced Analytical Technologies, Inc., (AATI) and Agilent DNF-471RNA kit. The library was prepared taking 4 μg of RNA sample. To isolate the mRNA, molecules containing poly-A, poly-T-oligo attached magnetic beads (Illumina) were used. Then the mRNA was purified and fragmented (200–700 nt) by divalent cations at 94 °C for 5 min. The purified mRNA was used for the construction of the cDNA library using the KAPA Stranded RNA-Seq Library Preparation Kit Illumina® Platforms. Fragment analyzer system was used to evaluate the quality of the library. The libraries obtained were sequenced in Illumina Nextseq550 at the ChileGenómico research center (Facultad de Medicina, Universidad de Chile). After sequencing, the output was transformed by base-calling into sequences, which is the "raw reads" output in fastq format. All reads have been uploaded in the Sequence Read Archive (SRA) at NCBI, under accession numbers PRJNA698241 and BioProject: SAMN17709520.

Analysis, *de novo* Transcriptome Assembly and Annotation

The raw reads were filtered to eliminate low quality regions (Quality score ≥ 30), in the prinseq-lite software (Schmieder and Edwards, 2011). Thus, pair-end reads with primer or adapter sequences and reads with more than 10% of the bases under the established quality were removed. After the read cleaning, *de novo* assembly was performed using the Trinity program (Grabherr et al., 2011). The functional annotation of the assembled sequences was performed using BLAST algorithm (*E*-value of < 10-5) against the databases: UniProt (UniProt Consortium, 2019), GO (Ashburner et al., 2000), and NCBI non-redundant protein database (NR) (Deng et al., 2006). To generate the gene ontology (GO) assignments, the Blast2GO program was applied (Conesa et al., 2005; Götz et al., 2008).

RESULTS

Morphological and Ultrastructural Features

Light microscopy revealed the presence of vegetative cells of ellipsoidal or ellipsoidal-cylindrical shape with rounded or even spherical posterior end, of 9–11 μm long and 6–12 μm width. **Figure 2**, with a smooth but noticeable cell wall and a discrete, hemispherical papilla (**Figure 3**). Two flagella, located apically, of equal length, 1.0 × cell length or longer, emerged under the papilla. TEM micrographs corroborate the presence of flagella with a cross section showing the axonema (**Figure 3F**). The young cells presented a single parietal chloroplast (dorsal side of the cell), laminated, shaped like a C, which occupies a large part of the cell volume. Eyespots were not observed in all stages of the vegetative phase, nor pyrenoids, but small grains of starch were distinguished, which were dispersed between the intertylakoidal spaces, along the chloroplast (**Figure 3A**). The size of the starch grains increases in cells from old cultures (**Figure 3G**). In mature cells it is possible to note how the chloroplast partially surrounds the nucleus (**Figure 3B**) until cell division occurs. Therefore, this alga reproduces asexually by forming two (**Figures 3C–E**) to eight motile zoospores (sometimes ten zoospores can be formed, even up 16). Motility was observed when the aliquots of the mother culture were transferred to a fresh medium, similar as has been reported for *Chloromonas arctica* (Barcytė et al., 2018a). However, unlike *Chloromonas arctica,* in *Chlorominima collina* motility was only maintained at low temperatures. A single nucleus was observed, which was located in the posterior region of the cell, eccentric, rather lateral (**Figure 3A**). In addition, in young cells, a wide periplasmic space was noted. Several cytoplasmatic globular vacuoles were observed, which can be empty or containing electron-dense deposits. Large oil droplets were evident only in cells from old cultures (**Figure 3G**). In these cells, plastoglobuli were also noted in the chloroplast (**Figure 3H**).

Molecular Phylogeny and Secondary Structure Analysis of ITS2

Chlorominima (Cm.) collina was located within clade C, one of the four main lineages identified for the *Chloromonas (Cr.)* and *Chlamydomonas (Cd.)* complex (Buchheim et al., 1997; Hoham et al., 2002). Specifically, *Cm. collina* is assigned within the *Stephanosphaerinia* phylogroup, which is one of the 21 monophyletic groups recognized for the class Chlorophyceae, order Chlamydomonadales (Nakada et al., 2008). In the phylogeny of the rbcL gene (**Figure 4**) the new

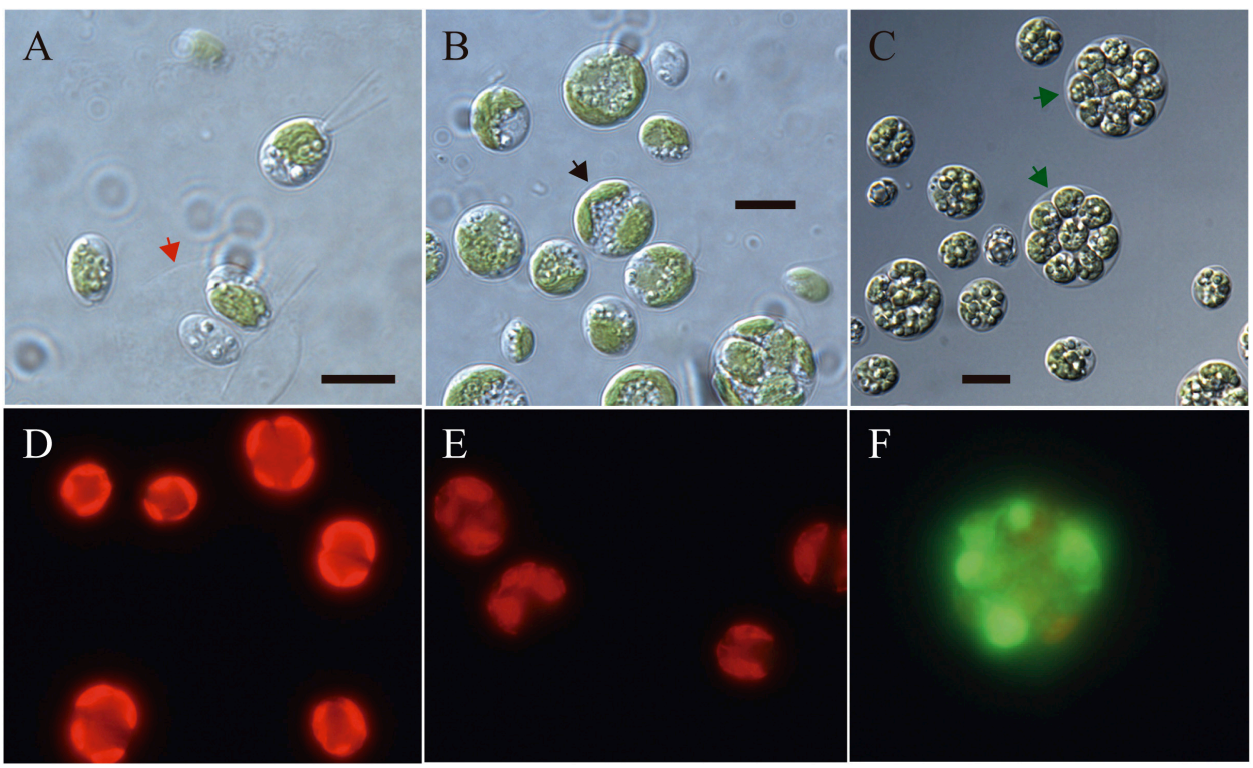

FIGURE 2 | (A–C) Light microscopy images of morphology of *Chlorominima collina* CCAP 6/1 **(A)** Zoospores with two flagella of equal length. The red arrow indicates the maternal cell wall, from which the zoospores emerged. **(B)** Vegetative cells in the process of cell division. Black arrow points to a cell in division. **(C)** Mature cells with higher amounts of starch grains and lipid droplets. Green arrows indicate zoospores within mother cell wall. **(D–F)** Fluorescence images of *Chlorominima collina* using CellROX Green dye for detection of ROS *in vivo* on the third day of exposure at the control temperature of 2°C **(D)** and at the treatment temperatures of 10°C **(E)** and 20°C **(F)**. In panels **(D,E)** red stained chloroplasts of dividing cells are observed and in panel **(F)** the dividing cell (≥4 zoospores) is almost completely stained green. Scale bars: 10 μm.

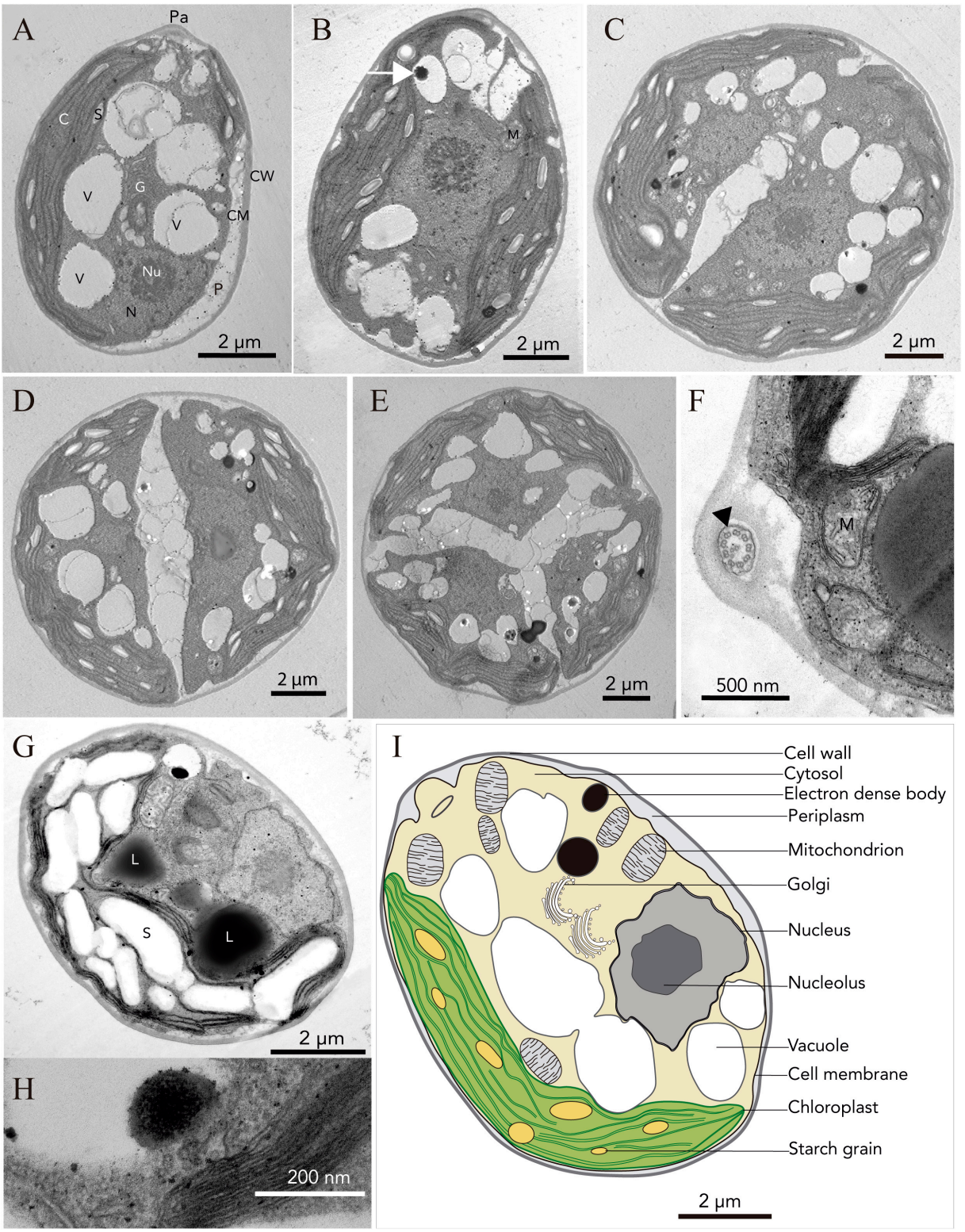

FIGURE 3 | Ultrastructure (TEM) of *Chlorominima collina* CCAP 6/1 **(A)** Longitudinal section of a zoospore. **(B)** Mature vegetative cell (white arrow: electron dense body). **(C–E)** Zoospores in the process of cell division, where the protoplast is divided transversely. **(F)** Cross section of the flagellum showing the 9 + 2 axonema structure (black arrow). **(G)** Old culture cell. Pa, papilla; C, chloroplast; S, starch grains; V, vacuole; N, nucleus; Nu, nucleolus; G, Golgi apparatus; P, periplasm; CM, cell membrane; CW, cell wall; M, mitochondria; L, lipid droplet. **(H)** Plastoglobule in the chloroplast. **(I)** Consensus schematic drawing of a vegetative cell of *Cm. collina*.

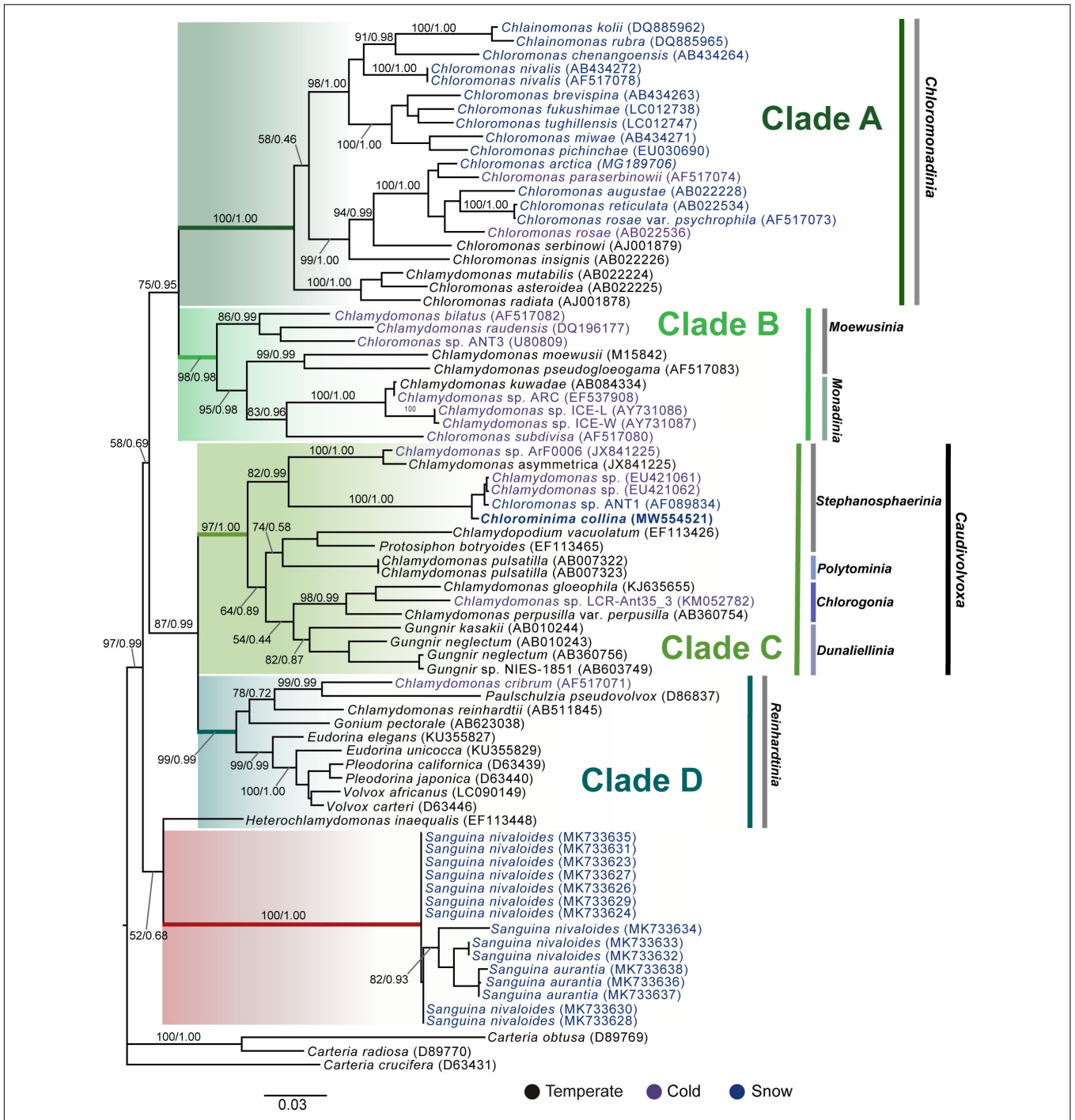

FIGURE 4 | Maximum-likelihood phylogram of rbcL gene sequences. The position of *Chlorominima collina* CCAP 6/1 and other related members of the order Chlamydomonadales. Clades A, B, C, and D were delimited according to Hoham et al. (2002). The names of the clades were designated according to Nakada et al. (2008). The new genus of *Sanguina* snow algae is specified (Procházková et al., 2019a). Representatives of the genus *Carteria* were used as outgroup. The numbers on the branches indicate statistical support values (Maximum-likelihood bootstraps/Bayesian posterior probabilities). Snow taxa are marked in blue, taxa from other cold environments, not from snow, are marked in purple and the rest of the taxa from other temperate environments are written in black. The lower bar indicates changes by nucleotide position (0.03).

strain is located with high support [Maximum likelihood support (ML): 100/Bayesian inference (BI): 1.00] within clade C, in a subclade that contains unidentified polar strains assigned to the genus *Chloromonas* and *Chlamydomonas*. In this subclade, *Cm. collina* is more similar to the rbcL gene sequences of Genbank of *Chloromonas* sp. ANT1 (AF089834)

and *Chlamydomonas* sp. CCMP681 (EU421062 and EU421061) of which it differs by 11 nucleotides. Compared with other similar rbcL gene sequences, *Cm. collina* differs by 90 and 98 nucleotides from *Chlamydomonas gloeophila* UTEX_607 (KJ635655) and *Chlamydomonas pulsatilla* CCAP11-106 (AB007322), respectively. Phylogenetic analyses based on 18S rRNA gene corroborated the assignment of *Cm. collina* in the *Stephanosphaerinia* phylogroup (**Figure 5**), where it also forms a subclade highly supported (ML: 100/BI: 1.00), with other unidentified polar strains assigned to *Chloromonas* and *Chlamydomonas*. *Cm. collina* presents 100% identity to the 18S rRNA gene sequence of *Chloromonas* sp. KNF0032 (KU886306) and differs by two nucleotides from *Chloromonas* sp. CCCryo273-06 (HQ404890) and from *Chlamydomonas* sp. CCMP681 (EF106784). The secondary structure analyses of the ITS2 rDNA revealed a high similarity between *Cm. collina* and strains of *Chloromonas* sp. (CCCryo273-06, CCCryo244-06, and CCCryo257-06) with identity of 99.6–100%. These sequences did not show CBCs (**Figure 6**). Other strains with similar ITS2 sequences were *Chloromonas perforata* CCAP 11/43 and *Chlamydomonas applanata* CCAP 11/9, which are representatives of *Caudivolvoxa* and differ from *Cm. collina* by 1–5 CBCs, respectively, presenting an identity percent of 80.6 and 78.5, respectively (**Figure 6**).

Thermal Responses of *Chlorominima collina*

The isolated alga tolerates only temperatures < 10°C (**Figure 7**), while at 20°C declines in growth (based RFU values) and in the specific growth rates (**Supplementary Figure 1**) were observed. Preliminary tests indicated that the optimum growth temperature for *Cm. collina* is around 4°C (results not shown). Low F_v/F_m values indicated that temperatures of 20°C in interaction with time were stressful to photochemistry of *Cm. collina* (glmmTMB; $p < 0.001$; **Supplementary Table 1** and **Figure 7B**). In fact, after 3 days at 20°C, F_v/F_m reached values close to 0.1, which was accompanied by the *in vivo* detection of ROS (**Figure 2F**). This caused a significant decrease in growth (RFU) at 20°C over time (glmer; $p < 0.001$; **Supplementary Table 1** and **Figure 7A**). Conversely, *Cm. collina* cells kept under control temperature (2°C) showed active growth (**Figure 7A**) and high levels of photochemical activity (F_v/F_m values ≤ 0.6; **Figure 7B**), while *in vivo* ROS was not detected (**Figure 2D**). Interestingly, the new strain maintains relatively constant F_v/F_m and growth values during the first days at 10°C (**Figure 7**) and ROS formation was not evident on the third day at this temperature (**Figure 2E**). After this period, a decline in F_v/F_m and growth was observed, suggesting that 10°C is a thermal tolerance limit for *Cm. collina*.

De novo Transcriptome Assembly and Annotation

In total, 2,670,333 crude Ilumina PE readings were obtained. Following removal of low-quality readings and with adapters, 1,539,352 readings were obtained. These RNA-seq reads were subjected to a *de novo* transcriptome assembly, which yielded 37,401 transcripts with N50 of 881 bp and an average length of 643.88 bp (**Table 1**). A number of annotated sequences (10,676) had a significant hit identified by BLAST search against Uniprot and NCBI, 79% of these hits were assigned to sequences of green algae (Chlorophyta), mainly members of the Chlamydomonadales order, while the rest corresponded to other divisions of algae (**Figure 8**). From the annotations against the GO database, it was possible to infer the presence of genes in the categories of GO (**Figure 9**). In the category "biological process" the top GO terms were "cellular process" (GO: 0009987), "metabolic process" (GO: 0008152), and "cellular metabolic process" (GO: 0044237). For "molecular function" the top GO terms were "catalytic activity" (GO: 0003824) and "binding" (GO: 0005488). In the "cellular component" category, the GO terms "cellular anatomical entity" (GO: 0110165) and "intracellular" (GO: 0005622) were the most enriched (**Figure 9**). Transcripts annotated against the Uniprot database using BLAST similarity, indicated well-known stress-responsive genes (**Table 2**), e.g., genes encoding "ABC transporters" or "calcium/calmodulin-dependent protein kinase" and "heat shock proteins." The identification of several genes related to photosynthesis such as "oxygen-evolving enhancer proteins" (e.g., TRINITY_DN6396), or "Rubisco" (TRINITY_DN13299), together with other genes involved in the translation process such as "elongation factors" (e.g., TRINITY_DN21381) and "ribosomal proteins" (e.g., TRINITY_DN10395) indicate an active metabolism of *Cm. collina* at 2°C. At least 12 transcripts (**Table 3**) encoding antifreeze glycoprotein and ice-binding proteins were observed. A large number of transcripts associated with biosynthesis of fatty acids, especially polyunsaturated fatty acids (PUFAs), triacylglycerol (TAG), secondary carotenoids were also identified (**Table 4**). Additionally, genes involved in synthesis of betaine were identified (**Table 5**).

Taxonomic Treatment

Chlorominima Gálvez gen nov.

Type species: *Chlorominima collina* Gálvez sp. nov.

Etymology: the name reflects the morphological similarity with the genus *Chloromonas*, and in turn refers to a small cell size.

Registration: http://phycobank.org/102721

Description: ellipsoidal cells with rounded posterior end, approximately 11 μm long and 12 width, with two flagella of equal length at the anterior end. A single parietal chloroplast on the dorsal side of the cell, without pyrenoids, eyespot absent, and starch grains scattered between intertylakoidal spaces. Nucleus single, positioned in the posterior region of the cell, eccentric. Smooth and noticeable cell wall. Discrete hemispheric papilla. More than five contractile vacuoles irregularly distributed on the protoplast surface. Asexual reproduction through the formation of 2–16 zoospores within the parental cell wall.

Chlorominima collina Gálvez sp. nov.

Registration: http://phycobank.org/102722

Description: vegetative cells, ellipsoidal, ellipsoidal-cylindrical or spherical with rounded posterior end, of 9–11 μm length and 6–12 μm width, biflagellate with flagella of equal length (1.0 × cell length or longer). Single chloroplast, laminate and parietal in the dorsal side of the cell, defined as C-shaped,

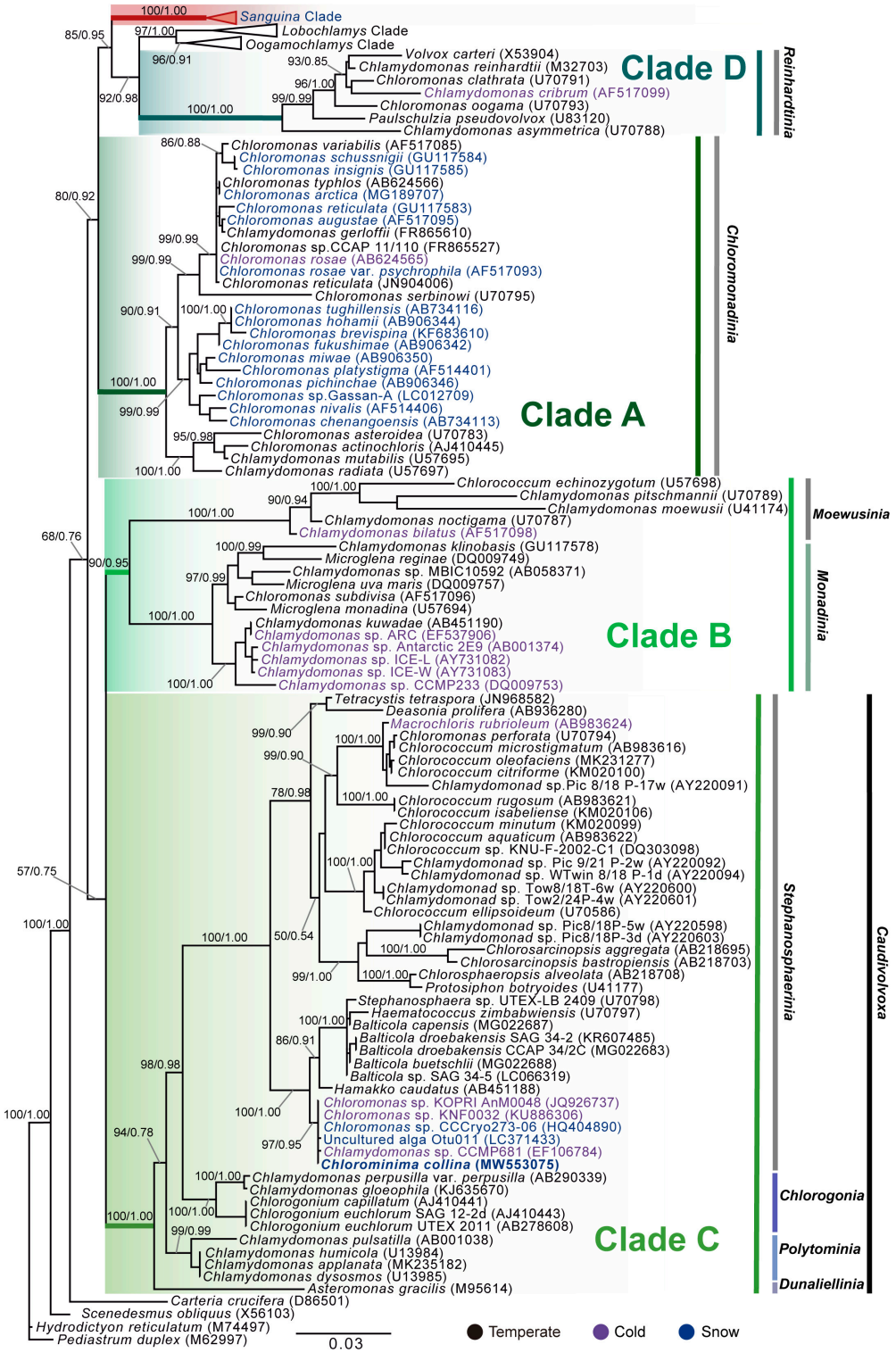

FIGURE 5 | Maximum-likelihood phylogram of the sequences of the 18S rRNA gene of *Chlorominima collina* CCAP 6/1 and other representative members of the order Chlamydomonadales. Clades A, B, C, and D were circumscribed according to Buchheim et al. (1997) and Hoham et al. (2002). The new genus of *Sanguina* snow algae is specified (Procházková et al., 2019a). *Carteria crucifera*, *Tetradesmus obliquus*, *Hydrodictyon reticulatum*, and *Pediastrum duplex* were considered as outgroup. The names of the clades were designated according to Nakada et al. (2008). The numbers on the branches indicate statistical support values (Maximum-likelihood bootstraps/Bayesian posterior probabilities). Snow taxa are marked in blue, taxa from other cold environments, not from snow, are marked in purple and the rest of the taxa from other temperate environments are written in black. The lower bar indicates changes by nucleotide position (0.03).

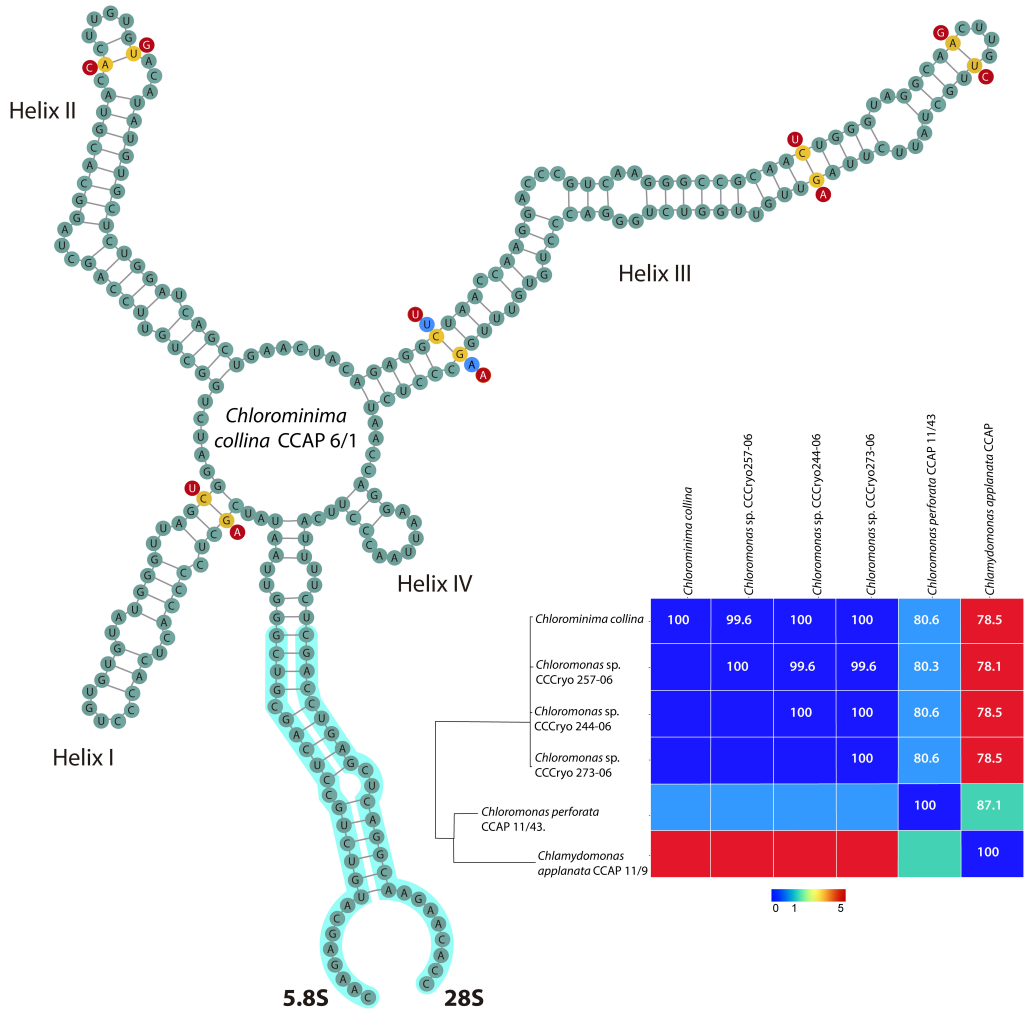

FIGURE 6 | Secondary structure model of the ITS2 rDNA of *Chlorominima collina* CCAP 6/1. The positions of CBC are shown in yellow circles between *Chlorominima collina* and *Chloromonas perforata* CCAP 11/43 (light blue circles) and *Chlamydomonas applanata* CCAP 11/9 (red circles). The Matrix under the structure shows compensatory base changes (CBCs) by color under diagonal and identity percent (above diagonal) among the respective strains considered for the analysis of the secondary structure of ITS2.

with starch grains scattered between intertylakoidal spaces. Pyrenoid and eyespot absent. Nucleus single, positioned in the posterior region of cell, eccentric, rather lateral. Approximately 5–6 contractile vacuoles distributed irregularly on the protoplast. Discrete and hemispherical anterior papilla. Young cells present wide periplasmic space. Old cells lose their flagella, are globular in shape with cytoplasmic lipid droplets that occupy most of the cell volume and increase the size of starch grains. Asexual reproduction through the formation of generally up to eight zoospores within the cell wall. In old cultures, formations of up to 16 zoospores can also be observed within the cell wall. Sexual reproduction was not evident. Cell aggregates were not observed in cultures.

Holotype: the strain is preserved permanently at 2°C at the Photobiology Laboratory of the Universidad Austral de Chile, Valdivia, Chile. It has also been deposited in the CCAP, based in Scottish Association for Marine Science near Oban, Scotland, United Kingdom[4], under strain number CCAP 6/1. **Figures 2**, **3** show the morphology of the holotype.

Type locality: red snow from the Collins Glacier, King George Island, South Shetland Islands (62°10′5.412″S, 58°51′18.216″W), Western Antarctic Peninsula.

Etymology: the species name was chosen to emphasize the holotype's sampling area, the Collins Glacier.

Distribution: Antarctica.

DISCUSSION

Recent studies have demonstrated that snow algae are taxonomically diverse. In part, this has been possible due to the application of polyphasic approaches that have allowed

[4]http://www.ccap.ac.uk

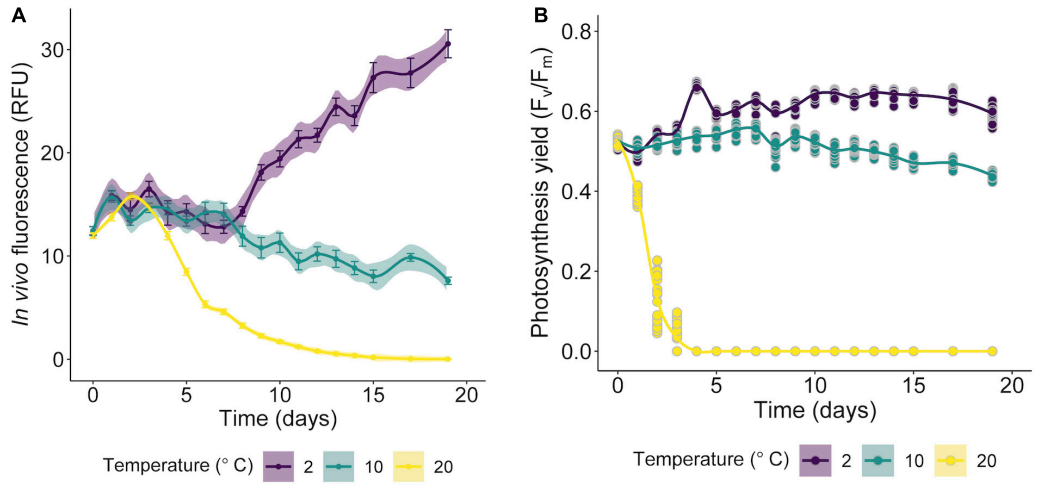

FIGURE 7 | Growth curves of *Chlorominima collina* CCAP 6/1 based on RFU values **(A)** and efficiency of the quantum yield of photosystem II (PSII) (F_v/F_m) **(B)** exposed to 2, 10, and 20°C. The lines show the trends, and the shading indicates the confidence intervals (CI). In the RFU graphs, each point is the mean of 24 replicates and the bars represent the standard error (SE). For F_v/F_m data, each point is an average of 24 replicates (raw data).

the identification of new species (Matsuzaki et al., 2018, 2019; Procházková et al., 2019b), even a new genus, *Sanguina* has been recognized as a dominant component of the snow communities (Procházková et al., 2019a). This knowledge is crucial, since it allow building a basis for characterizing the colored snow blooms, allowing to describe the genetic diversity of snow algae and their dispersal (Segawa et al., 2018; Soto et al., 2020). Thus, the description of a new Antarctic genus, *Chlorominima* with the species type *Cm. collina*, together with the integration of molecular and physiological approaches serves not only to improve our knowledge about Antarctic taxonomic diversity, but also provides elements to understand its functional attributes, reflecting adaptations to the snow ecosystem.

New characterizations of snow communities developed in the Fildes peninsula, King George Island, have reported in the red snow a low abundance of *Chloromonas* sp. CCCryo273-06 (HQ404890) a integrant of the polar subclade of *Chlorominima* (Luo et al., 2020). This only confirms the presence of representatives of *Chlorominima* in the red snow, which probably coexist with members of *Sanguina* and *Chlainomonas* (Procházková et al., 2019a; Luo et al., 2020) but does not prove that the cells of *Chloromonas* sp. CCCryo273-06 or the isolated strain in this study have germinated from cysts, as a conclusive methodology it is suggested to perform single-cell sequencing, to verify the taxonomic identity of the cysts.

TABLE 1 | Transcriptome sequencing and summary statistics of *de novo* assembly.

Number/length	
Number of reads from Nextseq550 (2 × 150 pb)	2,670,333
High-quality (HQ) reads	1,539.352
Total trinity transcripts	37,401
Total trinity genes	33,337
Percent GC	54,82
Average contig length	643,88 bp
N50	881

Morphology and Ultrastructure of *Chlorominima collina*

The characteristics observed in the vegetative phase of our new strain were similar to the morphological traits described for snow or ice species of *Chloromonas* (Ettl, 1970, 1983), including the common absence of pyrenoids. This contrasts with the presence of pyrenoids in taxa phylogenetically related to *Cm. collina*, such as *Chlamydomonas perpusilla* var. *perpusilla* (Nakada and Nozaki, 2007), *Hamakko caudatus* (Nakada and Nozaki, 2009), or *Haematococcus zimbabwiensis* (Buchheim et al., 2013), confirming that this structural trait may be absent or present within the *Chloromonas-Chlamydomonas* complex and therefore could not be relevant for the natural history of these algae (Hoham et al., 2002; Matsuzaki et al., 2012). In addition, *Cm. collina* lacks an eyespot, suggesting that this structure is not an essential component of the photoreceptor apparatus (Morel-Laurens and Feinleib, 1983), which has also been reported for other snow algal strains such as *Cr. pichinchae* (Hoham, 1975a), *Cr. krienitzii* (Matsuzaki et al., 2015), or *Cr. fukushimae* (Matsuzaki et al., 2014). Similar to the latter species, *Cm. collina* has a parietal, laminate chloroplast but is defined as C-shaped, that is unusual among snow algal species of *Chloromonas* exhibiting a cup-shaped chloroplast (Ling and Seppelt, 1998; Matsuzaki et al., 2014, 2019). Species closely related to *Cm. collina* such as *Hamakko caudatus* (Nakada and Nozaki, 2009) also have a parietal chloroplast, it also has a similar cell width (6–10 μm) to *Cm. collina*, but *Hamakko caudatus* have spindle cell shape and can have 10 contractile vacuoles and *Cm. collina* only 6. Other close species such as *Cd. perpusilla* var. *perpusilla* only present two apical contractile vacuoles (Nakada and Nozaki, 2007).

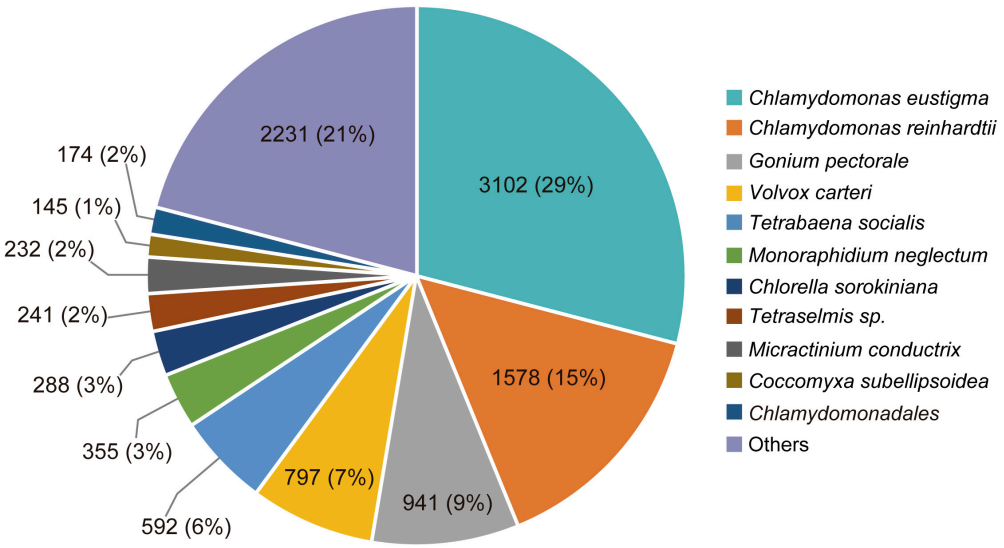

FIGURE 8 | Species distribution of the top BLAST hits by NR database annotation for *Chlorominima collina* CCAP 6/1. Percentage distribution of the 10 most successful species identified for each BLAST-assembled sequence against the NCBI non-redundant protein database. In addition to the percentage value, the number of genes noted per species is indicated.

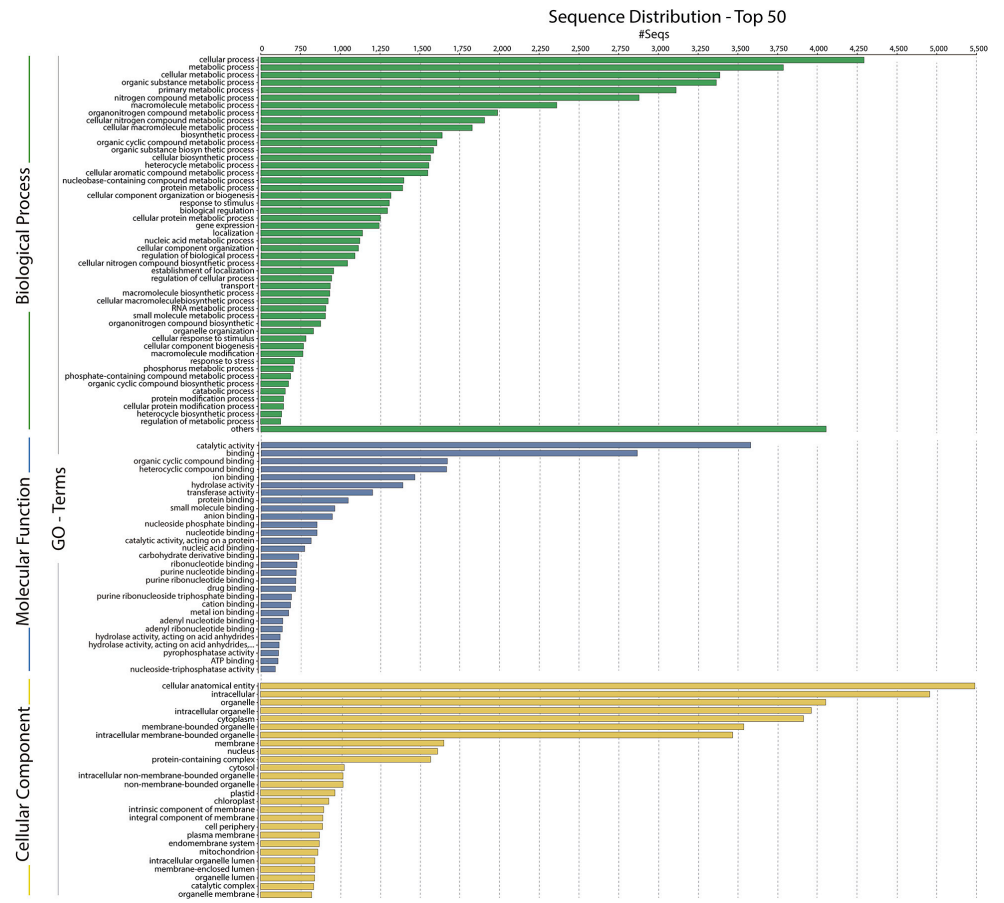

FIGURE 9 | Gene ontology (GO) assignments for the *Chlorominima collina* CCAP 6/1 transcriptome. Assignments generated in Blast2GO predict the participation of genes in biological processes (green); molecular functions (blue) and cellular components (yellow).

TABLE 2 | Stress-responsive genes present in the *Chlorominima collina* trascriptome.

De novo assembled sequence ID	GO molecular function (species)
TRINITY_DN1216	ABC transporter F family member 5 (*Tetrabaena socialis*)
TRINITY_DN25081	ABC transporter B family member 25 *(Anthurium amnicola*)
TRINITY_DN19387	Leucine-rich repeat-containing protein 1 *(Tetrabaena socialis*)
TRINITY_DN747	Leucine-rich repeat-containing protein 40 (*Auxenochlorella protothecoides*)
TRINITY_DN7218	Hypersensitive-induced response protein 3 (*Tetrabaena socialis*)
TRINITY_DN6510	Calcium/calmodulin-dependent protein kinase 1 Da (*Lepisosteus oculatus)*
TRINITY_DN10034	Heat shock factor 1 (*Chlamydomonas reinhardtii*)
TRINITY_DN4825	Activator heat shock protein ATPase (*Monoraphidium neglectum*)
TRINITY_DN9027	Heat shock cognate 71 kDa protein-like (*Saccoglossus kowalevskii*)
TRINITY_DN10375	Heat shock protein 70a (*Dunaliella salina*)
TRINITY_DN10700	Heat shock protein 70D (*Chlamydomonas reinhardtii*)

TABLE 3 | Putative Antifreeze and Ice-Binding proteins found in transcriptome of *Chlorominima collina.*

De novo assembled sequence ID	GO molecular function (species)
TRINITY_DN12789	Antifreeze glycoprotein (*Rhodosporidium toruloides*)
TRINITY_DN1603	Ice-binding protein-2 (*Chlamydomonas* sp. CCMP681)
TRINITY_DN1624	Ice-binding protein-4 (*Chlamydomonas* sp. CCMP681)
TRINITY_DN16614	Ice-binding protein-4 (*Chlamydomonas* sp. CCMP681)
TRINITY_DN25734	Ice-binding protein-4 (*Chlamydomonas* sp. CCMP681)
TRINITY_DN26347	Ice-binding protein-4 (*Chlamydomonas* sp. CCMP681)
TRINITY_DN27778	Ice-binding protein (*Chloromonas* sp.)
TRINITY_DN4443	Ice-binding protein-4 (*Chlamydomonas* sp. CCMP681)
TRINITY_DN6301	Ice-binding protein-4 (*Chlamydomonas* sp. CCMP681)
TRINITY_DN6423	Ice-binding protein-4 (*Chlamydomonas* sp. CCMP681)
TRINITY_DN7238	Ice-binding protein-3 (*Chlamydomonas* sp. CCMP681)
TRINITY_DN8708	Ice-binding protein (*Chloromonas* sp.)

TABLE 4 | Putative desaturases and other enzymes involved in the biosynthesis of fatty acids, triacylglycerol and secondary carotenoids present in the transcriptome of *Chlorominima collina.*

De novo assembled sequence ID	GO molecular function (species)
TRINITY_DN12058	Fatty acid elongase 1 (*Orychophragmus violaceus*)
TRINITY_DN12819	Fatty acid desaturase 4 (*Klebsormidium nitens*)
TRINITY_DN1377	Delta-12-fatty acid desaturase (*Glaciozyma antarctica*)
TRINITY_DN15049	Putative long-chain-alcohol O-fatty-acyltransferase 5 (*Chlorella sorokiniana*)
TRINITY_DN18272	Fatty acid synthase subunit alpha (*Rhodosporidium toruloides*)
TRINITY_DN22769	Cyclopropane-fatty-acyl-phospholipid synthase (*Tetrabaena socialis*)
TRINITY_DN27022	Elongation of fatty acids protein (*Rhodotorula graminis*)
TRINITY_DN30110	Putative long-chain-alcohol O-fatty-acyltransferase (*Tetrabaena socialis*)
TRINITY_DN6285	Fatty acid desaturase 2 (*Jatropha curcas*)
TRINITY_DN6913	Fatty acid desaturase 5 (*Theobroma cacao*)
TRINITY_DN6936	Fatty acid delta-6-desaturase (*Lobosphaera incisa*)
TRINITY_DN7069	Omega-3-fatty acid desaturase (*Chlamydomonas reinhardtii*)
TRINITY_DN6274	Stearoyl-ACP-desaturase (*Haematococcus lacustris*)
TRINITY_DN15482	Cytochrome P450, C-22 desaturase (*Chlamydomonas reinhardtii*)
TRINITY_DN9974	Triacylglycerol lipase-like protein (*Chlamydomonas reinhardtii*)
TRINITY_DN11143	Diacylglycerol kinase (*Chlamydomonas eustigma*)
TRINITY_DN18922	Putative phospholipid:diacylglycerol acyltransferase 2 (*Arabidopsis thaliana*)
TRINITY_DN19602	Diacylglycerol kinase (*Volvox carteri* f. *nagariensis*)
TRINITY_DN3878	Diacylglycerol acyltransferase type 2 (*Ettlia oleoabundans*)
TRINITY_DN6178	Diacylglycerol acyltransferase type 2 (*Chlamydomonas reinhardtii*)
TRINITY_DN6279	Glycerol-3-phosphate acyltransferase, chloroplastic (*Chlamydomonas eustigma*)
TRINITY_DN7159	1-acyl-sn-glycerol-3-phosphate acyltransferase (*Chlamydomonas reinhardtii*)
TRINITY_DN7140	Glycerol-3-phosphate dehydrogenase [NAD(+)] *(Chlamydomonas reinhardtii*)
TRINITY_DN239	Putative stearoyl-CoA 9-desaturase (*Leucosporidium creatinivorum*)
TRINITY_DN10651	Zeta-carotene desaturase (*Auxenochlorella protothecoides*)
TRINITY_DN19166	Zeta-carotene desaturase (*Haematococcus lacustris*)
TRINITY_DN2370	Phytoene desaturase (*Haematococcus lacustris*)

Furthermore, cells of *Cm. collina* have an average length between 9 and 11 μm, while the width does not exceed 12 μm, resembling cells of *Cr. alpina* and *Cr. miwae*, but they differ in chloroplast and cell morphology (Matsuzaki et al., 2019). Rather, the ellipsoidal shape of the cells of *Cm. collina* are comparable to *Cr. hoshawii* cells (Matsuzaki et al., 2018). This species does not present a discernible papilla and can only form up to four zoospores (rarely eight) within the parental cell wall, while *Cm. collina* can form up to eight zoospores (rarely 16), a feature

TABLE 5 | Putative betaine aldehyde dehydrogenases genes present in the transcriptome of *Chlorominima collina*.

De novo assembled sequence ID	GO molecular function (species)
TRINITY_DN13477	Betaine aldehyde dehydrogenase 2, mitochondrial (*Arabidopsis thaliana*)
TRINITY_DN21321	Betaine aldehyde dehydrogenase 2, mitochondrial (*Tarenaya hassleriana*)
TRINITY_DN5490	Betaine aldehyde dehydrogenase 2 (*Phoenix dactylifera*)

reported also in *Cr. nivalis* (Matsuzaki et al., 2018) and *Cr. fukushimae* (Matsuzaki et al., 2014). Similar to the latter species, *Cm. collina* does not form cellular aggregates in cultures.

Although *Cm. collina* displays several typical characteristics of the *Chloromonas*, it is distinguished from the species described for this genus and from phylogenetically close species such as *Hamakko caudatus* by showing an unusual position of the nucleus, a wide periplasmic space between the inner and outer cell membranes, the presence of 5–6 contractile vacuoles, the small cell size that did not exceed 12 μm in both length and width, and the absence of pyrenoid and eyespot.

Phylogenetic Position of *Chlorominima collina* and Phylogeny of Cold Tolerant Chlamydomonadales

Chlorominima collina CCAP 6/1 is placed in the phylogroup *Stephanosphaerinia*, or clade C (Nakada et al., 2008). This is unexpected since most snow algae occur in clade A or *Chloromonadinia* (Hoham et al., 2002). Specifically, within clade C, *Cm. collina* forms an independent lineage, close to other polar strains unidentified, but assigned to *Chloromonas* and *Chlamydomonas* (**Supplementary Table 2**). With the rbcL gene, *Cm. collina* is sister to *Chloromonas* ANT1 and *Chlamydomonas* sp. CCM681, for which there are no morphological descriptions that allow comparisons, only their adaptations to cold environments have been characterized (Devos et al., 1998; Raymond et al., 2009). By using the 18S rRNA gene, *Cm. collina* exhibits high identity with *Chloromonas* sp. KNF0032, both strains have a small cell size and an ovoid cell shape but differ in the shape of their chloroplasts and by the apparent presence of pyrenoid in *Chloromonas* sp. KNF0032 (Jung et al., 2016b). The insufficient description of *Chloromonas* sp. KNF0032 limits further conclusions, but it must also be taken into account that the evolutionary highly conserved 18S rRNA gene does not provide sufficient resolution to discriminate between closely related species (Barcytė et al., 2018a; Remias et al., 2018; Lutz et al., 2019). When the taxonomic status of *Cm. collina* was verified under the CBC species concept (Coleman, 2000; Müller et al., 2007) we observe the absence of CBC among *Cm. collina* and other strains known as *Chloromonas* sp. (CCCryo273-06, CCCryo244-06, and CCCryo257-06), which could indicate with a probability of ∼ 0.76 that these algae belong to the same species (Coleman, 2000; Müller et al., 2007). This scenario may be quite feasible given the proximity between the sampling sites of these algae (**Supplementary Table 2**). Although, it should also be noted that even without CBC, the named strains may belong to different species with a probability of ∼ 0.24 (Caisová et al., 2013; Škaloud and Rindi, 2013; Procházková et al., 2018). Even in some cases it has been suggested that morphological changes precede the emergence of a CBC (Pawłowska et al., 2013). However, these strains have not been described at the species level, so there are no descriptions that allow morphological comparisons. On the other hand, the presence of CBCs was found in helix III, one with *Chloromonas perforata* CCAP 11/43 and five with *Chlamydomonas applanata* CCAP 11/9, revealing that *Cm. collina* is a distinct taxon within *Caudivolvoxa* with a probability of ∼ 0.93 (Müller et al., 2007; Wolf et al., 2013).

In the phylogenies of the 18S rRNA gene and the rbcL gene it was possible to observe the four previously described clades (A, B, C, and D) for cold-tolerant taxa of *Chlamydomonas* and *Chloromonas* complex (Buchheim et al., 1997; Hoham et al., 2002), which reaffirms that these genera have colonized cold habitats at least five times during their evolutionary history (Hoham et al., 2002; Remias et al., 2010; Hoham and Remias, 2020). Additionally, by including the recent clade of *Sanguina*, another origin in cold habitats is added (Procházková et al., 2019a). In *Stephanosphaerinia*, in addition to the polar subclade of *Cm. collina* and related strains, there are other cold-adapted members such as *Macrochloris rubrioleum* CCCryo 340b-08, suggesting that there is more than one origin of cold-adaptation within of this clade. In addition, the present phylogenies show that the representatives of both *Chlamydomonas* and *Chloromonas* are not closely related, confirming the reported polyphilia of both genera (Nakayama et al., 1996; Pröschold et al., 2001; Barcytė et al., 2018a). This can be the result of a combination of factors such as the use of symplesiomorphies, environmentally variable characters, evolutionary convergence of vegetative morphologies, or maybe the omission of ecological preferences that can drive sympatric differentiation (Nakayama et al., 1996; Pröschold et al., 2001; Malavasi et al., 2016). In fact, this last point has resolved the classification of genera attaining problematic morphologies such as *Coccomyxa* (Malavasi et al., 2016). Interestingly, in *Chloromonas-Chlamydomonas* complex, the habitat has been strongly correlated with the phylogenetic history of these genera irrespective of morphology (Buchheim et al., 1997; Hoham et al., 2002; Barcytė et al., 2018b). The discovery of polar subclades in the Chlamydomonadales (Demchenko et al., 2012; Procházková et al., 2019a), such as observed in the present study, support the idea that extreme environments have promoted the evolution and speciation in unicellular chlorophytes (Pollio et al., 2005; Fučíková et al., 2014; Malavasi et al., 2016).

Considering that *Cm. collina* (i) forms an independent lineage within *Stephanosphaerinia*, (ii) it is sister to strains assigned to *Chloromonas* or *Chlamydomonas,* but which are not monophyletic with the type species of *Chloromonas* (*Cr. reticulata*) or *Chlamydomonas* (*Cd. reinhardtii*), so it is not can maintain the assigned generic identity and must be transferred to other genera (Pröschold et al., 2001), we propose a new genus *Chlorominima*, describing the type species *Cm. collina*, with the aim of generating a baseline to identify the rest of the members of

this polar monophyletic lineage, contributing to the biodiversity of Chlamydomonadales.

The Psychrophilic Character of *Chlorominima collina*: A Typical Feature of True Snow Algae

Physiological experiments revealed that *Cm. collina* is a psychrophilic organism, therefore the increase in temperature to 20°C causes in this strain a marked decrease of the maximum quantum yield of the PSII and oxidative stress on the third day of exposure. These responses were also correlated with a decline in growth. Probably it was a direct result of thermal stress, which can affect key metabolic functions, disrupting cellular homeostasis and uncoupling physiological processes (Suzuki and Mittler, 2006; Barati et al., 2019). Likewise, the effects of ROS vary not only according to temperature, but also according to the duration of heat stress (Dunn et al., 2004), which in this case was in scale of days. The maintenance of growth and photosynthetic performance or F_v/F_m during the first days of exposure to 10°C and the subsequent decline of these parameters may indicate that this temperature is a physiological limit for *Cm. collina* similar to that observed in other snow algae (Hoham, 1975b; Devos et al., 1998). In addition to growth, the psychrophilic character was evaluated through the maximum quantum yield of PSII (F_v/F_m), since this physiological parameter is sensitive to alterations in early photochemical reactions revealing stress (Maxwell and Johnson, 2000). These changes were observed in *Cm. collina* after 24 h of exposure at 20°C with a decrease in F_V/F_m below 0.4 compared to F_V/F_m above 0.5 at 2°C (**Figure 7B**). Such alterations may not be detected using growth alone, so evaluating growth alone is inappropriate to define a psychrophilic organism (Feller and Gerday, 2003).

True snow algae are regarded as psychrophilic organisms that thrive exclusively in snow (Komárek and Nedbalová, 2007; Leya, 2013). This classification is valid for some algae of the genus *Chloromonas* such as *Cr. pichinchae* (Hoham, 1975a), *Cr. tughillensis*, and *Cr. chenangoensis* (Hoham et al., 2008). However, other snow isolates such as *Cr. rosae* v. *psychrophile* (Hoham et al., 2008), *Cr. arctica* (Barcytė et al., 2018a) and *Cr. svalbardensis* (Barcytė et al., 2018b) can be regarded as psychrotolerant. These algae, in contrast to true snow algae, can inhabit other substrates (e.g., soil, freshwater) (Stibal and Elster, 2005; Komárek and Nedbalová, 2007), nevertheless, under persistent cold conditions they can acquire psychrophilic adaptions (Cvetkovska et al., 2017).

The psychrophilic nature of *Cm. collina* is also supported by the presence of plastoglobuli in the chloroplast, which contains specialized proteomes and metabolomes to respond to abiotic stress (van Wijk and Kessler, 2017). In addition, stressors such as high doses of UV-B radiation (Tian and Yu, 2009) or sulfur deficiency (Mizuno et al., 2013) have been reported to cause an increase in starch grains. The latter was observed in old cells of *Cm. collina* similar to *Cr. arctica* (Barcytė et al., 2018a), but unlike this alga, *Cm. collina* cells retain their flagella only at low temperature. When *Cm. collina* cells are exposed to elevated temperatures, they lose their flagella, similar to observed in the snow algae *Chlainomonas kolii* and *Chlainomonas rubra* (Hoham, 1975b).

The Transcriptome of *Chlorominima collina* Reflects Adaptations to the Antarctic Snow Environment

Based on the functional annotation of the transcriptome, it is possible to identify the expression of the following groups of key genes: (i) stress-responsive genes, including genes that encode "heat shock proteins." The expression of these genes is common in polar algae and cannot only be stimulated by heat, but also by cold (Liu et al., 2010, 2016; Kim et al., 2013). In addition, we identified CaM genes or "calmodulin," whose expression is regulated by non-optimal temperature conditions, high UV-B radiation and salinity, conditions commonly found in Maritime Antarctica (He et al., 2017). Besides, the presence of genes of ABC transporters, linked to transport of metabolic intermediates and compounds for detoxification, as observed in other polar algae suggests a functional role in cold acclimatization (Mock et al., 2006; Liu et al., 2016; Poong et al., 2018). We also identified (ii) ice-active genes, such as genes encoding "antifreeze glycoprotein" and "ice-binding proteins" or IBPs, which have been found only in psychrophilic species (Oude Vrielink et al., 2016), particularly in snow species of the Chlamydomonadales (Leya, 2013). Therefore there are no homologs to IBPs in mesophilic species (Raymond et al., 2009; Dolhi et al., 2013). The novel IBPs discovered the Antarctic strain *Chlamydomonas* sp. CCMP681 showed effects on the inhibition of recrystallization and on the retention of brine in ice (Raymond et al., 2009), likewise the expression of IBP genes can also be regulated by heat (Jung et al., 2016a) and light stress (Gwak et al., 2014). The origin of these genes, whose resemblance to bacterial IBPs genes suggests the idea of a possible horizontal gene transfer (HGT), which can be facilitated by transposases (Raymond and Kim, 2012; Liu et al., 2016). Although some transposases were identified in the *Cm. collina* transcriptome, (TRINITY_DN1269; TRINITY_DN2803), evidence for HGT is still not conclusive. We also observe (iii) genes encoding cryoprotectants and fatty acids such as "Omega-3-fatty acid desaturase" involved in the biosynthesis of polyunsaturated fatty acids or PUFAs (Garba et al., 2017). Since PUFAs regulate membrane fluidity, their prevalence is regarded as one of the most common adaptations of psychrophilic organisms (De Maayer et al., 2014). Likewise, the presence of "Cytochrome P450, C-22 desaturase" genes can be indicative of sterol biosynthesis that also regulates the fluidity of the membrane (Brumfield et al., 2017). Furthermore, "Diacylglycerol acyltransferase" genes involved in the biosynthesis of triacylglycerol (TAG) were found, which is related to tolerance to freezing (Zienkiewicz et al., 2016; Tan et al., 2018). The presence of "Phytoene desaturase" genes may suggest an active synthesis of secondary carotenoids (Grünewald et al., 2000), whose antioxidant activity is also induced by cold (Gocheva et al., 2009; Lemoine and Schoefs, 2010). Other genes, such as those that encode "Betaine aldehyde dehydrogenase," suggest the accumulation of betaine that reduce the freezing point in the cytoplasm (De Maayer et al., 2014). Thus, it is proposed that

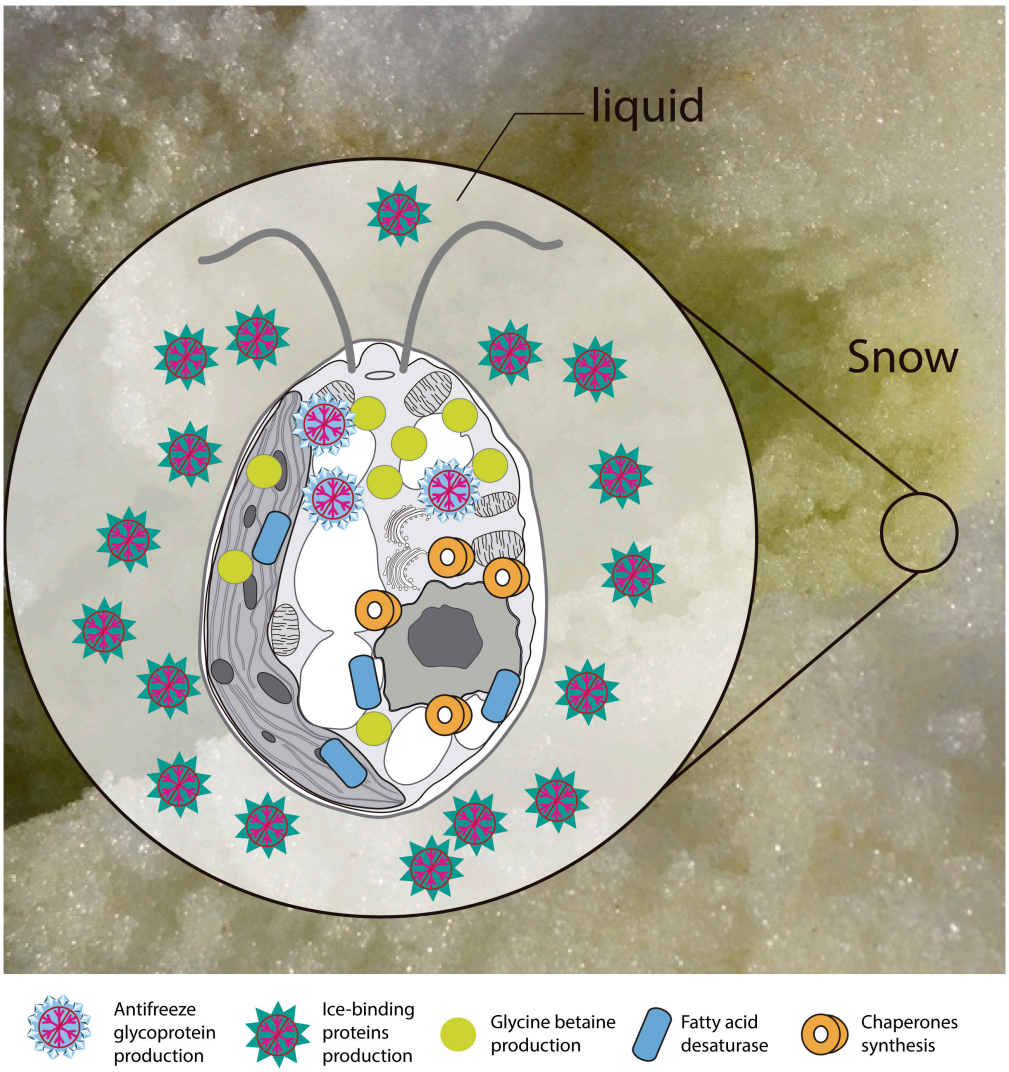

FIGURE 10 | Scheme of the main transcriptional responses at low temperature. Putative proteins and enzymes present in the *Chlorominima collina* CCAP 6/1 transcriptome are represented.

joint regulation of the above-mentioned genes allows *Cm. collina* (**Figure 10**) to thrive in Antarctic snow.

CONCLUSION

Our study corroborates the suitability of using a polyphasic approach to identify and characterize snow alga *Cm. collina*. This new strain presents some typical morphological features of *Chloromonas*-like algae but differs from this genus by the unusual position of the nucleus, the shape of the chloroplast, the number of vacuoles and the small size of the cells. The phylogenies confirm that the new alga is not *Chloromonas* but forms an independent lineage, sister to other strains uncertainly assigned to *Chloromonas-Chlamydomonas*, forming a polar subclade within *Stephanosphaerinia*. Within the Chlamydomonadales, *Cm. collina* is proposed as a distinct taxon according to the comparisons with models of the secondary structures of the ITS2 rDNA. Based on these results, we propose a new Antarctic genus, *Chlorominima* with the species type *Cm. collina*. The integration of physiological and transcriptomic approaches revealed psychrophilic characteristics that reflect adaptations to the snow environment. Therefore, the description of *Cm. collina,* improves our knowledge on the diversity of snow algae within *Stephanosphaerinia.*

NOMENCLATURE

Resource Identification Initiative

To take part in the Resource Identification Initiative, please use the corresponding catalog number and RRID in your current manuscript. For more information about the project and for steps on how to search for an RRID, please click here.

Life Science Identifiers

Life Science Identifiers (LSIDs) for ZOOBANK registered names or nomenclatural acts should be listed in the manuscript before the keywords with the following format:

urn:lsid: < Authority > : < Namespace > : < ObjectID > [: < Version >]

For more information on LSIDs please see Inclusion of Zoological Nomenclature section of the guidelines.

DATA AVAILABILITY STATEMENT

The datasets presented in this study can be found in online repositories. The names of the repository/repositories and accession number(s) can be found in the article/ **Supplementary Material**.

AUTHOR CONTRIBUTIONS

FEG sampled the algal material in the Antarctic, performed the isolation of the strain from cysts, and conducted the light microscopy and assisted in the electron microscopy studies. Also, carried out the physiological experiment and measurements for thermal threshold and transcriptomic analysis. PH supervised at the beginning the cultivation and maintenance procedures in the laboratory as well as the fluorescence techniques for growth rate measurement. AS and FEG with the help of the AUSTRAL-omics team and obtained the DNA sequences and performed the RNA extraction. MS-C performed the phylogenetic analyses and the sequence structure of the ITS2 rDNA. AS was in charge of the RNA library sequencing and transcriptional analysis. The first draft of manuscript was written by FEG and edited by IG. Finally, all authors contributed with inputs to the final stage of the manuscript.

FUNDING

This research was funded by the grants Fondecyt 1161129, Fondecyt 1201053 and Fondap IDEAL 15150003 to IG and PH, and INACh DG_12_19 to FEG.

ACKNOWLEDGMENTS

The Instituto Antártico Chileno (INACh) granted the necessary permissions to obtain snow samples in the Antarctic in accordance with the Protocol on Environmental Protection to the Antarctic Treaty and provided the logistic support at the Professor Julio Escudero scientific station during the campaign 2018-ECA54. We would like to thank Dayane Osman for her valuable technical assistance during field sampling and during laboratory work. We would also like to thank the Electron Microscopy Unit (UME) of the Universidad Austral de Chile for TEM analysis. We are grateful to Carolina Encina and Luis Guzman for helpful assistance during sequencing and library preparation at AUSTRAl-omics, and Nelson Valdivia and Cristian Molina for their help with data analysis and bioinformatics, respectively. We are also grateful for the valuable comments and criticisms of two reviewers and editor LN, who substantially improved the manuscript.

SUPPLEMENTARY MATERIAL

The Supplementary Material for this article can be found online at: https://www.frontiersin.org/articles/10.3389/fpls.2021.662298/full#supplementary-material

REFERENCES

Abadi, S., Azouri, D., Pupko, T., and Mayrose, I. (2019). Model selection may not be a mandatory step for phylogeny reconstruction. *Nat. Commun.* 10:934. doi: 10.1038/s41467-019-08822-w

Altschul, S. F., Gish, W., Miller, W., Myers, E. W., and Lipman, D. J. (1990). Basic local alignment search tool. *J. Mol. Biol.* 215, 403–410. doi: 10.1016/S0022-2836(05)80360-2

Andersen, R. A. (2005). *Algal Culturing Techniques*. Cambridge, MA: Academic Press.

Anesio, A. M., and Laybourn-Parry, J. (2012). Glaciers and ice sheets as a biome. *Trends Ecol. Evol.* 27, 219–225.

Anesio, A. M., Lutz, S., Chrismas, N. A. M., and Benning, L. G. (2017). The microbiome of glaciers and ice sheets. *NPJ Biofilms Microbiomes* 3, 1–11.

Ashburner, M., Ball, C. A., Blake, J. A., Botstein, D., Butler, H., Cherry, J. M., et al. (2000). Gene ontology: tool for the unification of biology. *Nat. Genet.* 25, 25–29. doi: 10.1038/75556

Barati, B., Gan, S.-Y., Lim, P.-E., Beardall, J., and Phang, S.-M. (2019). Green algal molecular responses to temperature stress. *Acta Physiol. Plant.* 41:26. doi: 10.1007/s11738-019-2813-1

Barcytė, D., Hodač, L., Nedbalová, L., and Elster, J. (2018a). *Chloromonas arctica* sp. nov., a psychrotolerant alga from snow in the High Arctic (Chlamydomonadales, Chlorophyta). *Int. J. Syst. Evol. Microbiol.* 68, 851–859. doi: 10.1099/ijsem.0.002595

Barcytė, D., Hodač, L., Nedbalová, L., and Elster, J. (2018b). *Chloromonas svalbardensis* n. sp. with Insights into the Phylogroup Chloromonadinia (Chlorophyceae). *J. Eukaryot. Microbiol.* 65, 882–892. doi: 10.1111/jeu.12633

Barton, K. (2019). *MuMIn: Multi-Model Inference. R package version 1.43.6*.

Bates, D., Mächler, M., Bolker, B., and Walker, S. (2015). Fitting linear mixed-effects models using lme4. *J. Stat. Softw.* 67, 1–48.

Bischoff, H. W., and Bold, H. C. (1963). *Some Algae from Enchanted Rock and Related Algal Species*. Austin, TX: University of Texas.

Boetius, A., Anesio, A. M., Deming, J. W., Mikucki, J. A., and Rapp, J. Z. (2015). Microbial ecology of the cryosphere: sea ice and glacial habitats. *Nat. Rev. Microbiol.* 13, 677–690. doi: 10.1038/nrmicro3522

Bolker, B., and Team, R. C. (2017). *bbmle: Tools for General Maximum Likelihood Estimation. R Package version 1.0. 19*.

Breslow, N. E., and Clayton, D. G. (1993). Approximate inference in generalized linear mixed models. *J. Am. Stat. Assoc.* 88:9. doi: 10.2307/2290687

Broady, P. (1996). Diversity, distribution and dispersal of Antarctic terrestrial algae. *Biodivers. Conserv.* 5, 1307–1335. doi: 10.1007/BF00051981

Brooks, M. E., Kristensen, K., van Benthem, K. J., Magnusson, A., Berg, C. W., Nielsen, A., et al. (2017). glmmTMB balances speed and flexibility among packages for zero-inflated generalized linear mixed modeling. *R J.* 9, 378–400. doi: 10.32614/RJ-2017-066

Brumfield, K. M., Laborde, S. M., and Moroney, J. V. (2017). A model for the ergosterol biosynthetic pathway in *Chlamydomonas reinhardtii*. *Eur. J. Phycol.* 52, 64–74. doi: 10.1080/09670262.2016.1225318

Buchheim, M. A., Buchheim, J. A., and Chapman, R. L. (1997). Phylogeny of *Chloromonas* (Chlorophyceae): a study of 18S ribosomal RNA gene sequences. *J. Phycol.* 33, 286–293. doi: 10.1111/j.0022-3646.1997.00286.x

Buchheim, M. A., Sutherland, D. M., Buchheim, J. A., and Wolf, M. (2013). The blood alga: phylogeny of *Haematococcus* (Chlorophyceae) inferred from ribosomal RNA gene sequence data. *Eur. J. Phycol.* 48, 318–329. doi: 10.1080/09670262.2013.830344

Caisová, L., Marin, B., and Melkonian, M. (2013). A consensus secondary structure of ITS2 in the Chlorophyta identified by phylogenetic reconstruction. *Protist* 164, 482–496. doi: 10.1016/j.protis.2013.04.005

Coleman, A. W. (2000). The significance of a coincidence between evolutionary landmarks found in mating affinity and a DNA sequence. *Protist* 151, 1–9. doi: 10.1078/1434-4610-00002

Conesa, A., Götz, S., García-Gómez, J. M., Terol, J., Talón, M., and Robles, M. (2005). Blast2GO: a universal tool for annotation, visualization and analysis in functional genomics research. *Bioinformatics* 21, 3674–3676. doi: 10.1093/bioinformatics/bti610

Cook, A. J. (2005). Retreating glacier fronts on the Antarctic Peninsula over the past half-century. *Science* 308, 541–544. doi: 10.1126/science.1104235

Cornejo-Corona, I., Thapa, H. R., Browne, D. R., Devarenne, T. P., and Lozoya-Gloria, E. (2016). Stress responses of the oil-producing green microalga *Botryococcus braunii* Race B. *PeerJ* 4:e2748. doi: 10.7717/peerj.2748

Cvetkovska, M., Hüner, N. P. A., and Smith, D. R. (2017). Chilling out: the evolution and diversification of psychrophilic algae with a focus on Chlamydomonadales. *Polar Biol.* 40, 1169–1184. doi: 10.1007/s00300-016-2045-4

Darty, K., Denise, A., and Ponty, Y. (2009). VARNA: interactive drawing and editing of the RNA secondary structure. *Bioinformatics* 25:1974.

De Maayer, P., Anderson, D., Cary, C., and Cowan, D. A. (2014). Some like it cold: understanding the survival strategies of psychrophiles. *EMBO Rep.* 15, 508–517. doi: 10.1002/embr.201338170

Demchenko, E., Mikhailyuk, T., Coleman, A. W., and Pröschold, T. (2012). Generic and species concepts in Microglena (previously the *Chlamydomonas monadina* group) revised using an integrative approach. *Eur. J. Phycol.* 47, 264–290. doi: 10.1080/09670262.2012.678388

Deng, Y. Y., Li, J. Q., Wu, S. F., Zhu, Y. P., Chen, Y. W., and He, F. (2006). Integrated nr database in protein annotation system and its localization. *Comput. Eng.* 32, 71–72.

Devos, N., Ingouff, M., Loppes, R., and Matagne, R. F. (1998). RUBISCO adaptation to low temperatures: a comparative study in psychrophilic and mesophilic unicellular algae. *J. Phycol.* 34, 655–660. doi: 10.1046/j.1529-8817.1998.340655.x

Dolhi, J. M., Maxwell, D. P., and Morgan-Kiss, R. M. (2013). Review: the Antarctic *Chlamydomonas raudensis*: an emerging model for cold adaptation of photosynthesis. *Extremophiles* 17, 711–722. doi: 10.1007/s00792-013-0571-3

Dunn, S. R., Thomason, J. C., Le Tissier, M. D. A., and Bythell, J. C. (2004). Heat stress induces different forms of cell death in sea anemones and their endosymbiotic algae depending on temperature and duration. *Cell Death Differ.* 11, 1213–1222. doi: 10.1038/sj.cdd.4401484

Ettl, H. (1970). Die Gattung *Chloromonas* Gobi emend. Wille (Chlamydomonas und Die Nächstverwandten Gattungen I). Nov. *Hedwigia Beihefte* 34, 1–283.

Ettl, H. (1983). *Chlorophyta I. Phytomonadina*. Portland, OR: Gustav Fischer.

Feller, G., and Gerday, C. (2003). Psychrophilic enzymes: hot topics in cold adaptation. *Nat. Rev. Microbiol.* 1, 200–208. doi: 10.1038/nrmicro773

Fogg, G. E. (1967). Observations on the snow algae of the South Orkney Islands. *Philos. Trans. R. Soc. Lond. B. Biol. Sci.* 252, 279–287. doi: 10.1098/rstb.1967.0018

Friedl, T. (1996). Evolution of the polyphyletic genus *Pleurastrum* (Chlorophyta): inferences from nuclear-encoded ribosomal DNA sequences and motile cell ultrastructure. *Phycologia* 35, 456–469. doi: 10.2216/i0031-8884-35-5-456.1

Fučíková, K., Lewis, P. O., and Lewis, L. A. (2014). Putting incertae sedis taxa in their place: a proposal for ten new families and three new genera in Sphaeropleales (Chlorophyceae, Chlorophyta). *J. Phycol.* 50, 14–25. doi: 10.1111/jpy.12118

Garba, L., Shukuri Mo, M., Nurbaya Os, S., and Noor Zalih, R. (2017). Review on fatty acid desaturases and their roles in temperature acclimatisation. *J. Appl. Sci.* 17, 282–295. doi: 10.3923/jas.2017.282.295

Garcia-Lopez, E., and Cid, C. (2017). "The role of microbial ecology in glacier retreat," in *Glaciers Evolution in a Changing World*, ed. D. Godone (London: InTech), 105. doi: 10.5772/intechopen.69097

Gocheva, Y. G., Tosi, S., Krumova, E. T., Slokoska, L. S., Miteva, J. G., Vassilev, S. V., et al. (2009). Temperature downshift induces antioxidant response in fungi isolated from Antarctica. *Extremophiles* 13, 273–281. doi: 10.1007/s00792-008-0215-1

Götz, S., García-Gómez, J. M., Terol, J., Williams, T. D., Nagaraj, S. H., Nueda, M. J., et al. (2008). High-throughput functional annotation and data mining with the Blast2GO suite. *Nucleic Acids Res.* 36, 3420–3435. doi: 10.1093/nar/gkn176

Grabherr, M. G., Haas, B. J., Yassour, M., Levin, J. Z., Thompson, D. A., Amit, I., et al. (2011). Full-length transcriptome assembly from RNA-Seq data without a reference genome. *Nat. Biotechnol.* 29, 644–652. doi: 10.1038/nbt.1883

Gradinger, R., and Nürnberg, D. (1996). Snow algal communities on Arctic pack ice floes dominated by *Chlamydomonas nivalis* (Bauer) Wille. *Proc. NIPR Symp. Polar Biol.* 9, 35–43.

Grünewald, K., Eckert, M., Hirschberg, J., and Hagen, C. (2000). Phytoene desaturase is localized exclusively in the chloroplast and up-regulated at the mRNA Level during accumulation of secondary carotenoids in *Haematococcus pluvialis* (Volvocales, Chlorophyceae). *Plant Physiol.* 122, 1261–1268. doi: 10.1104/pp.122.4.1261

Gwak, Y., Jung, W., Lee, Y., Kim, J. S., Kim, C. G., Ju, J.-H., et al. (2014). An intracellular antifreeze protein from an Antarctic microalga that responds to various environmental stresses. *FASEB J.* 28, 4924–4935. doi: 10.1096/fj.14-256388

Hamby, K. R., Sims, L., Issel, L., and Zimmer, E. (1988). Direct ribosomal RNA sequencing: optimization of extraction and sequencing methods for work with higher plants. *Plant Mol. Biol. Report.* 6, 175–192. doi: 10.1007/BF02669591

Hamilton, T. L., and Havig, J. (2017). Primary productivity of snow algae communities on stratovolcanoes of the Pacific Northwest. *Geobiology* 15, 280–295. doi: 10.1111/gbi.12219

Hammer, Ø, Harper, D. A. T., and Ryan, P. D. (2001). PAST: Paleontological statistics software package for education and data analysis. *Palaeontol. Electron.* 4:9.

Hartig, F. (2020). *DHARMa: Residual Diagnostics for Hierarchical (Multi-Level/Mixed) Regression Models. R Package V. 0.3.3.0.*

Havig, J. R., and Hamilton, T. L. (2019). Snow algae drive productivity and weathering at volcanic rock-hosted glaciers. *Geochim. Cosmochim. Acta* 247, 220–242. doi: 10.1016/j.gca.2018.12.024

He, Y., Wang, Y., Zheng, Z., Liu, F., An, M., He, X., et al. (2017). Cloning and stress-induced expression analysis of calmodulin in the Antarctic alga *Chlamydomonas* sp. ICE-L. *Curr. Microbiol.* 74, 921–929. doi: 10.1007/s00284-017-1263-5

Hofacker, I. L. (2003). Vienna RNA secondary structure server. *Nucleic Acids Res.* 31, 3429–3431. doi: 10.1093/nar/gkg599

Hoham, R. W. (1975a). Optimum temperatures and temperature ranges for growth of snow algae. *Arct. Alp. Res.* 7, 13–24. doi: 10.2307/1550094

Hoham, R. W. (1975b). The life history and ecology of the snow alga *Chloromonas pichinchae* (Chlorophyta, Volvocales). *Phycologia* 14, 213–226. doi: 10.2216/i0031-8884-14-4-213.1

Hoham, R. W., Bonome, T. A., Martin, C. W., and Leebens-Mack, J. H. (2002). A combined 18S rDNA and rbcL phylogenetic analysis of *Chloromonas* and *Chlamydomonas* (Chlorophyceae, Volvocales) emphasizing snow and other cold-temperature habitats. *J. Phycol.* 38, 1051–1064. doi: 10.1046/j.1529-8817.2002.t01-1-01227.x

Hoham, R. W., Frey, F. M., Mohn, W. W., Felio, J. H., Todd, S., Duncan, J. E., et al. (2008). Optimum growth temperatures of three species of green *Chloromonas* snow algae from Upstate New York and the White Mountains, Arizona. *Arctic Antarct. Alp. Res.* 40, 355–363.

Hoham, R. W., and Remias, D. (2020). Snow and glacial algae: a review. *J. Phycol.* 56, 264–282. doi: 10.1111/jpy.12952

Hothorn, T., Bretz, F., and Westfall, P. (2008). Simultaneous inference in general parametric models. *Biometrical J.* 50, 346–363. doi: 10.1002/bimj.200810425

Huovinen, P., Ramírez, J., and Gómez, I. (2018). Remote sensing of albedo-reducing snow algae and impurities in the Maritime Antarctica. *ISPRS J. Photogramm. Remote Sens.* 146, 507–517. doi: 10.1016/j.isprsjprs.2018.10.015

Jukes, T. H., and Cantor, C. R. (1969). "Evolution of protein molecules," in *Mammalian Protein Metabolism*, ed. H. N. Munro (Amsterdam: Elsevier), 21–132.

Jung, W., Campbell, R. L., Gwak, Y., Kim, J. I., Davies, P. L., and Jin, E. (2016a). New cysteine-rich ice-binding protein secreted from Antarctic microalga, *Chloromonas* sp. *PLoS One* 11:e0154056. doi: 10.1371/journal.pone.0154056

Jung, W., Kim, E. J., Lim, S., Sim, H., Han, S. J., Kim, S., et al. (2016b). Cellular growth and fatty acid content of Arctic chlamydomonadalean. *Algae* 31, 61–71. doi: 10.4490/algae.2016.31.2.8

Keller, A., Schleicher, T., Schultz, J., Müller, T., Dandekar, T., and Wolf, M. (2009). 5.8S-28S rRNA interaction and HMM-based ITS2 annotation. *Gene* 430, 50–57. doi: 10.1016/j.gene.2008.10.012

Kim, S., Kim, M. J., Jung, M. G., Lee, S., Baek, Y.-S., Kang, S.-H., et al. (2013). De novo transcriptome analysis of an Arctic microalga, *Chlamydomonas* sp. *Genes Genomics* 35, 215–223. doi: 10.1007/s13258-013-0085-5

Koetschan, C., Förster, F., Keller, A., Schleicher, T., Ruderisch, B., Schwarz, R., et al. (2010). The ITS2 Database III—sequences and structures for phylogeny. *Nucleic Acids Res.* 38, D275–D279. doi: 10.1093/nar/gkp966

Koetschan, C., Hackl, T., Müller, T., Wolf, M., Förster, F., and Schultz, J. (2012). ITS2 database IV: interactive taxon sampling for internal transcribed spacer 2 based phylogenies. *Mol. Phylogenet. Evol.* 63, 585–588. doi: 10.1016/j.ympev.2012.01.026

Kol, E. (1968). "Kryobiologie. Biologie und limnologie des schnees und eises. I. Kryovegetation," in *Die Binnengewiisser*, Vol. 24, eds A. Thienemann, J. Elster, and W. Ohle (Stuttgart: Schweizerbart'sche Verlagsbuchhandlung), 216.

Kol, E. (1971). Green snow and ice from the Antarctica. *Ann. Hist. Nat. Mus. Natl. Hung.* 63, 51–56.

Kol, E., and Flint, E. A. (1968). Algae in green ice from the Balleny Islands, Antarctica. *New Zeal. J. Bot.* 6, 249–261. doi: 10.1080/0028825X.1968.10428810

Komárek, J., and Nedbalová, L. (2007). "Green cryosestic algae," in *Algae and Cyanobacteria in Extreme Environments. Cellular Origin, Life in Extreme Habitats and Astrobiology*, Vol. 11, ed. J. Seckbach (Dordrecht: Springer), 321–342. doi: 10.1007/978-1-4020-6112-7_17

Komárek, O., and Komárek, J. (1999). Diversity of freshwater and terrestrial habitats and their oxyphototroph microflora in the Arctowski Station region, South Shetland Islands. *Polish Polar Res.* 20, 259–282.

Komárek, O., and Komárek, J. (2001). Contribution to the taxonomy and ecology of green cryosestic algae in the summer season 1995-96 at King George Island, S. Shetland Islands. *Nov. Hedwigia* 123, 121–140.

Krug, L., Erlacher, A., Markut, K., Berg, G., and Cernava, T. (2020). The microbiome of alpine snow algae shows a specific inter-kingdom connectivity and algae-bacteria interactions with supportive capacities. *ISME J.* 14, 2197–2210.

Kumar, S., Stecher, G., Li, M., Knyaz, C., and Tamura, K. (2018). MEGA X: molecular evolutionary genetics analysis across computing platforms. *Mol. Biol. Evol.* 35, 1547–1549. doi: 10.1093/molbev/msy096

Lemoine, Y., and Schoefs, B. (2010). Secondary ketocarotenoid astaxanthin biosynthesis in algae: a multifunctional response to stress. *Photosynth. Res.* 106, 155–177. doi: 10.1007/s11120-010-9583-3

Lenth, R. (2019). *emmeans: Estimated Marginal Means, Aka Least-Squares Means. R Package Version 1.4.3.01*.

Leya, T. (2013). "Snow algae: adaptation strategies to survive on snow and ice," in *Polyextremophiles. Cellular Origin, Life in Extreme Habitats and Astrobiology*, eds J. Seckbach, A. Oren, and H. Stan-Lotter (Dordrecht: Springer), 401–423. doi: 10.1007/978-94-007-6488-0_17

Ling, H. U. (1996). 10. Snow algae of the Windmill Islands region, Antarctica. *Hydrobiologia* 336, 99–106. doi: 10.1007/BF00010823

Ling, H. U., and Seppelt, R. D. (1998). Snow algae of the Windmill Islands, continental Antarctica 3. *Chloromonas polyptera* (Volvocales, Chlorophyta). *Polar Biol.* 20, 320–324. doi: 10.1007/s003000050309

Liu, C., Wang, X., Wang, X., and Sun, C. (2016). Acclimation of Antarctic Chlamydomonas to the sea-ice environment: a transcriptomic analysis. *Extremophiles* 20, 437–450. doi: 10.1007/s00792-016-0834-x

Liu, C., Zhao, X., and Wang, X. (2018). Identification and characterization of the psychrophilicbacterium CidnaK gene in the Antarctic *Chlamydomoas* sp. ICE-L under freezing conditions. *J. Appl. Phycol.* 30, 3519–3528. doi: 10.1007/s10811-018-1492-4

Liu, S., Zhang, P., Cong, B., Liu, C., Lin, X., Shen, J., et al. (2010). Molecular cloning and expression analysis of a cytosolic Hsp70 gene from Antarctic ice algae *Chlamydomonas* sp. ICE-L. *Extremophiles* 14, 329–337. doi: 10.1007/s00792-010-0313-8

Lüdecke, D., Makowski, D., Waggoner, P., and Patil, I. (2020). *performance: Assessment of Regression Models Performance. R Package Version 0.4.6*.

Luo, W., Ding, H., Li, H., Ji, Z., Huang, K., Zhao, W., et al. (2020). Molecular diversity of the microbial community in coloured snow from the Fildes Peninsula (King George Island, Maritime Antarctica). *Polar Biol.* 43, 1391–1405. doi: 10.1007/s00300-020-02716-0

Lutz, S., Anesio, A. M., Edwards, A., and Benning, L. G. (2015). Microbial diversity on Icelandic glaciers and ice caps. *Front. Microbiol.* 6:307. doi: 10.3389/fmicb.2015.00307

Lutz, S., Anesio, A. M., Jorge Villar, S. E., and Benning, L. G. (2014). Variations of algal communities cause darkening of a Greenland glacier. *FEMS Microbiol. Ecol.* 89, 402–414. doi: 10.1111/1574-6941.12351

Lutz, S., Prochazkova, L., Benning, L. G., Nedbalova, L., and Remias, D. (2019). Evaluating amplicon high-throughput sequencing data of microalgae living in melting snow: improvements and limitations. *Fottea* 19, 115–131. doi: 10.5507/fot.2019.003

Lyon, B. R., and Mock, T. (2014). Polar microalgae: new approaches towards understanding adaptations to an extreme and changing environment. *Biology (Basel)* 3, 56–80. doi: 10.3390/biology3010056

Malavasi, V., Škaloud, P., Rindi, F., Tempesta, S., Paoletti, M., and Pasqualetti, M. (2016). DNA-based taxonomy in ecologically versatile microalgae: a re-evaluation of the species concept within the coccoid green algal genus *Coccomyxa* (Trebouxiophyceae, Chlorophyta). *PLoS One* 11:e0151137. doi: 10.1371/journal.pone.0151137

Marchant, H. J. (1982). Snow algae from the Australian snowy mountains. *Phycologia* 21, 178–184. doi: 10.2216/i0031-8884-21-2-178.1

Matsuzaki, R., Hara, Y., and Nozaki, H. (2012). A taxonomic revision of *Chloromonas reticulata* (Volvocales, Chlorophyceae), the type species of the genus Chloromonas, based on multigene phylogeny and comparative light and electron microscopy. *Phycologia* 51, 74–85. doi: 10.2216/11-18.1

Matsuzaki, R., Kawai-Toyooka, H., Hara, Y., and Nozaki, H. (2015). Revisiting the taxonomic significance of aplanozygote morphologies of two cosmopolitan snow species of the genus *Chloromonas* (Volvocales, Chlorophyceae). *Phycologia* 54, 491–502. doi: 10.2216/15-33.1

Matsuzaki, R., Nozaki, H., and Kawachi, M. (2018). Taxonomic revision of *Chloromonas nivalis* (Volvocales, Chlorophyceae) strains, with the new description of two snow-inhabiting *Chloromonas* species. *PLoS One* 13:e0193603. doi: 10.1371/journal.pone.0193603

Matsuzaki, R., Nozaki, H., Takeuchi, N., Hara, Y., and Kawachi, M. (2019). Taxonomic re-examination of "*Chloromonas nivalis* (Volvocales, Chlorophyceae) zygotes" from Japan and description of *C. muramotoi* sp. nov. *PLoS One* 14:e0210986. doi: 10.1371/journal.pone.0210986

Matsuzaki, R., Yoshiaki, H., and Hisayoshi, N. (2014). A taxonomic study of snow *Chloromonas* species (Volvocales, Chlorophyceae) based on light and electron microscopy and molecular analysis of cultured material. *Phycologia* 53, 293–304. doi: 10.2216/14-3.1

Maxwell, K., and Johnson, G. N. (2000). Chlorophyll fluorescence—a practical guide. *J. Exp. Bot.* 51, 659–668. doi: 10.1093/jexbot/51.345.659

Mikhailyuk, T. I., Sluiman, H. J., Massalski, A., Mudimu, O., Demchenko, E. M., Kondratyuk, S. Y., et al. (2008). New streptophyte green algae from terrestrial habitats and an assessment of the genus *Interfilum* (Klebsormidiophyceae, Streptophyta). *J. Phycol.* 44, 1586–1603. doi: 10.1111/j.1529-8817.2008.00606.x

Mizuno, Y., Sato, A., Watanabe, K., Hirata, A., Takeshita, T., Ota, S., et al. (2013). Sequential accumulation of starch and lipid induced by sulfur deficiency in *Chlorella* and *Parachlorella* species. *Bioresour. Technol.* 129, 150–155. doi: 10.1016/j.biortech.2012.11.030

Mock, T., Krell, A., Glockner, G., Kolukisaoglu, U., and Valentin, K. (2006). Analysis of expressed sequence TAGS (ESTS) from the polar diatom *Fragilariopsis cylindrus*. *J. Phycol.* 42, 78–85. doi: 10.1111/j.1529-8817.2006.00164.x

Morel-Laurens, N. M. L., and Feinleib, M. E. (1983). Photomovement in an "eyeless" mutant of *Chlamydomonas*. *Photochem. Photobiol.* 37, 189–194. doi: 10.1111/j.1751-1097.1983.tb04457.x

Müller, T., Bleiß, W., Martin, C.-D., Rogaschewski, S., and Fuhr, G. (1998). Snow algae from northwest Svalbard: their identification, distribution, pigment and nutrient content. *Polar Biol.* 20, 14–32. doi: 10.1007/s003000050272

Müller, T., Philippi, N., Dandekar, T., Schultz, J., and Wolf, M. (2007). Distinguishing species. *RNA* 13, 1469–1472. doi: 10.1261/rna.617107

Muramoto, K., Nakada, T., Shitara, T., Hara, Y., and Nozaki, H. (2010). Re-examination of the snow algal species *Chloromonas miwae* (Fukushima) Muramoto et al., comb. nov. (Volvocales, Chlorophyceae) from Japan, based on molecular phylogeny and cultured material. *Eur. J. Phycol.* 45, 27–37. doi: 10.1080/09670260903272607

Nakada, T., Misawa, K., and Nozaki, H. (2008). Molecular systematics of Volvocales (Chlorophyceae, Chlorophyta) based on exhaustive 18S rRNA phylogenetic analyses. *Mol. Phylogenet. Evol.* 48, 281–291. doi: 10.1016/j.ympev.2008.03.016

Nakada, T., and Nozaki, H. (2007). Two species of *Chlamydomonas* (Volvocales, Chlorophyceae) new to Japan. *J. Japanese Bot.* 82, 179–189.

Nakada, T., and Nozaki, H. (2009). Taxonomic study of two new genera of fusiform green flagellates, *Tabris* gen. nov. and *Hamakko* gen. nov. (Volvocales, Chlorophyceae). *J. Phycol.* 45, 482–492. doi: 10.1111/j.1529-8817.2009.00652.x

Nakayama, T., Watanabe, S., Mitsui, K., Uchida, H., and Inouye, I. (1996). The phylogenetic relationship between the Chlamydomonadales and Chlorococcales inferred from 18SrDNA sequence data. *Phycol. Res.* 44, 47–55. doi: 10.1111/j.1440-1835.1996.tb00037.x

Oude Vrielink, A. S., Aloi, A., Olijve, L. L. C., and Voets, I. K. (2016). Interaction of ice binding proteins with ice, water and ions. *Biointerphases* 11:018906. doi: 10.1116/1.4939462

Pawłowska, J., Walther, G., Wilk, M., de Hoog, S., and Wrzosek, M. (2013). The use of compensatory base change analysis of ITS2 as a tool in the phylogeny of Mucorales, illustrated by the *Mucor circinelloides* complex. *Org. Divers. Evol.* 13, 497–502. doi: 10.1007/s13127-013-0139-1

Pollio, A., Cennamo, P., Ciniglia, C., De Stefano, M., Pinto, G., and Huss, V. A. R. (2005). *Chlamydomonas pitschmannii* Ettl, a little known species from thermoacidic environments. *Protist* 156, 287–302. doi: 10.1016/j.protis.2005.04.004

Poong, S.-W., Lee, K.-K., Lim, P.-E., Pai, T.-W., Wong, C.-Y., Phang, S.-M., et al. (2018). RNA-Seq-mediated transcriptomic analysis of heat stress response in a polar *Chlorella* sp. (Trebouxiophyceae, Chlorophyta). *J. Appl. Phycol.* 30, 3103–3119. doi: 10.1007/s10811-018-1455-9

Procházková, L., Leya, T., Křížková, H., and Nedbalová, L. (2019a). *Sanguina nivaloides* and *Sanguina aurantia* gen. et spp. nov.(Chlorophyta): the taxonomy, phylogeny, biogeography and ecology of two newly recognised algae causing red and orange snow. *FEMS Microbiol. Ecol.* 95:fiz064. doi: 10.1093/femsec/fiz064

Procházková, L., Remias, D., Řezanka, T., and Nedbalová, L. (2018). *Chloromonas nivalis* subsp. tatrae, subsp. nov. (Chlamydomonadales, Chlorophyta): re–examination of a snow alga from the High Tatra Mountains (Slovakia). *Fottea* 18, 1–18. doi: 10.5507/fot.2017.010.Chloromonas

Procházková, L., Remias, D., Řezanka, T., and Nedbalová, L. (2019b). Ecophysiology of *Chloromonas hindakii* sp. nov. (chlorophyceae), causing orange snow blooms at different light conditions. *Microorganisms* 7, 1–22. doi: 10.3390/microorganisms7100434

Pröschold, T., and Leliaert, F. (2007). "Systematics of the green algae: conflict of classic and modern approaches," in *Unravelling the Algae: The Past, Present, and Future of Algal Systematics*, eds J. Brodie and J. Lewis (Boca Raton, FL: CRC Press), 123–153. doi: 10.1201/9780849379901

Pröschold, T., Marin, B., Schlösser, U. G., and Melkonian, M. (2001). Molecular phylogeny and taxonomic revision of *Chlamydomonas* (Chlorophyta). I. Emendation of *Chlamydomonas* Ehrenberg and *Chloromonas* Gobi, and description of *Oogamochlamys* gen. nov. and *Lobochlamys* gen. nov. *Protist* 152, 265–300. doi: 10.1078/1434-4610-00068

R Core Team (2018). *R: A Language and Environment for Statistical Computing, Version 3.5.2*. Vienna: R Foundation for Statistical Computing.

Rambaut, A., and Drummond, A. J. (2018). *FigTree v1. 4.4. Institute of Evolutionary Biology*. Edinburgh: University of Edinburgh.

Raymond, J. A., Janech, M. G., and Fritsen, C. H. (2009). Novel ice-binding proteins from a psychrophilic Antarctic alga (Chlamydomonadaceae, Chlorophyceae). *J. Phycol.* 45, 130–136. doi: 10.1111/j.1529-8817.2008.00623.x

Raymond, J. A., and Kim, H. J. (2012). Possible role of horizontal gene transfer in the colonization of sea ice by algae. *PLoS One* 7:e35968. doi: 10.1371/journal.pone.0035968

Remias, D., Karsten, U., Lütz, C., and Leya, T. (2010). Physiological and morphological processes in the Alpine snow alga *Chloromonas nivalis* (Chlorophyceae) during cyst formation. *Protoplasma* 243, 73–86. doi: 10.1007/s00709-010-0123-y

Remias, D., Procházková, L., Holzinger, A., and Nedbalová, L. (2018). Ecology, cytology and phylogeny of the snow alga *Scotiella cryophila* K-1 (Chlamydomonadales, Chlorophyta) from the Austrian Alps. *Phycologia* 57, 581–592. doi: 10.2216/18-45.1

Remias, D., Schwaiger, S., Aigner, S., Leya, T., Stuppner, H., and Lütz, C. (2012). Characterization of an UV- and VIS-absorbing, purpurogallin-derived secondary pigment new to algae and highly abundant in *Mesotaenium berggrenii* (Zygnematophyceae, Chlorophyta), an extremophyte living on glaciers. *FEMS Microbiol. Ecol.* 79, 638–648. doi: 10.1111/j.1574-6941.2011.01245.x

Remias, D., Wastian, H., Lütz, C., and Leya, T. (2013). Insights into the biology and phylogeny of *Chloromonas polyptera* (Chlorophyta), an alga causing orange snow in Maritime Antarctica. *Antarct. Sci.* 25, 648–656. doi: 10.1017/S0954102013000060

Ronquist, F., Teslenko, M., van der Mark, P., Ayres, D. L., Darling, A., Höhna, S., et al. (2012). MrBayes 3.2: efficient Bayesian phylogenetic inference and model choice across a large model space. *Syst. Biol.* 61, 539–542. doi: 10.1093/sysbio/sys029

Saitou, N., and Nei, M. (1987). The neighbour-joining method: a new method for reconstructing phylogenetic trees. *Mol. Biol. Evol.* 4, 406–425. doi: 10.1093/oxfordjournals.molbev.a040454

Schmieder, R., and Edwards, R. (2011). Quality control and preprocessing of metagenomic datasets. *Bioinformatics* 27, 863–864. doi: 10.1093/bioinformatics/btr026

Schultz, J., Müller, T., Achtziger, M., Seibel, P. N., Dandekar, T., and Wolf, M. (2006). The internal transcribed spacer 2 database—a web server for (not only) low level phylogenetic analyses. *Nucleic Acids Res.* 34, W704–W707. doi: 10.1093/nar/gkl129

Segawa, T., Matsuzaki, R., Takeuchi, N., Akiyoshi, A., Navarro, F., Sugiyama, S., et al. (2018). Bipolar dispersal of red-snow algae. *Nat. Commun.* 9:3094. doi: 10.1038/s41467-018-05521-w

Seibel, P. N., Müller, T., Dandekar, T., Schultz, J., and Wolf, M. (2006). 4SALE – A tool for synchronous RNA sequence and secondary structure alignment and editing. *BMC Bioinformatics* 7:498. doi: 10.1186/1471-2105-7-498

Seibel, P. N., Müller, T., Dandekar, T., and Wolf, M. (2008). Synchronous visual analysis and editing of RNA sequence and secondary structure alignments using 4SALE. *BMC Res. Notes* 1:91. doi: 10.1186/1756-0500-1-91

Selig, C., Wolf, M., Müller, T., Dandekar, T., and Schultz, J. (2008). The ITS2 Database II: homology modelling RNA structure for molecular systematics. *Nucleic Acids Res.* 36, D377–D380. doi: 10.1093/nar/gkm827

Simoes, C. L., Rosa, K. K., Czapela, F. F., Vieira, R., and Simoes, J. C. (2015). Collins glacier retreat process and regional climatic variations, King George Island, Antarctica. *Geogr. Rev.* 105, 462–471. doi: 10.1111/j.1931-0846.2015.12091.x

Škaloud, P., and Rindi, F. (2013). Ecological differentiation of cryptic species within an asexual protist morphospecies: a case study of filamentous green alga *Klebsormidium* (Streptophyta). *J. Eukaryot. Microbiol.* 60, 350–362. doi: 10.1111/jeu.12040

Soto, D. F., Fuentes, R., Huovinen, P., and Gómez, I. (2020). Microbial composition and photosynthesis in Antarctic snow algae communities: integrating metabarcoding and pulse amplitude modulation fluorometry. *Algal Res.* 45:101738. doi: 10.1016/j.algal.2019.101738

Stibal, M., and Elster, J. (2005). Growth and morphology variation as a response to changing environmental factors in two Arctic species of *Raphidonema* (Trebouxiophyceae) from snow and soil. *Polar Biol.* 28, 558–567. doi: 10.1007/s00300-004-0709-y

Suzuki, N., and Mittler, R. (2006). Reactive oxygen species and temperature stresses: a delicate balance between signaling and destruction. *Physiol. Plant.* 126, 45–51. doi: 10.1111/j.0031-9317.2005.00582.x

Tan, W.-J., Yang, Y.-C., Zhou, Y., Huang, L.-P., Xu, L., Chen, Q.-F., et al. (2018). DIACYLGLYCEROL ACYLTRANSFERASE and DIACYLGLYCEROL KINASE modulate triacylglycerol and phosphatidic acid production in the plant response to freezing stress. *Plant Physiol.* 177, 1303–1318. doi: 10.1104/pp.18.00402

Tian, J., and Yu, J. (2009). Changes in ultrastructure and responses of antioxidant systems of algae (*Dunaliella salina*) during acclimation to enhanced ultraviolet-B radiation. *J. Photochem. Photobiol. B Biol.* 97, 152–160. doi: 10.1016/j.jphotobiol.2009.09.003

Trifinopoulos, J., Nguyen, L., von Haeseler, A., and Minh, B. Q. (2016). W-IQ-TREE: a fast online phylogenetic tool for maximum likelihood analysis. *Nucleic Acids Res.* 44, W232–W235. doi: 10.1093/nar/gkw256

UniProt Consortium (2019). UniProt: a worldwide hub of protein knowledge. *Nucleic Acids Res.* 47, D506–D515. doi: 10.1093/nar/gky1049

van Wijk, K. J., and Kessler, F. (2017). Plastoglobuli: plastid microcompartments with integrated functions in metabolism, plastid developmental transitions, and environmental adaptation. *Annu. Rev. Plant Biol.* 68, 253–289. doi: 10.1146/annurev-arplant-043015-111737

Vaughan, D. G., Marshall, G. J., Connolley, W. M., Parkinson, C., Mulvaney, R., Hodgson, D. A., et al. (2003). Recent rapid regional climate warming on the Antarctic Peninsula. *Clim. Change* 60, 243–274.

Vilgalys, R., and Hester, M. (1990). Rapid genetic identification and mapping of enzymatically amplified ribosomal DNA from several *Cryptococcus* species. *J. Bacteriol.* 172, 4238–4246. doi: 10.1128/JB.172.8.4238-4246.1990

White, T. J., Bruns, T., Lee, S. J. W. T., and Taylor, J. (1990). Amplification and direct sequencing of fungal ribosomal RNA genes for phylogenetics. *PCR Protoc.* 18, 315–322. doi: 10.1016/b978-0-12-372180-8.50042-1

Williams, W. E., Gorton, H. L., and Vogelmann, T. C. (2003). Surface gas-exchange processes of snow algae. *Proc. Natl. Acad. Sci. U.S.A.* 100, 562–566.

Wolf, M., Chen, S., Song, J., Ankenbrand, M., and Müller, T. (2013). Compensatory base changes in ITS2 secondary structures correlate with the biological species concept despite intragenomic variability in ITS2 sequences–a proof of concept. *PLoS One* 8:e66726. doi: 10.1371/journal.pone.0066726

Yallop, M. L., Anesio, A. M., Perkins, R. G., Cook, J., Telling, J., Fagan, D., et al. (2012). Photophysiology and albedo-changing potential of the ice algal community on the surface of the Greenland ice sheet. *ISME J.* 6, 2302–2313. doi: 10.1038/ismej.2012.107

Zienkiewicz, K., Du, Z.-Y., Ma, W., Vollheyde, K., and Benning, C. (2016). Stress-induced neutral lipid biosynthesis in microalgae – Molecular, cellular and physiological insights. *Biochim. Biophys. Acta Mol. Cell Biol. Lipids* 1861, 1269–1281. doi: 10.1016/j.bbalip.2016.02.008

Conflict of Interest: The authors declare that the research was conducted in the absence of any commercial or financial relationships that could be construed as a potential conflict of interest.

frontiers in Plant Science

ORIGINAL RESEARCH
published: 16 June 2021
doi: 10.3389/fpls.2021.671981

Remote Sensing Phenology of Antarctic Green and Red Snow Algae Using WorldView Satellites

Andrew Gray[1,2]*, *Monika Krolikowski*[1], *Peter Fretwell*[3], *Peter Convey*[3], *Lloyd S. Peck*[3], *Monika Mendelova*[1], *Alison G. Smith*[1] and *Matthew P. Davey*[1,4]

[1] Department of Plant Sciences, University of Cambridge, Cambridge, United Kingdom, [2] Field Spectroscopy Facility (Natural Environment Research Council), University of Edinburgh, Edinburgh, United Kingdom, [3] British Antarctic Survey, Natural Environment Research Council, Cambridge, United Kingdom, [4] The Scottish Association for Marine Science, Oban, United Kingdom

Snow algae are an important group of terrestrial photosynthetic organisms in Antarctica, where they mostly grow in low lying coastal snow fields. Reliable observations of Antarctic snow algae are difficult owing to the transient nature of their blooms and the logistics involved to travel and work there. Previous studies have used Sentinel 2 satellite imagery to detect and monitor snow algal blooms remotely, but were limited by the coarse spatial resolution and difficulties detecting red blooms. Here, for the first time, we use high-resolution WorldView multispectral satellite imagery to study Antarctic snow algal blooms in detail, tracking the growth of red and green blooms throughout the summer. Our remote sensing approach was developed alongside two Antarctic field seasons, where field spectroscopy was used to build a detection model capable of estimating cell density. Global Positioning System (GPS) tagging of blooms and *in situ* life cycle analysis was used to validate and verify our model output. WorldView imagery was then used successfully to identify red and green snow algae on Anchorage Island (Ryder Bay, 67°S), estimating peak coverage to be 9.48×10^4 and 6.26×10^4 m^2, respectively. Combined, this was greater than terrestrial vegetation area coverage for the island, measured using a normalized difference vegetation index. Green snow algae had greater cell density and average layer thickness than red blooms (6.0×10^4 vs. 4.3×10^4 cells ml^{-1}) and so for Anchorage Island we estimated that green algae dry biomass was over three times that of red algae (567 vs. 180 kg, respectively). Because the high spatial resolution of the WorldView imagery and its ability to detect red blooms, calculated snow algal area was 17.5 times greater than estimated with Sentinel 2 imagery. This highlights a scaling problem of using coarse resolution imagery and suggests snow algal contribution to net primary productivity on Antarctica may be far greater than previously recognized.

Keywords: snow algae, Antarctica, remote sensing, snow, satellites, WorldView, ecology

OPEN ACCESS

Edited by:
Linda Nedbalová,
Charles University, Czechia

Reviewed by:
Biagio Di Mauro,
National Research Council (CNR), Italy
Roman Dial,
Alaska Pacific University, United States

***Correspondence:**
Andrew Gray
andrew.gray@ed.ac.uk

Specialty section:
This article was submitted to Marine and Freshwater Plants, a section of the journal Frontiers in Plant Science

Received: *24 February 2021*
Accepted: *20 April 2021*
Published: *16 June 2021*

Citation:
Gray A, Krolikowski M, Fretwell P, Convey P, Peck LS, Mendelova M, Smith AG and Davey MP (2021) Remote Sensing Phenology of Antarctic Green and Red Snow Algae Using WorldView Satellites. Front. Plant Sci. 12:671981. doi: 10.3389/fpls.2021.671981

1. INTRODUCTION

Blooms of microalgae were noted in Antarctic snow fields by several expeditions in the early 1900s, in a period when scientific discovery became a major driving force for exploration of the continent (Hirano, 1965). Since these early records, blooms of red, green, and orange snow algae in Antarctica have been revealed as diverse ecosystems that play an active role in biogeochemical cycling of

nutrients and carbon (Ling and Seppelt, 1993; Dierssen et al., 2002; Hodson et al., 2008; Remias et al., 2013; Boetius et al., 2015; Davey et al., 2019; Procházková et al., 2019). Antarctica has relatively little exposed land to support terrestrial vegetation, with 98.7% of its surface area permanently covered in snow or ice (Fretwell et al., 2011). Thus, growth within the interstitial water of melting snow may be a successful, or even dominant, strategy for photosynthetic life there. Indeed, previous work has identified green snow algal blooms covering 1.9 km^2 of the Antarctic Peninsula within a melt season (Gray et al., 2020), which compares with standing area estimates for other terrestrial vegetation of between 2.44 and 44.6 km^2 (depending on the level of certainty) (Fretwell et al., 2011). Monitoring snow algae is important in the face of warming in Antarctica, as snow loss from low-lying islands competes with increases in snow melt at higher elevations to influence the area and distribution of habitable snow (Gray et al., 2020). Moreover, snow algae are impurities within the snowpack, absorbing more solar radiation than clean snow, reducing its albedo and enhancing melt (Lutz et al., 2016; Ganey et al., 2017; Khan et al., 2021). The study of snow algae in Antarctica, in particular optimizing approaches to accurately monitor their ecology and influence on snow albedo, is timely and crucial to improve understanding of the effect of climatic changes on their distribution and abundance.

Satellite remote sensing greatly increases our ability to map and monitor the extent of Antarctica's terrestrial biosphere, because other approaches, such as airborne or drone-based remote sensing missions cover relatively small areas and are geographically tethered to research station infrastructure. Satellite imagery has provided valuable insight into the distribution and biomass of terrestrial vegetation in Antarctica (Fretwell et al., 2011; Casanovas et al., 2015; Jawak et al., 2019), but these studies do not include snow algae as their spectral reflectance profile, measured using field spectroscopy (Painter et al., 2001; Cook et al., 2017; Huovinen et al., 2018; Di Mauro et al., 2020; Gray et al., 2020), is not identified using classical vegetation indices. There are, however, several studies that focus specifically on remote sensing snow algae, from early work using airborne hyperspectral imaging (Painter et al., 2001), projects utilizing satellite observations (Takeuchi et al., 2006; Huovinen et al., 2018; Tedstone et al., 2019; Di Mauro et al., 2020; Gray et al., 2020), and drone-based observations (Tedstone et al., 2019). Each technology has advantages and disadvantages, with airborne sensors giving high spatial and spectral resolution across moderate areas, satellites offering relatively coarse spatial and spectral resolution across large areas, and drones offering custom spectral resolution at very high resolutions, but over small areas.

Our previous work mapping snow algae on the Antarctic Peninsula used the freely available European Space Agency's (ESA) Sentinel 2 satellite imagery and gave the first insight into the distribution of blooms in Antarctica over a large scale (Gray et al., 2020). However, the spatial resolution of satellite imagery was too coarse to capture blooms at the edges of snow patches, and importantly, it was not able to determine the presence of blooms of red snow algae, as their secondary carotenoids reduce the effectiveness of the spectral index used. Moreover, this analysis focused only on a snapshot of growth from 1 year's worth of imagery at each bloom location. The problem of red bloom detection in Sentinel 2 imagery has been somewhat addressed by the work of Khan et al. (2020), yet large uncertainties remain when deriving area and biomass estimates from 10 m spatial resolution pixels. Key to using remotely sensed observations to study Antarctic terrestrial ecology lies in this balance between spatial resolution and area coverage. Using higher resolution commercial satellite imagery may help to address some of the uncertainties of coarser resolution Sentinel 2 or Landsat imagery, yet it can also be used to study blooms over larger areas.

Here, we apply the Painter et al. (2001)-adapted methodology from Gray et al. (2020) to high spatial resolution WorldView 2 and 3 satellite imagery to study the ecology of snow algae in Antarctica. WorldView satellites (Maxar Technologies) offer some of the highest spatial and spectral resolution satellite imagery that are commercially available and have shown great utility for studying Antarctica's ecology (LaRue et al., 2011; Fretwell et al., 2012; Cubaynes et al., 2019; Jawak et al., 2019). We aimed to assess the use of high-resolution optical satellite remote sensing as a tool to study snow algae, and in so doing improve upon estimates of area, biomass, and uncertainty from our earlier study (Gray et al., 2020). The band configuration of WorldView satellites enabled us to adapt our earlier methodology to include red snow algae in our analysis, and higher spatial resolution (1.24 m^2) pixels meant we could improve our understanding of spatial scale when deriving remotely sensed ecological measures for snow algae. Finally, we use WorldView imagery to study the phenology of snow algae over a growth season in the Ryder Bay area of Adelaide Island, Antarctica.

2. MATERIALS AND METHODS

Fieldwork was conducted in the Fildes Peninsula area of King George Island (62°S) in January and February 2019 (**Figure 1A**) and the Ryder Bay (Rothera Research Station) area (67°S) in January and February 2018 (**Figure 1B**). Parallel work packages were undertaken to collect information on snow algal life cycle, collect field spectrometer measurements to build our remote sensing model, and to record the locations of blooms for later validation of satellite imagery. WorldView 3 imagery was tasked for collection during both field campaigns. Adverse cloud conditions on collection days meant that only one image was collected coincident to fieldwork, from February 1, 2019 on King George Island, and it suffers from over-saturation within the blue and green bands. Though we were able to use this image to partially verify our approach, the major remote sensing discussion herein is focused around a mixture of WorldView 2 and 3 imagery of Ryder Bay, captured in 2017, with images from February 6, February 28, November 23, and December 28.

2.1. Field Studies

2.1.1. Snow Algal Bloom Sampling

Previous work in the Ryder Bay area has shown green coloration of snow, mostly resulting from *Chloromonas*, *Chlamydomonas*, and *Chlorella* sp., in the slush layer between multiyear and seasonal snowpacks (Davey et al., 2019). Red coloration, largely a result of *Chloromonas* sp., was also visible on the surface

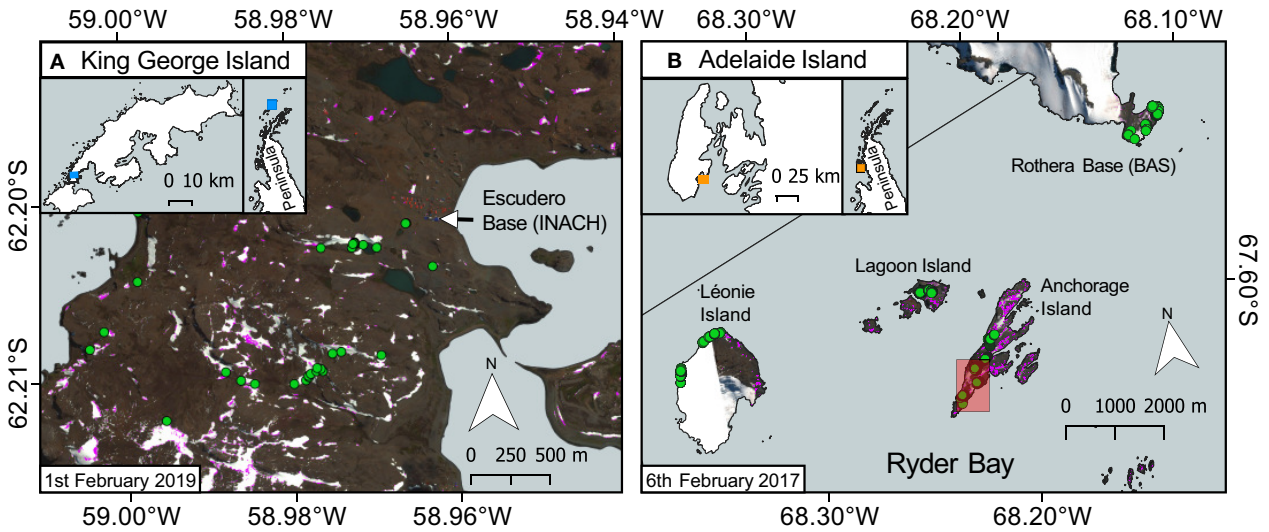

FIGURE 1 | Ground validation sites. WorldView 3 red–green–blue (RGB) images of our ground validation sites, the extent and location of which are denoted by the blue- or orange-shaded areas in their respective inset maps. Green circles show locations where snow algae were visibly growing on the snow surface, were geotagged, measured with the field spectrometer, and sampled for microscopy analysis. Pink pixel shading denotes areas of snow identified as containing snow algae within those WorldView 3 images, using the approach outlined below. **(A)** Sampling conducted in the Fildes Peninsula region of King George Island whilst stationed at Professor Julio Escudero Station and Refugio Collins in 2019. **(B)** Sampling conducted in the Ryder Bay area of Adelaide Island, showing Rothera Research Station and the outlying islands from which snow algae were sampled in 2018. Red shaded box on Anchorage Island denotes the area shown in **Figures 9**, **12**. Map data from the SCAR Antarctic Digital Database.

of seasonal snow (Davey et al., 2019). This stratification has been observed elsewhere in Antarctica, with green or orange coloration at depth (Bidigare et al., 1993; Mataloni and Tesolín, 1997; Remias et al., 2013; Hodson et al., 2017) as well as red/orange/pink coloration on the snow surface (Fujii et al., 2010; Segawa et al., 2018; Procházková et al., 2019; Soto et al., 2020).

Six blooms, in which snow was visibly colored red or green, were identified close to Rothera Research Station (Rothera Point) and on the nearby islands of Anchorage, Lagoon, and Léonie. GPS locations and photographs of the blooms were taken. Within the bloom, three sampling patches (sample pits) were identified, one central and one to the left and right of center, and carefully dug out with a snow shovel (pits are shown in **Figure 2**). One patch/pit with no visible snow algae was also sampled to provide a negative control at each location, close to the visible bloom area. At each patch, we sampled the surface white (or sometimes green or red algal top layer) snow, the algal layer (usually green), and the underlying snow or ice layer. The algal layers were sampled using 4 × 50 mL (28.98 cm^2) sterile plastic sample tubes and analyzed according to the methods described in Davey et al. (2019) and Gray et al. (2020). Briefly, the depth of layer was recorded as well as photosynthetically active radiation (PAR) (Skye PAR Quantum Sensor, Skye Instruments Ltd., Powys, UK) and temperature (Omega HH306A thermometer; OMEGA Engineering Inc) at the snow surface and algal layers at the start of each sampling period. The samples were then transferred to the Bonner Laboratory (Rothera Research Station, Ryder Bay, Antarctica) for processing. Within the research station, samples were melted in 4°C lit incubators (Sanyo). Algal cell density

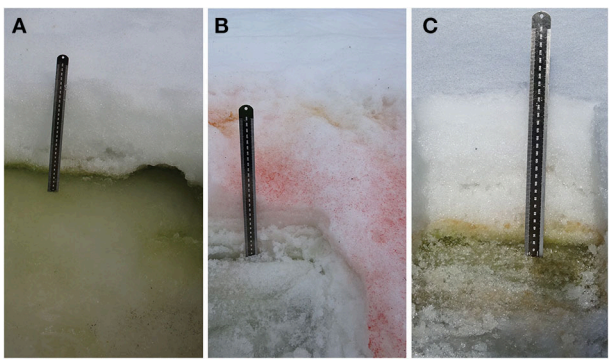

FIGURE 2 | Snow algae pits. Photographs showing **(A)** a green bloom underneath seasonal snow layer. Lagoon Island, January 12, 2018; **(B)** a red bloom on the surface of seasonal snow. Léonie Island, January 30, 2018; **(C)** red algae emerging on top of band of green snow algae. Anchorage Island, February 9, 2018.

was measured in 202 samples, by agitating and adding 6 μl of snowmelt into Hycor Kova® hemocytometer wells and counting the number of algal cells using bright field microscopy or adding a known volume (10–20 μL) to a slide, drying, and counting all the algal cells. Algal community dry cell mass was obtained by gravity filtration of 50 mL of melted snow through a pre-weighed dry filter (Whatman GF/C, 47 mm). Filters were dried at 80°C for at least 48 h prior to re-weighing.

TABLE 1 | WorldView 2 and 3 band positions.

Band	WorldView 2 center wavelength (nm)	WorldView 2 bandwidth (nm)	WorldView 3 center wavelength (nm)	WorldView 3 bandwidth (nm)
Coastal blue (B1)	447	62	426	57
Blue (B2)	478	73	481	72
Green (B3)	546	80	547	79
Yellow (B4)	608	48	605	49
Red (B5)	659	70	661	70
Red edge (B6)	724	50	724	51
NIR1 (B7)	833	136	832	134
NIR2 (B8)	949	187	948	182

The lower and upper band edges and center wavelengths for the VNIR sensors on board WorldView 2 and 3 VNIR multispectral satellites.

2.1.2. Remote Sensing Model Development and Validation

In situ hemispherical directional reflectance factors (HDRF) of green ($n = 91$) and red ($n = 57$) snow algae, control white snow patches ($n = 38$), and snow containing mineral dust but no algae ($n = 36$) were recorded at the locations noted by green circles in **Figure 1**. Spectra were collected under clear sky conditions with a Spectra Vista Corporation (SVC) 1024i field spectrometer using the methodology described in Gray et al. (2020). Fixed viewing geometry ensured that HDRF was recorded consistently over a 908 cm^2 field of view (FOV) (roughly 6% the area of a WorldView 3 pixel). The snow in the FOV was sub-sampled into a sterile 50 mL sample tube, with care taken not to compress the snow into the tube. The samples were then transferred to the Bonner laboratory or the Professor Julio Escudero Base laboratory [King George Island (KGI), Antarctica], where cell density was determined through analysis of color brightfield microscope images using the methodology described in Gray et al. (2020). Field samples were collected at Ryder Bay under the UK BAS Operating Permit and the Antarctic Act (1994; 2013) and at KGI under permit from INACH (Chile) Certificate number 209/2019.

As in Di Mauro et al. (2020) and Gray et al. (2020), chlorophyll absorbance features within reflectance factors were determined using the scaled integral method developed by Painter et al. (2001). Field-derived hyperspectral HDRF of red or green snow algae were convolved to the spectral response of WorldView 2 or 3, and the integral of chlorophyll a absorbance, I_{B5}, calculated using WorldView 2 or 3-simulated "yellow," "red," and "red-edge" bands (Equation 1). Band positions for the WorldView 2 and 3 sensors are shown in **Table 1**, and the position of the bands used in Equation (1) relative to the HDRF of snow algae is shown in the Results section (**Figure 3**). Since WorldView 2 and 3 have different spectral response functions, sensor-specific I_{B5} equations were used to analyze their respective imagery.

$$I_{B5} = \frac{R_{B4}(\lambda_{B6}-\lambda_{B5})+R_{B6}(\lambda_{B5}-\lambda_{B4})}{\lambda_{B6}-\lambda_{B4}} - R_{B5} \Big/ \frac{R_{B4}(\lambda_{B6}-\lambda_{B5})+R_{B6}(\lambda_{B5}-\lambda_{B4})}{\lambda_{B6}-\lambda_{B4}} \quad (1)$$

where I_{B5} is the scaled integral of Band 5, R_{Bn} is the HDRF for Band "n", and λ_{Bn} is the wavelength at the center point of Band "n" (see **Table 1**). Relative to the use of Sentinel 2 in Gray et al. (2020), where analysis was limited to green snow algae, WorldView's yellow band at 605 nm corresponds to the lower shoulder of the chlorophyll a absorption feature, without interference from astaxanthin absorption. This meant that Equation (1) could be used upon WorldView multispectral imagery to detect both red and green snow algae.

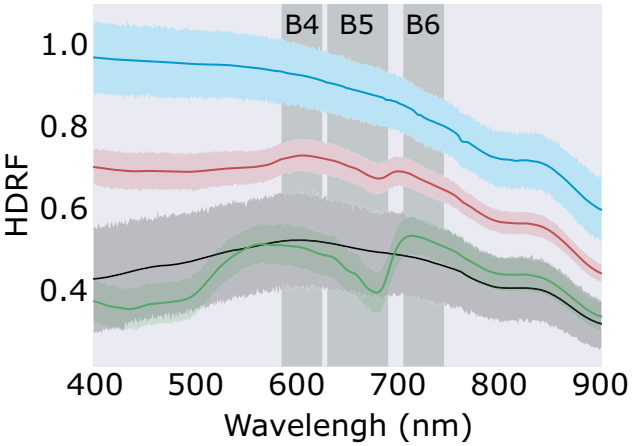

FIGURE 3 | Snow algae reflectance factors. Average hemispherical directional reflectance factors (HDRF) of red snow algae (red; $n = 70$), green snow algae (green; $n = 91$), clean snow (blue; $n = 38$), and mineral dust-entrained snow (black; $n = 36$). Error band shows the 95% confidence interval. Vertical shaded bands show the position of Bands 4, 5, and 6 of WorldView 3's multispectral sensor.

2.2. Remote Sensing

WorldView imagery over the Ryder Bay area from February 6, 2017 (WorldView 3), February 28, 2017 (Worldview 2), November 23, 2017 (Worldview 2), and December 28, 2017 (Worldview 2) was accessed through the DigitalGlobe Foundation. Imagery was processed and analyzed at 1.24 m ground sampling distance for Worldview 3 and 1.84 m for WorldView 2. Imagery was converted to surface reflectance using the Atmospheric and Radiometric Correction of Satellite Imagery (ARCSI) command line tool (Bunting and Clewley, 2019), which uses the 6S radiative transfer model (Vermote et al., 1997) to perform atmospheric correction. The 8m Reference Elevation Model of Antarctica (REMA) (Howat et al., 2019)

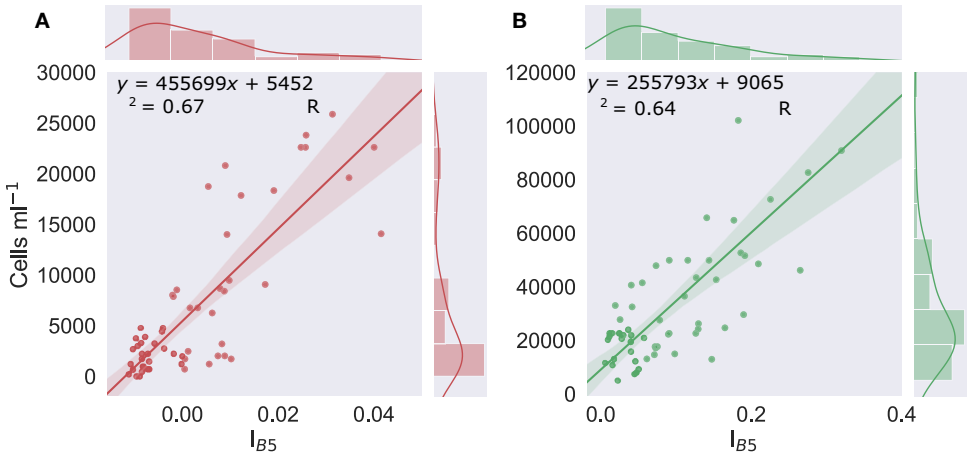

FIGURE 4 | Cell density vs. I_{B5}. Linear regression of the scaled integral of WorldView 3's Band 5 relative to Bands 4 and 6 (I_{B5}) (derived from resampled field HDRF), vs. concentrations of red (left, graph **A**) ($n = 57$) or green (right, graph **B**) ($n = 60$) algal cells within the snow. Shaded area shows the 95% confidence interval. Marginal histograms show data distribution.

was used to provide elevation data for atmospheric correction. Aerosol optical depth (AOD) data, collected on clear sky days by Rothera's POM 01 (Prede Co. Ltd) automatic sunphotometer and a handheld Microtops II sunphotometer (Solar Light), were used to provide values of AOD for the 6S atmospheric model. No corresponding AOD measurements were available for the 2017 Ryder Bay images, so average clear sky values recorded during the 2018 Ryder Bay field season were used. For the 2019 King George Island image, AOD was derived from an average of triplicate Microtops measurements, taken at the same time as the WorldView 3 image. Maritime aerosol profile and sub-arctic winter atmospheric profiles were used.

Each scene was masked using the filter functions presented in Gray et al. (2020). These remove false positives that return high I_{B5} values but correspond to saturated, noisy or mixed pixels, or other terrestrial vegetation. A spectral angle mapper (SAM) classification was performed in ENVI (Version 5.5 Exelis Visual Information Solutions, Boulder, Colorado) on the masked multispectral imagery to differenciate between green, red, dirty and clean snow. For this classification model, reference end-member spectra of red ($n = 57$) and green ($n = 91$) snow algae, mineral entrained snow ($n = 36$), and control plots of algae-free snow ($n = 38$) were derived from averaged HDRF, recorded using field spectroscopy (spectra of these end members are shown in **Figure 3** in the Results section).

Chlorophyll absorbance was then mapped by applying I_{B5} (Equation 1) to each masked image. To relate this mapped absorbance to cell density, we used the *in situ* data collected with the field spectrometer and microscope. The lines of least squares regression of field spectroscopy-derived I_{B5} vs. measured cell density, shown here in **Figure 4**, were used to relate the I_{B5} value of each pixel to a cell concentration. For pixels identified as red snow by the SAM classification, cell density was calculated using the linear regression of red snow algae vs. I_{B5} (**Figure 4A**; Equation 3), whereas, for pixels classified as green snow algae, cell density was calculated using the linear relationship between green algal cell density and I_{B5} (**Figure 4B**; Equation 4). Single isolated pixels were discarded from analysis as they predominantly corresponded to sun glint from rock or heavily crevassed ice. Pixels returning a lower cell density than the intercept of Equations (3) or (4) were also discarded. As in Gray et al. (2020), we estimated snow algal biomass (dry mass) using averaged *in situ* measurements of red or green bloom layer thickness and snow density, and the pixel area, calculated based on mean row and column pixel dimensions (which vary according to the cross and in track viewing angle to normalize per pixel cell concentrations by volume). Average measured dry mass of a single red or green snow alga was then used to calculate dry biomass per pixel, with the mass of carbon present determined using the average measured %C in red and green blooms. All of these data are presented in **Table 2**.

To compare with other terrestrial vegetation, the normalized difference vegetation index (NDVI), a proxy for detecting vegetation in multispectral imagery, was calculated using the image from February 28, 2017. This was done with Equation (2), utilizing the NDVI-2 band combination tested by Jawak et al. (2019) on Antarctic vegetation. We chose a lower NDVI threshold of 0.1 after Fretwell et al. (2011), as values less than this introduced significant noise into our analysis, where isolated pixels on targets known to not contain vegetation had NDVI values between 0.05 and 0.1. Pixels identified as snow algae that also had NDVI > 0.1 were clipped out of the NDVI map to allow comparison between snow algae and terrestrial vegetation.

$$NDVI = \frac{NIR\,2 - Red}{NIR\,2 + Red} \tag{2}$$

2.3. Accuracy Assessment

During the 2018 and 2019 field seasons, locations where algae were visible on the surface of the snow pack were traced using a Trimble 5700 GPS receiver and Zepher Antenna (Ryder Bay;

TABLE 2 | Snow algae *in situ* data.

	Green *in situ*	Red *in situ*	Green WorldView 28/02/17	Red WorldView 28/02/17
Snow algae cells ml^{-1} snow melt	$1.9 \times 10^5 \pm 3.8 \times 10^5$ ($n = 66$)	$3.4 \times 10^4 \pm 1.0 \times 10^5$ ($n = 108$)	$7.3 \times 10^4 \pm 3.0 \times 10^4$ ($n = 15{,}614$)	$3.3 \times 10^4 \pm 1.5 \times 10^4$ ($n = 23{,}956$)
Snow algae cells m^{-2} snow surface	$2.9 \times 10^9 \pm 3.8 \times 10^9$ ($n = 66$)	$8.0 \times 10^8 \pm 3.4 \times 10^9$ ($n = 136$)	$3.9 \times 10^8 \pm 1.6 \times 10^8$ ($n = 15{,}814$)	$3.1 \times 10^7 \pm 1.4 \times 10^7$ ($n = 23{,}956$)
Snow algae community dry mass (g m^{-2})	29.5 ± 29.9 ($n = 50$)	0.83 ± 1.4	9.1 ± 3.8 ($n = 15{,}814$)	1.9 ± 0.9 ($n = 23{,}956$)
Snow algal single cell mass (g)	$2.4 \times 10^{-8} \pm 2.2 \times 10^{-8}$ ($n = 90$)	$6.2 \times 10^{-8} \pm 1.2 \times 10^{-7}$ ($n = 57$)	–	–
Snow density (ml melt cc^{-1} snow)	0.58 ± 0.17 ($n = 90$)	0.49 ± 0.13 ($n = 57$)	–	–
Snow algal layer thickness (mm)	9.1 ± 5.9 ($n = 90$)	1.9 ± 3.3 ($n = 57$)	–	–
Snow algal %C	36.1 ± 9.5 ($n = 82$)	34.9 ± 10.3 ($n = 17$)	–	–

Cell counts, snow physical properties, and carbon data of Antarctic green and red snow algae compared to remote-sensed estimates from Anchorage Island using WorldView 2 on February 28, 2017. Reported values are mean values (±1 standard deviation) from a combination of field work conducted in the Ryder Bay area of Adelaide Island (2018) and the Fildes Peninsula area of King George Island (2019). In situ data for green snow algae is also reported in Gray et al. (2020).

see **Figure 5** for a photograph of GPS tracing), and an Emlid RS+ GNSS receiver (King George Island). Triplicate samples of green, red, and clean snow were collected from each bloom location and analyzed for cell density by light microscopy using the methodology described in Gray et al. (2020). GPS positions of field-checked blooms are shown in **Figure 1**. In the case of King George Island (**Figure 1A**), points were recorded within 1 day of the WorldView 3 image shown. GPS data of bloom locations in the Ryder Bay area were recorded in January and February 2018 (imagery from 2017). Accuracy of both the SAM classification and the location of snow algae identified using I_{B5} was assessed by calculating the Kappa coefficient of agreement using these ground-checked locations. For Ryder Bay images, where there was a significant time difference between ground observations and images, manual checking of true color imagery was also employed to corroborate Kappa scores. For the Ryder Bay images, 76 GPS referenced blooms were used to validate the images from February. Since we had near overlapping field observations for the Ryder Bay image from the December 28, 2017, 26 blooms locations recorded in early January 2018 were used to validate this image. For the King George Island image on February 1, 2019, 40 bloom locations that were recorded within 4 days of these dates were used for validation.

3. RESULTS

3.1. *In situ* Sampling

3.1.1. Bloom Phenology

Blooms in the Ryder Bay area, including those on Anchorage Island, were initially (early January 2018) observed as a green layer within the snowpack. Small patches of red snow were also noted on the surface of the snowpack in places in early January. Later in the season (early February), red and green snow algal blooms covered a visibly larger area. By mid-February, overlying snow had melted to expose the green algal layers, often on the surface of a dense, multi-year snowpack as shown in **Figure 5**.

FIGURE 5 | Snow algae blooms on Anchorage Island. Photograph of Andrew Gray GPS tracing a green snow algal bloom on south-western tip of Anchorage Island, January 31, 2018 (Credit: M. Davey).

Pit sampling revealed green layers turning red in some instances (**Figure 2C**), although red blooms mostly appeared on the top of fresh snow, with no green cells detected within the underlying

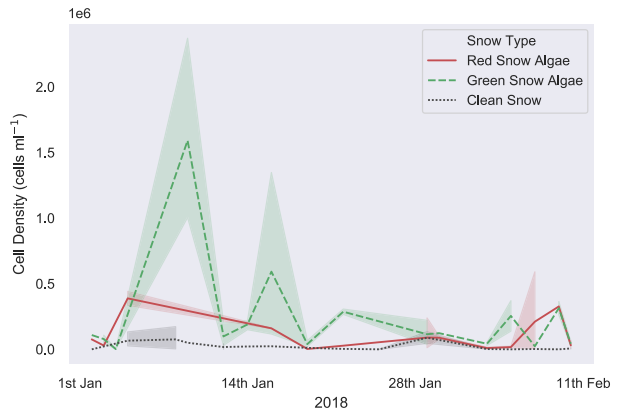

FIGURE 6 | *In situ* snow algal cell density. Measured *in situ* algal cell density within clean, visibly red or visibly green snow, sampled for life cycle analysis throughout the 2017/2018 growth season in the Ryder Bay area, Antarctica. Samples are from Rothera Point, Anchorage Island, Lagoon Island, and Léonie Island. Shaded area shows one standard deviation.

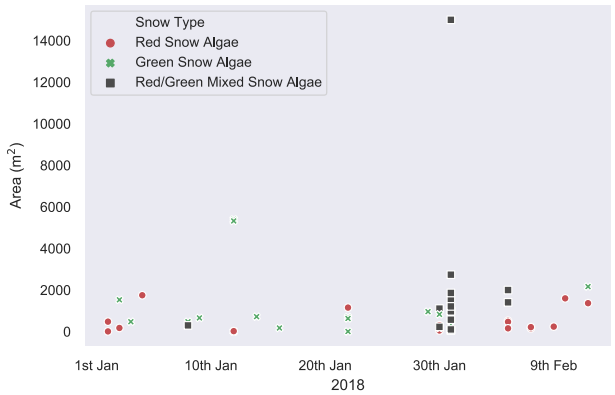

FIGURE 7 | *In situ* bloom area measurements. *In situ* measurements of visible bloom area, recorded with a Trimble dGPS throughout the 2018 field season in the Ryder Bay area. Blooms recorded are from Rothera Point, Anchorage Island, Lagoon Island, and Léonie Island.

snowpack (**Figure 2B**). Several patches of mixed red and green snow were also evident, though it was unclear whether this was representative of different stages of life cycle or two distinct populations mixed through snow-melt action.

Figure 6 shows the algal cell density of visibly red, green, or clean snow throughout the 2017/2018 growth season. No significant trends were observed across the 42 days of observation. Average cell density (shown in **Table 2**) was 1.9×10^5 cells ml^{-1} for green and 3.4×10^4 for red blooms, with considerable variation observed between different blooms of the same color (respective standard deviations of 3.8×10^5 and 1.0×10^5). There were also no changes in measured visible bloom area through January and February during our observations in 2018 (**Figure 7**). Average bloom area was $1{,}110 \pm 674$ m^2 for green blooms and 531 ± 364 m^2 for red blooms. The cell densities measured within strongly colored patches of snow in 2018 were consistent with those recorded for Ryder Bay snow algae in 2015 (Davey et al., 2019), and are similar to cell densities recorded elsewhere in Antarctica (Hodson et al., 2017).

3.1.2. Field Spectroscopy

Average HDRF of red and green snow algae, and clean and mineral entrained snow are shown in **Figure 3**. Both red and green algae exhibited strong absorption features at 680 nm from chlorophyll a, which were not present within the recorded spectra of clean or mineral dust-containing snow. Green snow algae HDRF also had strong absorption from chlorophyll b, a broad peak between c. 400 and 500 nm, which was present but less pronounced in red bloom spectra. Red blooms also showed absorption from carotenoids, such as astaxanthin, which when combined with chlorophyll b creates a broad flat absorption feature below 570 nm. Field HDRF indicate similar pigmentation to that observed through HPLC analysis of snow algae sampled from the same area (Davey et al., 2019) and are similar to red and green snow algae spectra reported elsewhere (Painter et al., 2001; Holzinger et al., 2016; Huovinen et al., 2018; Khan et al., 2021).

There was significant variation in the magnitude of HDRF within the visible/near infra-red (VNIR) region, as our sampling aimed to survey a wide range of cell densities to avoid extrapolation when applying our regression model to remotely sensed images. Lower cell concentrations, where coloration was just visible on the surface of the snow, typically had higher overall reflectance and a smaller chlorophyll absorption features at 680 nm. Where algae completely covered the snow surface, HDRF values were much lower within the VNIR range but also exhibited deeper chlorophyll a absorbance features. The relationship between cell density and the continuum-scaled integral of the chlorophyll a absorbance feature is shown in **Figure 4**. The linear relationship between cell density and I_{B5} (**Figure 4**) was high and significant for both red and green blooms, with respective Pearson's correlation coefficients of $r(58) = 0.82$, $p < 0.01$ and $r(55) = 0.80$, $p < 0.01$. R^2 was, respectively, 0.67 and 0.64, and the standard error 4.3×10^4 and 2.5×10^4 cells ml^{-1}. The lines of best fit, used to estimate cell density within a WorldView pixel, are shown in Equations (3) and (4), for red and green snow algae, respectively.

$$Red\ Cells\ ml^{-1} = (I_{B5} \times 455699) + 5452 \quad (3)$$

$$Green\ Cells\ ml^{-1} = (I_{B5} \times 255793) + 9065 \quad (4)$$

Likely causes of variation in these regression models include factors that affect the HDRF lineshape, for example, debris, mixed communities of red and green algal cells, and snow morphology, such as crystal structure and liquid water content (Cook et al., 2017). Variation may also arise from sampling geometry, with a fixed nadir viewing angle, but with aspect, slope angle, and the solar zenith varying between sampling sites. The y-intercepts of Equations (3) and (4) (the lines of best fit from **Figures 4A,B**) determined the lower limit of cell density detection within a

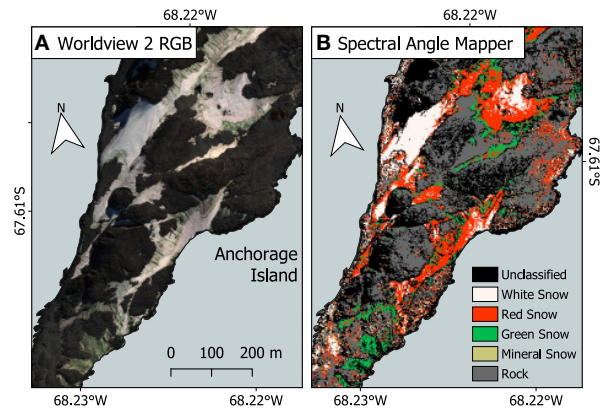

FIGURE 8 | Spectral angle mapper (SAM) classification example. **(A)** Red–green–blue (RGB) true color WorldView 2 image of a section of Anchorage Island from February 28, 2017. Image extent is highlighted in **Figure 1**. **(B)** Output from the spectral angle mapper classification (SAM), used to determine which pixels contained red, and green snow algae for later calculation of pixel cell density.

WorldView pixel using this approach: 5.5×10^3 cells ml^{-1} for red snow algae, and 9.1×10^3 cells ml^{-1} for green snow algae. This is, respectively, one and two orders of magnitude smaller than our averaged measured cell densities (**Table 2**).

3.2. Remote Sensing Snow Algae

3.2.1. Accuracy Assessment and Bias

Figure 8 shows the output from the SAM classification. Run only on snow within a scene, SAM performed well in classifying between red or green snow algae, white and mineral-entrained snow, with Kappa scores of 0.68 on December 28, 2017, 0.81 on February 6, 2017, and 0.64 on February 28, 2017, when compared to ground GPS data from the subsequent season. The November 23, 2017 image differed greatly from our ground GPS data, with seasonal snow covering most of the islands. Instead, SAM output was assessed by manual checking against true color imagery, where it correctly classified most clean snow but did not perform well with areas of shadow, misclassifying them as mineral-laden or red algal blooms. SAM misclassification in all images predominantly was related to red snow being assigned as mineral entrained snow or clean snow, or very dark patches of green snow algae (which may be classified as rock/terrestrial vegetation within our SAM end member framework). We were unable to classify or separate red or green snow in the image of King George Island, as its blue and green bands were saturated over snow.

Figure 9 shows the output of our approach to identifying snow algae within WorldView 2 and 3 images, combining filter masking, SAM, I_{B5}, and Equations (4) or (3). Since it was our only WorldView image with concurrent field measurements, we performed an accuracy assessment using georeferenced blooms on the saturated image of King George Island. All GPS-logged patches of snow algae were correctly identified by our model; however, its Kappa score was low (0.59) as we were unable to accurately differentiate algae from mineral-laden snow, with SAM classification performing poorly on the saturated image. For Ryder Bay images, Kappa scores of 0.79 on December 28, 2017, 0.59 on February 6, 2017, and 0.82 on February 28, 2017 were observed. As with SAM validation, November 23, 2017 scene was assessed by manually checking against true color imagery. Areas with visible green/orange coloration to the snow were classified as snow algae, as were patches close to Rothera Station that appeared white in this image, but had developed into green blooms by December 28, 2017, possibly indicating sub-surface blooms.

At center swath and on flat ground, WorldView 3 has a ground sampling distance of 1.24 m for its VNIR bands, with WorldView 2 only slightly larger at 1.84 m. This allows detection of smaller blooms than is possible using Sentinel 2 or Landsat imagery, yet our field observations indicate that blooms were still patchy and heterogeneous at this scale. Any chlorophyll absorbance from the presence of snow algae will be integrated across a pixel according to its point spread function (Radoux et al., 2016) with a theoretical lower limit of detection for bloom area being based upon the bloom's cell density and whether it crosses through the center or is positioned at the border of a pixel. Based upon average *in situ* cell densities from **Table 2**, the minimum detectable cell densities from Equations (4) and (3), and assuming a bloom crosses through the center of a pixel otherwise containing clean snow, we estimate the minimum detectable bloom area to be 0.09 and 0.06 m^2 for green blooms, and 0.3 and 0.2 m^2 for red blooms, in WorldView 2 and 3 imagery, respectively. Mixed pixels containing rock or vegetation alongside green snow algae would likely be excluded from the study based on the filter functions applied before analysis (Gray et al., 2020).

Spatial biases of remote-sensed snow algal area estimates may be caused by misclassification of pixels, subpixel blooms being counted as one pixel in area, blooms growing under the surface layer of snow being excluded from observation, and error associated with pixel dimensions on the snow surface. Each of these will cause over- or underestimation of area and will affect red and green blooms differently throughout the growth season. Misclassification likely led to underestimation of red bloom area, where pixels containing red snow algae were incorrectly labeled as mineral entrained or clean white snow by the SAM classifier. Conversely, misclassification likely caused overestimation of green bloom area, as some noisy or dark pixels with high I_{B5} remained after filtering and were often misclassified as green snow algae by our SAM classifier. These were typically on angular rocky structures or crevassed ice and required manual removal prior to analysis. Overestimation of the area of subpixel blooms will likely cause greater bias at the beginning of the season, where the exposed area of blooms may be smaller. However, this is also when we expect to have greater underestimation of bloom area, as overlying snow obscures growth from view. The latter will mostly affect green blooms, as red blooms in coastal Antarctica have predominantly been observed to inhabit the surface of snow (Remias et al., 2013; Davey et al., 2019). Spatial bias resulting from error in pixel dimension introduces uncertainty when comparing different images/sensors, as the off-nadir and azimuth viewing angles with respect to surface topography will result in different

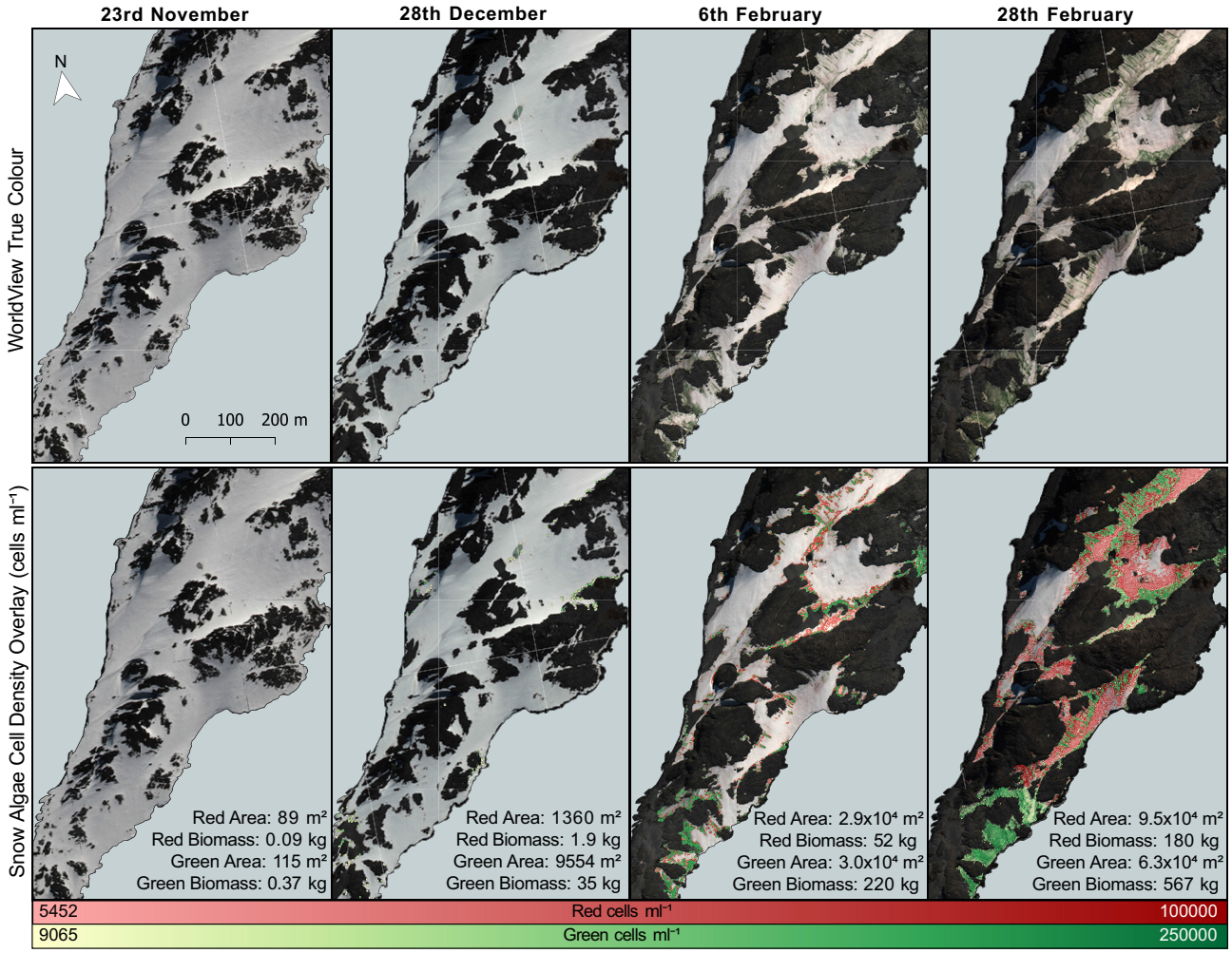

FIGURE 9 | Red and green snow algal distribution and modeled cell density. Area coverage and (dry) biomass estimates are given for red and green snow algae on Anchorage Island. All images are from 2017. Map extent is shown in **Figure 1B**.

pixel area errors for the same blooms within different images. The areas reported here are given minimum and maximum range bounds based upon potential bias from misclassification (based on that image's accuracy assessment) and the range of pixel area within a scene (based on image-specific viewing geometry only). Errors associated with foreshortening and elongation of pixels because of satellite viewing geometry were not considered in this paper and should be considered in greater depth in future study.

Assuming pixels contain only red or green snow, and do not contain mixed populations, error for remote-sensed cell density estimates is largely captured by the standard error of our regression models relating I_{B5} to cell density (**Figure 4**). This standard error would relate to errors in field spectroscopy-based I_{B5} measurements, the associated cell density measurement and non-snow algae factors that may influence lineshape and hence I_{B5}. These may be factors, such as mineral dust, snow crystal morphology, and bi-directional reflectance factor (BRDF) effects. Biomass estimates have greater uncertainty because they are parameterized using averaged field measurements rather than mapped or remote sensing-derived snow density, thickness, or cellular mass. Biomass estimates are given with maximum and minimum values based on propagated error from pixel area, the standard error of red or green snow algae regression models, and each empirically derived parameter used for calculation. Error is more complex where pixels contain mixed red and green populations, as SAM may classify a pixel as red or green based upon the greater number of red or green cells in that pixel rather than by greatest area coverage, although the position of red or green cells within a pixel relative to its point spread function will also influence classification. In this case, red snow algae in a pixel classified as green will be enumerated based upon the relationship between I_{B5} and green algae (Equation 4) rather than I_{B5} and red algae (Equation 3) and vice versa. Dry biomass estimates will similarly be based upon incorrect field measurements. Future work should address this uncertainty, through spectral unmixing approaches, or analysis of higher resolution drone imagery.

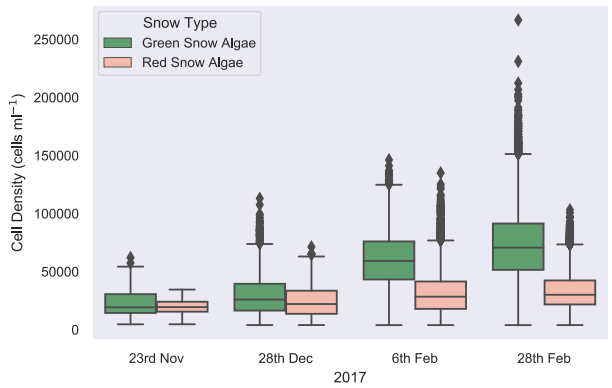

FIGURE 10 | Remotely sensed cell density. A boxplot showing the change in average snow algal cell density for Anchorage Island, recorded by WorldView 2 and 3 imagery, through a growing season.

3.2.2. WorldView Identification of Snow Algae on Anchorage Island

Remote sensing results reported here focus on Anchorage Island alone, as the footprint of each WorldView image of Ryder Bay was different, with sections of Léonie Island cropped from several images. **Figure 9** maps the change in distribution of snow algal biomass and area over the southwestern tip of Anchorage Island on February 6, February 28, November 23, and December 28. To complement this map, **Figure 10** shows the change in remote-sensed estimates of snow algal cell density across these time points. Although the images are from the same year, rather than the same growth season, our analysis is presented as a seasonal progression to explore changes from early (November/December) to late (February) season bloom development.

On November 23, 2017, green snow algae were identified at several locations where sea ice had thinned close to the shore and green or red/orange coloration appeared at the snow surface. These covered a small total area, with pixels identified as green snow algae covering 115 m^2 (min: 114 m^2; max: 118 m^2) and pixels identified as red snow algae covering 89 m^2 (min: 88 m^2; max: 91 m^2). These blooms were not densely populated, with a green pixel average cell density of 2.4 $\times$ 10^4 cells ml^{-1} $\pm$ 1.1 $\times$ 10^4 (n = 26) and a red pixel average cell density of 2.0 $\times$ 10^4 cells ml^{-1} $\pm$ 1.3 $\times$ 10^4 (n = 20). Dry biomass was, respectively, 0.37 kg (min: 6 g; max: 1.5 kg) and 0.09 kg (min: 38 g; max: 1.0 kg) for green and red blooms. By December 28, 2017, green snow algae were identified at the edges of snow packs and in troughs in the landscape. Both area (mean: 9.6 $\times$ 10^3 m^2; min: 8.7 $\times$ 10^3 m^2; max: 9.7 $\times$ 10^3 m^2) and average pixel cell density (3.0 $\times$ 10^4 cells ml^{-1} $\pm$ 1.3 $\times$ 10^4; n = 1749) had increased relative to the image from November 23, 2017, with dry biomass now totaling 42 kg (min: 0.6 kg; max: 179 kg) for Anchorage Island. Red snow algae were identified alongside these green patches, though they covered a smaller area (mean: 1.4 $\times$ 10^3 m^2; min: 1.2 $\times$ 10^3 m^2; max: 1.4 $\times$ 10^3 m^2). Here, red pixels averaged 2.5 $\times$ 10^4 cells ml^{-1} $\pm$ 1.5 $\times$ 10^4 (n = 249) and contained an estimated 1.9 kg (min: 0.7 kg; max: 20.3 kg) of dry biomass. By February 6, 2017, the area of visible green blooms had increased to 3.02 $\times$ 10^4 m^2 (min: 2.36 $\times$ 10^4 m^2; max: 3.20 $\times$ 10^4 m^2), as had the area of red snow algae, which was now similar to that of green (2.89 $\times$ 10^4 m^2; min: 2.10 $\times$ 10^4 m^2; max: 2.91 $\times$ 10^4 m^2). Average cell density for both red and green blooms had increased relative to December 28 image (5.0 $\times$ 10^4 cells ml^{-1} $\pm$ 1.7 $\times$ 10^4; n = 12,094 and 4.1 $\times$ 10^4 cells ml^{-1} $\pm$ 2.3 $\times$ 10^4 (n = 11,561), respectively), green blooms significantly so (t-test: t = 67; $P \leq 0.01$). Total dry biomass for Anchorage Island within this image was 52 kg (min: 15 kg; max: 537 kg) for red snow algae and 224 kg (min: 2.8 kg; max: 979 kg) for green snow algae. By February 28, 2017, red snow algae covered a greater area than green, averaging 9.48 $\times$ 10^4 m^2 vs. 6.26 $\times$ 10^4 m^2 (respective minimum area: 8.65 $\times$ 10^4 m^2 and 5.56 $\times$ 10^4 m^2; respective maximum area: 9.49 $\times$ 10^4 m^2 and 6.27 $\times$ 10^4 m^2). Green cell density had significantly increased (t-test: t = 41; $P \leq 0.01$) relative to February 6, 2017, averaging 6.0 $\times$ 10^4 cells ml^{-1} $\pm$ 2.2 $\times$ 10^4 (n = 15,814) in February 28, 2017 image, while red bloom cell densities remained similar within both February images (4.3 $\times$ 10^4 cells ml^{-1} $\pm$ 2.0 $\times$ 10^4; n = 23,956). Dry biomass on February 28, 2017 was 567 kg (min: 8 kg; max: 2,340 kg) for green blooms and 180 kg (min: 34 kg; max: 1,850 kg) for red blooms. The entirety of the WorldView 2 image from the February 28, 2017 (extent is shown in **Figure 1B**) contained 1.1 $\times$ 10^5 m^2 (min: 9.9 $\times$ 10^4 m^2; max:1.1 $\times$ 10^5 m^2) of green snow algae and 2.6 $\times$ 10^5 m^2 (min: 2.3 $\times$ 10^5 m^2; max: 2.6 $\times$ 10^5 m^2) of red snow algae, respectively, contributing 778 kg (min: 11 kg; max: 3220 kg) and 388 kg (min: 137 kg: max: 3,980 kg) of dry biomass to the area.

Red blooms had closer agreement between remote-sensed and *in situ* measurements of cell density, relative to green ones, with derived estimates, respectively, averaging 97 and 38% of *in situ* cell counts. It is likely this discrepancy is partially because the *in situ* mean overestimates average green bloom cell density due to sampling bias when in the field. Green blooms form dense mats of algae on relatively small patches of snow, whereas red blooms were typically more evenly distributed across a broader area, thus are less subject to bias when sampling. Integrating small dense patches of green algae over the area of one pixel may cause remote-sensed estimates of green algal cell density to underestimate real-world values. This spreading effect is also more likely to influence green blooms than red.

Based on dGPS data from two surveys on Anchorage Island, conducted on January 31 and February 12, 2018, blooms ranged from 60 to 2,739 m^2 in size, with the average bloom area being 962 m^2. Remotely sensed area estimates of discrete blooms from February 6, 2017 suggests the average bloom size was 12 m^2, with the maximum observed bloom being 1,035 m^2. At this point, Anchorage Island had 3,277 discrete blooms of snow algae with blooms under 100 m^2 contributing to 60% of total snow algal area. Blooms appear smaller within the satellite imagery because of differences by which blooms were separated into discrete entities. The remote sensing analysis rigidly separates blooms that do not intersect, whereas field dGPS surveys aggregate adjacent patches (as shown in **Figure 5**) where it was evident

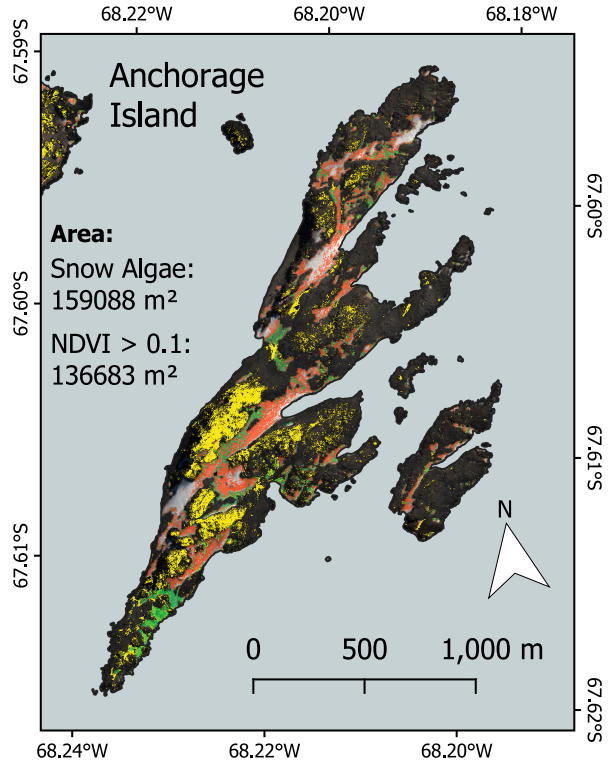

FIGURE 11 | Comparison between snow algal area and normalized difference vegetation index (NDVI) (a vegetation proxy) for Anchorage Island. Red and green pixels show the area covered by red and green snow algae, respectively. Yellow indicates pixels with an NDVI > 0.1, which indicates other vegetation (moss and lichen).

that subsurface algae connected blooms that were visible on the surface.

3.2.3. Snow Algae vs. Other Terrestrial Vegetation

Figure 11 shows snow algae alongside pixels with an NDVI > 0.1 on Anchorage Island on February 28, 2017. This image had the largest area coverage of snow algae, and the lowest area coverage of snow, meaning seasonally snow-covered terrestrial vegetation is likely to be exposed. For Anchorage Island, the total area covered by snow algae was 1.57×10^5 vs. 1.37×10^5 m^2 for pixels with an NDVI > 0.1. The average NDVI for pixels identified as vegetation (NDVI > 0.1) on Anchorage Island was 0.13 ± 0.07. Of 15 GPS-logged locations where moss or lichen covered an area larger than 1 m^2, recorded in February 2018, 80% had NDVI values > 0.1.

4. DISCUSSION

4.1. WorldView Satellites to Map Snow Algae

We have used WorldView 2 and 3 multispectral imagery to map changes in Antarctic snow algae during the summer growth season. The high spatial resolution of WorldView satellites has significantly improved upon previous satellite-based maps of snow algae, producing detailed area coverage and cell density estimates that let us explore the seasonal development of snow algal blooms. Additionally, WorldView's high spectral resolution meant we were able to map red algal blooms alongside green ones, addressing a major limitation of our previous study (Gray et al., 2020). Two ground validation campaigns (in 2018 and 2019) monitored the seasonal development of snow algae in Antarctica and collected field spectra of snow algae. These data were then used to develop a model to detect and estimate algal cell density in snow, by using the scaled integral of a chlorophyll absorption feature evident within both field reflectance factors and satellite pixels. Positional data were also collected to assess accuracy when applying this approach to WorldView imagery. Using this method, we successfully identified red and green snow algae on Anchorage Island, Antarctica, estimating peak coverage to be 9.48×10^4 and 6.26×10^4 m^2, respectively. Despite covering a smaller area, green snow algae had greater cell density than red blooms (6.0×10^4 and 4.3×10^4 cells ml^{-1}, respectively), and had higher average layer thickness (see **Table 2**). This meant that green algae contributed more overall to terrestrial biomass on the island than red algae (567 vs. 180 kg).

Our work builds upon previous use of Sentinel 2 imagery to study snow algae in Antarctica (Huovinen et al., 2018; Gray et al., 2020; Khan et al., 2020, 2021) and shows the advantage gained by using high spatial and spectral resolution satellites, such as WorldView 2 or 3. **Figure 12** compares snow algae identified through the methodology presented here, with that used in Gray et al. (2020), which used coarser-resolution Sentinel 2 satellite imagery. **Figure 12B** is a Sentinel 2 image that was captured 3 days after the WorldView 2 image in **Figure 12A**. Across the same area of Anchorage Island, Sentinel 2 was only able to detect 14.8% of the area of green snow algae identified by WorldView 2. Due to coarser spectral resolution, Sentinel 2 was unable to reliably detect red blooms, meaning that the total area of snow algae detected by Sentinel 2 was 5.7% of the combined area of red and green blooms detected with WorldView 2. WorldView 2 pixels cover a 25x smaller area than Sentinel 2 pixels, resulting in far fewer mixed pixels at the edges of blooms that would be filtered out when analyzing Sentinel 2 imagery. Smaller pixels also allows WorldView 2 to detect much smaller blooms [0.09 m^2 vs. 11 m^2 for Sentinel 2 (Gray et al., 2020)] with less chance of misclassification. The total bloom area for green snow algae on the Antarctic Peninsula detected using Sentinel 2 in Gray et al. (2020) was 1.9 km^2. Since a large proportion of this area was related to several very large blooms, where the limitation of Sentinel 2's minimum area detection limit would be less problematic, we cannot simply scale the difference observed between satellites for Anchorage Island in **Figure 12** to improve our Peninsula area estimate. Instead, it serves to highlight the importance of smaller blooms in contributing to the total area covered by snow algae. It also shows a need to refine methods for automatic sub-pixel bloom detection when using Sentinel 2 or similar imagery to study snow algae over large areas.

Of the methods employed here for identifying snow algae, most uncertainty relates to the SAM classifier as a method for discriminating between snow end members as "clean,"

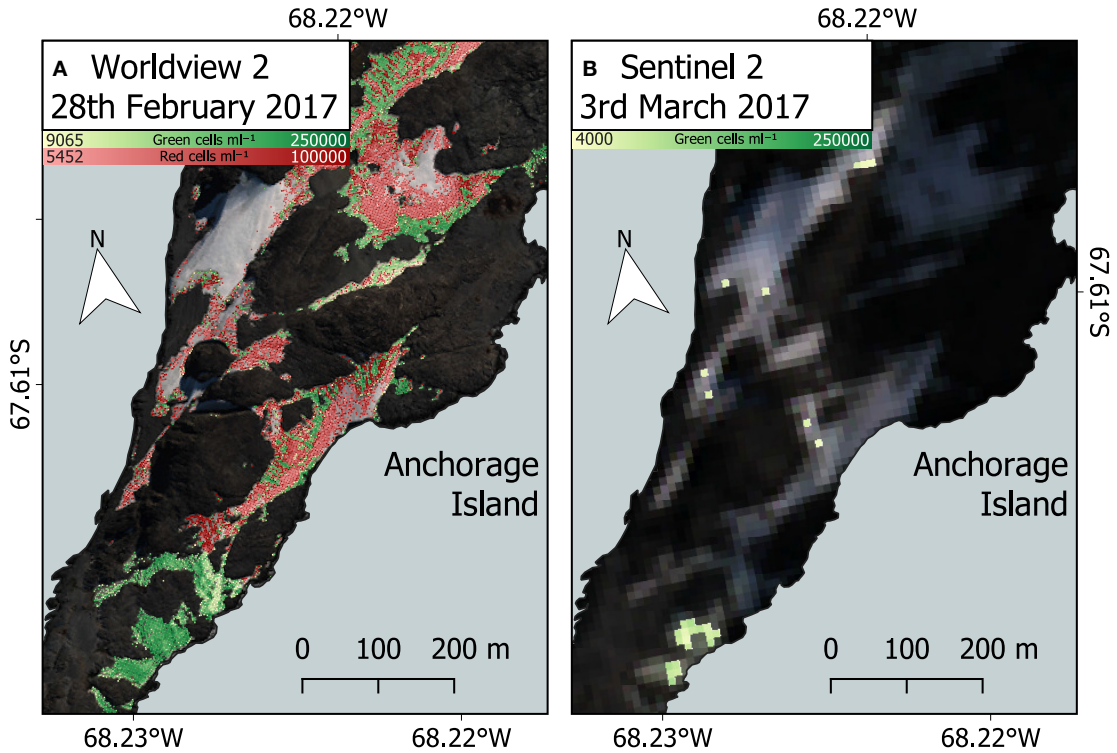

FIGURE 12 | Comparison between WorldView 2 and Sentinel 2. **(A)** WorldView 2 analysis of red and green snow algal distribution and cell density on February 28, 2017, Anchorage Island, Antarctica. **(B)** Green snow algal distribution and cell density based on a Sentinel 2 image from March 3, 2017, using methodology described by Gray et al. (2020). Note cloud shadow is partially obscuring the north east section in this image.

"mineral-laden," "red," or "green" snow algae. SAM was used over other classification methods for this study as it is relatively robust against BRDF effects (Weyermann et al., 2009). However, snow and ice have diverse and dynamic morphology, where grain size, density, and liquid water content may all change significantly throughout the day and influence the scattering of light (Dozier et al., 2009; Nolin, 2011). Moreover, our end member HDRF were collected over a narrow time period relative to the snow algal growth season, and so may not be representative of a full range of snow conditions. Spectral unmixing approaches have been used to separate mineral-laden snow from snow algae-containing snow with some success within Sentinel 2 images (Huovinen et al., 2018). However, unconstrained linear unmixing classification using the same end member spectra as used to populate our SAM classifier yielded poor performance on our WorldView imagery, and so was not considered further here. Indices methods for identifying mineral impurities within snow, such as those developed by Di Mauro et al. (2015) and Kokhanovsky et al. (2021), may improve the reliability of classifying red snow algae when combined with our SAM approach. Future work should focus on refining ensemble methods to improve classification of snow and its mineral and biological impurities over a wider range of seasonal conditions within multispectral satellite imagery.

For studying the ecology of snow algae, the synoptic view provided by satellites escapes the sampling bias of *in situ* observations while providing temporal characterization of fundamental properties, such as area and cell density across large areas. Remote sensing is not an alternative to field-based observations, however, as it misses the complexity of processes within the snow pack, both in terms of algal diversity and the physical stratification of algae within the snow itself. Moreover, coastal Antarctic snows are host to a variety of other microbial constituents that are not visible for remote detection, yet are important within biogeochemical processes, such as nutrient transfer and carbon cycling (Antony et al., 2016; Malard et al., 2019). Moreover, pixel size and processing routines used to identify snow algae introduce their own biases and are discussed here. The use of high spatial resolution WorldView imagery in this paper goes some way to addressing these biases to give a more complete picture of snow algae as an ecosystem relative to what has been achieved with the freely available Sentinel 2 imagery in Antarctica (Huovinen et al., 2018; Gray et al., 2020). Unfortunately, as this imagery needs to be tasked, and is relatively expensive, it is currently unsuitable for routine monitoring at large scales.

4.2. Snow Algal Seasonal Change and Phenology

The WorldView image of Anchorage Island from November 23, 2017 shows algae appearing where snow is overlying coastal inlets, where sea ice has persisted. With no *in situ* observations

this early in the season, it is hard to confidently state whether these pixels are snow algae. The inlets where algae were identified by our model coincide with valleys further inland, meaning that early melt water could have been channeled here, or snow may be saturated from proximity to ocean water, causing wet conditions for algae to grow in the snowpack. Alternatively, we may be seeing a false positive from light diffracting through thin sea ice, or marine algae exposed from ice disturbance. Nonetheless, December's WorldView image mirrored our field observations, with small patches of green and red snow algae appearing at the melting edge of snow banks. Observations from snow pits dug in January at both Ryder Bay and King George Island field sites suggest that this green snow algal layer will extend up into the snowpack within a melt water-rich layer of snow/slush, sandwiched between overlying seasonal and compacted multi-year snow layers. Depending on the thickness and freshness (Perovich, 2007) of overlying snow, this layer of snow algae may be shielded from satellite observation, and hence our area estimates for December likely underestimate the actual extent of growth.

A significant change was observed in the late-season images, where green snow algae had appeared in the upper elevations of snow banks, exposed where the seasonal snow pack had melted away in runnels (see **Figure 9**). Field observations from Anchorage Island on January 31, 2018 indicated less extensive green snow algae coverage relative to February 6, 2017 WorldView image, though larger green patches were starting to appear (see **Figure 5**) in the same locations that were identified as containing snow algae by 2017 remote sensing imagery. They also followed the same pattern of exposure, melting out from underneath seasonal snow on the upper margins of snow fields. Average remote-sensed cell density estimates increased significantly between November 23 and February 28 images, suggesting considerable green algal growth between early and late season. We postulate that the maximum area coverage of green snow algae was achieved while buried underneath seasonal snow cover, where liquid water and nutrients are supplied by snow melt percolating through the algal layer (Nowak et al., 2018). This means that late-season remote sensing observations can be diagnostic of processes occurring earlier in the melt season, yet also highlights a primary limitation of optical remote sensing methods for snow alga (or algae) ecology: uncertainty relating to buried and obscured blooms.

Field observations indicated that red blooms primarily occurred on the surface of seasonal snow, sometimes appearing to bloom after fresh snow fall, although red coloration could also appear on underlying multi-year snow, presumably having been deposited by snow melt. The blooms on the seasonal snow surface surveyed on Anchorage Island on January 31 were red and/or orange in color (e.g., **Figure 2B**), and again were evident in similar locations to red snow algae identified in February 6, 2017 image. By February 28, 2017, red snow algae covered a greater area than green and, combined, snow algae covered 72% of the snowpack on Anchorage Island. Despite snow algal area reaching its observed maximum in February 28, 2017 image, there had also been significant loss of algae-inhabited snow by this point in the melt season. Between February 6 and 28, 1.2×10^4 m^2 of snow containing green algae, and 1.0×10^4 m^2 of snow containing red algae had melted out completely, and 13.8% of the total bloom area is identified in February 28, 2017 image.

Interestingly, we observed green snow algal blooms of similar sizes on the same snow banks across multiple growth seasons. Imagery from 2017 closely matches field observations from 2018, and indeed green coloration is visible on these same snow patches on the southern tip of Anchorage Island within 2020 Sentinel 2 imagery (data not shown). This may be an indication that the previous year's bloom seeds subsequent year's growth, where blooms on multi-year snow are buried by fresh snowfall (Hoham and Duval, 2001; Hoham and Remias, 2020). **Figure 9** shows large red blooms forming adjacent to green. Along with observations of red cells forming on top of layers of green snow algae in several snow pits (see **Figure 2C**), this perhaps indicates that the red blooms on Anchorage Island are an encystment phase of an underlying green bloom. In some cases, this was confirmed, as snow that was red on February 6 was replaced with green snow by February 28, presumably as the cyst-containing seasonal snow melted out completely. Some in-field observations of red blooms, however, indicated that red snow algae were not associated with underlying vegetative cells, suggesting that aerial dispersal of cells onto the snowpack may also be an important factor influencing the colonization of snow (Marshall and Chalmers, 1997; Muller et al., 2001; Procházková et al., 2019). This may be possible to test with a remote-sensed phenology, such as in **Figure 9**, but we see no evidence of red blooms melting out to white snow in this case. Additionally, although there is increasing evidence that red cells have a bioalbedo advantage over green cells in seeding and establishing blooms (Dial et al., 2018), we do not have any systematic evidence in this study to support this and would require further investigation for such mixed green–orange–red color algal populations.

Our results indicate that 2017 snow algal coverage on Anchorage Island was greater in area than other terrestrial vegetation combined. Anchorage Island vegetation is predominantly mosses and lichens, with some *Prasiola* species also present (Bokhorst et al., 2007). Our results indicated that NDVI values on Anchorage Island were generally low (averaging 0.13), and consistent with those identified for lichen species in Landsat imagery by Casanovas et al. (2015). Casanovas et al. (2015) showed NDVI to perform relatively poorly when mapping Antarctic lichen species because of their low NDVI under dry conditions. However, though we did not perform species-specific ground validation for terrestrial vegetation, NDVI appeared to perform well, identifying large areas of lichen-covered rock toward the south of Anchorage Island. The results of Fretwell et al. (2011) and Casanovas et al. (2015) indicate that we may have missed some vegetation by choosing a 0.1 threshold for our NDVI value, in which case maximum snow algal area may be similar to that of terrestrial vegetation. We observed significant false positives when applying a lower 0.05 NDVI threshold on our February 28, 2017 image, however, and so cannot accurately use these data in our comparison. Future work may apply the full remote

sensing framework devised by Jawak et al. (2019) for more robust identification of terrestrial vegetation in WorldView scenes to allow for better comparison between Antarctic vegetation types.

5. CONCLUSIONS

Our primary aim here was to improve remote sensing methods for detecting and monitoring snow algal blooms and to use them to assess fundamental aspects of the ecology of these organisms. We have made the first use of high-resolution WorldView 2 and 3 imagery from 2017 to identify blooms of red and green snow algae as they grow in the snow pack on Anchorage Island, Antarctica. From this imagery, we have produced estimates of cell density and area coverage, showing how red and green blooms developed separately as the melt season progressed. Together, red and green blooms grew to cover an area greater than other terrestrial vegetation on the island. This remote sensing study was underpinned by two field seasons in Antarctica, in 2018 and 2019, to build the empirical model which relates spectral reflectance to cell density and to spatially validate our model output.

WorldView imagery provided a significant improvement over previous efforts using Sentinel 2 imagery, with both red and green blooms automatically detected using the methodology developed for Sentinel 2 imagery by Gray et al. (2020). The higher resolution allows blooms to be picked out in far greater detail than previously achieved, meaning that blooms occurring on the edge of snow packs can be included in our analyses. Comparison of snow algal area estimates between WorldView and Sentinel 2 imagery implied that the total area of snow algae on the Antarctic Peninsula estimated in Gray et al. (2020) was a significant underestimate. However, until higher resolution multispectral imagery is routinely recorded over Antarctica, and is freely distributed, Sentinel 2 remains a more practical option for monitoring snow algae on large scales. Although there are still significant uncertainties associated with using satellites to monitor snow algae, high-resolution satellite imagery, such as WorldView offers the chance to perform relatively detailed analyses of blooms in specific areas through time, and to study how they are affected by factors, such as temperature and precipitation and how they, in turn, influence the albedo of the snow surface. Synoptic monitoring of snow algal growth and development during the Antarctic summer may yield further insights into their ecological strategies, metabolic load and life cycle, and how either may be affected by climatic changes in Antarctica.

DATA AVAILABILITY STATEMENT

The raw data supporting the conclusions of this article will be made available by the authors, without undue reservation.

AUTHOR CONTRIBUTIONS

MD, AG, LP, and PC designed and planned the fieldwork and logistics. AG, MD, and MM carried out the fieldwork. MD, MK, AG, AS, and MM planned and analyzed the field samples at Rothera Research Station, Escudero Base, and Cambridge. AG led the remote sensing, validation, and geospatial analysis with input from PF and MD. AG led the writing of the manuscript with all authors contributing and editing the text. All authors have seen and approved the final version.

FUNDING

The research expeditions were funded by a Leverhulme Trust Research Grant (RPG-2017-077) and supported by the NERC British Antarctic Survey and the Chilean Antarctic Institute INACH. MD, MK, and AG were supported by the Leverhulme Trust Research Grant (RPG-2017-077). LP, PC, and PF were supported by NERC core funding to the BAS Biodiversity, Evolution and Adaptation Team and MAGIC. This work was currently funded under a NERC Standard Grant (NE/V000764/1).

ACKNOWLEDGMENTS

We thank staff at the Rothera Research Station, Antarctica, especially the Bonner laboratory manager Alison Massey and boating staff (Ritchie Southerton, Zac Priestley, Zoe Waring) and staff at King George Island Escudero Base (Elias Barticevic and César Cárdenas Alarcón), the Digital Globe Foundation for the WorldView imagery, and Steve Colwell for sunphotometer data. We thank Andrew Fleming, Kevin Newsham, Dan Clewley, and James Blake for scientific support. Thank you to James Rolfe at the Godwin Laboratory for Palaeoclimate Research, Department of Earth Sciences, University of Cambridge for the total C/N data acquisition, Lorraine Archer, Department of Plant Sciences, University of Cambridge for help with the microscopy, the NERC Field Spectroscopy Facility (loans 765.0617 and 796.0618), Macarena Henriquez (AGUNSA) for assistance and logistic support, and Jorge González Aravena (INACH) for freeze drying samples.

REFERENCES

Antony, R., Sanyal, A., Kapse, N., Dhakephalkar, P. K., Thamban, M., and Nair, S. (2016). Microbial communities associated with Antarctic snow pack and their biogeochemical implications. *Microbiol. Res.* 192, 192–202. doi: 10.1016/j.micres.2016.07.004

Bidigare, R. R., Ondrusek, M. E., Kennicutt, M. C., Iturriaga, R., Harvey, H. R., Hoham, R. W., et al. (1993). Evidence a photoprotective for secondary carotenoids of snow algae. *J. Phycol.* 29, 427–434. doi: 10.1111/j.1529-8817.1993.tb00143.x

Boetius, A., Anesio, A. M., Deming, J. W., Mikucki, J. A., and Rapp, J. Z. (2015). Microbial ecology of the cryosphere: sea ice and glacial habitats. *Nat. Rev. Microbiol.* 13, 1–14. doi: 10.1038/nrmicro3522

Bokhorst, S., Huiskes, A., Convey, P., and Aerts, R. (2007). The effect of environmental change on vascular plant and cryptogam communities from the Falkland Islands and the Maritime Antarctic. *BMC Ecol.* 7:15. doi: 10.1186/1472-6785-7-15

Bunting, P., and Clewley, D. (2019). *Atmospheric and Radiometric Correction of Satellite Imagery (ARCSI)*. Available online at: https://www.arcsi.remotesensing.info/ (accessed May 12, 2020).

Casanovas, P., Black, M., Fretwell, P., and Convey, P. (2015). Mapping lichen distribution on the Antarctic Peninsula using remote sensing, lichen spectra and photographic documentation by citizen scientists. *Polar Res.* 34:25633. doi: 10.3402/polar.v34.25633

Cook, J. M., Hodson, A. J., Gardner, A. S., Flanner, M., Tedstone, A. J., Williamson, C., et al. (2017). Quantifying bioalbedo: a new physically based model and discussion of empirical methods for characterising biological influence on ice and snow albedo. *Cryosphere* 11, 2611–2632. doi: 10.5194/tc-11-2611-2017

Cubaynes, H. C., Fretwell, P. T., Bamford, C., Gerrish, L., and Jackson, J. A. (2019). Whales from space: four mysticete species described using new VHR satellite imagery. *Mar. Mammal Sci.* 35, 466–491. doi: 10.1111/mms.12544

Davey, M. P., Norman, L., Sterk, P., Huete-Ortega, M., Bunbury, F., Loh, B. K. W., et al. (2019). Snow algae communities in Antarctica: metabolic and taxonomic composition. *New Phytol.* 222, 1242–1255. doi: 10.1111/nph.15701

Di Mauro, B., Fava, F., Ferrero, L., Garzonio, R., Baccolo, G., Delmonte, B., et al. (2015). Mineral dust impact on snow radiative properties in the European Alps combining ground, UAV, and satellite observations. *J. Geophys. Res. Atmos.* 120, 6080–6097. doi: 10.1002/2015JD023287

Di Mauro, B., Garzonio, R., Baccolo, G., Franzetti, A., Pittino, F., Leoni, B., et al. (2020). Glacier algae foster ice-albedo feedback in the European Alps. *Sci. Rep.* 10:4739. doi: 10.1038/s41598-020-61762-0

Dial, R. J., Ganey, G. Q., and Skiles, S. M. (2018). What color should glacier algae be? An ecological role for red carbon in the cryosphere. *FEMS Microbiol. Ecol.* 94:fiy007. doi: 10.1093/femsec/fiy007

Dierssen, H. M., Smith, R. C., and Vernet, M. (2002). Glacial meltwater dynamics in coastal waters west of the Antarctic peninsula. *Proc. Natl. Acad. Sci. U.S.A.* 99, 1790–1795. doi: 10.1073/pnas.032206999

Dozier, J., Green, R. O., Nolin, A. W., and Painter, T. H. (2009). Interpretation of snow properties from imaging spectrometry. *Rem. Sens. Environ.* 113, S25–S37. doi: 10.1016/j.rse.2007.07.029

Fretwell, P. T., Convey, P., Fleming, A. H., Peat, H. J., and Hughes, K. A. (2011). Detecting and mapping vegetation distribution on the Antarctic Peninsula from remote sensing data. *Polar Biol.* 34, 273–281. doi: 10.1007/s00300-010-0880-2

Fretwell, P. T., LaRue, M. A., Morin, P., Kooyman, G. L., Wienecke, B., Ratcliffe, N., et al. (2012). An emperor penguin population estimate: the first global, synoptic survey of a species from space. *PLoS ONE* 7:e33751. doi: 10.1371/annotation/32c246eb-3b73-4410-a44c-b41ddae11fc5

Fujii, M., Takano, Y., Kojima, H., Hoshino, T., Tanaka, R., and Fukui, M. (2010). Microbial community structure, pigment composition, and nitrogen source of red snow in antarctica. *Microb. Ecol.* 59, 466–475. doi: 10.1007/s00248-009-9594-9

Ganey, G. Q., Loso, M. G., Burgess, A. B., and Dial, R. J. (2017). The role of microbes in snowmelt and radiative forcing on an Alaskan icefield. *Nat. Geosci.* 10, 754–759. doi: 10.1038/ngeo3027

Gray, A., Krolikowski, M., Fretwell, P., Convey, P., Peck, L. S., Mendelova, M., et al. (2020). Remote sensing reveals Antarctic green snow algae as important terrestrial carbon sink. *Nat. Commun.* 11:2527. doi: 10.1038/s41467-020-16018-w

Hirano, M. (1965). "Freshwater algae in the Antarctic regions," in *Biogeography and Ecology in Antarctica, Chapter 4*, eds J. van Mieghem and P. van Oye (Heidelberg: Springer Science & Business Media), 127–193. doi: 10.1007/978-94-015-7204-0_4

Hodson, A. J., Anesio, A. M., Tranter, M., Fountain, A. G., Osborn, M., Priscu, J. C., et al. (2008). Glacial ecosystems. *Ecol. Monogr.* 78, 41–67. doi: 10.1890/07-0187.1

Hodson, A. J., Nowak, A., Cook, J., Sabacka, M., Wharfe, E. S., Pearce, D. A., et al. (2017). Microbes influence the biogeochemical and optical properties of maritime Antarctic snow. *J. Geophys. Res. Biogeosci.* 122, 1456–1470. doi: 10.1002/2016JG003694

Hoham, R. W., and Duval, B. (2001). "Microbial ecology of snow and freshwater ice with emphasis on snow algae," in *Snow Ecology: An Interdisciplinary Examination of Snow-Covered Ecosystems*, eds H. G. Jones, J. W. Pomeroy, D. A. Walker, and R. W. Hoham (Cambridge: Cambridge University Press), 168–228.

Hoham, R. W., and Remias, D. (2020). Snow and glacial algae: a review. *J. Phycol.* 56, 264–282. doi: 10.1111/jpy.12952

Holzinger, A., Allen, M. C., and Deheyn, D. D. (2016). Hyperspectral imaging of snow algae and green algae from aeroterrestrial habitats. *J. Photochem. Photobiol. B Biol.* 162, 412–420. doi: 10.1016/j.jphotobiol.2016.07.001

Howat, I. M., Porter, C., Smith, B. E., Noh, M.-J., and Morin, P. (2019). The reference elevation model of Antarctica. *Cryosphere* 13, 665–674. doi: 10.5194/tc-13-665-2019

Huovinen, P., Ramírez, J., and Gómez, I. (2018). Remote sensing of albedo-reducing snow algae and impurities in the Maritime Antarctica. *ISPRS J. Photogramm. Rem. Sens.* 146, 507–517. doi: 10.1016/j.isprsjprs.2018.10.015

Jawak, S. D., Luis, A. J., Fretwell, P. T., Convey, P., and Durairajan, U. A. (2019). Semiautomated detection and mapping of vegetation distribution in the antarctic environment using spatial-spectral characteristics of WorldView-2 imagery. *Rem. Sens.* 11:1909. doi: 10.3390/rs11161909

Khan, A. L., Dierssen, H., Scambos, T., Höfer, J., and Cordero, R. R. (2020). Spectral characterization, radiative forcing, and pigment content of coastal antarctic snow algae: approaches to spectrally discriminate red and green communities and their impact on snowmelt. *Cryosphere Discuss.* 2020, 1–27. doi: 10.5194/tc-2020-170

Khan, A. L., Dierssen, H. M., Scambos, T. A., Höfer, J., and Cordero, R. R. (2021). Spectral characterization, radiative forcing and pigment content of coastal antarctic snow algae: approaches to spectrally discriminate red and green communities and their impact on snowmelt. *Cryosphere* 15, 133–148. doi: 10.5194/tc-15-133-2021

Kokhanovsky, A., Di Mauro, B., Garzonio, R., and Colombo, R. (2021). Retrieval of dust properties from spectral snow reflectance measurements. *Front. Environ. Sci.* 9:644551. doi: 10.3389/fenvs.2021.644551

LaRue, M. A., Rotella, J. J., Garrott, R. A., Siniff, D. B., Ainley, D. G., Stauffer, G. E., et al. (2011). Satellite imagery can be used to detect variation in abundance of Weddell seals (*Leptonychotes weddellii*) in Erebus Bay, Antarctica. *Polar Biol.* 34, 1727–1737. doi: 10.1007/s00300-011-1023-0

Ling, H. U., and Seppelt, R. D. (1993). Snow algae of the Windmill Islands continental Antarctica. 2. *Chloromonas rubroleosa* sp. nov. (Volvocales, Chlorophyta), an alga of red snow. *Eur. J. Phycol.* 28, 77–84. doi: 10.1080/09670269300650131

Lutz, S., Anesio, A. M., Raiswell, R., Edwards, A., Newton, R. J., Gill, F., et al. (2016). The biogeography of red snow microbiomes and their role in melting arctic glaciers. *Nat. Commun.* 7:11968. doi: 10.1038/ncomms11968

Malard, L. A., Šabacká, M., Magiopoulos, I., Mowlem, M., Hodson, A., Tranter, M., et al. (2019). Spatial variability of Antarctic surface snow bacterial communities. *Front. Microbiol.* 10:461. doi: 10.3389/fmicb.2019.00461

Marshall, W., and Chalmers, M. (1997). Airborne dispersal of Antarctic terrestrial algae and cyanobacteria. *Ecography* 20, 585–594. doi: 10.1111/j.1600-0587.1997.tb00427.x

Mataloni, G., and Tesolín, G. (1997). A preliminary survey of cryobiontic algal communities from Cierva Point (Antarctic Peninsula). *Antarctic Sci.* 9, 250–258. doi: 10.1017/S0954102097000333

Muller, T., Thomas, L., and Fuhr, G. (2001). Persistent snow algal fields in Spitsbergen: field observations and a hypothesis about the annual cell circulation. *Arctic Antarctic Alpine Res.* 33, 42–51. doi: 10.1080/15230430.2001.12003403

Nolin, A. W. (2011). Recent advances in remote sensing of seasonal snow. *J. Glaciol.* 56, 1141–1150. doi: 10.3189/002214311796406077

Nowak, A., Hodson, A., and Turchyn, A. V. (2018). Spatial and temporal dynamics of dissolved organic carbon, chlorophyll, nutrients, and trace metals in Maritime Antarctic snow and snowmelt. *Front. Earth Sci.* 6:201. doi: 10.3389/feart.2018.00201

Painter, T. H., Duval, B., Thomas, W. H., Mendez, M., Heintzelman, S., and Dozier, J. (2001). Detection and quantification of snow algae with an airborne imaging spectrometer. *Appl. Environ. Microbiol.* 67, 5267–5272. doi: 10.1128/AEM.67.11.5267-5272.2001

Perovich, D. K. (2007). Light reflection and transmission by a temperate snow cover. *J. Glaciol.* 53, 201–210. doi: 10.3189/172756507782202919

Procházková, L., Leya, T., Křížková, H., and Nedbalová, L. (2019). *Sanguina nivaloides* and *Sanguina aurantia* gen. et spp. Nov. (Chlorophyta): The taxonomy, phylogeny, biogeography and ecology of two newly recognised algae causing red and orange snow. *FEMS Microbiol. Ecol.* 95:fiz064. doi: 10.1093/femsec/fiz064

Radoux, J., Chomé, G., Jacques, D. C., Waldner, F., Bellemans, N., Matton, N., et al. (2016). Sentinel-2's potential for sub-pixel landscape feature detection. *Rem. Sens.* 8:488. doi: 10.3390/rs8060488

Remias, D., Wastian, H., Lütz, C., and Leya, T. (2013). Insights into the biology and phylogeny of *Chloromonas polyptera* (Chlorophyta), an alga causing orange snow in Maritime Antarctica. *Antarctic Sci.* 25, 648–656. doi: 10.1017/S0954102013000060

Segawa, T., Matsuzaki, R., Takeuchi, N., Akiyoshi, A., Navarro, F., Sugiyama, S., et al. (2018). Bipolar dispersal of red-snow algae. *Nat. Commun.* 9:3094. doi: 10.1038/s41467-018-05521-w

Soto, D. F., Fuentes, R., Huovinen, P., and Gómez, I. (2020). Microbial composition and photosynthesis in Antarctic snow algae communities: integrating metabarcoding and pulse amplitude modulation fluorometry. *Algal Res.* 45:101738. doi: 10.1016/j.algal.2019.101738

Takeuchi, N., Dial, R., Kohshima, S., Segawa, T., and Uetake, J. (2006). Spatial distribution and abundance of red snow algae on the Harding Icefield, Alaska derived from a satellite image. *Geophys. Res. Lett.* 33, 1–6. doi: 10.1029/2006GL027819

Tedstone, A., Cook, J., Williamson, C., Hofer, S., McCutcheon, J., Irvine-Fynn, T., et al. (2019). Algal growth and weathering crust structure drive variability in Greenland Ice Sheet ice albedo. *Cryosphere Discuss.* 14, 521–538. doi: 10.5194/tc-14-521-2020

Vermote, E. F., Tanre, D., Deuze, J. L., Herman, M., and Morcette, J. (1997). Second simulation of the satellite signal in the solar spectrum 6s: an overview. *IEEE Trans. Geosci. Rem. Sens.* 35, 675–686. doi: 10.1109/36.581987

Weyermann, J., Schläpfer, D., Hueni, A., Kneubühler, M., and Schaepman, M. (2009). "Spectral Angle Mapper (SAM) for anisotropy class indexing in imaging spectrometry data," in *Imaging Spectrometry XIV*, Vol. 7457, eds S. S. Shen and P. E. Lewis (San Diego, CA: SPIE), 74570B. doi: 10.1117/12.825991

Conflict of Interest: The authors declare that the research was conducted in the absence of any commercial or financial relationships that could be construed as a potential conflict of interest.

frontiers in Plant Science

ORIGINAL RESEARCH
published: 28 June 2021
doi: 10.3389/fpls.2021.673614

Macro-Nutrient Stoichiometry of Glacier Algae From the Southwestern Margin of the Greenland Ice Sheet

Christopher J. Williamson[1], Thomas Turpin-Jelfs[1], Miranda J. Nicholes[1], Marian L. Yallop[2], Alexandre M. Anesio[3] and Martyn Tranter[1,3]*

[1] Bristol Glaciology Centre, School of Geographical Sciences, University of Bristol, Bristol, United Kingdom, [2] School of Biological Sciences, University of Bristol, Bristol, United Kingdom, [3] Department of Environmental Science, Aarhus University, Aarhus, Denmark

Glacier algae residing within the surface ice of glaciers and ice sheets play globally significant roles in biogeochemical cycling, albedo feedbacks, and melt of the world's cryosphere. Here, we present an assessment of the macro-nutrient stoichiometry of glacier algal assemblages from the southwestern Greenland Ice Sheet (GrIS) margin, where widespread glacier algal blooms proliferate during summer melt seasons. Samples taken during the mid-2019 ablation season revealed overall lower cellular carbon (C), nitrogen (N), and phosphorus (P) content than predicted by standard microalgal cellular content:biovolume relationships, and elevated C:N and C:P ratios in all cases, with an overall estimated C:N:P of 1,997:73:1. We interpret lower cellular macro-nutrient content and elevated C:N and C:P ratios to reflect adaptation of glacier algal assemblages to their characteristic oligotrophic surface ice environment. Such lower macro-nutrient requirements would aid the proliferation of blooms across the nutrient poor cryosphere in a warming world. Up-scaling of our observations indicated the potential for glacier algal assemblages to accumulate ∼ 29 kg C km^2 and ∼ 1.2 kg N km^2 within our marginal surface ice location by the mid-ablation period (early August), confirming previous modeling estimates. While the long-term fate of glacier algal autochthonous production within surface ice remains unconstrained, data presented here provide insight into the possible quality of dissolved organic matter that may be released by assemblages into the surface ice environment.

Keywords: glacier algae, C:N:P, Greenland Ice Sheet, stoichiometry, supraglacial

OPEN ACCESS

Edited by:
Linda Nedbalová, Charles University, Czechia

Reviewed by:
Elly Spijkerman, University of Potsdam, Germany
Daniel Remias, University of Applied Sciences Upper Austria, Austria

****Correspondence:***
Christopher J. Williamson
c.williamson@bristol.ac.uk

Specialty section:
This article was submitted to Marine and Freshwater Plants, a section of the journal Frontiers in Plant Science

Received: *27 February 2021*
Accepted: *23 April 2021*
Published: *28 June 2021*

Citation:
Williamson CJ, Turpin-Jelfs T, Nicholes MJ, Yallop ML, Anesio AM and Tranter M (2021) Macro-Nutrient Stoichiometry of Glacier Algae From the Southwestern Margin of the Greenland Ice Sheet. Front. Plant Sci. 12:673614. doi: 10.3389/fpls.2021.673614

INTRODUCTION

Microbial communities that reside on the surfaces of glaciers and ice sheets play globally significant roles in carbon (C) and nutrient cycling and surface ice melt (Hodson et al., 2008; Stibal et al., 2012; Anesio et al., 2017; Williamson et al., 2018, 2020). Of particular importance are Streptophyte "glacier algae" (Williamson et al., 2019), whose presence in surface ice lowers the bare ice albedo, enhances solar energy absorption, and drives surface melt through the process of "biologically driven albedo reduction" (Yallop et al., 2012; Stibal et al., 2017; Williamson et al., 2018, 2020; Cook et al., 2020). On the surface of the Greenland Ice Sheet (GrIS), summer blooms of glacier algae are responsible for widespread albedo decline that has paralleled accelerating surface melt since the early 1990s (Yallop et al., 2012; Tedesco et al., 2016; Stibal et al., 2017; van den Broeke et al., 2017; Cook et al., 2020; Tedstone et al., 2020; Williamson et al., 2020), with recent estimates attributing

an additional 5.5–8.0 Gt of runoff to glacier algal growth along the western ice sheet margin; 6–9% of the total runoff (Cook et al., 2020). Given that melt of the GrIS is the single largest cryospheric contributor to global eustatic sea level rise (Bamber et al., 2018), constraining bloom dynamics into the future remains a significant research priority (Williamson et al., 2019, 2020; Cook et al., 2020; Tedstone et al., 2020).

Glacier algal blooms initiate following snow line retreat (Williamson et al., 2018), with population doubling times on the GrIS ranging 3.75–5.5 days, and maximal cell densities approaching 10^5 cells mL^{-1} of melt water during major bloom years (Yallop et al., 2012; Stibal et al., 2017; Williamson et al., 2018, 2020). At these cell densities, widespread albedo decline is driven by significant secondary phenolic pigmentation produced by glacier algae to protect their low-light adapted chloroplasts (Williamson et al., 2020). By dissipating the intercepted incident irradiance as heat, this secondary pigmentation also generates liquid water proximal to the cells, driving surface ice ablation while providing access to nutrient and other resources required to promote algal growth (Dial et al., 2018; Williamson et al., 2020). Accordingly, growth proceeds as a function of bare-ice melt duration, such that strong patterning in accumulated biomass is apparent across the ablation zone, with maximal cell densities accumulated within the most marginal regions that experience the longest ablation periods, and a decreasing trend toward the equilibrium line (Williamson et al., 2020). As the ablation period progresses into polar winter, the fate of accumulated biomass remains unknown, although glacier algal species have been shown to overwinter in alpine locations (Remias et al., 2012b), and active glacier algal assemblages have been observed in GrIS shallow surface ice prior to snow line retreat (Nicholes et al., 2019).

One of the biggest questions remaining about glacier algal blooms asks, What factors limit the distribution and magnitude of blooms in space and time? While physical conditions such as snow-pack height, light availability, and temperature produce a first order control on the ability of blooms to form and proliferate in any given year (Tedstone et al., 2017; Williamson et al., 2020), little information currently exists on potential "bottom-up" or "top-down" regulation of blooms in supraglacial environments, restricting abilities to project bloom occurrence into the future (Williamson et al., 2019; McCutcheon et al., 2021). Within the marine environment, for example, top-down pressures such as zooplankton grazing and/or bottom-up availability of nutrients represent fundamental controls on phytoplankton biomass (Huppert et al., 2002). Supraglacial environments are characterized by truncated, microbially dominated trophic structures (Anesio and Laybourn-Parry, 2012; Anesio et al., 2017) and highly oligotrophic conditions (Hawkings et al., 2016; Wadham et al., 2016), indicating that large potential exists for bottom-up limitation of glacier algal blooms.

To date, field observations of ambient hydrochemistry during bloom progression have demonstrated a bulk phase shift toward organic over inorganic nutrient resources within surface ice (Holland et al., 2019), which coupled with 28-times lower secondary production relative to primary production (Yallop et al., 2012; Nicholes et al., 2019) has been interpreted to imply inefficient remineralization of inorganic nutrient resources within GrIS surface ice, and a potential mechanism of bottom-up control (Nicholes et al., 2019). Recently, McCutcheon et al. (2021) provided the first evidence for such bottom-up control of glacier algal blooms on the GrIS, highlighting inorganic phosphorus (P_i) limitation and the importance of locally sourced hydroxylapatite in supporting bloom proliferation, and likely important roles for heterotrophic bacterial and fungal communities in accelerating apatite weathering and thus P availability to glacier algal communities. This study did not, however, directly quantify glacier algal abundance within samples, precluding direct calculation of cellular elemental quotas. The importance of this information is illustrated by the findings of Holland et al. (2019) for the same bloom and sampling sites, who concluded that there was sufficient inorganic macro-nutrient availability within surface ice to support the magnitude of glacier algal bloom apparent during the 2016 ablation season when assuming Redfield stoichiometry for glacier algal C, nitrogen (N), and P requirements.

Fundamental to deciphering the importance of bottom-up controls on glacier algal blooms is therefore knowledge of the macronutrient cellular requirements of glacier algal cells. While Redfield stoichiometry provides an important framework against which ambient nutrient concentrations can be contrasted (Redfield, 1958), deviations from this ratio are well documented across several algal lineages (Hecky et al., 1993; Geider and La Roche, 2002; Quigg et al., 2003), with individual cell stoichiometry shown to be dynamic relative to a plethora of drivers (Geider and La Roche, 2002; Quigg et al., 2003; Dickman et al., 2006; Finkel et al., 2016). Here, we provide an estimate of glacier algal macro-nutrient (C, N, and P) cellular stoichiometry in assemblages sampled from the surface of the GrIS. A snapshot of glacier algae stoichiometry was determined for assemblages residing within surface ice sampled from the south western ice sheet margin during the 2019 ablation season in order to provide a first order approximation of the elemental requirements of glacier algal assemblages and to investigate the potential for divergence from Redfield dynamics. This data is important for efforts to project the occurrence of blooms into the future and to constrain bloom impacts to cycles of C and macro-nutrients.

MATERIALS AND METHODS

Study Area and Sampling Details

Surface ice containing glacier algal assemblages was sampled across August 8–10 (total number of samples = 28) from the marginal ablation zone in the south western GrIS proximal to Point 660. For all samples, the top 2 cm of surface ice was sampled using a pre-cleaned ice saw, transferred into sterile Whirl-Pak® bags (Madison, WI, United States), and melted slowly in the dark over 24 h at 4°C. The melted surface ice was subsequently homogenized and sub-sampled for further analyses including 1 mL sub-sampled into 15 mL centrifuge tubes and fixed immediately with 2% glutaraldehyde final concentration for subsequent algal cell enumeration; triplicate 100–200 mL subsamples filtered onto pre-combusted 25 mm diameter glass

microfiber filters (0.7 μm retention; Thermo Fisher Scientific, Pittsburgh, PA, United States), frozen immediately at −20°C for subsequent determination of glacier algal C, N content; and duplicate 100–200 mL subsamples filtered onto pre-combusted 47 mm diameter glass microfiber filters (0.7 μm retention; Thermo Fisher Scientific, Pittsburgh, PA, United States), frozen immediately at −20°C for subsequent determination of glacier algal P content. All samples were transported back to the University of Bristol for subsequent processing.

Algal Cell Enumeration and Cell Biovolume Estimation

Algal abundance (cells mL^{-1}) was determined using methods described by Williamson et al. (2018) on 1 mL aliquots of melted surface ice using a modified Fuchs-Rosenthal hemocytometer (0.2 mm by 1/16 mm^2; Hawksley, Lancing, United Kingdom) on a Leica M205 C stereomicroscope (Wetzlar, DE) with attached GXCAM HiChrome-Met HD microscope camera (GT Vision Ltd., Stansfield, United Kingdom). Glacier algal cellular biovolume (μm^3) was determined from measurements of cell length and diameter taken using ImageJ software (version 1.52n), for which glacier algal cells were considered to be regular cylinders (Hillebrand et al., 1999).

Algal Carbon and Nitrogen

Using methods outlined by Lorrain et al. (2003), the C (after the removal of carbonates by acid fumigation) and N content of glacier algae retained on 25 mm diameter glass microfiber filters (0.7 μm retention; Thermo Fisher Scientific, Pittsburgh, PA, United States), which had been freeze-dried over 24 h, were determined using an elemental analyzer (Elementar vario PYRO cube®, Langenselbold, Hesse, DE). The detection limits of elemental concentrations were 0.001% for both elements measured, and the coefficient of variation (CV) for C and N according to six replicates of an organic analytical standard (NC Soil Standard 338 40025, cert. 133317, C = 2.29%, N = 0.21%; Elemental Microanalysis Ltd., United Kingdom) were 5.60% and 2.74%, respectively. To determine the quantity of C and N associated with algal biomass (μg mL^{-1} of surface ice), the bulk glacier algal abundance (cells mL^{-1}) was multiplied by the quantity of cellular C and N (μg $cell^{-1}$).

Algal Phosphorus

Concentrations of total P (P_t) and P_i associated with glacier algae were determined using methods adapted from Hedley and Stewart (1982) and Stibal et al. (2008). Paired 47 mm diameter glass microfiber filters (0.7 μm retention) were added to separate pre-cleaned 15 mL polypropylene centrifuge tubes (Thermo Fisher Scientific), frozen at −80°C and subsequently freeze-dried for 24 h. After freeze-drying, 1 mL of ethanol-free chloroform ($CHCl_3$; Thermo Fisher Scientific) was added to one from each pair of centrifuge tubes. These tubes were then agitated three times for 10 s using a vortex mixer at 15 min intervals before being placed under a fume hood for 24 h to allow the $CHCl_3$ to evaporate. Both the unfumigated and $CHCl_3$-fumigated filters from each pair were then amended with 6 mL (∼ 1:60 w/v retained sample:extractant) of 1 M magnesium chloride ($MgCl_2$; Thermo Fisher Scientific), agitated at 200 rpm on a reciprocal shaker for 16 h and centrifuged at 1,217 × *g* at 0°C for 12 min. An aliquot of 1.5 mL from the resulting extracts was transferred to a 9 mL muffled digest tube, mixed with 0.5 mL of an oxidizing agent comprised of 9 g of NaOH and 40 g of potassium persulfate ($K_2S_2O_8$; Thermo Fisher Scientific) in 1 L of Milli-Q® water, and autoclaved for 60 min at 121°C (digested). The undigested and digested $MgCl_2$ extracts pertaining to both the unfumigated and $CHCl_3$-fumigated filters were then filtered to 0.45 μm using mixed cellulose ester membranes (Whatman®, Maidstone, United Kingdom). Concentrations of P_i and P_t were determined in the undigested and digested $MgCl_2$ extracts, respectively, using a standard orthophosphate colorimetric technique on a photometric meter (Gallery™ Plus Discrete Analyzer, Thermo Fisher Scientific, Waltham, MA, United States). The CV (six replicate mid-range standards) for P_i and P_t were ≤0.20%. In addition, the limits of detection (LoD; three times the standard deviation of six replicate method blanks) for P_i and P_t were 4.73 μg L^{-1} and 1.93 μg L^{-1}, respectively. Samples were blank corrected when blank concentrations exceeded the detection limits. All reagents used were of analytical grade. Algal P_i and P_t were calculated, respectively, as the differences between P concentrations in the undigested and digested $MgCl_2$ extracts for the $CHCl_3$-fumigated and unfumigated filters within each pair.

Ambient Chemistry

Concentrations of dissolved organic C (DOC) and dissolved total N (DTN) in filtered ice samples were determined on a total organic C analyzer (Shimadzu TOC-L_{CPH}, Kyoto, Japan) coupled with a total N measuring unit (Shimadzu TNM-L). The ammonium-N (NH_4^+-N), nitrate-N (NO_3^--N), and phosphate-P (PO_4^{3-}-P) contents of the same samples were quantified on a photometric meter (Gallery™ Plus Discrete Analyzer). According to six replicate standards, the CV for the DOC, DTN, NH_4^+-N, NO_3^--N, and PO_4^{3-}-P analyses were 3.71%, 7.38%, 0.20%, 0.26%, and 0.35%, respectively. The corresponding detection limits for the same analyses were 51.40 μg L^{-1}, 39.12 μg L^{-1}, 1.19 μg L^{-1}, 3.13 μg L^{-1}, and 4.95 μg L^{-1}. Dissolved organic N (DON) was calculated for each sample as the difference between concentrations of DTN and dissolved inorganic N (DIN; sum of NH_4^+-N and NO_3^--N).

Data Analyses

All plots and statistical analyses were performed using R version 3.4.1 in accordance with methods outlined by Crawley (2005).

RESULTS

Ambient Chemistry of Surface Ice

Major C and macro-nutrient phases were determined for GrIS surface ice from which glacier algal assemblages were sampled to provide contextual hydrochemistry information to contrast with glacier algal cellular stoichiometries. Dissolved nutrient phases measured from melted surface ice were dominated by organic phases (**Table 1**), with the majority comprised of DOC,

TABLE 1 | Concentrations of dissolved organic carbon (DOC), total dissolved nitrogen (DTN), organic nitrogen (DON), ammonium-nitrogen (NH_4^+-N), nitrate-nitrogen (NO_3^--N), and phosphate-phosphorus (PO_4^{3-}-P) in surface ice from the south western margin of the Greenland Ice Sheet (GrIS) during the 2019 ablation season (mean ± standard error, n = 12).

DOC (μg L^{-1})	DTN (μg L^{-1})	DON (μg L^{-1})	NH_4^+-N (μg L^{-1})	NO_3^--N (μg L^{-1})	PO_4^{3-}-P (μg L^{-1})
1,964 ± 162	113 ± 27	108 ± 27	2.8 ± 1.4	1.6 ± 1.1*	0.9 ± 0.4*

*Below limit of detection (three times the standard deviation of six replicate method blanks).

which exhibited concentrations ∼ 18 times greater than DON. In contrast, the concentrations of dissolved inorganic nutrients fell at or below the LoD. Dissolved inorganic N was only measurable in the form of NH_4^+ and accounted for ∼ 4% of the DTN, while PO_4^{3-}-P concentrations were below the LoD in all cases.

Assemblage Characteristics

Glacier algal assemblages ranged in abundance from 0 to 8.97 × 10^5 cells mL^{-1} and were comprised predominantly of *Ancylonema* cf. *nordenskiöldii* (67.9%) and cf. *Mesotaenium berggrenii* (31.7%; **Figure 1A**). Mean cellular biovolumes for *A.* cf. *nordenskiöldii* and cf. *M. berggrenii* were 2,788 ± 121 μm^3 $cell^{-1}$ and 2,197 ± 131 μm^3 $cell^{-1}$, respectively (**Figure 1B**). In contrast, fewer than 1% of cells were identified as *Cylindrocystis brebissonii*, though mean cellular biovolumes of these cells were an order of magnitude larger than *A.* cf. *nordenskiöldii* and cf. *M. berggrenii* (**Figure 1B**).

Cellular C and N contents of glacier algal assemblages averaged 106 ± 35 pg C $cell^{-1}$ and 4.5 ± 1.3 pg N $cell^{-1}$, respectively (**Figures 2A,B**), with cellular atomic C:N ratios ranging from 15.6 to 40.8. Using measured values of cellular C and N, we estimate an average of 27.4 ± 6.0 μg C mL^{-1} and 1.2 ± 0.25 μg N mL^{-1} to be contained within glacier algal biomass within the surface ice environment during our sampling period. In contrast to cellular C and N, quantifying algal P presented challenges as concentrations fell below the limit of detection (LoD), with P_t and P_i only detectable in seven and four of 28 samples, respectively. Across these, mean P_t is 0.14 ± 0.09 pg $cell^{-1}$ (**Figure 2C**). If organic P is defined as the difference between mean concentrations of P_t and P_i, we determined that up to 86% of algal P may be contained within the organic phase (∼ 0.12 pg $cell^{-1}$). Using the mean P_t, we estimate the atomic C:N:P stoichiometry of glacier algal assemblages to be 1,997:73:1; however, given the difficulty in detecting cellular P, this ratio should be considered with caution.

DISCUSSION

Understanding the macronutrient requirements of glacier algal cells is an important first step on the way to constraining potential bottom-up controls, which may ultimately restrict bloom magnitude and extent (McCutcheon et al., 2021). The present study examined the C, N, and P content of glacier algal assemblages sampled during the mid-2019 ablation season (early August) from the southwestern margin of the GrIS, providing a direct measurement of glacier algal cellular macronutrient content and stoichiometry. Through this we identify deviation from standard cell-constituent:volume ratios and classic Redfield stoichiometry, and we are able to estimate glacier-algal-associated macro-nutrient reservoirs within this highly oligotrophic environment.

The absolute cellular macronutrient content of glacier algal assemblages fell within the range of values reported across a diversity of algal lineages (Montagnes et al., 1994), though they deviated from cell-constituent:volume relationships established across microalgal taxa. For example, glacier algal cellular C and N content averaged 106 ± 35 pg C $cell^{-1}$ and 4.5 ± 1.3 pg N $cell^{-1}$ for cell volumes that ranged ∼ 2,000–3,000 μm^3. While absolute cellular contents were within the range reported across a host of microalgae (Montagnes et al., 1994; Finkel et al., 2016), values were conspicuously lower than would be predicted using established cell-constituent:volume ratios for cells of their size, whereby 2,000–3,000 μm^3 cells would be expected to contain 203–304 pg C $cell^{-1}$ and 40–62 pg N $cell^{-1}$, respectively (Montagnes et al., 1994). Glacier algal cellular C was thus approximately half that expected based on cell volume, with cellular N an order of magnitude lower.

Laboratory and field studies have consistently identified species-level differences in microalgal elemental requirements that reflect evolutionary histories and acclimation to environmental conditions (Geider and La Roche, 2002; Finkel et al., 2016; Garcia et al., 2018). Such differences are a product of the adaptations of cellular architecture and biochemistry that correspond to changes in macromolecular composition, with protein the primary reservoir of cellular N, phospholipids, polyphosphates, and nucleic acids the reservoirs of cellular P, and cellular C largely determined by the combination of protein, lipid, and carbohydrate (Geider and La Roche, 2002; Finkel et al., 2016; Barcyte et al., 2020). In this respect, lower cellular requirements for C and N may reflect adaptation of Streptophyte glacier algae to their oligotrophic surface ice environment; documented here and in numerous previous works to be highly deficient in inorganic nutrient supplies (**Table 1**; Hawkings et al., 2016; Wadham et al., 2016; Holland et al., 2019). It may also reflect the lower growth rates of glacier algal communities from icy environments (∼ 5 days doubling time; Stibal et al., 2017; Williamson et al., 2018) compared to more temperate microalgal taxa (e.g., Garcia et al., 2018), whereby species with lower growth rates have associated lower protein, and thus N, content (Finkel et al., 2016). Finally, divergence from typical cell volume:constituent relationships may also reflect the highly vacuolized nature of glacier algal cells, which results in an overall higher water content compared to many other algae (Remias et al., 2009, 2012a). Separating the phylogenetic signature of microalgal elemental requirements from e.g., dynamic responses to *in situ* nutrient regimes (see below) is ideally achieved through the assessment of actively growing microalgal cells

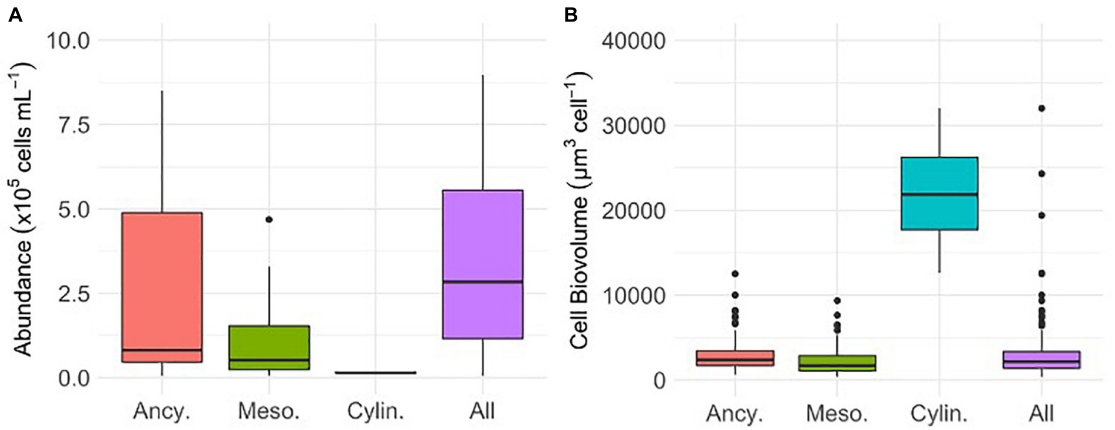

FIGURE 1 | The abundance **(A)** and cellular biovolume **(B)** of *Ancylonema* cf. *nordenskiöldii* (Ancy., *n* = 19 abundance, *n* = 215 biovolume), cf. *Mesotaenium berggrenii* (Meso., *n* = 20 abundance and *n* = 140 biovolume), *Cylindrocystis brebissonii* (Cylin., *n* = 2 abundance, *n* = 5 biovolume), and the total glacier algal assemblage (All, *n* = 21 abundance *n* = 360 biovolume) sampled in surface ice from the south western margin of the Greenland Ice Sheet (GrIS) during the mid-2019 ablation season. Plots show median ± interquartile range.

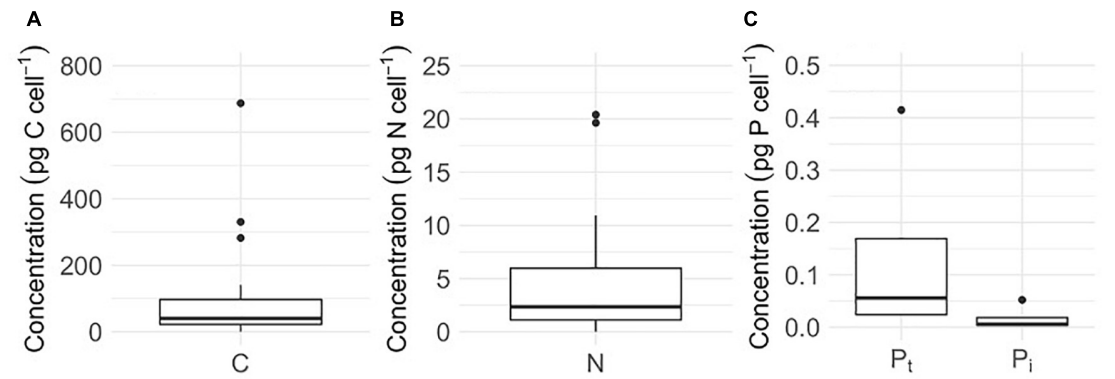

FIGURE 2 | Cellular concentrations of **(A)** carbon (C, *n* = 28), **(B)** nitrogen (N, *n* = 28), **(C)** total phosphorus (P_t, *n* = 4), and **(C)** inorganic phosphorus (P_i, *n* = 4) of glacier algal assemblages comprised of *Ancylonema* cf. *nordenskiöldii*, cf. *Mesotaenium berggrenii,* and *Cylindrocystis brebissonii* in surface ice from the south western margin of the Greenland Ice Sheet (GrIS) during the mid-2019 ablation season. Plots show median ± interquartile range.

cultured under nutrient replete conditions (Geider and La Roche, 2002; Finkel et al., 2016). To date, however, an inability to culture glacier algal taxa *ex situ* has hindered advances in our understanding of their physiology and interactions with key environmental stressors (Williamson et al., 2019), necessitating field-based approaches as here.

In contrast to C and N contents, measurement of cellular P from glacier algal assemblages proved challenging, with few samples yielding detectable concentrations. This was consistent with our aqueous hydrochemistry data whereby all dissolved PO_4^{3-}-P concentrations from melted surface ice samples fell below the LoD (LoD = 4.95 µg L^{-1}). For glacier algae, just four of 28 samples yielded quantifiable P, with a mean P_t content of 0.14 ± 0.09 pg P $cell^{-1}$ across samples. To compare to published values for major marine phyla (Ho et al., 2003), a glacier algal cell volume of 2,500 µm^3 was applied to convert to units of mmol P per liter cell volume (mmol L^{-1} cell volume), yielding ∼ 1.50 mmol P L^{-1} cell volume for our glacier algal assemblages. This is substantially lower than values reported for 15 marine eukaryote species (∼ 9.1–250 mmol P L^{-1} cell volume; see Table 2 in Ho et al., 2003), though likely reflects the nutrient deplete conditions under which glacier algal assemblages grow. For example, the cyanobacterium *Microcystis aeruginosa* demonstrated much lower cellular P content ranging from 0.2 to 1.2 pg P $cell^{-1}$ when cultured under ambient P conditions that ranged 0–256 µg P L^{-1}, with lower intracellular content associated with lower ambient P availability (Ghaffar et al., 2017). Similarly, for more closely related planktonic desmid species (Zygnematophyceae), Spijkerman and Coesel (1996) demonstrated how *Cosmarium abbreviatum var. planctonicum* originating from an oligo-meso-trophic lake was consistently capable of greater biomass production for a given amount of P (across the range 0.5–10 µmol P l^{-1}) than *Staurastrum pingue*, which originated from a eutrophic lake. Cellular P content ranged 0.2–2.17 pg P $cell^{-1}$, comparable to values reported here for glacier algae, with *C. planctonicum* shown to be an affinity species, possessing a competitive advantage in an environment where growth is permanently P limited (Spijkerman and Coesel, 1996).

While limited in sample size, our data demonstrate how glacier algal macro-nutrient content broadly reflects ambient inorganic nutrient availability within surface ice habitats of the GrIS, and suggests an overall lower cellular macro-nutrient requirement likely advantageous in the ultra-oligotrophic supraglacial. These findings are consistent with recent advances in understanding potential bottom-up controls on glacier algal bloom proliferation (McCutcheon et al., 2021).

Assessment of glacier algal cellular macro-nutrient quotients allowed for a first order approximation of organic C and N stocks within assemblages inhabiting our sampling location on the marginal southwestern GrIS. Based on cellular C and N contents and abundances recorded across our samples, we calculated an average of 27.4 ± 6.0 μg C mL^{-1} and 1.2 ± 0.25 μg N mL^{-1} to be contained within glacier algal cells within our marginal sampling location. Upscaling from these point observations to the km^2 scale (i.e., μg C or N mL^{-1} × 1.061 = kg C or N km^2, after Williamson et al., 2018) provides an estimate of ∼ 29.0 kg C km^2 and ∼ 1.2 kg N km^2 stored within glacier algal assemblages inhabiting surface ice at the mid-ablation season (early August). Previously, Williamson et al. (2018) modeled glacier algal net production in southwestern Greenland forced by the number of days since snowline retreat. They estimated an overall average of 15.82 ± 8.14 kg C km^2 produced by glacier algal assemblages across their 8.24 × 10^4 km^2 model region during the 2016 ablation period, with spatial variability ranging from <10 kg C km^2 toward the equilibrium line up to ∼ 40–50 kg C km^2 at their most marginal model regions by the end of the 2016 ablation season (Williamson et al., 2018). Our measurements of glacier algal cellular macro-nutrient content corroborate modeling estimates by Williamson et al. (2018) and extend these trends into the most marginal zone of the ice sheet, omitted by this previous study given uncertainties regarding microbial activity within such locations (Hodson et al., 2010; Stibal et al., 2012). We confirm here that glacier algal cells represent a significant producer of autochthonous organic C and N within the most marginal zone of the GrIS, likely driving the high rates of net production previously recorded for surface ice in this region (e.g., Musilova et al., 2017).

Additional to the cellular quotient of macro-nutrients, our data further demonstrate strong divergence in the relative abundance, i.e., cellular stoichiometry, of glacier algal C, N, and P relative to Redfield stoichiometry (106:16:1 C:N:P; Redfield, 1958), which we interpret here to represent the true stoichiometry of glacier algal communities under normal surface ice conditions as opposed to a dynamic response to e.g., nutrient limitation. Atomic C:N ratios of glacier algal assemblages ranged 15.6–40.8 across all samples, approximately two to six times greater than the Redfield C:N ratio of 6.6, and while P measurements proved challenging (see above), we estimate here an overall glacier algal C:N:P stoichiometry in the range 1,997:73:1. Under high light, low nutrient conditions, algal photosynthesis is often uncoupled from growth, with surplus photosynthate reallocated to storage carbohydrates and lipids that require minimal or no N and/or P inputs (Geider and La Roche, 2002; James et al., 2011; Pichrtová et al., 2014; Talmy et al., 2014). This results in a C-rich but N- and P-poor assemblage (Sterner et al., 1997), higher C:N and C:P ratios than predicted by Redfield stoichiometry, and typically conclusion that the community under study is nutrient limited (Berman-Frank, 1999; Dickman et al., 2006). For glacier algae residing within the high-light surface ice environment, it is likely that their abundant secondary phenolic pigmentation contributes to the elevated C:N and C:P ratios recorded here. This C-rich pigmentation is required to protect the cells against excess irradiance and provide a mechanism to convert abundant light energy into heat in order to liberate meltwater adjacent to the cell (Remias et al., 2012b; Dial et al., 2018; Williamson et al., 2018, 2020), likely also acting as an effective sink for excess photosynthate. However, given the characteristic oligotrophy of surface ice environments (Holland et al., 2019), and the contrasting ability of glacier algae to form widespread blooms under such conditions cryosphere wide (Williamson et al., 2019), we argue that our low absolute macro-nutrient content and elevated C:N and C:P ratios also likely signify overall reduced requirements for N and P resources by glacier algal communities, a potentially key adaptation to life in oligotrophic surface ice. This assertion is consistent with the findings of McCutcheon et al. (2021), who though concluding mineral phosphorus to be a first order control on glacier algal bloom presence, demonstrated that responses to nutrient addition (specifically phosphorous) were only evident in incubated field assemblages after 5 days of incubation, suggesting sufficient nutrient resources for glacier algal growth under ambient conditions. For context, this study reported highly comparable C:N:P stoichiometry to the present study, with POC:N:P_{org} ranging 690:48:1 to 2,615:196:1 across eight samples dominated by glacier algae at their main study location (McCutcheon et al., 2021). This putative lower macro-nutrient requirement would allow glacier algal assemblages to continue to progress into new oligotrophic areas of bare ice as the climate warms and the GrIS ablation zone expands into the future (Ryan et al., 2019), exacerbating local albedo decline and surface ablation in a positive feedback mechanism (Cook et al., 2020). It may also form a key consideration for ongoing efforts to culture glacier algal taxa *ex situ* under laboratory conditions.

To aid the balancing of internal stoichiometry, microalgae can actively release excess C into the ambient environment via the production and release of exopolymeric substances (EPS) (Berman-Frank, 1999; Hessen and Anderson, 2008; Palmucci et al., 2011) and/or divert excess photosynthate into the production of abundant secondary pigmentation as discussed above (Berman-Frank, 1999). For glacier algae blooming within ablating surface ice environments, EPS production has been postulated as a potentially important mechanism to aid retention of cells within the melting surface ice matrix (Williamson et al., 2019). While glacier algal EPS release remains unquantified, higher cellular C:N and C:P ratios likely impact the quality of dissolved organic matter available within surface ice environments, with consequences for other functional groups. For example, the dissolved organic nutrient phases that dominated the ambient hydrochemistry data presented here showed a DOC:DON ratio of ∼18, and a DOC:DOP ratio in the range 1,000–5,000 (**Table 1**). These data are highly consistent with Holland et al. (2019) who documented molar dissolved organic nutrient ratios in surface ice dominated

by a glacier algal bloom further into the southwestern GrIS, with DOC:DON ranging 16–17 and DOC:DOP ranging 800–2,000. For that same 2016 glacier algal bloom, Nicholes et al. (2019) further demonstrated how bacterial secondary production was on average 28 times lower than rates of glacier algal primary production, indicating an inefficient microbial loop potentially limited by N and P resources (Holland et al., 2019; Nicholes et al., 2019). It is thus likely that glacier algal cellular stoichiometry is reflected in the quality of dissolved organic matter available within surface ice environments during blooms and may potentially limit the activity of associated communities. Constraining the short-term (within season) and long-term (inter-annual) fate of glacier algal autochthonous organic carbon and macro-nutrient production within surface ice will be the next step toward understanding their role as the dominant primary producer within supraglacial systems, and their wider impacts to biogeochemical cycling.

CONCLUSION

We provide here a snapshot of glacier algal cellular macro-nutrient content and stoichiometry from assemblages sampled during the mid-ablation season at the ice margin of the southwestern GrIS. Our findings highlight comparatively lower cellular C, N, and P absolute content in glacier algal cells that deviates from standard cellular content:biovolume relationships, and high C:N and C:P ratios that likely reflect adaptation to this highly oligotrophic surface ice environment as well as the dominance of abundant secondary phenolic pigmentation within glacier algal cells. Based on these observations, we confirm the role of glacier algal blooms in the most marginal region of the ice sheet in driving autochthonous macro-nutrient accumulation, estimating that approximately 29 kg C km^2 and 1.2 kg N km^2 was amassed by glacier algal assemblages by the middle of the 2019 ablation season. While the long-term fate of these nutrient reservoirs remains unconstrained, our findings indicate the potential for comparatively low quality (i.e., low N and P content) dissolved organic matter release into the surface ice by glacier algal assemblages, with consequences for associated heterotrophic activity.

DATA AVAILABILITY STATEMENT

The raw data supporting the conclusions of this article will be made available by the authors, without undue reservation.

AUTHOR CONTRIBUTIONS

CW led the design of the study and completed all fieldwork. TT-J carried out all laboratory work. TT-J and MN performed the data analysis. All authors contributed to the manuscript.

FUNDING

This work was funded as part of the UK Natural Environment Research Council Consortium Grant "Black and Bloom" (NE/M021025/1). CW acknowledges support from The Leverhulme Trust Research Project Grant "iDAPT" (RPG-2020-199).

ACKNOWLEDGMENTS

We would like to recognize Dr. Fotis Sgouridis for providing guidance relating to elemental concentrations.

REFERENCES

Anesio, A. M., and Laybourn-Parry, J. (2012). Glaciers and ice sheets as a biome. *Trends Ecol. Evol.* 27, 219–225.

Anesio, A. M., Lutz, S., Chrismas, N. A. M., and Benning, L. G. (2017). The microbiome of glaciers and ice sheets. *Npj Biofilms Microbiomes* 3:10.

Bamber, J. L., Westaway, R. M., Marzeion, B., and Wouters, B. (2018). The land ice contribution to sea level during the satellite Era. *Environ. Res. Lett.* 13:063008. doi: 10.1088/1748-9326/aac2f0

Barcyte, D., Pilátová, J., Mojzeš, P., and Nedbalová, L. (2020). The arctic Cylindrocystis (Zygnematophyceae, Streptophyta) green algae are genetically and morphologically diverse and exhibit effective accumulation of polyphosphate. *J. Phycol.* 56, 217–232. doi: 10.1111/jpy.12931

Berman-Frank, I. (1999). Balanced growth in aquatic plants: myth or reality? phytoplankton use the imbalance between carbon assimilation and biomass production to their strategic advantage. *BioScience* 49, 29–37. doi: 10.2307/1313491

Cook, J. M., Tedstone, A. J., Williamson, C. J., McCutcheon, J., Hodson, A., Dayal, A., et al. (2020). Glacier algae accelerate melt rates on the south-western greenland ice sheet. *Cryosphere* 14, 309–330. doi: 10.5194/tc-14-309-2020

Crawley, M. J. (2005). *Statistics: an Introduction Using R*. Chichester, UK: John Wiley & Sons, Ltd.

Dial, R. J., Ganey, G. Q., and Skiles, M. (2018). What color should glacier algae be? an ecological role for red carbon in the cryosphere. *FEMS Microbiol. Ecol.* 94:fiy007.

Dickman, E. M., Vanni, M. J., and Horgan, M. J. (2006). Interactive effects of light and nutrients on phytoplankton stoichiometry. *Oecologia* 149, 676–689. doi: 10.1007/s00442-006-0473-5

Finkel, Z. V., Follows, M. J., Liefer, J. D., Brown, C. M., Benner, I., and Irwin, A. J. (2016). Phylogenetic diversity in the macromolecular composition of microalgae. *PLoS One* 11:e0155977. doi: 10.1371/journal.pone.0155977

Garcia, N. S., Sexton, J., Riggins, T., Brown, J., Lomas, M. W., and Martiny, A. C. (2018). High Variability In Cellular Stoichiometry Of Carbon, Nitrogen, And Phosphorous Within Classes Of Marine Eukaryotic Phytoplankton Under Sufficient Nutrient Conditions. *Front. Microbiol.* 9:543.

Geider, R. J., and La Roche, J. (2002). Redfield revisited: variability of C:N:P in marine microalgae and its biochemical basis. *Eur. J. Phycol.* 37, 1–17. doi: 10.1017/s0967026201003456

Ghaffar, S., Stevenson, R. J., and Khan, Z. (2017). Effect of phosphorous stress on *Microcystis aeruginosa* growth and phosphorous uptake. *PLoS One* 12:e0174349. doi: 10.1371/journal.pone.0174349

Hawkings, J., Wadham, J., Tranter, M., Telling, J., and Bagshaw, E. (2016). The greenland ice sheet as a hot spot of phosphorus weathering and export in the arctic. *Global Biogeochem. Cycles* 30, 191–210. doi: 10.1002/2015gb005237

Hecky, R. E., Campbell, P., and Hendzel, L. L. (1993). The stoichiometry of carbon, nitrogen, and phosphorus in particulate matter of lakes and oceans. *Limnol. Oceanogr.* 38, 709–724. doi: 10.4319/lo.1993.38.4.0709

Hedley, M. J., and Stewart, J. W. B. (1982). Method to measure microbial phosphate in soils. *Soil Biol. Biochem.* 14, 377–385. doi: 10.1016/0038-0717(82)90009-8

Hessen, D. O., and Anderson, T. R. (2008). Excess carbon in aquatic organisms and ecosystems: physiological, ecological, and evolutionary implications. *Limnol. Oceanogr.* 53, 1685–1696. doi: 10.4319/lo.2008.53.4.1685

Hillebrand, H., Dürselen, C. D., Kirschtel, D., Pollingher, U., and Zohary, T. (1999). Biovolume calculation for pelagic and benthic microalgae. *J. Phycol.* 35, 403–424. doi: 10.1046/j.1529-8817.1999.3520403.x

Ho, T. Y., Quigg, A., Finkel, Z. V., Milligan, A. J., Wyman, K., Falkowski, P. G., et al. (2003). The elemental composition of some marine phytoplankton. *J. Phycol.* 39, 1145–1159.

Hodson, A., Anesio, A. M., Tranter, M., Fountain, A., Osborn, M., Priscu, J., et al. (2008). Glacial ecosystems. *Ecol. Monogr.* 78, 41–67.

Hodson, A., Boggild, C., Hanna, E., Hyubrechts, P., Langfort, H., Cameron, K., et al. (2010). The cryoconite ecosystem on the greenland ice sheet. *Ann. Glaciol.* 51, 123–129. doi: 10.3189/172756411795931985

Holland, A. T., Williamson, C. J., Sgouridis, F., Tedstone, A. J., McCutcheon, J., Cook, J. M., et al. (2019). Dissolved organic nutrients dominate melting surface ice of the dark zone (Greenland ice sheet). *Biogeosciences* 16, 3283–3296. doi: 10.5194/bg-16-3283-2019

Huppert, A., Blasius, B., and Stone, L. (2002). A model of phytoplankton blooms. *Am. Nat.* 159, 156–171.

James, G. O., Hocart, C. H., Hillier, W., Chen, H., Kordbacheh, F., Price, G. D., et al. (2011). Fatty acid profiling of *Chlamydomonas reinhardtii* under nitrogen deprivation. *Bioresour. Technol.* 102, 3343–3351. doi: 10.1016/j.biortech.2010.11.051

Lorrain, A., Savoye, N., Chauvaud, L., Paulet, Y. M., and Naulet, N. (2003). Decarbonation and preservation method for the analysis of organic C and N contents and stable isotope ratios of low-carbonated suspended particulate material. *Anal. Chim. Acta* 491, 125–133. doi: 10.1016/s0003-2670(03)00815-8

McCutcheon, J., Lutz, S., Williamson, C., Cook, J. M., Tedstone, A. J., Vanderstraeten, A., et al. (2021). Mineral phosphorous drives glacier algal blooms on the greenland ice sheet. *Nat. Commun.* 12:570.

Montagnes, D. J. S., Berges, J. A., Harrison, P. J., and Taylor, F. J. R. (1994). Estimating Carbon, Nitrogen, Protein, and Chlorophyll a from volume in marine phytoplankton. *Limnol. Oceanogr.* 39, 1044–1060. doi: 10.4319/lo.1994.39.5.1044

Musilova, M., Tranter, M., Wadham, J., Telling, J., Tedstone, A., and Anesio, A. M. (2017). Microbially driven export of labile organic carbon from the greenland ice sheet. *Nat. Geosci.* 10, 360–365. doi: 10.1038/ngeo2920

Nicholes, M. J., Williamson, C. J., Tranter, M., Holland, A., Poniecka, E., Yallop, M. L., et al. (2019). Bacterial dynamics in supraglacial habitats of the greenland ice sheet. *Front. Microbiol.* 10:1366.

Palmucci, M., Ratti, S., and Giordano, M. (2011). Ecological and evolutionary implications of carbon allocation in marine phytoplankton as a function of nitrogen availability: a fourier transform infrared spectroscopy approach. *J. Phycol.* 47, 313–323. doi: 10.1111/j.1529-8817.2011.00963.x

Pichrtová, M., Kulichová, J., and Holzinger, A. (2014). Nitrogen limitation and slow drying induce desiccation tolerance in conjugating green algae (Zygnematophyceae, Streptophyta) from polar habitats. *PLoS One* 9:e113137. doi: 10.1371/journal.pone.0113137

Quigg, A., Finkel, Z. V., Irwin, A. J., Rosenthal, Y., Ho, T.-Y., Reinfelder, J. R., et al. (2003). The evolutionary inheritance of elemental stoichiometry in marine phytoplankton. *Nature* 425, 291–294. doi: 10.1038/nature01953

Redfield, A. C. (1958). The biological control of chemical factors in the environment. *Am. Sci.* 46, 205–221.

Remias, D., Holzinger, A., Aigner, S., and Lutz, C. (2012a). Ecophysiology and ultrastructure of *Ancylonema nordenskiöldii* (Zygnematales, Streptophyta), causing brown ice on glaciers in Svalbard (high arctic). *Polar Biol.* 35, 899–908. doi: 10.1007/s00300-011-1135-6

Remias, D., Holzinger, A., and Lütz, C. (2009). Physiology, ultrastructure and habitat of the ice alga *Mesotaenium berggrenii* (Zygnematophyceae, Chlorophyta) from glaciers in the European Alps. *Phycologia* 48, 302–312. doi: 10.2216/08-13.1

Remias, D., Schwaiger, S., Aigner, S., Leya, T., Stuppner, H., and Lütz, C. (2012b). Characterization of an UV- and VIS-Absorbing, purpurogallin-derived secondary pigment new to algae and highly abundant in Mesotaenium berggrenii (Zygnematophyceae, Chlorophyta), an extremophyte living on glaciers. *FEMS Microbiol. Ecol.* 79, 638–648. doi: 10.1111/j.1574-6941.2011.01245.x

Ryan, J. C., Smith, L. C., van As, D., Cooley, S. W., Cooper, M. G., Pitcher, L. H., et al. (2019). Greenland ice sheet surface melt amplified by snowline migration and bare ice exposure. *Sci. Adv.* 5:eaav3738. doi: 10.1126/sciadv.aav3738

Spijkerman, E., and Coesel, P. F. M. (1996). Phosphorous uptake and growth kinetics of two planktonic desmid species. *Eur. J. Phycol.* 31, 53–60. doi: 10.1080/09670269600651191

Sterner, R. W., Elser, J. J., Fee, E. J., Guildford, S. J., and Chrzanowski, T. H. (1997). The light:nutrient ratio in lakes: the balance of energy and materials affects ecosystem structure and process. *Am. Nat.* 150, 663–684. doi: 10.1086/286088

Stibal, M., Box, J. E., Cameron, K. A., Langen, P. L., Yallop, M. L., Mottram, H., et al. (2017). Algae drive enhanced darkening of bare ice on the greenland ice sheet. *Geophys. Res. Lett.* 44, 11463–11471.

Stibal, M., Telling, J., Cook, J., Mak, K. M., Hodson, A., Anesio, A. M., et al. (2012). Environmental controls on microbial abundance and activity on the greenland ice sheet: a multivariate analysis approach. *Microb. Ecol.* 63, 74–84. doi: 10.1007/s00248-011-9935-3

Stibal, M., Tranter, M., Telling, J., and Benning, L. G. (2008). Speciation, phase association and potential bioavailability of phosphorus on a svalbard glacier. *Biogeochemistry* 90, 1–13. doi: 10.1007/s10533-008-9226-3

Talmy, D., Blackford, J., Hardman-Mountford, N. J., Polimene, L., Follows, M. J., and Geider, R. J. (2014). Flexible C: N ratio enhances metabolism of large phytoplankton when resource supply is intermittent. *Biogeosciences* 11, 4881–4895. doi: 10.5194/bg-11-4881-2014

Tedesco, M., Doherty, S., Fettweis, X., Alexander, P., Jeyaratnam, J., and Stroeve, J. (2016). The darkening of the greenland ice sheet: trends, drivers, and projections (1981-2100). *Cryosphere* 10, 477–496. doi: 10.5194/tc-10-477-2016

Tedstone, A. J., Bamber, J. L., Cook, J. M., Williamson, C. J., Fettweis, X., Hodson, A. J., et al. (2017). Dark ice dynamics of the south-west Greenland Ice Sheet. *Cryosphere* 11, 2491–2506. doi: 10.5194/tc-11-2491-2017

Tedstone, A. J., Cook, J. M., Williamson, C. J., Hofer, S., McCutcheon, J., Irvine-Fynn, T., et al. (2020). Algal growth and weathering crust state drive variability in Western Greenland Ice sheet ice albedo. *Cryosphere* 14, 521–538. doi: 10.5194/tc-14-521-2020

van den Broeke, M., Box, J., Fettweis, X., Hanna, E., Noel, B., Tedesco, M., et al. (2017). Greenland ice sheet surface mass loss: recent developments in observation and modelling. *Curr. Climate Chang. Rep.* 3, 345–356. doi: 10.1007/s40641-017-0084-8

Wadham, J. L., Hawkings, J., Telling, J., Chandler, D., Alcock, J., and Lawson, E. (2016). Sources, cycling and export of nitrogen on the Greenland ice sheet. *Biogeoscience* 13, 6339–6352. doi: 10.5194/bg-13-6339-2016

Williamson, C. J., Anesio, A. M., Cook, J., Tedstone, A., Poniecka, E., Holland, A., et al. (2018). Ice algal bloom development on the surface of the Greenland ice sheet. *FEMS Microbiol. Ecol.* 94:fiy025.

Williamson, C. J., Cameron, K. A., Cook, J. M., Zarsky, J. D., Stibal, M., and Edwards, A. (2019). Glacier algae: a dark past and a darker future. *Front. Microbiol.* 10:524.

Williamson, C. J., Cook, J. M., Tedstone, A., Yallop, M. L., McCutcheon, J., Poniecka, E., et al. (2020). Algal photophysiology drives darkening and melt of the Greenland ice sheet. *Proc. Natl. Acad. Sci. USA* 117, 5694–5705. doi: 10.1073/pnas.1918412117

Yallop, M. L., Anesio, A. M., Perkins, R. G., Cook, J. M., Telling, J., Fagan, D., et al. (2012). Photophysiology and Albedo-changing potential of the ice algal community on the surface of the Greenland ice sheet. *ISME J.* 6, 2302–2313. doi: 10.1038/ismej.2012.107

Conflict of Interest: The authors declare that the research was conducted in the absence of any commercial or financial relationships that could be construed as a potential conflict of interest.

frontiers in Plant Science

ORIGINAL RESEARCH
published: 05 July 2021
doi: 10.3389/fpls.2021.689119

Spatial and Temporal Variations in Pigment and Species Compositions of Snow Algae on Mt. Tateyama in Toyama Prefecture, Japan

Tomomi Nakashima[1], *Jun Uetake*[2], *Takahiro Segawa*[3], *Lenka Procházková*[4], *Akane Tsushima*[1] *and Nozomu Takeuchi*[1]*

[1] *Graduate School of Science, Chiba University, Chiba, Japan,* [2] *Field Science Center for Northern Biosphere, Hokkaido University, Sapporo, Japan,* [3] *Center for Life Science Research, University of Yamanashi, Kofu, Japan,* [4] *Department of Ecology, Faculty of Science, Charles University, Prague, Czechia*

Snow algae are photosynthetic microbes that inhabit the melting snow surface in alpine and polar regions. We analyzed the pigment and species composition of colored snow collected on Mt. Tateyama in Japan during the melting seasons of 2015 and 2016. High-performance liquid chromatographic analyses of the pigments extracted from the colored snow showed that their composition varied within the study area and were classified into four types: Type A (astaxanthin-monoester dominant), Type B (medium astaxanthin-monoester content), Type C (abundant primary carotenoids and free-astaxanthin), and Type D (abundant primary carotenoids and astaxanthin diesters). Types A and B were most commonly observed in the study area, whereas Types C and D appeared only at specific sites. Analysis of the 18S ribosomal RNA (18S rRNA) gene revealed six major amplicon sequence variants (ASVs) of snow algae, belonging to the *Sanguina, Chloromonas*, and *Chlainomonas* groups. The relative abundance of the algal ASVs showed that *Sanguina* was dominant (>48%) in both Types A and B, suggesting that the difference in astaxanthin abundance between the two types was caused by the production of pigments in the algal cells. The algal community structures of Types C and D differed from those of Types A and B, indicating that the primary carotenoids and astaxanthin diesters were derived from certain algal species in these types. Therefore, astaxanthin-rich *Sanguina* algae mostly induced the red snow that appeared widely in this alpine area; however, they were partially dominated by *Chloromonas* or *Chlainomonas* algae, causing different pigment compositions.

Keywords: snow algae, red snow, pigment composition, astaxanthin, 18S rRNA, phylogenetic analysis, *Sanguina, Chloromonas*

OPEN ACCESS

Edited by:
Eric Marechal, UMR5168 Laboratoire de Physiologie Cellulaire Vegetale (LPCV), France

Reviewed by:
Katerina Bišová, Institute of Microbiology, Czechia
Yoshihisa Hirakawa, University of Tsukuba, Japan

***Correspondence:**
Nozomu Takeuchi
ntakeuch@faculty.chiba-u.jp

Specialty section:
This article was submitted to Marine and Freshwater Plants, a section of the journal Frontiers in Plant Science

Received: *31 March 2021*
Accepted: *31 May 2021*
Published: *05 July 2021*

Citation:
Nakashima T, Uetake J, Segawa T, Procházková L, Tsushima A and Takeuchi N (2021) Spatial and Temporal Variations in Pigment and Species Compositions of Snow Algae on Mt. Tateyama in Toyama Prefecture, Japan. Front. Plant Sci. 12:689119. doi: 10.3389/fpls.2021.689119

INTRODUCTION

Snow algae are photosynthetic microbes that inhabit the melting snow surface in alpine and polar regions. Their blooms on the snow surface cause visible red- or green-colored snow because of various pigments in the algal cells. This phenomenon is observed worldwide, including in Japan, and is referred to as red or green snow. The blooms of snow algae can affect carbon and nitrogen

cycles within the snowpacks and can also affect the melting rate of snow because of their light-absorbing effect (Onuma et al., 2020). Thus, it is important to understand the spatial distribution and the factors controlling the occurrence of algal blooms.

The pigments in snow algal cells are mainly chlorophylls and carotenoids, which have specific physiological functions in their cells (Bidigare et al., 1993; Müller et al., 1998). Chlorophylls play a role in photosynthesis and are present in active algal cells. However, carotenoids play a role in protecting cells from ultraviolet (UV) damage and potential photoinhibition, and transferring excitation energy to chlorophyll *a* (Takaichi, 2011). Carotenoids in algal cells are usually classified as primary and secondary carotenoids. Primary carotenoids, such as xanthophyll cycle pigments, are present in trace amounts in algal chloroplasts and are directly associated with photosynthesis. Secondary carotenoids, such as astaxanthin, are present in the algal cytoplasm and are more abundant than the primary carotenoids, and most exist as astaxanthin fatty acid esters (Remias and Lütz, 2007; Řezanka et al., 2008).

The abundance of pigments, in particular carotenoids, determines the visible coloration of algal cells, such as green, red, or orange, and varies seasonally and spatially on snowpacks. For example, astaxanthin and xanthophyll cycle pigments increased in algal cells of *Chloromonas nivalis* later during the melting season (Remias et al., 2010). Lutz et al. (2014) observed that white snow turned into red or green snow in 2 or 3 days on a Greenlandic glacier. The pigment composition of snow algae spatially varied in different locations in Svalbard and in different topographies, snow conditions, slope angles, and altitudes (Müller et al., 1998). Furthermore, astaxanthin contains various derivatives, and its composition in algal cells of *C. nivalis* has been reported to vary geographically in European Alps (Řezanka et al., 2013).

Variations in pigment compositions of colored snow are associated with algal species composition in the snow or with the relative abundance of carotenoid pigments controlled by the environmental conditions. One of the major groups of snow algae is the genus *Sanguina* (previously a part of *Chlamydomonas*), usually rich in astaxanthin in mature cyst cells and causes red-colored snow (Remias et al., 2005; Remias and Lütz, 2007; Holzinger et al., 2016). Another major group of snow algae is the genus *Chloromonas*, usually rich in primary carotenoids, such as zeaxanthin, violaxanthin, and secondary carotenoids, which causes green-colored snow or slightly brown orange-colored or pink-colored snow (Nedbalová et al., 2008; Remias et al., 2010).

Snow algae in colored snow usually consist of several species, and their community structure varies spatially in mountainous regions (Brown et al., 2016; Yakimovich et al., 2020). For example, *Sanguina* was dominant in red snow above the tree line, whereas *Chloromonas* was dominant in green- and orange-colored snow at lower elevations (Engstrom et al., 2020). In Antarctica, green-colored snow consists of *Chloromonas, Sanguina*, and *Chlorella*, usually rich in chlorophylls *a* and *b*, β-carotene, and lutein, whereas red-colored snow consists of *Chloromonas* alga containing abundant astaxanthin esters (Davey et al., 2019). The algal community of red-colored snow in Svalbard and Sweden consisted of *Chloromonas* and *Sanguina*; however, that of green-colored snow differed in two locations: *Microglena* sp. and *Raphidonema semperviens* were dominant in Svalbard, whereas *Sanguina* and *Chloromonas* were dominant in Sweden (Lutz et al., 2017).

Pigment composition also varies during the lifecycle of snow algae. For example, the cyst stage of algae contains abundant astaxanthin, whereas, in later stage, the flagellated green cells contain abundant primary carotenoids such as lutein (Osterrothová et al., 2019). *Sanguina* snow algae have more primary carotenoids during the earlier season, whereas they have astaxanthin during the later season (Remias et al., 2005).

The community structure and the pigment composition of snow algae can change depending on the physical or chemical conditions of the snow surface (Remias et al., 2005, 2010). Snow algae under conditions of strong ultraviolet radiation (UVR) or nutrient limitations produce more carotenoids and induce red-colored snow, whereas snow algae in weak radiation or rich nutrients produce fewer carotenoids and induce green-colored snow (Thomas and Duval, 1995; Leya et al., 2009). In particular, under limited nitrogen conditions, snow algal cells contain more abundant carotenoids (Britton and Edgar, 1998). However, Fujii et al. (2010) reported that astaxanthin-rich algae were found in snow with high nitrogen content. In contrast, Müller et al. (1998) showed no direct correlation between the secondary carotenoids of snow algal cells and the nutrient content of meltwater. Thus, there is still uncertainty between the environmental conditions and the pigment composition of snow algae. It is important to clarify the relationship between algal species and the pigment composition to understand their ecology on the snow surface.

Colored snow is widely observed on snowpacks in Japan and has been taxonomically studied in recent decades (Fukushima, 1963; Segawa et al., 2005; Muramoto et al., 2008; Tanabe et al., 2011; Matsuzaki et al., 2015; Terashima et al., 2017). Mt. Tateyama, an alpine area at elevations between 2,000 and 3,000 m above sea level (a.s.l.), is one of the snowiest mountains in Japan and is a place where colored snow frequently occurs during spring and summer. Red snow appears every year on the snow surface above the tree line at ∼2,100 m a.s.l.; however, its distribution is spatially and seasonally heterogeneous in this alpine area. The variations in algal pigments and the community structure in this area are still not well-understood.

In this study, we analyzed the pigment composition and the 18S rRNA gene of snow algae in the colored snow collected from various sites in Mt. Tateyama during the melting seasons of 2015 and 2016. This study describes the spatial and temporal variations of algal pigments and the community structure in snowfields and discusses the relationships between species, life cycles, and pigments.

MATERIALS AND METHODS

Study Site and Sample Collection

Mt. Tateyama is located in the Toyama Prefecture in the western part of Japan. It is a northern part of the Hida mountain range, one of the major mountain ranges on the main island (Honshu Island) of Japan, extending over 150 km from north to south. The elevation of the highest peak of Mt. Tateyama is 3,015 m

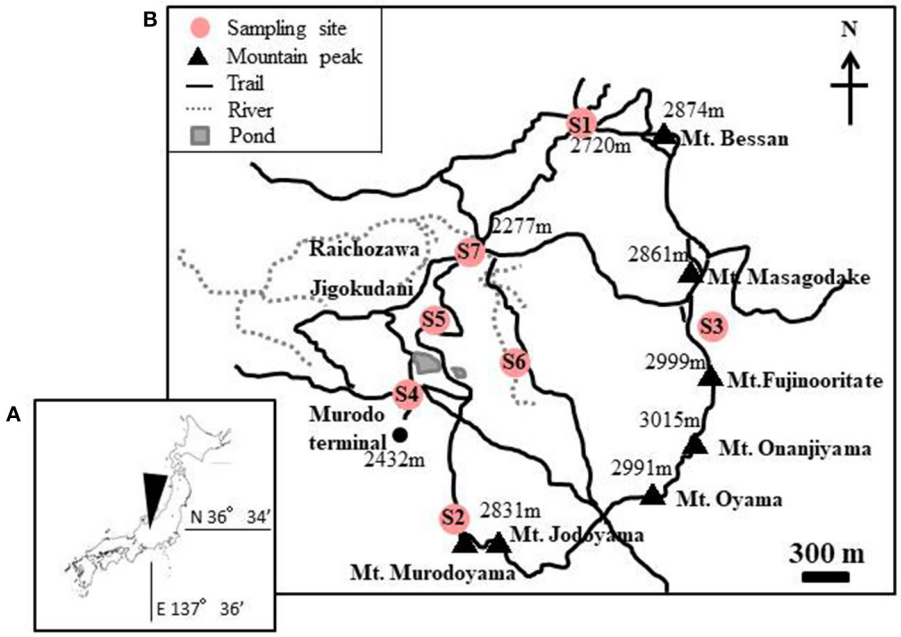

FIGURE 1 | (A) Maps showing the location of the study area in Mt. Tateyama, Japan. **(B)** Locations of the sites where the red snow samples were collected. Numbers in the map indicate the altitude above sea level.

a.s.l. Because the strong monsoon westerly blows from the Sea of Japan to the mountains during winter, heavy snow accumulates more than 5 m in depth in the mountain every year. The snow usually starts to melt in April and continues until the end of August. On the snow surface, red or green snow of algal blooming is commonly observed above the tree line (∼2,100 m a.s.l.) from May to July every year.

Snow samples were collected at seven sites in Murodo-Daira, a flat and old lava plateau in this alpine area at an elevation of ∼2,400 m a.s.l (**Figure 1**, **Table 1**). Fieldwork was conducted in June and July of 2015 and June of 2016. We found visible red snow at all times and collected a total of 54 colored surface snow samples (**Figure 2**, **Table 2**). Red snow appeared widely in June 2015; however, it was patchy on a scale of ∼10 cm in July 2015 and June 2016. The snow color varied slightly among the study sites; it was deep red and orange at S2 but red to brown at S7. The samples were transported in a frozen state to the laboratory at Chiba University and were stored in a freezer at −20°C until analysis. A part of the samples was kept at 0°C and used for microscopic observation. The algal cells in the samples were observed with an optical microscope (BX51, Olympus, Japan). Cell concentrations of each algal morpho-type were quantified by direct cell counting with the microscope.

Analysis of Algal Pigments

Frozen snow samples (−20°C) were thawed in a refrigerator (4°C) before analysis. The meltwater of the samples was filtered through a glass fiber filter (Whatman Glass Microfiber Filters, GF/F, 25 mm). The filter was then placed in 6 mL of N, N′-dimethylformamide (DMF: density 99.5%) in an 8-mL polypropylene tube and left in the refrigerator for 24 h. The extracted pigments were stored at −20°C before analysis.

The extracted pigments in the DMF were quantified by high-performance liquid chromatography (HPLC; SHIMADZU LC-20A Series, Japan), composed of liquid chromatography (LC-20AT, Shimadzu), refractive index detector (RID-20A, Shimadzu), UV and visible detector (SPD-20A, Shimadzu), diode array detector (SPD-M20A, spectra from 300 to 800 nm, Shimadzu), solvent degasser, autosampler unit set at 4°C, and a column thermostat set at 60°C. The column [Phenomenex LUNA-C8 (2), 3 μm, 150 × 4.6 mm] is used a reverse-phase column. Solvent A contained 28 mM tetrabutylammonium acetate (1.0 M solution in water, Sigma-Aldrich)/methanol (HPLC grade, Wako) = 30/70 (v/v). Solvent B contained methanol (HPLC grade, Wako). The HPLC pump flow rate was 1 mL/min. The UV and visible detectors were set at 450 nm, and the diode array detector was set at 480 and 663 nm. Liquid chromatography and solvent were purged for 10 min before a new sample was injected. The injection contained 600 μL of solvent A and 400 μL of the filtered sample.

Analysis was undertaken with two methods in the different time sequences of the mixing ratio of the solvents.

Method 1 (percentage of solvent B): 0 min (20%)−18 min (45%)−65 min (90%)−66 min (95%)−71 min (95%)−72 min (20%)−82 min (20%).
Method 2: 0 min (20%)−10 min (50%)−15 min (80%)−45 min (95%)−48 min (20%)−53 min (20%).

Methods 1 and 2 were used for the samples collected in 2015 and in 2016, respectively.

TABLE 1 | List of study sites showing the number of samples collected.

Site No.	Elevation (m)	GPS coordinates	2015		2016	Total
			June	July	June	
S1	2,720	N36.596614 E137.610712	1	1	0	2
S2	2,670	N36.568770 E137.600069	4	–	2	6
S3	2,650	N36.582900 E137.620111	3	–	–	3
S4	2,450	N36.578007 E137.597709	1	2	2	5
S5	2,360	N36.583555 E137.599125	1	3	0	4
S6	2,350	N36.581005 E137.605004	5	·	·	5
S7	2,300	N36.587690 E137.599254	10	12	7	29
Total			25	18	11	54

–, No data; ·, No snow cover.

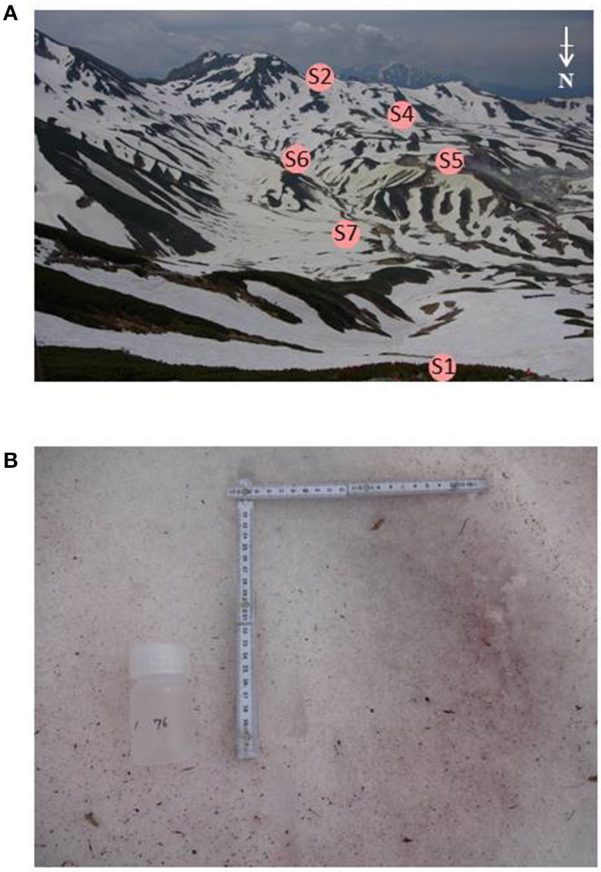

FIGURE 2 | (A) Photographs of the study area, Murodo-Daira, alpine plateau, Mt. Tateyama. The site S3 is not visible from this shooting point. **(B)** Red snow surface at the site S6 observed in June 2015.

Peaks that appeared in the chromatograms of 450 nm wavelength were identified and quantified with carotenoid and chlorophyll standards: chlorophyll *a*, chlorophyll *b*, lutein, β-carotene (3S, 3S′) astaxanthin, violaxanthin, antheraxanthin, zeaxanthin, canthaxanthin, echinenone, and pheophytin *a* (DHI Pigment Standards, Denmark). Chlorophyll *a* was quantified using the chromatograms of 663 nm wavelength since its peak often overlapped with those of antheraxanthin in the 450 nm chromatogram. Astaxanthin esters were quantified only for the trans-isomer in the 480 nm chromatogram using (3S, 3S′) astaxanthin standard. The standard was measured within 1 month before or after the sample was measured.

The pigment content of each sample quantified in this study is summarized in **Supplementary Table 1**. The hierarchical clustering of samples, as by calculating the Bray–Curtis dissimilarity index of pigment compositions, was conducted with R (version 4.0.5) and a VEGAN library (R Core Team, 2017).

DNA Extraction

For samples collected in 2015, 10 mL of melted snow was filtered through a glass fiber filter (Whatman Glass Microfiber Filters, GF/F, 25 mm), combusted at 300°C for 1 h to remove DNA contamination before use. For samples collected in 2016, melted snow was directly added to the DNA extraction tube without filtration. DNA on the filter was extracted using a DNA extraction kit (FastDNA SPIN Kit for Soil, MP Biomedicals) by following the standard protocol of the manufacturer. Glass fiber filters were placed in lysing tubes directly and homogenized together with filtrates. The extracted DNA samples were stored at −30°C until subsequent analysis.

18S rRNA Gene Analysis by Illumina Sequencing

Partial 18S rRNA gene sequences (V4 region, ∼380 bp) were amplified using primers Euk454F (5′-CCAGCASCYGCGGTAATTCC-3′) and EukR (5′-ACTTTCGTTCTTGATYRA-3′) (Logares et al., 2012). Polymerase chain reaction (PCR) mixture (20 μL) contained 1× KAPA *Taq* EXtra HotStart ReadyMix (Roche, Basel, Switzerland), 0.2 μM of each primer, and 1–5 μL template DNA. PCR was performed under the following cycling conditions: initial annealing at 95°C for 3 min, followed by 25–35 cycles of 95°C for 30 s, 50°C for 30 s, and 72°C for 60 s, and with a final extension at 72°C for 5 min. All PCR products were purified with AMPure XP (Beckman Coulter). As some of the PCR products included

TABLE 2 | Number of samples classified into four pigment types at each study site and month.

Site No. (m a.s.l.)		Pigment type				Total			
		A	B	C	D	A	B	C	D
	June 2015	1	0	0	0				
S1	July 2015	1	0	0	0	2	0	0	0
(2,720)	June 2016	0	0	0	0				
	June 2015	4	0	0	0				
S2	July 2015	–	–	–	–	4	1	0	1
(2,670)	June 2016	0	1	0	1				
	June 2015	3	0	0	0				
S3	July 2015	–	–	–	–	3	0	0	0
(2,650)	June 2016	–	–	–	–				
	June 2015	0	1	0	0				
S4	July 2015	0	0	2	0	0	3	2	0
(2,450)	June 2016	0	2	0	0				
	June 2015	0	1	0	0				
S5	July 2015	0	3	0	0	0	4	0	0
(2,360)	June 2016	0	0	0	0				
	June 2015	2	3	0	0				
S6	July 2015	·	·	·	·	2	3	0	0
(2,350)	June 2016	·	·	·	·				
	June 2015	3	7	0	0				
S7	July 2015	4	8	0	0	12	17	0	0
(2,300)	June 2016	5	2	0	0				
Total						23	28	2	1

–, No data; ·, No snow cover.

multiband or smeared bands, after agarose gel electrophoresis, PCR products were excised from the gel and purified using a NucleoSpin Gel and PCR clean-up kit (Macherey Nagel, Germany). The PCR products were labeled with a sample-unique index and Illumina adapter sequences at their 5′ end using the Nextera XT index kit v2 (Illumina, San Diego, CA, the United States). The PCR mixture (10 μL) contained 1× KAPA HiFi HS ReadyMix, 2 μL each of forward and reverse primers, and 1 μL of the recovered PCR products. PCR was performed under the following cycling conditions: 95°C for 3 min, followed by 8 cycles of 95°C for 30 s, 50°C for 30 s, and 72°C for 60 s, and with a final extension at 72°C for 5 min. All index PCR products were purified with AMPure XP and measured using a Qubit 2.0 Fluorometer (ThermoFisher Scientific) with Qubit dsDNA HS Assay Kit (ThermoFisher Scientific). Tagged amplicons were mixed with PhiX control DNA at a ratio of 80:20 and used as a template for MiSeq paired-end sequencing (2 × 300 bp) using Reagent kit v3 (Illumina) at the National Institute of Polar Research.

Phylogenetic Analyses

All sequence libraries were clustered into amplicon sequence variants (ASVs) using the R package "DADA2" (Callahan et al., 2016). Taxonomy was assigned by the "assignTaxonomy" function (Wang et al., 2007) in DADA2 using the custom Silva 132 database (Quast et al., 2013). DADA2 removed all potential chimeric sequences. After removing identifiable plant sequences (order: Rosales, Sapindales, Pinales, Fagales, Lamiales), only Chlorophyta ASVs were filtered out, and the ASV composition was analyzed using the R package "Phyloseq" (McMurdie and Holmes, 2013). The taxonomy of ASVs was assigned using BLAST against the NCBI nr/nt database.

The 18S rDNA alignment of snow-inhabiting *Chloromonas/Chlainomonas* contained 47 sequences (1,567 bp) examined in the previous studies (e.g., Matsuzaki et al., 2019; Procházková et al., 2019a), as well as five ASVs (377 bp long) generated in this study (ASV2-ASV6), and the 18S rDNA matrix focused on *Sanguina* spp. consisted of 30 sequences (1,581 bp) published before (e.g., Procházková et al., 2019b), as well as one ASV (378 bp long) acquired in this study (ASV1). For the former dataset, the mesophilic species of the *Chloromonas* clade (Pröschold et al., 2001) or the *Chloromonadinia* clade (Nakada et al., 2008) were selected as the outgroup; and for the latter dataset, the mesophilic species of Reinhardtii clade sensu (Pröschold et al., 2001) were selected as the outgroup. The best-fit nucleotide substitution model was estimated using jModeltest 2.0.1 (Posada, 2008). Based on the Akaike information criterion, the TIM2+I+G and TIM3+I+G models were selected for the former and latter datasets, respectively. The phylogenetic tree of 18S rDNA was inferred by Bayesian inference (BI) using MrBayes (version 3.2.6) (Ronquist et al., 2012). Two parallel Markov chain Monte Carlo runs for 3,000,000 generations with one cold

and three heated chains were conducted for both alignments using the selected best-fit evolutionary models, with trees sampled every 100 generations. The first 25% were discarded as burn-in. The maximum-likelihood (ML) phylogenetic tree was constructed using GARLI 2.0 (Zwickl, 2006). ML analysis consisted of rapid heuristic searches (100 pseudo-replicates) using automatic termination (genthreshfortopoterm command set to 100,000). The convergence of the two cold chains was checked by the average standard deviation of split frequencies (0.000868 and 0.000384 for the former and latter datasets, respectively). Bootstrap analyses and Bayesian posterior probabilities were used to assess the support of the clades. Values of posterior probabilities and bootstrap support were treated as weak (BI $<$ 0.5, ML $<$ 50%), moderate (BI 0.54-0.94, ML 50-79%) and high (BI $>$ 0.94, ML $>$ 79%) (Skaloud and Peksa, 2010).

Data Availability

Raw sequence data are available from BioProject: PRJNA726817 in the Sequence Read Archive of National Center for Biotechnology Information (NCBI; https://www.ncbi.nlm.nih.gov/sra/). Sequences of 6 major ASVs are deposited in NCBI Genbank (Accession number: MZ317533 - MZ317538).

RESULTS

Microscopic Observation of Algal Cells

Microscopic observation revealed that all of the red snow samples contained algal cells of various colors and cell shapes as described previously by Nakashima and Takeuchi (2017). The algal cells were often attached to small mineral particles. The algal cells were roughly classified into seven types based on the color and morphology: (1) Red or deep red spherical cells with thick cell walls (**Figure 3A**). Chloroplasts were observed at the center of the cell. The size of cells was 23.7 $\pm$ 6.0 μm in diameter. (2) Light red or orange spherical cells with thick cell walls (**Figure 3B**). The size of cells was 20.8 $\pm$ 3.2 μm in diameter. (3) Green and small-sized spherical cells (**Figure 3C**). The size of cells was 13.8 $\pm$ 2.6 μm in diameter. (4) Deep red ellipsoidal cells, with smooth cell wall (**Figure 3D**). The size of cells was 46.9 $\pm$7.6 μm in the major axis and 36.7 $\pm$ 5.1 μm in the minor axis. (5) Orange-colored oval cells, with cell wall flanges (**Figure 3E**). The size of cells was 44.4 $\pm$ 5.9 μm in the major axis and 24.1 $\pm$ 2.6 μm in the minor axis. (6) Yellow-colored and spindle-shaped cells (**Figure 3F**). The cell size was 27.4 $\pm$ 5.0 μm in the major axis and 16.0 $\pm$ 2.1 μm in the minor axis, smaller than (5) and larger than (7). (7) Green-colored oval cells (**Figure 3G**). Whole cell or center of the cell was colored light green and oval. The size of cells was 16.7 $\pm$ 3.1 μm in the major axis and 10.6 $\pm$ 1.9 μm in the minor axis.

The relative abundance of these cell types varied among the samples. Red, orange, and green spherical cells and green oval cell were contained in almost all samples in this study area. The other cell morphology appeared only at the specific site. Red ellipsoidal cells were included only in the samples at the site S2. Orange oval cell included in the samples at the sites S2, S4, and S7. Yellow oval cell was included in the samples at the sites S2 and S4; however, its abundance was relatively small.

Algal Pigment Composition

HPLC analysis of algal pigments revealed that the algal snow collected in this contained mainly two chlorophylls (chlorophyll *a* and chlorophyll *b*) and primary and secondary carotenoids (violaxanthin, lutein, β-carotene, and astaxanthin) (**Figure 4**). Astaxanthin included mainly three different forms: 3S, 3S′ trans-astaxanthin (free-astaxanthin), astaxanthin-monoester, and astaxanthin diesters. The astaxanthin esters showed several peaks in the chromatogram.

In this study, the composition of these pigments varied among the samples. Based on the cluster analysis, the samples can be classified into four pigment types (Types A, B, C, and D as shown in **Figure 5**). **Figure 6** shows the mean proportion of each pigment for the four pigment types. Type A was characterized by the dominance of astaxanthin-monoester, which accounted for 43.4–76.3% (mean: 63.6%) of the total pigments. Type B was characterized by the medium astaxanthin-monoester content, which accounted for 7.5–35.1% (mean: 22.0%) of the total pigments. The primary carotenoids were in trace levels in both Types A and B. Type C was characterized by the relatively high abundance of free-astaxanthin and primary carotenoids, mainly lutein. The mean abundance of free-astaxanthin and the mean abundance of lutein were 20.0 and 11.6%, respectively, of the total pigment. Type D was characterized by the high abundance of astaxanthin diesters, which accounted for 38.1% of the total pigment. The number of samples classified as Types A, B, C, and D were 23, 28, 2, and 1, respectively (**Table 2**).

The mean compositions of algal cell morphology in the four pigment types are shown in **Supplementary Figure 1**. The red, orange, and green spherical cells were dominant in both Types A and B (>90%), however red spherical cells was more abundant in Type A than Type B. Type C was dominated by the orange oval cell, accounting for 84% in the total cells. Type D was dominated by the red ellipsoidal cell, accounting for 89% in the total cells.

Spatial Variation in Pigment Types

Table 2 shows the number of samples of the four pigment types in each study site, indicating that the pigment types varied spatially in the study area. Types A and B were most commonly observed in this area: Type A occurred at five sites (S1, S2, S3, S6, and S7) and Type B occurred at five sites (S2, S4, S5, S6, and S7) among seven study sites. Types C and D occurred only at sites S4 and S2, respectively. There was almost no difference in the appearance of pigment type among the different months of sample collection. Types A and B were always observed at site S7 in all field investigations (June 2015, July 2015, and June 2016).

Phylogenetic Analyses of the 18S rRNA Gene of the Snow Algae

After quality filtering, the 18S rRNA gene amplicon sequence reads from the red snow comprised 2,568,681 high-quality paired-end sequence reads, which were clustered into 689 ASVs, with an average amplicon length of 381.52 bp (**Supplementary Table 2**). Classification of the sequence

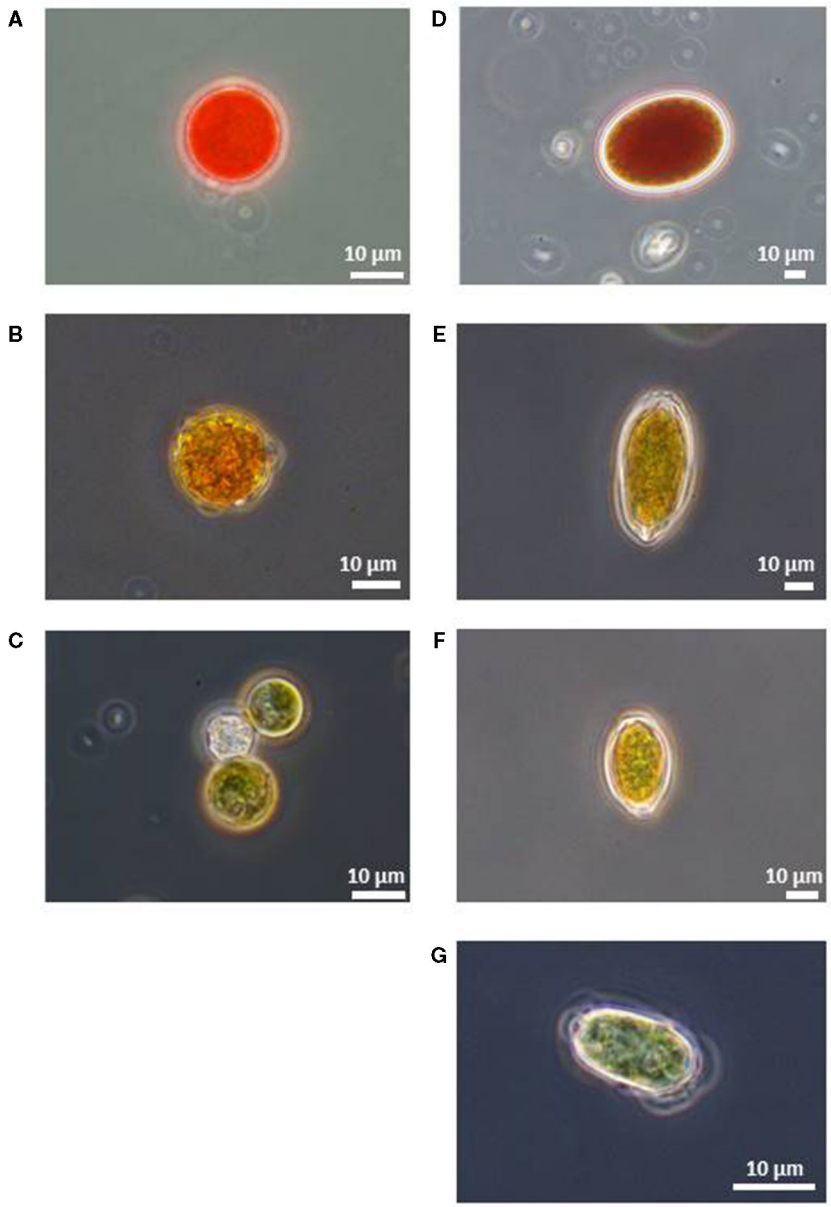

FIGURE 3 | Microscopic photographs of snow algal cells in red snow samples collected in Mt. Tateyama (reproduced from Nakashima and Takeuchi, 2017). **(A)** Red spherical cell, **(B)** Orange spherical cell, **(C)** Green spherical cell, **(D)** Red ellipsoidal cell, **(E)** Orange oval cell with cell wall flanges, **(F)** Yellow oval cell with cell wall flanges, and **(G)** Green oval cell.

data revealed that Chlorophyceae dominated the snow algal communities (99.9% in the total Chlorophyta). Chlamydomonadales contained major 6 ASVs, and the observed number of ASVs in Chlamydomonadales were 15, 18, and 24 ASVs for the samples from June 2015, July 2015, and June 2016, respectively (**Supplementary Table 3**). The most abundant ASV was ASV1 (MZ317533), accounting for 45.6% of Chlorophyta sequences, it was closely related to *Sanguina nivaloides* CCCryo RS 0015-2010 (JQ790560) and *Sanguina aurantia* CCCryo RS 0017-2010 (MK728645) classified in the highly/highly (BI/ML) supported *Sanguina* clade (**Figure 7**). The second abundant ASV was ASV2 (MZ317534), accounting for 32.1% of Chlorophyta sequences, and it was a member of highly/moderately supported subclade of the *Chloromonas* clade-B (**Figure 8**). ASV2 was closely related to snow algae and consists of *Chloromonas hindakii* WP129/CCCryo 531-19 (MN251865), *Chloromonas polyptera* DRAnt023 (JQ790556), *Chloromonas* sp. Gassan-B (LC012714), and *Chloromonas* sp. TA-8 (AB902996) (**Table 3**).

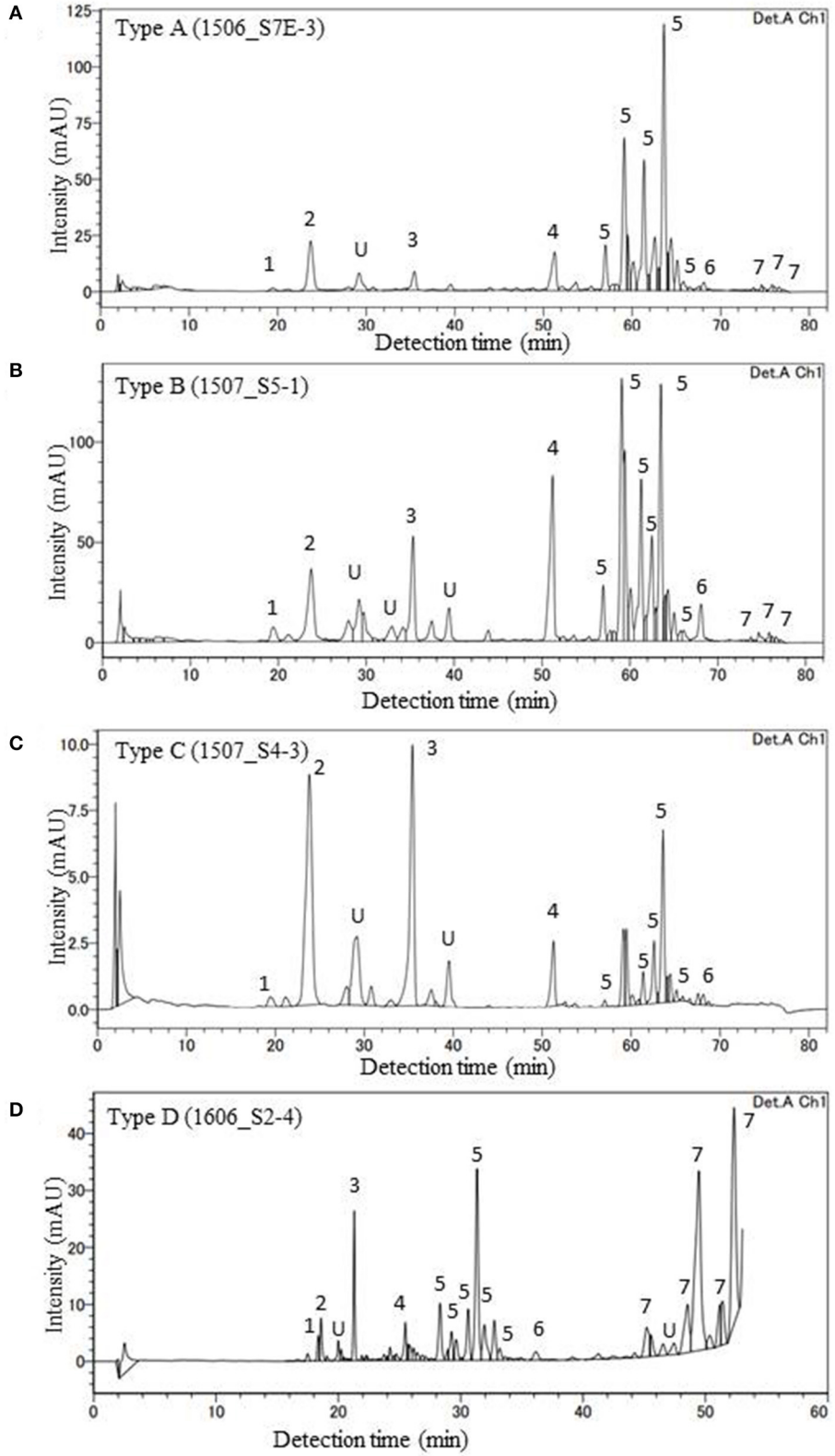

FIGURE 4 | HPLC chromatograms of four major pigment types of red snow samples (**A**: Type A, **B**: Type B, **C**: Type C, **D**: Type D) in this study (detection wavelength: 450 nm). Peaks with numbers or alphabet in the chromatograms indicate the algal pigments identified in this study. 1: Violaxanthin, 2: Astaxanthin, 3: Lutein, 4: Chlorophyll *b*, 5: trans-Astaxanthin (monoester), 6: β-carotene, 7: trans-Astaxanthin (diesters), and U: Unknown.

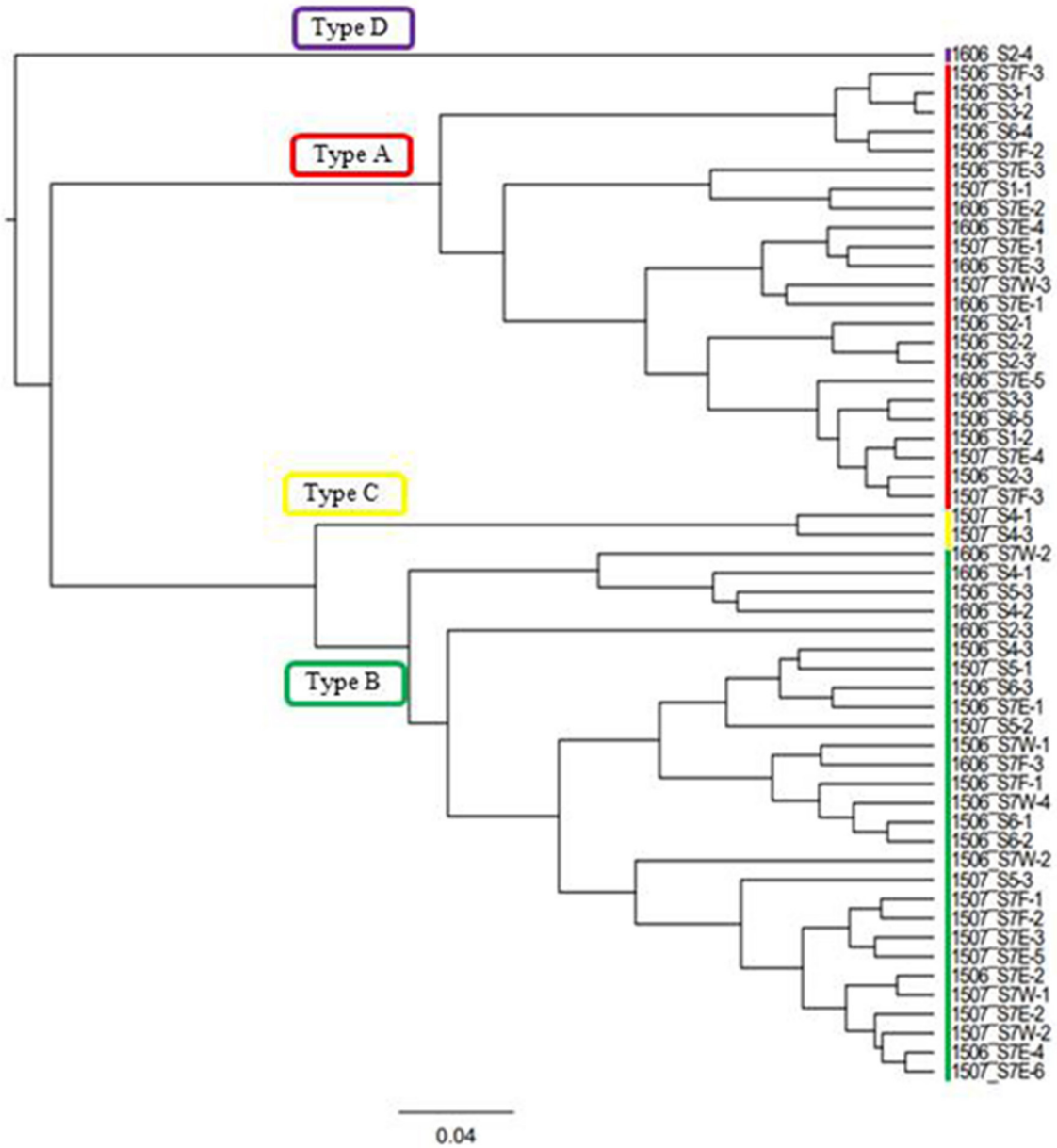

FIGURE 5 | Cluster analysis performed based on the algal pigment composition of red snow samples. Four groups classified in this study based on the result were shown (Types A, B, C, and D).

The third most abundant ASV was ASV3 (MZ317535), representing 7.6% of Chlorophyta sequences reads and belonged to an unnamed moderately/highly supported *Chloromonas* clade. It consisted of uncultured alga OTU003 (LC371421.1), uncultured *Chloromonas* sp. TA-9 (AB903024), uncultured *Chloromonas* SV-3 (AB903022), etc. (**Figure 8**).

The ASV5 (MZ317537), representing 3.5% reads of Chlorophyta sequences, was a member of the *Chloromonas* clade-D (**Figure 8**) and closely related to *Chlainomonas* sp. DL06/LP03 (MF803743, MF803745). ASV5 was 100% identical with the two algae tentatively assigned as "*Chloromonas*_sp_TA_1" (AB903004) and "*Chloromonas*_sp_TA_3" (AB902981) by single cell sequencing.

Figure 9 shows the relative abundance of the ASVs of snow algae among the four pigment types. Both Types A and B were dominated by ASV1 and ASV2. ASV1 was most dominant in Types A and B, accounting for 48 and 69%, respectively. ASV2 was secondary dominant in the types, accounting for 31 and 20%,

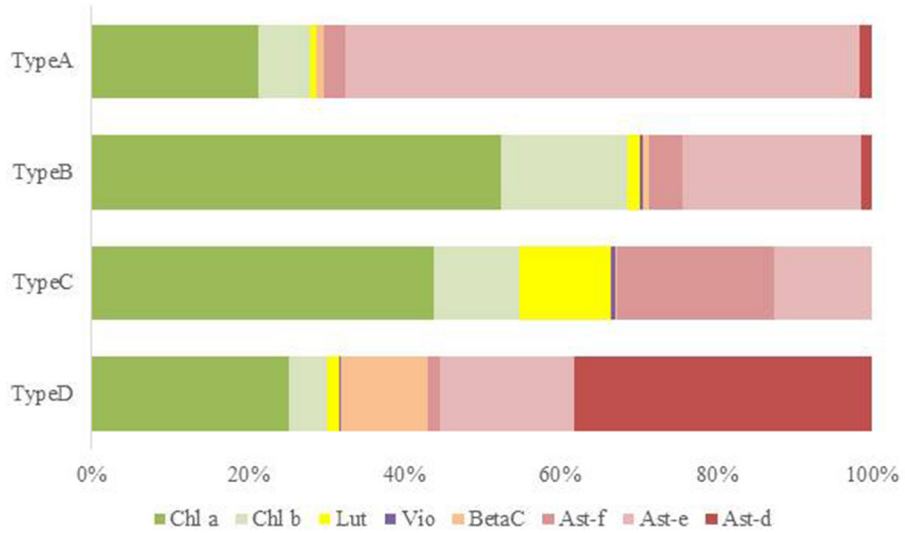

FIGURE 6 | Mean pigment composition of four types of red snow samples in Mt. Tateyama. Abbreviations: Chl a: chlorophyll a; Chl b: chlorophyll b; Lut: lutein; Vio: violaxanthin; BetaC: β-carotene; Ast-f: free-astaxanthin; Ast-e: astaxanthin-monoester; Ast-d: astaxanthin-diesters.

respectively. Types C and D were dominated by ASV2 (94%) and ASV5 (95%), respectively.

DISCUSSION

Red Snow Commonly Appeared in This Area (Types A and B)

Types A and B, which were dominated by the secondary carotenoid of astaxanthin-monoester, were the most common types of red snow in this study area, suggesting that most of the red snow is due to snow algae containing abundant astaxanthin-monoester. Phylogenetic analysis showed that the dominant ASV in both Types A and B was ASV1 was a part of *Sanguina*-clade in the 18S rRNA gene phylogenetic tree (formerly assigned to *Chlamydomonas*, Procházková et al., 2019b). As *Sanguina* sp., a typical snow alga distributed worldwide, has been reported as an astaxanthin-rich snow alga (Remias et al., 2005), it is reasonable to suggest that the red snow of Types A and B was dominated by *Sanguina* sp. rich in astaxanthin.

Types A and B were both dominated by ASV1; therefore, the difference in the abundance of astaxanthin between these two types was probably due to the astaxanthin content in each algal cell. In Type A, algal cells exhibited higher astaxanthin-to-chlorophyll *a* ratio (range: 1.31–6.20, mean: 3.3:1), whereas algal cells in Type B had a lower astaxanthin-to-chlorophyll *a* ratio (range: 0.16–0.92, mean: 0.54:1). A previous study suggested that the pigment composition in the *Sanguina* group alga cells varied depending on the environmental conditions—for example, abundant production of astaxanthin under intense UV radiation (Remias et al., 2005) or under nitrogen-limited conditions (Lutz et al., 2016). Also the ratio of astaxanthin to chlorophyll *a* varied with the individual extent of maturation of a population in course of the summer season (Procházková et al., 2021). In this study, at the higher elevation sites, only Type A appeared (S1, S2, and S3), whereas in the lower elevation sites both Types A and B appeared (S6 and S7), and only Type B appeared at the low elevation site (S2, S4, and S5). At the higher elevation sites, the melt rate of snow was probably lower because the air temperature was lower than at lower elevations. The increase in astaxanthin in cells benefits snow surface-dwelling hypnoblasts (Dial et al., 2018) and is consistent with this conclusion. Furthermore, all the sites were located near the mountain ridge, where there was less vegetation due to windy conditions. The abundance of astaxanthin in the algal cells of ASV1 may be affected by the environmental conditions of the snow surface and cell maturation process.

Since the fragment of 18S rDNA (this study) or even the whole length of 18S rDNA is insufficient to distinguish the different *Sanguina* species (i.e., *S. nivaloides* and *S. aurantia*) (Procházková et al., 2019b), the distinct pigment compositions of Types A and B are also possibly due to abundance of different *Sanguina* species. Microscopy showed that, red and orange spherical cells contained in the samples of Types A and B were morphologically very similar to the mature cyst of *S. nivaloides* and *S. aurantia*, respectively, however, the size of the orange cells was significantly larger than that of *S. aurantia* (Procházková et al., 2019b, 2021). Thus, we cannot exclude that an undescribed *Sanguina* sp. may occur in snow in Mt. Tateyama.

Red Snow of Special Properties Appeared in Specific Sites (Types C and D)

Pigment Type C, which is rich in primary carotenoids, including lutein and free-astaxanthin, appeared only at the site S4 in this study area, suggesting that special conditions induce this type of red snow at the site. However, we did not find any specific chemical (pH or EC) or topographical conditions at this site.

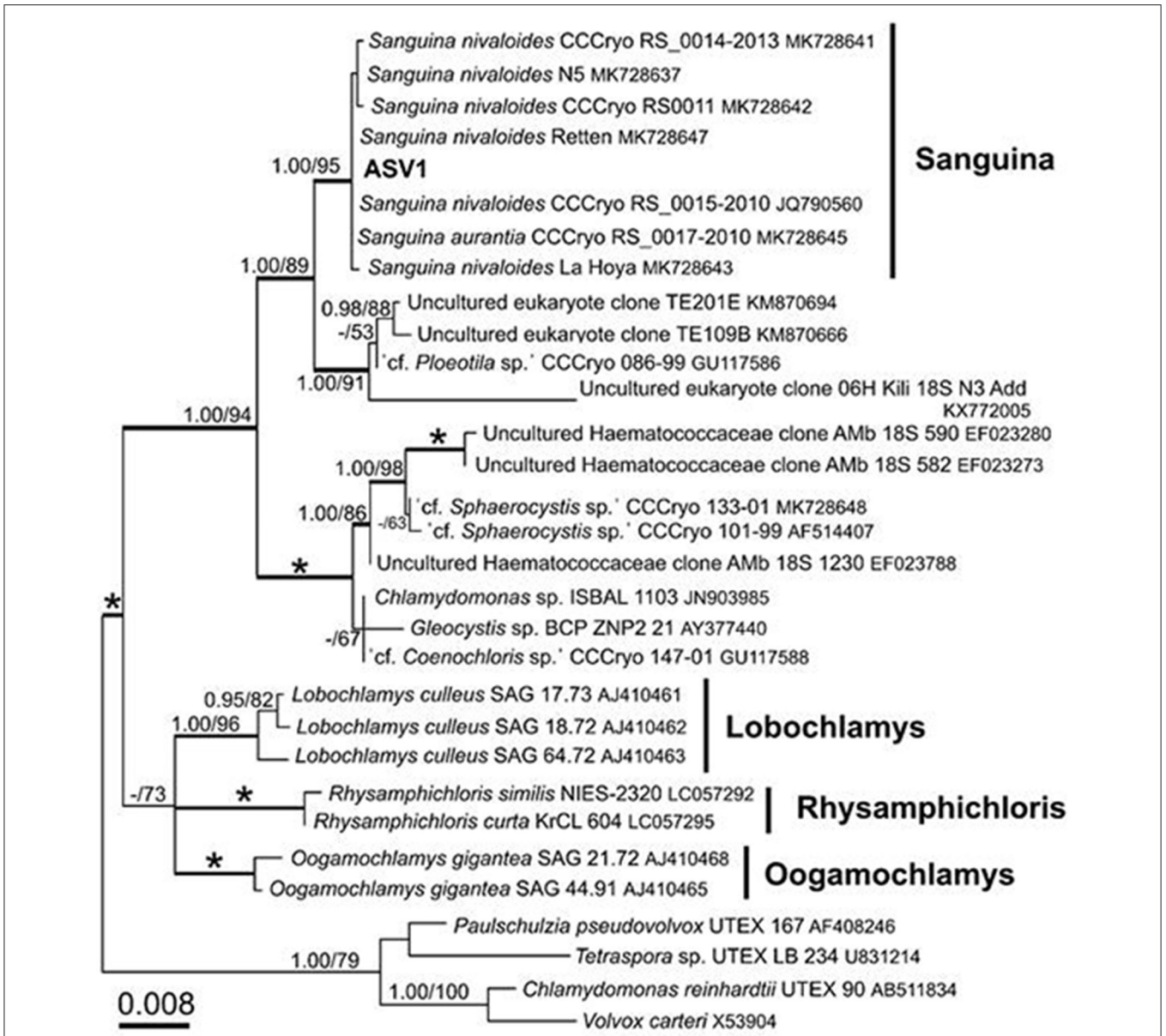

FIGURE 7 | 18S rRNA-gene-based maximum likelihood phylogeny of *Sanguina* spp. showing phylogenetic position of one of the major ASV reads (ASV1) detected in the red snow samples in Mt. Tateyama, Japan. Posterior probabilities (≥0.95) and bootstrap values from maximum likelihood analysis (≥50%) are shown. Full statistical support (1.00/100) is marked with an asterisk. Thick branches represent nodes receiving the highest posterior probability support (1.00). Accession numbers, strain, or field sample codes are indicated after each species name.

When we collected the sample, the snow depth at this site was shallower (<20 cm) compared with those at the other sites (more than 50 cm). DNA analysis showed that this type was mostly dominated by ASV2, indicating that the primary carotenoids in Type C were derived from the algal cells of ASV2. ASV2 was one of the common algal species in this study area, as it was detected in many samples, including in Types A and B samples The phylogenetic tree showed that ASV2 was closely related to *Chloromonas* spp., which is consistent with their dominant pigments. Previous studies have shown that cells of *C. nivalis* have abundant primary carotenoids such as xanthophyll cycle pigments and lutein, which is distinctive from *Sanguina* sp. that contains mainly secondary carotenoids such as astaxanthin (Remias et al., 2010). Therefore, this type of snow probably has conditions to be dominated by the *Chloromonas* alga.

Pigment Type D, which was characterized by abundant astaxanthin diesters, was dominated by ASV5, indicating that the pigment was derived from this algal species. The lack of ASV1 (*Sanguina* sp.) in this snow type was distinctive from the other types in this study. This type appeared only at the

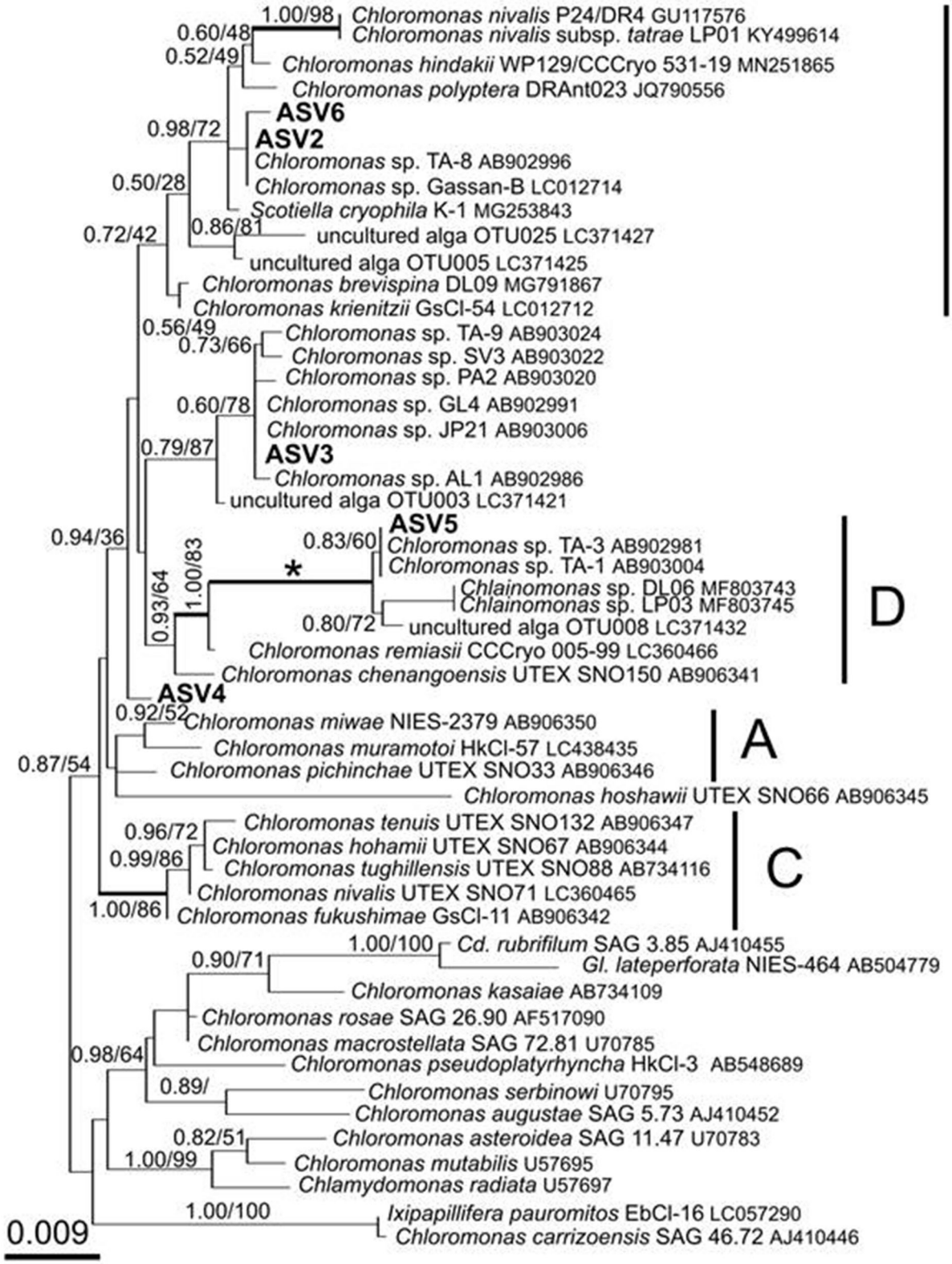

FIGURE 8 | 18S rRNA-gene-based maximum-likelihood phylogeny of snow-inhabiting *Chloromonas/Chlainomonas* spp. showing phylogenetic positions of the five major ASV reads (ASV2–ASV6) detected in the red snow samples in Mt. Tateyama, Japan. The labeled clades "A," "B," and "C" correspond to Matsuzaki et al. (2019). Posterior probabilities and bootstrap values from maximum likelihood analysis are shown. Full statistical support (1.00/100) is marked with an asterisk. Thick branches represent nodes receiving the highest posterior probability support (1.00). Accession numbers, strain, or field sample codes are indicated after each species name.

TABLE 3 | Top six ASVs (377-378 bp long) of 18S rRNA genes aligned and assigned to Chlorophyta in the samples, the closest relatives of the 18S rRNA genes that are based on the Nucleotide BLAST search in NCBI, and the sequence identity of 18S rRNA gene (%).

ASV No.	Relative abundance (%)	Closest identified relatives	Accession numbers	Sequence identity (%)
ASV 1	45.6	*Sanguina nivaloides* CCCryo RS 0015-2010	JQ790560.1	100
		Sanguina aurantia CCCryo RS 0017-2010	MK728645.1	100
ASV 2	32.1	*Chloromonas hindakii* WP129/CCCryo 531-19	MN251865.1	100
		Chloromonas polyptera DRAnt023	JQ790556.1	100
		Chloromonas sp. Gassan-B	LC012714.1	100
		Chloromonas sp. TA-8	AB902996.1	100
ASV 3	7.6	Uncultured alga: OTU003	LC371421.1	100
		Chloromonas sp. TA-9	AB903024.1	100
		Chloromonas sp. SV-3	AB903022.1	100
		*Chloromonas*_sp_PA2	AB903020.1	100
		*Chloromonas*_sp_GL4	AB902991.1	100
		*Chloromonas*_sp_JP21	AB903006.1	100
		And many others		
ASV 4	3.6	Uncultured alga: Otu025	LC371427.1	99.2
		Uncultured alga: Otu005	LC371425.1	99.2
		Uncultured alga: Otu003	LC371421.1	99.2
		Chloromonas sp. TA-9	AB903024.1	99.2
		Chloromonas sp. SV-3	AB903022.1	99.2
		And many others		
ASV 5	3.5	*Chloromonas*_sp_TA_1	AB903004.1	100
		*Chloromonas*_sp_TA_3	AB902981.1	100
		Uncultured alga: OTU008	LC371432.1	99.5
		Chlainomonas sp. LP03	MF803745.1	98.7
		Chlainomonas sp. DL06	MF803743.1	98.7
ASV 6	2.5	*Chloromonas hindakii* WP129/CCCryo 531-19	MN251865.1	99.7
		Chloromonas polyptera DRAnt023	JQ790556.1	99.7
		Chloromonas sp. Gassan-B	LC012714.1	99.7
		Chloromonas sp. TA-8	AB902996.1	99.7

Top six ASVs were chosen which contained more than 1% in total ASVs.

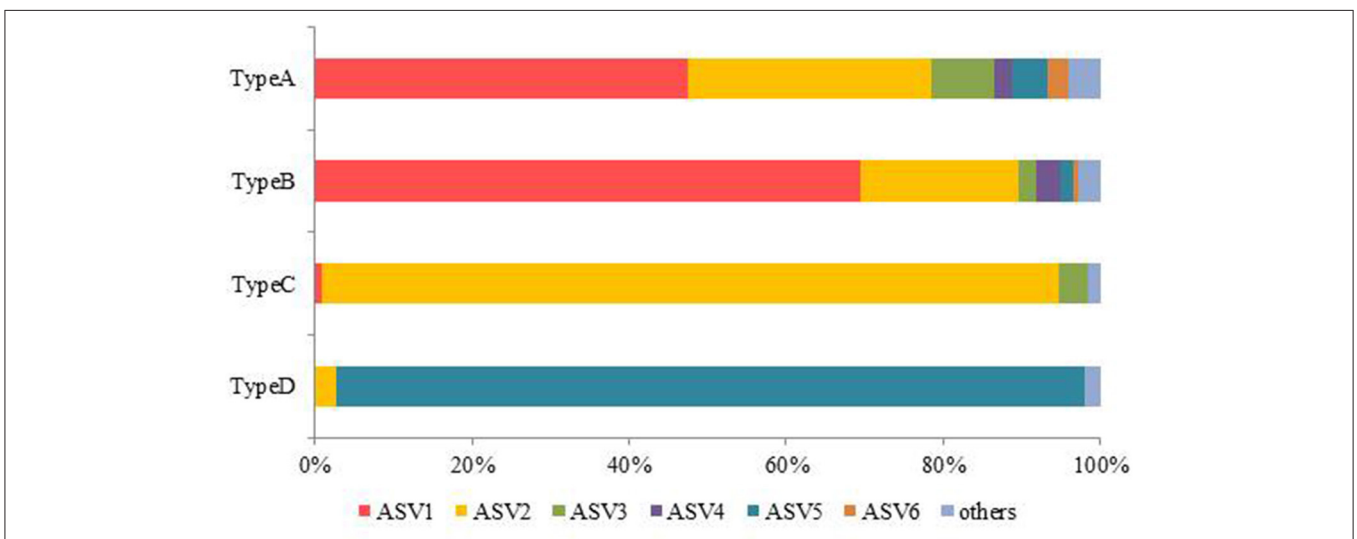

FIGURE 9 | Mean relative abundance of algal ASVs containing the four pigment types.

site S2, suggesting special conditions induced this type of red snow at the site. Astaxanthin in algal cells is present in various molecular forms and often combines with one or two fatty acids and glucose. Fatty acids play an important role in cell survival at low temperatures (Řezanka et al., 2013). A previous study revealed that such molecular forms of astaxanthin in algal cells were changed by species. For example, the algal cells of the *Sanguina* group, which have abundant astaxanthin, mainly contained monoesters in the stage of resting spores, whereas the algal cells of *Chlainomonas* group were mainly present as astaxanthin diesters in the vegetative cell stage (Bidigare et al., 1993, Remias et al., 2016). The phylogenetic tree showed that ASV5 was closely related to *Chlainomonas* sp. and algal cell morphology in Type D was distinctive from other pigment types—red ellipsoidal cell dominant resembled in cell size, cell shape and pigment colouration of snow *Chlainomonas*. The snow surface at this site may be a suitable condition for the growth of this alga in this region. The site S2 was located on a southern mountain ridge in this study area; however, we did not find any other specific chemical (pH or EC) or topographical conditions at this site.

Variations in the Algal Community in Red Snow in Tateyama Mountain Region

Our results showed that the community structure of red snow in the Tateyama Mountains area varied seasonally and spatially among the sites and largely affected the pigment composition. The presence of diverse algal communities within a relatively small mountainous area suggests that the algal community of red snow is determined by local environmental conditions and the migration process of algal cells to the snow surface.

Most of the red snow in this area is dominated by ASV1, *Sanguina* sp., a typical algal species in red snow worldwide. The previous study showed the presence of cosmopolitan species of snow algae, which appeared in the Arctic and Antarctic regions, and *Sanguina* [i.e., "*Chlamydomonas*"-snow group B) was one of them (Segawa et al., 2018)]. The snow alga *Sanguina* sp. observed in the red snow in this study may have originated from common sources of the world and migrated from the atmosphere onto the snow surface. However, another study described that the *Sanguina* snow alga in red snow does not have a homogeneous population structure across worldwide locations (Brown and Tucker, 2020), therefore, it may be derived locally.

ASV2, which close to putative *Chloromonas* sp., was also commonly present in the red snow in the study area. *Chloromonas* reported to be regionally endemic distribution (Segawa et al., 2018). The broad distribution of ASV2 in the study area may disperse locally.

ASV5 dominant, which close to putative *Chlainomonas* sp. appeared only at the specific sites (S2) and was rarely observed in other red snow samples. However, we did not find any specific chemical (pH or EC) or topographical conditions at this site. The previous study showed that snow-dwelling *Chlainomonas* spp. were distributed in forested sites or close to coniferous canopies (Hoham, 1974a,b), in waterlogged snow overlying lakes (Novis et al., 2008, Procházková et al., 2018), or at other high alpine sites which were not notably wetter than the surrounding snow, nor were they located over frozen lakes (Engstrom et al., 2020). The life cycle of *Chlainomonas* includes flagellates (e.g., Procházková et al., 2018) which are important for migration processes from the ground soil to the snow surface during snow melting (Hoham and Remias, 2020). To reveal reasons for the distinct distribution of this alga in this region (when compared to other species in this dataset), measurement of physical and chemical snow parameters may be helpful.

Seasonal and spatial variations in the appearance of each algal species suggest that they have different dispersal processes, life cycles, and suitable conditions for growth on the snow surface. However, this remains largely questionable. This snowy area of the Tateyama Mountains is one of the best places in the world to study snow algae. However, global climate warming is changing the environmental conditions of this alpine area and will affect the snowpack in this unique ecosystem soon. Thus, understanding the ecology of the snow algae in this area is urgently required.

CONCLUSIONS

This study revealed that red snow appeared extensively on the Mt. Tateyama snowfields during the melting seasons. HPLC analysis showed that the algal pigment compositions of the red snow varied spatially and seasonally and could be classified into four distinctive types (Types A–D), although they appeared visually to be almost the same color. Types A and B contained abundant astaxanthin-monoester; however, its abundance was relatively greater in Type A than in Type B. These two types occurred most commonly in the study area. Types C and D were characterized by primary carotenoids, free-astaxanthin, and astaxanthin diesters. These two types occurred only at specific sites. Phylogenic analysis using the 18S rRNA gene showed no significant difference in community structure between Types A and B, dominated by ASV1 and ASV2, which are close to *Sanguina* sp. and *Chloromonas* sp., respectively. Types C and D were dominated by ASV2, close to *Chloromonas* sp., and by ASV5, close to *Chlainomonas* sp., respectively. As both Types A and B are dominated by *Sanguina* spp., the difference in the abundance of astaxanthin between the two types was probably due to the environmental conditions and also cell maturation process as well. The pigment composition of Type C was likely induced by ASV2 because *Chloromonas* algae have abundant primary carotenoids. The pigment composition of Type D was likely derived from ASV5, *Chlainomonas* algae, which have abundant astaxanthin diesters. The factors determining the pigment composition or community structure in red snow remain uncertain. Further detailed studies examining the physical parameters such as snow water content, the amount of snow and solar radiation intensity, and chemical conditions of the snow at each site are required. The dispersal process and annual life cycle of each algal species are also important for understanding their spatial and seasonal variations.

DATA AVAILABILITY STATEMENT

Raw sequence data are available from BioProject: PRJNA726817 in the Sequence Read Archive of National Center for Biotechnology Information (NCBI; https://www.ncbi.nlm.nih.gov/sra/).

AUTHOR CONTRIBUTIONS

TN and NT designed the study. TN collected the samples. TN and AT conducted HPLC analyses. TN and JU performed DNA extractions and sequencing. JU, TS, and LP performed DNA data analyses. TN, NT, JU, TS, and LP wrote the manuscript. All authors contributed to the article and approved the submitted version.

FUNDING

This work was supported from JSPS KAKENHI (19H01143, 20K21840, 21H03612, and 21H03588), and from the Arctic Challenge for Sustainability II (ArCS II), Program Grant Number JPMXD1420318865, the Institute for Fermentation, Osaka (G-2020-2-133), and by Czech Science Foundation (GACR) projects 18-02634S. LP has been supported by Charles University Research Centre program No. 204069.

ACKNOWLEDGMENTS

We would like to thank Drs. Hajime Iida and Kotaro Fukui for kind support for field works in Mt. Tateyama, Dr. Yukiko Tanabe for kind support for HPLC analysis, and Drs. Daniel Remias and Shinichi Takaichi for their valuable comments for algal pigment identification on HPLC chromatogram. We would also like to thank two reviewers for their helpful comments.

SUPPLEMENTARY MATERIAL

The Supplementary Material for this article can be found online at: https://www.frontiersin.org/articles/10.3389/fpls.2021.689119/full#supplementary-material

REFERENCES

Bidigare, R. R., Ondrusek, M. E., Kennicutt, M. C., Iturriaga, R., Harvey, H. R., Hoham, R. W., et al. (1993). Evidence a photoprotective for secondary carotenoids of snow algae 1. *J. Phycol.* 29, 427–434. doi: 10.1111/j.1529-8817.1993.tb00143.x

Britton, J. S., and Edgar, B. A. (1998). Environmental control of the cell cycle in Drosophila: nutrition activates mitotic and endoreplicative cells by distinct mechanisms. *Development* 125, 2149–2158. doi: 10.1242/dev.125.11.2149

Brown, S. P., and Tucker, A. E. (2020). Distribution and biogeography of *Sanguina* snow algae: fine-scale sequence analyses reveal previously unknown population structure. *Ecol. Evol.* 10, 11352–11361. doi: 10.1002/ece3.6772

Brown, S. P., Ungerer, M. C., and Jumpponen, A. (2016). A community of clones: snow algae are diverse communities of spatially structured clones. *Int. J. Plant Sci.* 177, 432–439. doi: 10.1086/686019

Callahan, B. J., McMurdie, P. J., Rosen, M. J., Han, A. W., Johnson, A. J. A., and Holmes, S. P. (2016). DADA2: High-resolution sample inference from Illumina amplicon data. *Nat. Methods* 13, 581–583. doi: 10.1038/nmeth.3869

Davey, M. P., Norman, L., Sterk, P., Huete-Ortega, M., Bunbury, F., Loh, B. K. W., et al. (2019). Snow algae communities in Antarctica: metabolic and taxonomic composition. *New Phytol.* 222, 1242–1255. doi: 10.1111/nph.15701

Dial, R. J., Ganey, G. Q., and Skiles, S. M. (2018). What color should glacier algae be? An ecological role for red carbon in the cryosphere. *FEMS Microbiol. Ecol.* 94:fiy007. doi: 10.1093/femsec/fiy007

Engstrom, C. B., Yakimovich, K. M., and Quarmby, L. M. (2020). Variation in snow algae blooms in the Coast Range of British Columbia. *Front. Microbiol.* 11:569. doi: 10.3389/fmicb.2020.00569

Fujii, M., Takano, Y., Kojima, H., Hoshino, T., Tanaka, R., and Fukui, M. (2010). Microbial community structure, pigment composition, and nitrogen source of red snow in antarctica. *Microb. Ecol.* 59, 466–475. doi: 10.1007/s00248-009-9594-9

Fukushima, H. (1963). Studies on cryophytes in Japan. *Yokohama Municipal Univ. Ser. C. Nat. Sci.* 43, 1–146.

Hoham, R. W. (1974a). *Chlainomonas kolii* (Hardy et Curl) comb. nov. (Chlorophyta, Volvocales), a revision of the snow alga, *Trachelomonas kolii* Hardy et Curl (Euglenophyta, Euglenales). *J. Phycol.* 10, 392–396. doi: 10.1111/j.1529-8817.1974.tb02731.x

Hoham, R. W. (1974b). New findings in the life history of the snow alga, *Chlainomonas rubra* (Stein et Brooke) comb. nov. (Chlorophyta, Volvocales). *Syesis* 7, 239–247.

Hoham, R. W., and Remias, D. (2020). Snow and glacial algae: a review. *J. Phycol.* 56, 264–282. doi: 10.1111/jpy.12952

Holzinger, A., Allen, M. C., and Deheyn, D. D. (2016). Hyperspectral imaging of snow algae and green algae from aeroterrestrial habitats. *J. Photochem. Photobiol. B Biol.* 162, 412–420. doi: 10.1016/j.jphotobiol.2016.07.001

Leya, T., Rahn, A., Lütz, C., and Remias, D. (2009). Response of arctic snow and permafrost algae to high light and nitrogen stress by changes in pigment composition and applied aspects for biotechnology. *FEMS Microbiol. Ecol.* 67, 432–443. doi: 10.1111/j.1574-6941.2008.00641.x

Logares, R., Audic, S., Santini, S., Pernice, C. M., Vargas, C., and Massana, R. (2012). Diversity patterns and activity of uncultured marine heterotrophic flagellates unveiled with pyrosequencing, *ISME J.* 6, 1823–1833. doi: 10.1038/ismej.2012.36

Lutz, S., Anesio, A. M., Edwards, A., and Benning, L. G. (2017). Linking microbial diversity and functionality of arctic glacial surface habitats. *Environ. Microbiol.* 19, 551–565. doi: 10.1111/1462-2920.13494

Lutz, S., Anesio, A. M., Raiswell, R., Edwards, A., Newton, R. J., Gill, F., et al. (2016). The biogeography of red snow microbiomes and their role in melting arctic glaciers. *Nat. Commun.* 7, 1–9. doi: 10.1038/ncomms11968

Lutz, S., Anesio, A. M., Villar, S. E. J., and Benning, L. G. (2014). Variations of algal communities cause darkening of a Greenland glacier. *FEMS Microbiol. Ecol.* 89, 402–414. doi: 10.1111/1574-6941.12351

Matsuzaki, R., Kawai – Toyooka, H., Hara, Y., and Nozaki, H. (2015). Revisiting the taxonomic significance of aplanozygote morphologies of two cosmopolitan snow species of the genus *Chloromonas* (Volvocales, Chlorophyceae). *Phycologia* 54, 491–502. doi: 10.2216/15-33.1

Matsuzaki, R., Nozaki, H., Takeuchi, N., Hara, Y., and Kawachi, M. (2019). Taxonomic re-examination of "*Chloromonas nivalis* (Volvocales, Chlorophyceae) zygotes" from Japan and description of *C. muramotoi* sp. nov. *PLoS ONE* 14:e0210986. doi: 10.1371/journal.pone.0210986

McMurdie, P. J., and Holmes, S. (2013). phyloseq: an R package for reproducible interactive analysis and graphics of microbiome census data. *PLoS ONE* 8:e61217. doi: 10.1371/journal.pone.0061217

Müller, T., Bleiß, W., Martin, C. D., Rogaschewski, S., and Fuhr, G. (1998). Snow algae from northwest Svalbard: their identification, distribution, pigment and nutrient content. *Polar Biol.* 20, 14–32. doi: 10.1007/s003000050272

Muramoto, K., Kato, S., Shitara, T., Hara, Y., and Nozaki, H. (2008). Morphological and genetic variation in the cosmopolitan snow alga *Chloromonas nivalis* (Volvocales, Chlorophyta) from Japanese mountainous area. *Cytologia* 73, 91–96. doi: 10.1508/cytologia.73.91

Nakada, T., Misawa, K., and Nozaki, H. (2008). Molecular systematics of Volvocales (Chlorophyceae, Chlorophyta) based on exhaustive 18S rRNA phylogenetic analyses. *Mol. Phylogenet. Evol.* 48, 281–291. doi: 10.1016/j.ympev.2008.03.016

Nakashima, T., and Takeuchi, N. (2017). Variations in algal pigment composition of red snow during the melting season at Mount Tateyama, Toyama prefecture, Japan. *J. Jpn. Soc. Snow Ice* 79, 549–563. doi: 10.5331/seppyo.79.6_549

Nedbalová, L., Kociánová, M., and Lukavský, J. (2008). Ecology of snow algae in the Giant Mts. *Opera Corcontica* 45, 59–68.

Novis, P. M., Hoham, R. Q., Beer, T., and Dawson, M. (2008). Two snow species of the quadriflagellate green alga *Chlainomonas* (Chlorophyta, Volvocales): ultrastructure and phylogenetic position within the *Chloromonas* clade. *J. Phycol.* 44, 1001–1012. doi: 10.1111/j.1529-8817.2008.00545.x

Onuma, Y., Takeuchi, N., Tanaka, S., Nagatsuka, N., Niwano, M., and Aoki, T. (2020). Physically based model of the contribution of red snow algal cells to temporal changes in albedo in northwest Greenland. *Cryosphere* 14, 2087–2101. doi: 10.5194/tc-14-2087-2020

Osterrothová, K., Culka, A., Němečková, K., Kaftan, D., Nedbalová, L., Procházková, L., et al. (2019). Analyzing carotenoids of snow algae by Raman microspectroscopy and high-performance liquid chromatography. *Spectrochim. Acta Part A Mol. Biomol. Spectrosc.* 212, 262–271. doi: 10.1016/j.saa.2019.01.013

Posada, D. (2008). jModelTest: phylogenetic model averaging. *Mol. Biol. Evol.* 25, 1253–1256. doi: 10.1093/molbev/msn083

Procházková, L., Leya, T., KríŽková, H., and Nedbalová, L. (2019b). *Sanguina nivaloides* and *Sanguina aurantia* gen. et spp. nov. (Chlorophyta): the taxonomy, phylogeny, biogeography and ecology of two newly recognised algae causing red and orange snow. *FEMS Microbiol. Ecol.* 95:fiz064. doi: 10.1093/femsec/fiz064

Procházková, L., Remias, D., Holzinger, A., Řezanka, T., and Nedbalová, L. (2018). Ecophysiological and morphological comparison of two populations of *Chlainomonas* sp. (Chlorophyta) causing red snow on ice-covered lakes in the High Tatras and Austrian Alps. *Euro. J. Phycol.* 53, 230–243. doi: 10.1080/09670262.2018.1426789

Procházková, L., Remias, D., Holzinger, A., Řezanka, T., and Nedbalová, L. (2021). Ecophysiological and ultrastructural characterisation of the circumpolar orange snow alga *Sanguina aurantia* compared to the cosmopolitan red snow alga *Sanguina nivaloides* (Chlorophyta). *Polar Biol.* 44, 105–117. doi: 10.1007/s00300-020-02778-0

Procházková, L., Remias, D., Řezanka, T., and Nedbalová, L. (2019a). Ecophysiology of *Chloromonas hindakii* sp. nov. (Chlorophyceae), causing orange snow blooms at different light conditions. *Microorganisms* 7:434. doi: 10.3390/microorganisms7100434

Pröschold, T., Marin, B., Schlösser, U. G., and Melkonian, M. (2001). Molecular phylogeny and taxonomic revision of (Chlorophyta). I. Emendation of *Chlamydomonas* Ehrenberg and *Chloromonas* Gobi, and Description of *Oogamochlamys* gen. nov. and gen. nov. and Lobochlamys gen. nov. *Protist* 152, 265–300. doi: 10.1078/1434-4610-00068

Quast, C., Pruesse, E., Yilmaz, P., Gerken, J., Schweer, T., Yarza, P., et al. (2013). The SILVA ribosomal RNA gene database project: improved data processing and web-based tools. *Nucleic Acids Res.* 41, D590–D596. doi: 10.1093/nar/gks1219

R Core Team (2017). *R: A Language and Environment for Statistical Computing*. Vienna: R Foundation for Statistical Computing. Available online at: https://www.r-project.org/ (accessed May 28, 2021).

Remias, D., Karsten, U., Lütz, C., and Leya, T. (2010). Physiological and morphological processes in the Alpine snow alga *Chloromonas nivalis* (Chlorophyceae) during cyst formation. *Protoplasma* 243, 73–86. doi: 10.1007/s00709-010-0123-y

Remias, D., and Lütz, C. (2007). Characterisation of esterified secondary carotenoids and of their isomers in green algae: a HPLC approach. *Arch. Hydrobiol. Suppl. Algol. Stud.* 124, 85–94. doi: 10.1127/1864-1318/2007/0124-0085

Remias, D., Lütz-Meindl, U., and Lütz, C. (2005). Photosynthesis, pigments and ultrastructure of the alpine snow alga *Chlamydomonas nivalis*. *Eur. J. Phycol.* 40, 259–268. doi: 10.1080/09670260500202148

Remias, D., Pichrtová, M., Pangratz, M., Lütz, C., and Holzinger, A. (2016). Ecophysiology, secondary pigments and ultrastructure of *Chlainomonas* sp. (Chlorophyta) from the European Alps compared with *Chlamydomonas nivalis* forming red snow. *FEMS Microbiol. Ecol.* 92:fiw030. doi: 10.1093/femsec/fiw030

Řezanka, T., Nedbalová, L., Kolouchová, I., and Sigler, K. (2013). LC–MS/APCI identification of glucoside esters and diesters of astaxanthin from the snow alga *Chlamydomonas nivalis* including their optical stereoisomers. *Phytochemistry* 88, 34–42. doi: 10.1016/j.phytochem.2013.01.003

Řezanka, T., Nedbalová, L., Sigler, K., and Cepák, V. (2008). Identification of astaxanthin diglucoside diesters from snow alga *Chlamydomonas nivalis* by liquid chromatography–atmospheric pressure chemical ionization mass spectrometry. *Phytochemistry* 69, 479–490. doi: 10.1016/j.phytochem.2007.06.025

Ronquist, F., Teslenko, M., Van Der Mark, P., Ayres, D. L., Darling, A., Höhna, S., et al. (2012). Mrbayes 3.2: Efficient bayesian phylogenetic inference and model choice across a large model space. *Syst. Biol.* 61, 539–542. doi: 10.1093/sysbio/sys029

Segawa, T., Matsuzaki, R., Takeuchi, N., Akiyoshi, A., Navarro, F., Sugiyama, S., et al. (2018). Bipolar dispersal of red-snow algae. *Nat. Commun.* 9, 1–8. doi: 10.1038/s41467-018-05521-w

Segawa, T., Miyamoto, K., Ushida, K., Agata, K., Okada, N., and Kohshima, S. (2005). Seasonal change in bacterial flora and biomass in mountain snow from the Tateyama Mountains, Japan, analyzed by 16S rRNA gene sequencing and real-time PCR. *Appl. Environ. Microbiol.* 71, 123–130. doi: 10.1128/AEM.71.1.123-130.2005

Skaloud, P., and Peksa, O. (2010). Evolutionary inferences based on ITS rDNA and actin sequences reveal extensive diversity of the common lichen alga *Asterochloris* (Trebouxiophyceae, Chlorophyta). *Mol. Phylogenet. Evolut.* 54, 36–46. doi: 10.1016/j.ympev.2009.09.035

Takaichi, S. (2011). Carotenoids in algae: distributions, biosyntheses and functions. *Mar. Drugs* 9, 1101–1118. doi: 10.3390/md9061101

Tanabe, Y., Shitara, T., Kashino, Y., Hara, Y., and Kudoh, S. (2011). Utilizing the effective xanthophyll cycle for blooming of *Ochromonas smithii* and *O. itoi* (Chrysophyceae) on the snow surface. *PLoS ONE* 6:e14690. doi: 10.1371/journal.pone.0014690

Terashima, M., Umezawa, K., Mori, S., Kojima, H., and Fukui, M. (2017). Microbial community analysis of colored snow from an alpine snowfield in northern Japan reveals the prevalence of Betaproteobacteria with snow algae. *Front. Microbiol.* 8:1481. doi: 10.3389/fmicb.2017.01481

Thomas, W. H., and Duval, B. (1995). Sierra Nevada, California, USA, snow algae: snow albedo changes, algal-bacterial interrelationships, and ultraviolet radiation effects. *Arctic Alpine Res.* 27, 389–399. doi: 10.2307/1552032

Wang, Q., Garrity, G. M., Tiedje, J. M., and Cole, J. R. (2007). Naïve Bayesian classifier for rapid assignment of rRNA sequences into the new bacterial taxonomy. *Appl. Environ. Microbiol.* 73, 5261–5267. doi: 10.1128/AEM.00062-07

Yakimovich, K. M., Engstrom, C. B., and Quarmby, L. M. (2020). Alpine snow algae microbiome diversity in the Coast Range of British Columbia. *Front. Microbiol.* 11:1721. doi: 10.3389/fmicb.2020.01721

Zwickl, D. J. (2006). *Genetic algorithm approaches for the phylogenetic analysis of large biological sequence datasets under the maximum likelihood criterion (dissertation)*. The University of Texas, Austin, TX, United States.

Conflict of Interest: The authors declare that the research was conducted in the absence of any commercial or financial relationships that could be construed as a potential conflict of interest.

frontiers in Plant Science

HYPOTHESIS AND THEORY
published: 27 January 2022
doi: 10.3389/fpls.2021.735020

Cryogenian Glacial Habitats as a Plant Terrestrialisation Cradle – The Origin of the Anydrophytes and Zygnematophyceae Split

Jakub Žárský[1], Vojtěch Žárský[2,3], Martin Hanáček[4,5] and Viktor Žárský[6,7]*

[1] CryoEco Research Group, Department of Ecology, Faculty of Science, Charles University, Prague, Czechia, [2] Department of Botany, University of British Columbia, Vancouver, BC, Canada, [3] Department of Parasitology, Faculty of Science, Charles University, BIOCEV, Vestec, Czechia, [4] Polar-Geo-Lab, Department of Geography, Faculty of Science, Masaryk University, Brno, Czechia, [5] Regional Museum in Jeseník, Jeseník, Czechia, [6] Laboratory of Cell Biology, Institute of Experimental Botany of the Czech Academy of Sciences, Prague, Czechia, [7] Department of Experimental Plant Biology, Faculty of Science, Charles University, Prague, Czechia

OPEN ACCESS

Edited by:
Eric Marechal, UMR 5168 Laboratoire de Physiologie Cellulaire Vegetale (LPCV), France

Reviewed by:
Denis Baurain, University of Liège, Belgium
Alberto Amato, CEA Grenoble, France

***Correspondence:**
Jakub Žárský
jakub.dan.zarsky@gmail.com

Specialty section:
This article was submitted to Marine and Freshwater Plants, a section of the journal Frontiers in Plant Science

Received: *01 July 2021*
Accepted: *17 December 2021*
Published: *27 January 2022*

Citation:
Žárský J, Žárský V, Hanáček M and Žárský V (2022) Cryogenian Glacial Habitats as a Plant Terrestrialisation Cradle – The Origin of the Anydrophytes and Zygnematophyceae Split. Front. Plant Sci. 12:735020. doi: 10.3389/fpls.2021.735020

For tens of millions of years (Ma), the terrestrial habitats of Snowball Earth during the Cryogenian period (between 720 and 635 Ma before present–Neoproterozoic Era) were possibly dominated by global snow and ice cover up to the equatorial sublimative desert. The most recent time-calibrated phylogenies calibrated not only on plants but on a comprehensive set of eukaryotes indicate that within the Streptophyta, multicellular charophytes (Phragmoplastophyta) evolved in the Mesoproterozoic to the early Neoproterozoic. At the same time, Cryogenian is the time of the likely origin of the common ancestor of Zygnematophyceae and Embryophyta and later, also of the Zygnematophyceae–Embryophyta split. This common ancestor is proposed to be called Anydrophyta; here, we use anydrophytes. Based on the combination of published phylogenomic studies and estimated diversification time comparisons, we deem it highly likely that anydrophytes evolved in response to Cryogenian cooling. Also, later in the Cryogenian, secondary simplification of multicellular anydrophytes and loss of flagella resulted in Zygnematophyceae diversification as an adaptation to the extended cold glacial environment. We propose that the Marinoan geochemically documented expansion of first terrestrial flora has been represented not only by Chlorophyta but also by Streptophyta, including the anydrophytes, and later by Zygnematophyceae, thriving on glacial surfaces until today. It is possible that multicellular early Embryophyta survived in less abundant (possibly relatively warmer) refugia, relying more on mineral substrates, allowing the retention of flagella-based sexuality. The loss of flagella and sexual reproduction by conjugation evolved in Zygnematophyceae and zygomycetous fungi during the Cryogenian in a remarkably convergent way. Thus, we support the concept that the important basal cellular adaptations to terrestrial environments were exapted in streptophyte algae for terrestrialization and propose that this was stimulated

by the adaptation to glacial habitats dominating the Cryogenian Snowball Earth. Including the glacial lifestyle when considering the rise of land plants increases the parsimony of connecting different ecological, phylogenetic, and physiological puzzles of the journey from aquatic algae to terrestrial floras.

Keywords: plant evolution, Cryogenian glaciation, Streptophyta, Charophyta, Anydrophyta, Zygnematophyceae, Embryophyta, Snowball Earth

INTRODUCTION–THE TIMING OF THE TERRESTRIAL FLORA RISE

The timing of the evolution of terrestrial flora, the branching of Streptophyta lineages resulting in Embryophyta establishment, and their further diversification have been a subject of interest since the 19th century. The most recent debate is fueled by the emergence of large genomic and transcriptomic datasets (summarized in Rensing, 2020). The categorization of terrestrialization is used differently in different contexts. It is often mixed with the wet-to-dry transition, e.g., in some chlorophyte or streptophyte aerophytic algae (for terrestrialisation in the geology context see further). The wet-to-dry transition of some streptophyte algae might be a very initial part of following terrestrialization. However, during this report, we use the category of terrestrialization *sensu stricto* as only related to the establishment of Embryophyta–land plants–starting, however, in the common ancestor of Embryophyta and Zygnematophyceae–anydrophytes (see further).

The investigation of these ancient events is based on a combination of data sources, and there are apparent challenges linked with their interpretations. Firstly, an almost complete lack of fossil record of transition stages of terrestrialization in addition to the extinction of the close relatives of the early land plants. This was highlighted recently by the support of the monophyly of the Bryophyta as the sister clade to Tracheophyta (Nishiyama et al., 2004; Civáň et al., 2014; Cox et al., 2014; Puttick et al., 2018), leaving a larger gap in our understanding of the land plant evolution. There are still textbooks in use that state the assumption that the Tracheophyta evolved from Bryophyta, which is a scenario now invalidated. Secondly, the uncertainty of the timing estimates (contrasting predictions and large confidence intervals) based on molecular clock reaching deeper back in time. And thirdly, there is difficulty with interpreting an independent source of information on primary production on land provided by the geological/geochemistry record, as it has almost no taxonomic resolution.

Fossil Evidence of Terrestrialization

Due to the well-acknowledged poor fossilization of plant remnants, spores are considered to be the best early markers of land plant occurrence. Currently, the oldest trilete spores (narrow Y shape lines radiating from a spore surface center indicating an origin in a single meiosis quadruple structure product) assignable to Embryophyta are known from the Upper Ordovician (Steemans et al., 2009; Edwards et al., 2014; Rubinstein and Vajda, 2019), along with poorly preserved seemingly polysporangiate mesofossils (Salamon et al., 2018). The widespread occurrence of non–trilete cryptospores–i.e., variable first spore types of the presumptive terrestrial origin without trilete scar–(Edwards et al., 2014) in the Ordovician, starting in the middle Ordovician (Dapingian), is proposed to be a sign for the great Ordovician diversification of land plants (Servais et al., 2019). Current data support the hypothesis that in the Ordovician, there were already diversified tiny, possibly polysporangiate, cryptophyte-type floras. During the following Silurian, cryptospores producing plants decline while trilete producers prevail (Pšenička et al., 2021). It is important to note that cryptophytes *sensu* Edwards (Edwards et al., 2014) are extinct plants producing cryptospores, not to be confused with Cryptophyceae algae. Therefore the very first adaptations of Streptophyta to the dry land occurred much earlier, most probably in the Precambrian (Hedges et al., 2018; Servais et al., 2019; Shinohara and Nishitani, 2021; Strassert et al., 2021; Su et al., 2021). The first Silurian flora documented by macrofossils (e.g., Cooksonia, Baragwanathia) suggests an undocumented evolution and diversification of land plants preceding the earliest known fossils (Pšenička et al., 2021). We will discuss the potential importance of Cryogenian acritarchs for understanding the evolution of land plants in section "Zygnematophyceae Diverged From Multicellular Anydrophytes Later in the Cryogenian, Adapting to Ice–Dominated Surface" and the "Discussion."

Time-Calibrated Phylogeny

The land plants (Embryophyta), along with their algal relatives (streptophyte algae), constitute a clade called Streptophyta. Together with the algal group Chlorophyta and a small group Prasinodermatophyta, they constitute the green plants (Viridiplantae; Li et al., 2020). The deepest basal lineage of Streptophyta is formed by the unicellular biflagellate monotypic genera *Mesostigma*, described as a rarely but regularly occurring inhabitant of freshwater phytobenthos in wintertime (Lauterborn, 1894), and an aerophytic colonial monotypic genera *Chlorokybus* (Lemieux et al., 2007). The algal representatives of Streptophyta further include the filamentous Klebsormidiophyceae (Stewart and Mattox, 1975). Klebsormidiophyceae have biflagellate zoospores and combine the features of the early Streptophyta with terrestrial plants due to remarkable stress tolerance of vegetative cells (Holzinger et al., 2014). These three lineages are also referred to as the "lower-branching KCM grade" of Streptophyta (Klebsormidiophyceae, Chlorokybophyceae, and Mesostigmatophyceae, de Vries and Archibald, 2018). A further distinct streptophyte lineage is Charophyceae (Rabenhorst, 1870), characterized by their complex multicellular body architecture, which intuitively led to their traditional placement as the sister group to plants from

the 19th century until the early molecular studies (Karol et al., 2001). Together with the lineages Coleochaetophyceae (Delwiche et al., 2002) and Zygnematophyceae (= Conjugatophyceae, Guiry, 2013; Cheng et al., 2019), they are referred to as "higher branching ZCC-grade" of Streptophyta by de Vries and Archibald (2018)–along with Embryophyta called Phragmoplastophyta. The recently generally accepted topology of the streptophyte phylogenetic tree recognizes Zygnematophyceae as the closest living lineage to land plants (Clarke et al., 2011; Wodniok et al., 2011; Wickett et al., 2014; Morris et al., 2018b; Leebens-Mack et al., 2019; Su et al., 2021). Rensing (2020) proposed to call the common ancestor of Zygnematophyceae and Embryophyta "Anydrophyta"–pointing out their key drought-resistant abilities. We use anydrophytes throughout this report instead, as this name is not yet generally accepted as part of the plant systematic nomenclature. New molecular clock analyses (Strassert et al., 2021; Su et al., 2021) date the main splits of the streptophyte lineages and the split between Zygnematophyceae and Embryophyta way earlier than the estimates based on the appearance of the first spores in the fossil material (**Figures 1A**, **2**) or even relatively recent influential time-calibrated phylogeny by Morris et al. (2018b). The new time-calibrated phylogenies based on the Viridiplantae (Su et al., 2021) and Eukaryota (Strassert et al., 2021) suggest a likely Cryogenian origin of anydrophytes as well as the split of Zygnematophyceae. This dating was indicated very recently by Shinohara and Nishitani (2021) for Zygnematophyceae and acknowledged as a possibility by Lutzoni et al. (2018) and Jiao et al. (2020).

Isotopic and Chemical Evidence of Early Land Plants in the Geological Record–Green Cryogenian

There is an independent line of evidence integrating the signal of terrestrial productivity over large temporal and spatial scales, namely, the isotopic composition of marine sediments containing interstitial precipitates with a distinct isotopic fingerprint (Fayek et al., 2001). There is evidence for significant terrestrial primary production from the isotopic analyses of the Neoproterozoic marine interstitial carbonates based on combined oxygen and carbon isotope data (Knauth and Kennedy, 2009; Cole et al., 2020). These studies suggest that the terrestrial expansion of photosynthesizing communities preceded the significant climate perturbations of the Neoproterozoic glaciations. It needs to be noted that the term "terrestrialization" is understood often differently among biologists *versus* geologists (see also a distinction to wet-to-dry transition discussed above). Biologists define it as organisms inhabiting soils, surfaces of rocks–dry land in contrast to water inhabitants, while geologists mean inhabited surface of the whole continents, which also includes aquatic habitats as lakes, rivers, and melting glaciers. The conclusions of Knauth and Kennedy (2009) on the late Precambrian greening are formulated in the latter sense; they compared the signal of exploding terrestrial photosynthesizing communities with phanerozoic terrestrial primary production where there is no doubt about its origin in terrestrial habitats. Moreover, the study of Hoshino et al. (2017) finds that C_{29} 24-ethylsteranes are systematically absent from sediments deposited before the onset of the Snowball Earth events but are present in rocks deposited during and directly after the Marinoan glaciation. These findings imply an origin of stigmasteroid biosynthesis, compounds characteristic of photosynthetic Eukaryota, during the glaciation. The authors concluded that this extended glaciation period was an evolutionary stimulant rather than just a bottleneck (Hoshino et al., 2017). We can thus draw a simplified framework where fossil record shows solid evidence for already complex multicellular land plants (Embryophyta) in the Ordovician/Silurian (Pšenička et al., 2021). Molecular data models extend the possible timing for the origin of the anydrophytes and phylogenetic split between Zygnematophyceae and Embryophyta to either the Mesoproterozoic to early Neoproterozoic (Su et al., 2021), the Cryogenian (Strassert et al., 2021), or the Ediacaran/Cambrian (Morris et al., 2018a; see also **Figure 1**). Additionally, the rise in terrestrial primary productivity documented in sedimentary geologic isotopic records dates to the Tonian and Cryogenian (Knauth and Kennedy, 2009) or, based on sterol biosynthesis evolution, to the final Marinoan glaciation (Hoshino et al., 2017). It is likely that missing fossil evidence of earlier evolutionary stages of land floras is related not only to their poor ability to fossilize (rather than their absence) but also to the Rodinia continent break up and erosion of the Cryogenian. This allows us to infer that the Cryogenian origin of the first land floras is a highly parsimonious scenario and needs to be further critically considered and developed due to the important implications for the physiology and ecology of early terrestrial floras and extant land plants.

PALEOGEOGRAPHY OF THE CRYOGENIAN

When searching for critical aspects or features of the environment inhabited by the ancestors of the Embryophyta, speculation is inevitable, except for one generally accepted feature: their freshwater origin (Wodniok et al., 2011; de Vries et al., 2016; for deeper evolution and freshwater see Sánchez-Baracaldo et al., 2017; for review see Rensing, 2020). Thus, we focus on the presence, character, and spatiotemporal extent of the freshwater habitats in the mid to late Neoproterozoic world–especially in the Cryogenian.

The Cryogenian marks the period when the supercontinent Rodinia broke up. At the beginning of the Cryogenian (720 Ma), the first rift basins developed in the continental crust of Rodinia, and in 635 Ma (i.e., at the end of Cryogenian), the continued rifting resulted in the break-up of the supercontinent into several blocks (Li et al., 2013). The early advanced chemical weathering of the Rodinia continent resulted in the sequestration of the atmospheric carbon dioxide (CO_2) in quantity sufficient for global cooling, resulting in the Snowball Earth glaciation conditions (Hoffman and Schrag, 2002). Under these conditions, the oceans were covered with sea ice, and the glaciers covered most of the Rodinia land surface between 0–70° latitude (Li et al., 2013). There are two major glaciations

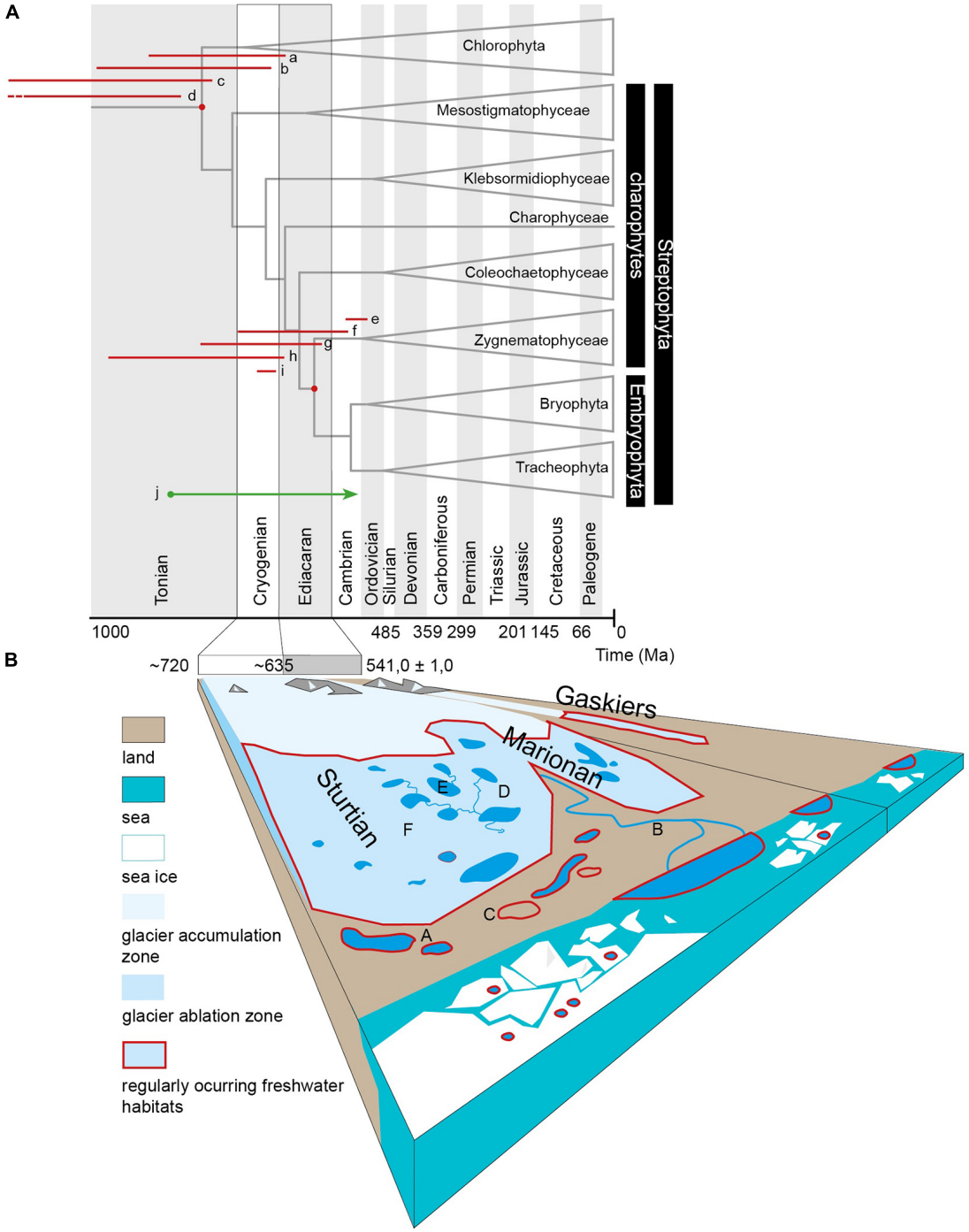

FIGURE 1 | (A) The phylogenetic tree with time estimates for the splits of Chlorophyta–Streptophyta and Zygnematophyceae–Embryophyta. Tree adapted from Morris et al. (2018b), projected over timescale based on international geostratigraphic chart (2020). The red lines at the respective node represent 95% highest posterior densities of estimates presented by Hedges et al. (2018), Morris et al. (2018b), Strassert et al. (2021), and Su et al. (2021): a–Streptophyta, Morris et al. (2018b) all calibrations, b–Streptophyta, Hedges et al. (2018) Mesozoic calibrations, c–Streptophyta, Hedges et al. (2018) Spermatophyta calibration, d–Streptophyta, Strassert et al. (2021), e–Embryophyta, Morris et al. (2018b) all calibrations, f–Embryophyta, Hedges et al. (2018) Mesozoic calibrations, g–Embryophyta, Hedges et al. (2018) Spermatophyta calibration, h–Embryophyta, Su et al. (2021), Strassert et al. (2021). j–Influx of terrestrial carbon is apparent in carbonates younger than 850 Ma, according to a study of Knauth and Kennedy (2009), who infer an explosion of photosynthesizing communities on late Precambrian land surfaces. **(B)** Schematic presentation of the potential freshwater habitats in a low latitude Cryogenian catchment. The picture represents habitats populated by members of streptophyte algae in the current biosphere (A) Lentic habitats (*Mesostigma, Chara*), (B) fluvial habitats with various *Zygnematophyceae* in the phytobenthos and e.g., *Coleochaete* on submerged surfaces, (C) subaeric habitats, moist or periodically submerged surfaces, and biological soil crusts (e.g., *Klebsormidium*, *Chlorokybus*, and some *Zygnematophyceae*).

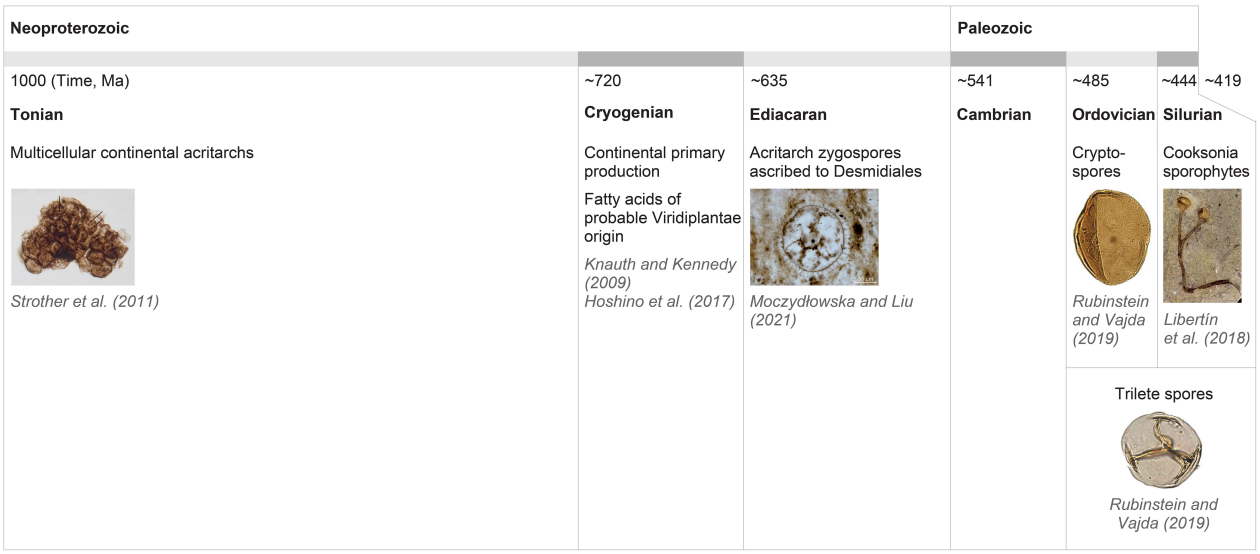

FIGURE 2 | Paleontological and geological evidence for the continental (most probably eukaryotic) organisms and primary production by photosynthetic organisms/plants from the Neoproterozoic through Cryogenian to the early Paleozoic. For our hypothesis, the existence of desmids in the early Ediacaran, as indicated by the Acritarch zygospores ascribed to Desmidiales (Moczydłowska and Liu, 2021), is of central importance.

recognized over the course of Cryogenian; the Sturtian and the Marinoan. The Snowball Earth hypothesis assumes complete glaciation of the Earth's surface (Hoffman and Schrag, 2002), which would intuitively turn the biotic colonization of the continents impossible. However, as summarized and discussed by Eyles (2008), the Snowball Earth glaciations possibly took place as a series of consecutive geo-tectonically predisposed regional glaciations. In the Marinoan glacial epoch, the sedimentological and geochemical records support a deglaciation interval with the onset of glaciolacustrine, non-glacial lacustrine, and ice-free marine conditions (Wang et al., 2008; Williams et al., 2008; Hoffman et al., 2012, 2017). The continents were possibly not completely glaciated even in the maxima of actual glaciation epochs. Exposed alluvial plains and tidal flats allowed the development of subaeric periglacial zones with permafrost (Retallack et al., 2015; Bai et al., 2020). The constituents of petroleum phytane, pristane (isoprenoid alkanes formed from phytol, a constituent of chlorophyll), and sterane (derived from steroids or sterols) in marine sediments provide evidence that there was no break in the activity of photosynthetic eukaryotes during the Cryogenian glacial epochs (Wang et al., 2008; Hoshino et al., 2017). The Neoproterozoic land system differed from the Phanerozoic by the absence of a continuous vegetation cover with a root system (Bose et al., 2012). The Neoproterozoic land system was thus similar to recent arid regions, or the continental polar areas. The dominant terrestrial environment was alluvial plains with unstable riverbeds even though meandering rivers also occurred (Barkat et al., 2020). Along the coast, there were river deltas and tidal flats where the eolic sedimentation of loess and wadded sands also took place (Williams et al., 2008; Retallack, 2011). Additionally, the surface of melting glaciers must be included within the list of potential freshwater habitats.

Habitats occupied by members of streptophyte algae in the current biosphere are represented in **Figure 1**. For lentic habitats, *Mesostigma* or *Chara* are typical, lentic to slow fluvial phytobenthos often hosts various *Zygnematophyceae*; and the subaeric, moist, or periodically submerged surfaces are occupied by *Klebsormidium* and also *Chlorokybus* or *Coleochaete* and some *Zygnematophyceae*. To some extent, recent supraglacial habitats represent functional analogs to all three previous types of habitats *via* supraglacial lakes and cryoconite melt ponds as lentic habitats, supraglacial streams as fluvial habitats, and by the melting surface of bare ice as a functional analog to subaeric habitat where desiccation is substituted by freezing as the main physiological stress. The last-named habitat is typically inhabited by zygnematophycean genera *Mesotaenium*, *Ancylonema,* and *Cylindrocystis,* where the first two taxa develop regularly large-scale blooms, e.g., on the Greenland ice sheet, but are reported in the ablation zones of glaciers worldwide (**Figure 1B**; Williamson et al., 2019).

Any glacial system in or close to balance with a climate, which allows the hydrological cycle to develop, must have an ablation zone where melting periodically occurs on an annual (polar areas) or daily (tropics) basis (Benn and Evans, 2010). For organisms that can cope with the supraglacial conditions, this environment can provide a habitat for long-term survival (Hodson et al., 2008; Anesio and Laybourn-Parry, 2012; Stibal et al., 2012). It includes different kinds of cyanobacteria and algae (Yallop et al., 2012; Lutz et al., 2018; Williamson et al., 2019), but sometimes also moss balls ("glacier mice") which are able to sustain cold-adapted invertebrates (Zawierucha et al., 2015, 2021) and the populations possibly survive over Holocene timescale (Heusser, 1972). However, in the polar glacial condition, the moss life cycle is disrupted and reduced to a vegetative phase, missing

sexual reproduction (e.g., Hotaling et al., 2020) in contrast to glacial Zygnematophyceae (e.g., Permann et al., 2021a,b; Procházková et al., 2021).

ADAPTATIONS TO COLD, SNOW, ICE, DROUGHT, AND HIGH IRRADIANCE EXPOSED CONDITIONS OF CRYOGENIAN AND THE EVOLUTION OF ANYDROPHYTES AND THEIR CELLULAR EXAPTATIONS FACILITATING FURTHER TERRESTRIALIZATION

Plant terrestrialization or land plant evolution started most probably at the single-cell stage of Streptophyta evolution by the first wet-to-dry transition–i.e., before the complex multicellularity evolved (Stebbins and Hill, 1980; Becker, 2013; Harholt et al., 2016). Certain aerophytic Chlorophyta adapted on the cellular level to dry land conditions (i.e., were subject to wet-to-dry transition), most probably even much earlier in the Proterozoic (Strassert et al., 2021; Su et al., 2021; Zhang et al., 2021). This hypothesis was recently further supported by studies of the plant cell wall and stress response evolution (Harholt et al., 2016; de Vries et al., 2018; Jensen et al., 2018). The streptophyte algae were living on the land for some time before the emergence of land plants (Harholt et al., 2016). Similarly, de Vries et al. (2018) show that the embryophyte stress signaling evolved in the algal progenitors of land plants. However, environments similar to our extant freshwater to land transitions (lake shores, periodic water bodies, wet aerophytic algae environments) are considered as possible terrestrialisation biotopes in most published cases (e.g., Fürst-Jansen et al., 2020; Rensing, 2020). Based on our new scenario, Streptophyta dry land adaptation started on a single cell level in the late Mesoproterozoic/Tonian before the Cryogenian glaciations. It continued until the establishment of multicellular lineages of Streptophyta–Charophyceae and Coleochaetophyceae in the Mesoproterozoic or the Tonian (at the beginning of the Neoproterozoic). Here, we argue and hypothesize that the tens of millions of years of prevalently cold or freezing environments of the Cryogenian period is the key environmental factor that crucially shaped future land plant cellular adaptations. These adaptations turned to exaptations in Embryophyta exposed to terrestrial conditions and their transition to the dry land.

Rensing (2020) highlighted the ability to survive desiccation as a key factor in the terrestrial ancestors of Zygnematophyceae and Embryophyta. However, we emphasize that on physical, physiological, and molecular levels, the stress imposed by desiccation has similar consequences on the plant organisms as the stress imposed by freezing. The surfaces of recent glaciers with bare ice inhabited by simple Zygnematophyceae (Williamson et al., 2019) and cryoconite occasionally colonized by long term populations of vegetatively propagating mosses (Heusser, 1972; Belkina and Vilnet, 2015) are a living example of survival and growth strategies on glacial surfaces with possible implications for their common ancestor. Life on a melting glacial surface has one crucial advantage over life in the proglacial area in terms of the predictability of water availability driven by seasonal or daily changes in insolation. The production of liquid water can be facilitated by the attachment of organisms to darker particles with lower albedo than the surrounding ice, as observed in globular mosses (glacier mice) attaching to and accumulating cryoconite sediment (Porter et al., 2008; Belkina and Vilnet, 2015). Alternatively, the same effect can be achieved by lowering the albedo of the cells by production and accumulation of pigments, such as purpurogallin in the case of glacial Zygnematophyceae (Remias et al., 2012). Accepting the supraglacial habitats such as cryoconite pans (Hoffman, 2016), lakes, melting snow, or melting bare ice inhabited by Cryogenian Chlorophyta and Streptophyta as freshwater aquatic habitats (**Figure 1B**) has important implications for understanding early land plant adaptations and refugia in the Cryogenian context. We emphasize this aspect, especially when generating a hypothetical yet realistic scenario for the survival of multicellular (though small and simple) anydrophytes.

Recent genomic analyses of the basal Streptophyta representatives (*Mesostigma* and *Chlorokybus*) and inference for their common ancestor indicate terrestrial adaptations of the photosynthetic apparatus. This is especially true when considering adaptations to high irradiance (photo-oxidative damage and photorespiration) and transcription factors (TFs) regulating dry land stress responses (Wang et al., 2020). Many studies of both Embryophyta and streptophyte algae indicate a tight coupling between the adaptation to high irradiation and cold and drought stress (e.g., de Vries et al., 2017, 2018; Chen X. et al., 2021). These stresses result in the major energetic cellular disbalance and reactive oxygen species (ROS) production and are best studied in model plants, esp. *Arabidopsis* (e.g., Kilian et al., 2007; Rasmussen et al., 2013). de Vries et al. (2018) systematically compared KCM (basal) v. ZCC (Zygnematophyceae, Coleochaetophyceae, Charophyceae) streptophyte algae and concluded more elaborated stress response, especially toward the cold in ZCC-grade streptophyte algae. The intimate connection between drought and cold/freeze stresses are well documented in C-repeat binding factor/dehydration responsive element binding factor (CBF/DREB – dehydratation-responsive element-binding protein) TFs functional involvement, and it is clear that their evolution was boosted in Streptophyta, especially in the lineage leading to Embryophyta (Jiao et al., 2020; Rensing, 2020). The activation of DREB TFs is positively regulated by the inducer of CBF expression 1 (ICE1) transcriptional regulator, which is a direct target of Open Stomata 1 (OST1) kinase (Zhu, 2016; Chen X. et al., 2021). OST1 (a member of the SNF1-related protein kinases 2/SnRK2 family), which was originally identified for its role in stomatal closure (Mustilli et al., 2002), is the central regulator of the cold signaling pathway *via* the activation of DREB TFs (Lamers et al., 2020; Chen X. et al., 2021). The CKIN2 (A) family of proteins in chlorophyte *Chlamydomonas reinhardtii* is closely related to the

land plant SnRK2 and contains a conserved SnRK2 box and abscisic acid (ABA) box (but without relation to ABA-dependent signaling which evolved later in Embryophyta) after the kinase domain (Komatsu et al., 2020). The ABA box of *C. reinhardtii* CKIN2 (A) is smaller and contains fewer acidic residues than in *Arabidopsis*. Obvious SnRK2s with an ABA box similar to land plants have been identified in *Klebsormidium* (Komatsu et al., 2020). The overall conservation of sequence structure and gene expression profile strongly links CKIN2 and abiotic stress response regulation. Indeed, many CKIN2s are expressed in response to abiotic stresses, such as hyperosmolarity, ultraviolet (UV) radiation exposure, and low temperatures (Colina et al., 2019; Komatsu et al., 2020). In response to the cold, SNRK2/OST1 phosphorylates the TFs ICE1, in addition to Basic Transcription Factor3 (BTF3; Ding et al., 2015, 2018). Low-temperature-induced OST1 phosphorylation activity is upregulated independently of the plant hormone ABA, a known inducer of OST1 activity in response to osmotic stress (Ding et al., 2015). The OST1/SNRK2 kinase of land plants evolved early in Streptophyta, and SNRK2 from *Klebsormidium nitens* complements quadruple mutant in moss (Shinozawa et al., 2019). It would therefore be interesting to test its functions during cold adaptation.

Late embryogenesis abundant (LEA) proteins protect other cytoplasmic proteins from aggregation during desiccation, osmotic, and low-temperature stress conditions (Shinde et al., 2012). Among several sub-clades of LEA proteins, LEA2 proteins are not found in chlorophyte algae, suggesting they evolved after the split of Chlorophyta and Streptophyta (Becker et al., 2020). A newly evolved class of LEA proteins might provide essential protection to cellular proteins during cold/freeze stress in addition to desiccation. The anydrophytes evolved two additional subfamilies for better protection (Becker et al., 2020) and we propose that this happened under the environmental pressure of Cryogenian glaciations.

The origin of anydrophytes (and later also the Zygnematophyceae) was linked to several crucial horizontal gene transfers (HGTs)–facilitated by the co-existence of streptophyte algae with different kinds of microbes and fungi on the surfaces of land (Lutzoni et al., 2018; Chen R. et al., 2021; Shinohara and Nishitani, 2021). Three TF families (GRAS, HDKNOX2, and BBR/BPC), a homolog of the PYR/PYL/RCAR-like ABA receptor and genes involved in 1,4 b-xylan formation (GUX1–5, PARVUS) and galactan/RG I pectin synthesis (GALS1-3), were likely gained in the common anydrophyte ancestor of Zygnematophyceae and Embryophyta (Cheng et al., 2019). Interestingly, Jiao et al. (2020) found that the desiccation regulating TFs of the GRAS and DREB families expanded in representatives of Desmidiales, *Penium* (Rensing, 2020).

The evolution of land plant chloroplast–embryoplast–with innovations as resistance to exposure to high light stress and desiccation, transfer of particular genes to the nucleus, and the emergence of additional control mechanisms could be hypothesized as being promoted during the Cryogenian glaciations in anydrophytes and then became exaptations for the ongoing terrestrialization (de Vries et al., 2016). We postulate that an important phase of the evolution of the embryoplast occurred during the Cryogenian and its glaciations. For example, the transfer of specific genes from the plastid to the nuclear genome and the evolution of nuclear-encoded plastid RNA polymerase/NEP (de Vries et al., 2016; Cheng et al., 2019).

The exposure of early streptophyte algae to high irradiance (including UV light) under the prevalent cold glaciation conditions of Cryogenian land surfaces might be potentially linked to the well documented large regulatory overlap in stress gene expression reaction to high irradiance, drought, and cold stresses (de Vries et al., 2018; Chen X. et al., 2021). Moreover, the light signal is necessary to fully develop cold (not heat) acclimation (Catalá et al., 2011). This is best studied in the *Arabidopsis* model, where it was shown that this signaling input into the cold adaptation is mediated by HY5 bZIP TF and the COP1 photomorphogenesis regulator is also possibly involved (Catalá et al., 2011). While COP1 was present already in the Archaeplastida ancestor, the HY5 TF evolved only in the common Chlorophyta and Streptophyta ancestor. Low-temperature pathways stimulated by HY5 include genes encoding chalcone isomerase (CHI), chalcone synthase (CHS), and flavonol synthase (FLS). These are three key enzymes in the anthocyanin biosynthetic pathway, important in cold response and especially in high irradiation protection due to their antioxidative/anti-ROS properties (Saigo et al., 2020). The key enzyme in the phenylpropanoid pathway (PAL) was acquired by horizontal gene transfer (HGT) in Streptophyta (Emiliani et al., 2009; Cheng et al., 2019), and precursors of the lignin biosynthetic pathway were possibly involved in stress responses and biotic interactions in basal Streptophyta (de Vries et al., 2017). Blue–light receptor phototropin (evolved previously in a common ancestor of Viridiplantae – Li et al., 2015) was found to function as a cold sensor in the liverwort *Marchantia polymorpha*, suggesting that low temperature and light cues are integrated immediately at the sensor level (Fujii et al., 2017). Phytochromes, which are crucial for red light signaling and temperature stress signaling, evolved in a common ancestor of Streptophyta (Han et al., 2019; Wang et al., 2020). Data from Angiospermophyta indicate that phytochromes can also contribute to the regulation of the isoprenoid metabolism in response to the temperature shift (Bianchetti et al., 2020).

The detailed experimental analysis summarized above clearly shows that the co-regulation of high light and cold stress responses is present already in basal Streptophyta. This co-regulation led de Vries et al. (2017) to conclude that embryophyte stress signaling had already evolved in streptophyte algae. Data from other studies (de Vries J. et al., 2020; Jiao et al., 2020; Wang et al., 2020) supports the interpretation proposed by de Vries et al. (2017) and Fürst-Jansen et al. (2020). We argue that these basal cellular adaptations to dry land in the streptophyte lineage evolved in a long cold and freezing period of the Cryogenian. Therefore, we postulate that adaptations to cold oligotrophic freshwater and periodic freezing/desiccation high irradiance exposed land conditions were later co-opted as exaptations that allowed multicellular early Embryophyta to continue in the transition to dry land in the warm Ediacaran period (Retallack, 2013).

ZYGNEMATOPHYCEAE DIVERGED FROM MULTICELLULAR ANYDROPHYTES LATER IN THE CRYOGENIAN, ADAPTING TO ICE–DOMINATED SURFACES

Current dating (e.g., Jiao et al., 2020; but also above summarized other timing reports) excludes the original hypothesis of Becker (2013), which proposes that the Streptophyta and Chlorophyta split occurred during the Cryogenian, as the Streptophyta lineage emerged most probably before or during the Tonian (e.g., Cheng et al., 2019; Jiao et al., 2020; Strassert et al., 2021). As we propose above–an interesting and appealing possibility opened by these recent timings is that multicellular streptophyte algae evolved at or even before the Tonian, and anydrophytes clade of Streptophyta evolved at the beginning or during the first part of the Cryogenian (Jiao et al., 2020; Strassert et al., 2021). Crucial to the further elaboration of our hypothesis is the dating of the diversification of Zygnematophyceae from anydrophytes to within the Cryogenian (Strassert et al., 2021). We propose that the Cryogenian encompasses, firstly, the anydrophyte evolution from the common multicellular streptophyte algae ancestor (closest relatives are Coleochaetophyceae). Secondly, the diversification into extremely cold-adapted cryophilic early Zygnematophyceae (Conjugatophyceae) and early Embryophyta, later in the Cryogenian. Embryophyta were not reduced to single-cell/filamentous level (see further) and also kept flagellated cells, with sexual processes based on motile gametes. It is possible to speculate that early Embryophyta survived the Cryogenian glaciations as a minority flora in the relatively warmer edaphic refugia. It is reasonable to consider that the Cryogenian continental greening (see above Knauth and Kennedy, 2009; Hoshino et al., 2017) was dominated not only by terrestrial Chlorophyta and single-cell/filamentous streptophytes (Lutzoni et al., 2018) but also, and maybe especially, by anydrophytes and later also extremely well cold-adapted early Zygnematophyceae. Therefore, we propose that the biota after the onset of the Cryogenian should also include streptophyte anydrophytes, which split later during the Cryogenian into extremely cold-adapted and reduced (from multicellular to unicellular status–see following chapter) early Zygnematophyceae and early Embryopyta lineages. This is in contrast to Knauth and Kennedy (2009), who speculate on the expansion of a primitive land biota possibly composed of protists, mosses, fungi, and liverworts starting by 1 Ga ago.

Stebbins and Hill (1980) argued that the same evolutionary constraint of dry land drove the convergent evolution of Zygnematophyceae and zygomycetous fungi (incl. Mucoromycota; former Zygomycota–Naranjo-Ortiz and Gabaldón, 2019b; Chang et al., 2021) *via* the loss of flagella and sexuality by conjugation. "Zygomycetous" refers to a paraphyletic phylum (Zygomycota), and this in turn to a sexual structure, the zygospore, that is common to most lineages ascribed to it (Naranjo-Ortiz and Gabaldón, 2019b). These authors hypothesize that a fungal transition to icy environmental niches acts as a facilitator of the transition from water to the terrestrial environment. They elaborate *via* the following scenario: (i) Snowball Earth created a diversification of niches, including microbial ones. (ii) Fungi moved into glacial environments as zoosporic predators of algae, and (iii) necrotic algal mass supported the evolution of hyphal growth and osmotrophy, loss of flagella, the evolution of conjugation, and resistant zygospores (Naranjo-Ortiz and Gabaldón, 2019b). Here we develop a similar hypothesis, suggesting that the split of conjugating Zygnematophyceae from anydrophytes happened under the same selective pressure of Cryogenian glaciations. This is supported by the evidence that the loss of flagella and sex by conjugation of zygomycetous fungi coincides with the Cryogenian glaciations (Taylor and Berbee, 2006; Lutzoni et al., 2018; Naranjo-Ortiz and Gabaldón, 2019a; Chang et al., 2021). Sexuality based on mere conjugation without flagellated gametes is more effective (and therefore evolutionarily more adaptive) for the life cycle completion in comparison to flagellated gamete mediated sexuality of other Cryogenian land inhabiting organisms. It is generally accepted that in contrast to microbes or single-cell organisms, the lower limit for the completion of the life cycle in multicellular organisms (except for endothermic animals) appears to be between 0 and 2°C (Clarke et al., 2013). Basal bodies and flagella are functionally constrained in glacial conditions. This even applies to snow-adapted chlorophyte flagellates*; Haematococcus pluvialis* become cysts in response to cold stress (de Carpentier et al., 2019), and *Chlamydomonas nivalis* cells resorb their flagella after a temperature downshift (Valledor et al., 2013). The microtubular cytoskeleton in plants is sensitive to cold conditions (Nick, 2013), and it is generally accepted that cold-resistant microtubular networks are much less dynamic, while dynamic microtubules are overly sensitive to the cold (Wallin and Strömberg, 1995).

The overall preference of basal extant Zygnematophyceae to bare ice or extremely oligotrophic low-pH freshwater habitats may be reminiscent of the original early Zygnematophyceae Cryogenian adaptation. This would mean that Chlorophyta (Lutzoni et al., 2018), anydrophytes, early Zygnematophyceae, and early Embryophyta co-evolved and radiated contemporaneously with land fungi already in the Cryogenian. This may also explain an early evolution of symbiosis genes that regulate biotic interactions between plants and microbes in Streptophyta (de Vries and Archibald, 2018; de Vries S. et al., 2020).

Stebbins and Hill (1980), proposed that the conjugation in algae and fungi evolved under the same dry land stress conditions, and independent convergent evolution of conjugation in zygomycetous fungi and Zygnematophyceae supports our conclusions (see above and also the "Discussion"). Moreover, the conjugation among streptophyte algae is a homoplasious feature, resulting from the independent convergent evolution (Cheng et al., 2019), as demonstrated by the streptophyte algal genus *Spirotaenia*, which has been shown to be a member of the Mesostigmatophyceae and not Zygnematophyceae despite conjugation sexual process (Gontcharov and Melkonian, 2004; Wickett et al., 2014)—in both cases potentially linked to glaciation conditions.

Stress resistant zygospores of Zygnematophyceae are covered by surface cell wall sporopollenin-like material (Permann et al., 2021a,b) so we looked into known Cryogenian acritarchs and despite an overall reduction in acritarchs diversity during the Cryogenian (Huntley et al., 2006) few new types of acritarchs appeared, among which it seems to be possible to find forms that can be potentially interpreted as Zygnematophyceae zygospores (Moczydłowska, 2008) even on the ultrastructural level (Moczydłowska et al., 2010). This possibility will undoubtedly require the attention of specialists in the future (see also Discussion–Moczydłowska and Liu, 2021).

EVOLUTIONARY REDUCTION FROM MULTICELLULARITY OF ANYDROPHYTES TO SINGLE-CELL OR FILAMENTOUS STATUS IN ZYGNEMATOPHYCEAE

It is generally assumed that Zygnematophyceae evolved by the reduction or loss of morphological complexity, based on the loss of flagella, plasmodesmata, and apical tip growth (Moody, 2020). This assumption is also well supported by the topology of the phylogenetic tree, as both the sister clade of anydrophytes (Coleochaetophyceae) and the sister clade of Zygnematophyceae (Embryophyta) are multicellular. It was proposed that the different mechanisms of cell division between land plants and Zygnematophyceae resulted partially from the simplification of the phragmoplast of the putative common anydrophyte ancestor in the Zygnematophyceae. In more derived Zygnematophyceae, phragmoplast is lost totally (Buschmann and Zachgo, 2016). We used recently published analyses of the early evolution of land plant receptor kinases (Gong and Han, 2021) and several reports on TF evolution to support the idea of secondary Zygnematophyceae simplification. The comparison of independently evolved multicellular organisms indicates evolutionary multiplication of receptor kinases and TFs–both crucial mediators of intercellular communication and tissue differentiation–as a convergent feature of multicellular animals, land plants, Chlorophyta, and brown algae (Cock et al., 2010; de Clerck et al., 2018). Comparing the data from Cheng et al. (2019), Jiao et al. (2020), and Gong and Han (2021), we conclude that along with Lys-M symbiosis-related and S-domain receptor kinases, some others are lost in Zygnematophyceae. Overall, kinase-associated domain types are significantly reduced in Zygnematophyceae compared to *Chara* or Embryophyta (Gong and Han, 2021). However, an exceptionally high number of different types of TFs are retained in single-cell Zygnematophyceae. This might suggest that secondary reductions in structural complexity toward the unicellular status are not necessarily accompanied by reductions in total TF complements as proposed by Jiao et al. (2020). Using the ratio between evolutionary losses and gains of gene orthologous groups as a proxy of evolutionary reduction, it is evident that in Zygnematophyceae, losses prevail–even in contrast to quite a large proportion of losses in *Chara* (Cheng et al., 2019). For *Chara braunii*, there are 834 gains (G) reported against 667 losses (L) (L/G–0.8). While, for *Spirogloea muscicola*, 479 gains are reported against 578 losses (L/G–1.2), and for *Mesotaenium endlicherianum*, 513 gains are reported against 511 losses (L/G–1.0; based on Cheng et al., 2019). These features of Zygnematophyceae compared to sister clades support the concept of secondary reduction of multicellularity of parental anydrophyte clade in the Zygnematophyceae lineage (**Figure 3**). This secondary simplification of Zygnematophyceae also agrees well with the differences between lower temperature limits for unicellular (−20°C) *versus* multicellular (around 0°C) organisms in respect to the survival and life cycle completion (Clarke et al., 2013) in low temperatures, as discussed above.

DISCUSSION–LIQUID WATER TO ICE PHASE TRANSITION AS A LAND PLANT EVOLUTION DRIVER

The timing of the beginning of the Cryogenian was shifted from 850 to 720 Ma recently (Shields-Zhou et al., 2015), and the nature of the Cryogenian period is the subject of vivid and ongoing discussions (e.g., Hoffman et al., 2017; Bai et al., 2020). Therefore, data published on the Cryogenian before 2015 (including, e.g., acritarchs) should be carefully considered within the context of the current timing. However, in the context of our hypothesis, the consensus that the Cryogenian was millions of years of extremely cold climate dominated by continental glaciations is sufficient. Scenarios for the climate extremity range from severe "Snowball Earth" to milder–"Slushball Earth" (Hoffman et al., 2017; Bai et al., 2020). With the interruption of more than 10 Ma of warmer interlude, the Cryogenian lasted approximately 80 Ma.

The crucial contentious point for our hypothesis is the timing of major evolutionary splits in the streptophyte lineage. Late dating of Streptophyta establishment to the late Tonian/early Cryogenian and the Zygnematophyceae–Embryophyta split to the late Ediacaran or Cambrian as proposed by Morris et al. (2018b) was challenged directly first by Hedges et al. (2018) and others more recently. Particularly relevant are Jiao et al. (2020), Nie et al. (2020), Moczydłowska and Liu (2021), Strassert et al. (2021) and Su et al. (2021), as these studies used different approaches for molecular clock calibrations or dating. Su et al. (2021) was based solely on Archaeplastida data to compare three dating strategies. Here, it was proposed that the Streptophyta lineage was established in the Paleoproteozoic/Mesoproterozoic, and the anydrophytes emergence and diversification into Zygnematophyceae and Embryophyta occurred in the late Tonian or Cryogenian. Strassert et al. (2021) used a robust approach for their calculations which involved the context of the whole Eukaryota. This resulted in the common ancestors of Coleochaetophyceae and Embryophyta—i.e., the immediate ancestor of anydrophytes–being placed essentially within the Cryogenian era. Su et al. (2021) found that studies favoring a Neoproterozoic origin of land plants (980–682 Ma) are constrained by molecular data while those proposing a Phanerozoic origin (518–500 Ma) are constrained more by the fossil record. They highlighted the important contribution

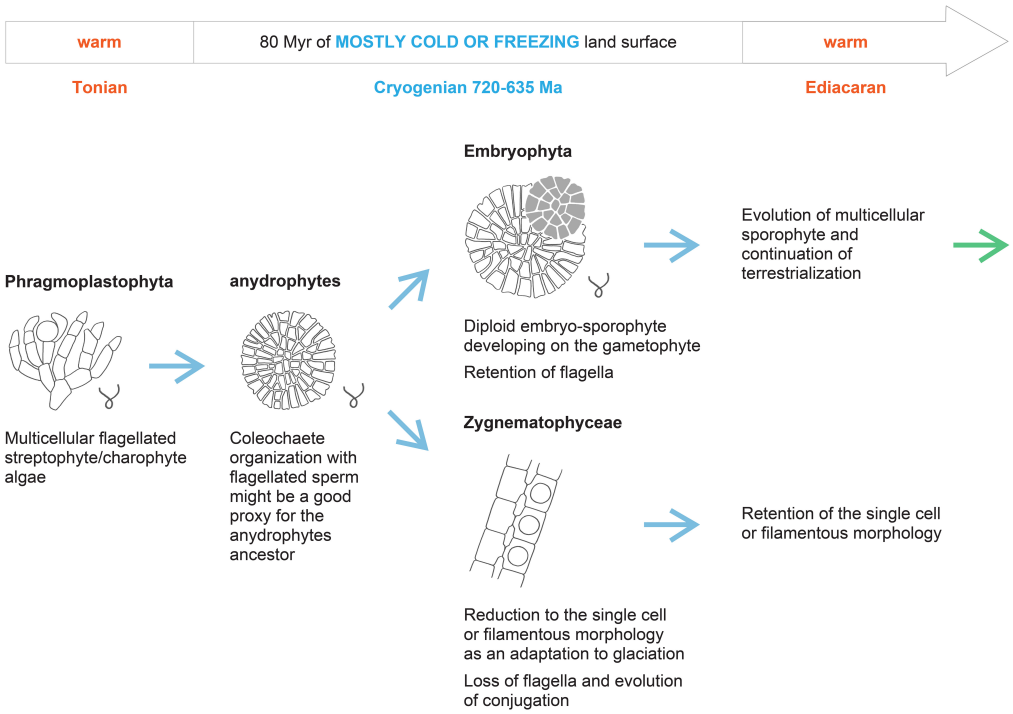

FIGURE 3 | Hypothetical scenario of anydrophyte establishment and Zygnematophyceae split off by the evolutionary reduction under the extended Cryogenian glaciations.

of molecular data (time-dependent molecular change) in the situation of the scarce or very limited fossil record. Importantly, the critical evaluation of how molecular clock-partitioning and fossil calibration strategies affect the uncertainty of evolutionary time scales computation of green plant evolution not only allows but directly indicates possible establishment and diversification of anydrophytes in the Cryogenian (Nie et al., 2020). The time scale ranges of the terrestrial co-evolution of plants and fungi also allow a possibility that the terrestrial colonization by Embryophyta could have occurred as early as 727 Ma (i.e., around the beginning of the Cryogenian; Lutzoni et al., 2018). Timescales by Jiao et al. (2020) also permit the Cryogenian as a possible time of anydrophytes origin and the late Cryogenian as a period of Zygnematophyceae differentiation (Supplementary Table 1E in Jiao et al., 2020). We can therefore conclude that it is reasonable to consider the Cryogenian as a possible time of anydrophyte origin and the diversification of Zygnematophyceae. This is in agreement with the "early" pre-Cryogenian and possibly pre-Tonian timing of the establishment of multicellular streptophyte algae (Su et al., 2021). It also agrees with evidence that Viridiplantae and Rhodophyta were well established by 1,400 Ma (recently based on fossils analyses Zhang et al., 2021; Archaeplastida origin 1,900 Ma, e.g., Strassert et al., 2021), while acritarchs with clear affinity to recent Desmidiales were present in early Ediacaran (Moczydłowska and Liu, 2021; **Figure 2** and see also further).

The current plant terrestrialization timing debate (see above, **Figure 1**), including the emergence of anydrophytes and Zygnematophyceae streptophyte clades, results in consideration of the Cryogenian Snowball Earth, with continents covered by ice, snow, and (periodic) cold freshwater masses as a period relevant to the shaping of plant cellular and developmental adaptations to continental dry land. It is clear that all green algae inhabiting Cryogeninan continents had to adapt to specific chronic glaciations conditions, regardless of the exact timing of Chlorophyta and Streptophyta clades divergences. For example, the case study of *Draparnaldia* chlorophyte aerophytic alga from order Chaetophorales describes how it implements wet-to-dry transition (Caisová, 2020). Recent advancements in deep plant phylogenetics unequivocally resolved *Mesostigma* and *Chlorokybus* as the most basal clade of Streptophyta (Wang et al., 2020). In this context, it is interesting that these extant basal streptophyte algae are oligotrophic, cold-adapted, and are also represented by aerophytic species (*Chlorokybus atmophyticus*). We propose that all early streptophyte lineages living under such conditions were fully adapted to different types of glacial or proglacial environments resulting from tens of Ma of adaptation to the cold Cryogenian. We highlight that they were psychrophilic or cryophilic to different degrees. Current ambient temperature conditions would have been heat stress conditions for them. The evolution of Cryogenian psychrophilic land flora of Chlorophyta, anydrophytes, and later in the Cryogenian also Zygnematophyceae might explain at least part of the geochemical greening of Neoproterozoic (Knauth and Kennedy, 2009; Hoshino et al., 2017), while also contributing to the possible rise in oxygen level before the end of the Cryogenian along with oceanic algal plankton (several models in Cole et al., 2020).

Becker (2013) proposed an interesting hypothesis that Snowball Earth conditions of the long Cryogenian era of the Neoproterozoic were the time of evolutionary split leading to the divergence between the Streptophyta and Chlorophyta lineages. This was based upon the diversification estimates of chlorophyte vs. streptophyte algae in the early 21st century and appreciation of the Cryogenian as an important evolutionary driver for photosynthesis mechanisms. However, we disagree with this scenario because of the improved current time-calibrated phylogeny calculations. Instead, we suggest that the Cryogenian cold and dry continents were the arena for the evolutionary origin of the common Embryophyta–Zygnematophyceae ancestor; anydrophytes. Due to the extended duration of global glaciations, Zygnematophyceae split off from the anydrophytes by simplification as cold-adapted cryophilic flora in later stages of the Cryogenian. Well-established regulatory interconnection between cold/freeze, high light, and drought stress physiological responses is possibly best illustrated by the DREB/CBF TF family regulating drought and cold stress responses (Lamers et al., 2020; Chen X. et al., 2021–see above). Light input into the cold adaptation is mediated by both red light and blue light receptors. It affects the upregulation of anthocyanin antioxidants biosynthesis to protect cells against cold stress enhanced ROS production. This is well documented to be mediated by the DREB/CBF transcriptional regulation in extant land plants (including *Arabidopsis* or *Marchantia*, Fujii et al., 2017; Shi et al., 2018; Bianchetti et al., 2020). This light–cold response coupling feature should also be expected in anydrophytes, as strongly supported by the comparative cold and light stress experiments with basal streptophyte algae *versus* Zygnematophyceae (de Vries et al., 2018).

Inevitably, both green plant lineages–Chlorophyta and Streptophyta–inhabiting continents' surfaces during the Cryogenian era had to pass through the same extended environmental bottleneck. These constraints resulted in the evolution of important cellular and physiological adaptations (wet-to-dry transitions; see above), which then became exaptations within the streptophyte lineage in the early Embryophyta for the further course of actual terrestrialization in the warmer Ediacaran and early Paleozoic. This agrees with the original hypothesis of Stebbins and Hill (1980), updated by Harholt et al. (2016)–that transition/adaptation to land started already on the single-cell level. It is also experimentally supported by de Vries et al. (2018), showing that terrestrialisation might have started on the single-cell level in algae by wet-to-dry transitions.

However, for our point here, it is important that single cell or filamentous Zygnematophyceae evolved from a multicellular ancestor by a reductive process, so that features relevant for the dry land adaptations described specifically for "ZCC-grade" of Streptophyta (de Vries and Archibald, 2018; see above) are not a result of evolution starting at the single-cell level of streptophyte algal organization. In this respect, it is very interesting that Bowles et al. (2020) recently proposed, based on phylogenomic comparative analyses, the separation of first the evolutionary origins of multicellularity and only later, as the second phase, the terrestrialization in Embryophyta. Our hypothesis that multicellular streptophyte algae evolved into anydrophytes, and were reduced to single-cell/filamentous organization in Zygnematophyceae during the Cryogenian while making crucial dry land adaptations during this epoch agrees with this two-step scenario of Bowles et al. (2020). However, we consider that dry land adaptation started by wet-to-dry transitions in streptophyte algae already on a single-cell level in the late Mesoproterozoic–early Neoproterozoic/Tonian (i.e., before the Cryogenian glaciations) and led to the establishment of freshwater multicellular streptophyte algae in the Mesoproterozoic or Tonian (see timings above and Strother et al., 2011; **Figure 2**). This means that streptophytes entered the Cryogenian not only as wet-to-dry adapted single cell/colonial or filamentous algae (*Chlorokybus*, *Klebsormidium*) but already also as multicellular organisms (e.g., extant *Chara or Coleochaete*). Anydrophytes, therefore, evolved as an adaptation of already multicellular streptophyte algae to the Cryogenian harsh glacial conditions. Zygnematophyceae evolved by secondary simplification from anydrophytes still in the Cryogenian as cryophilic algae with a life cycle (i.e., sexual process) optimized for cold and dry/freezing conditions (**Figure 3**). This was due to an extended selective pressure of 80 Ma of the Cryogenian glacial conditions. It is accepted that in the same period, zygomycetous fungi (originally Zygomycota) also lost the flagella and evolved conjugation as a mechanism of sexual reproduction (Liu et al., 2006; Taylor and Berbee, 2006; Lutzoni et al., 2018; Naranjo-Ortiz and Gabaldón, 2019b; Chang et al., 2021). The hypothesis that the same selective pressure of dry land stress conditions resulted in an independent evolution of conjugation in algae and fungi was originally proposed by Stebbins and Hill (1980). We believe that an independent convergent (homoplasy) evolution of conjugation in zygomycetous fungi and Zygnematophyceae supports our whole concept; Zygnematophyceae evolved under the same Cryogenian selective environmental conditions as zygomycetous fungi. This idea is further supported by an independent evolution of conjugation among the Mesostigmatophyceae (Wickett et al., 2014; see above).

A fascinating example of the possible convergent evolution of cell wall dynamics regulating xyloglucan endotransglucosylase/hydrolases (XTHs) and related enzymes between Zygnematophyceae and zygomycetous fungi in Cryogenian was shown recently by Shinohara and Nishitani (2021). Using comparative phylogenomic analyses, they traced the non-plant origins of the XTH family to Alphaproteobacteria, pre-XTH enzymes were integrated into zygnematophycean algae in the Cryogenian *via* the likely HGT. Subsequent HGT event of the zygnematophycean XTHs in the Cryogenian may have led to fungal Congo Red Hypersensitive (CRH) enzymes that cleave and reconnect chitin and glucans in fungal cell walls (name from yeast knockout mutants with increased sensitivity to cell-wall-interfering congo red stain). The HGTs of cell wall plasticity regulating enzyme encoding genes may have supported the adaptation of plants and fungi to the ancient icy environment by facilitating their dry land sessile lifestyles (Shinohara and Nishitani, 2021). In both instances, this might have contributed

to the regulation of the conjugation process requiring large local cell wall modifications of conjugating partner gametes.

The emergence of Zygnematophyceae is expected to have contributed to the acritarch diversity (Moczydłowska et al., 2010; see above). Several morphotypes of acritarchs allow zygnematophycean zygospore interpretation. Additionally, during the Tonian and the Cryogenian new types of acritarchs appeared (Agić et al., 2017). A recent report by Moczydłowska and Liu (2021) further supports our hypothesis. This study showed the existence of advanced zygospores ascribed to Desmidiales (i.e., relatively derived Zygnematophyceae) at the beginning of the Ediacaran. Therefore, the timings of anydrophyte emergence and split to Zygnematophyceae *versus* Embryophyta proposed by Morris et al. (2018a,b) are rather improbable also based on the recent fossil record.

We further propose the hypothesis that the reduction of organismal complexity from the characean Phragmoplastophyta and anydrophyte multicellularity to unicellularity or filamentous growth in Zygnematophycea was the result of an original evolutionary adaptation and specialization to glacial conditions. On the other hand, Embryophyta ancestors might have occupied relatively warmer refugia/habitats on Rodinia palaeosols (or cryoconite) around the equatorial latitudes or volcanic areas. The survival and life cycle completion lower temperature limits for unicellular (up to −20°C) *versus* multicellular (around 0°C; Clarke et al., 2013) organisms may have played a crucial role in Zygnematophyceae evolution. In this context, it might not be surprising that the basal aerophytic Zygnematophyceae are cold-tolerant or directly psychro- or cryophilic (e.g., *Mesotaenium* or *Ancylonema*–as examples of typical glacial algae; Williamson et al., 2019; Procházková et al., 2021). The loss of dependence on microtubuli-based motility of gametes during the sexual process could be explained as an adaptation for the persistent cold or freezing conditions and possibly the lack of stable mineral substrate in both zygomycetous fungi as well as Zygnematophyceae (see above).

We propose that anydrophytes emergence in the Cryogenian was a crucial initial event in the terrestrialisation and land plant evolution. The following Zygnematophyceae split off was a result of reductive evolution to glacial habitats based on further cold adaptations during the extended Cryogenian period.

DATA AVAILABILITY STATEMENT

The original contributions presented in the study are included in the article/supplementary material, further inquiries can be directed to the corresponding author.

AUTHOR CONTRIBUTIONS

JŽ and ViŽ coined the initial idea of this hypothesis and were joined from the beginning by VoŽ with expertise in phylogenetic analyses and MH with expertise in polar geology. JŽ, ViŽ, MH, and VoŽ wrote the manuscript. All authors read and approved the submitted manuscript.

FUNDING

This work was supported by the Grant Agency of Charles University project (GAUK 279715) and Czech Science Foundation project (GAČR 19–21341S) to JŽ; Czech Science Foundation (GAČR)–projects 21–10799S and 20–11642S to ViŽ; part of ViŽ income was covered by the Ministry of Education, Youth and Sports of the Czech Republic from European Regional Development Fund–Project "Centre for Experimental Plant Biology" CZ.02.1.01/0.0/0.0/16_019/0000738.

ACKNOWLEDGMENTS

JŽ, ViŽ, and VoŽ thank their grandfather and father–in–law Jan Zeno Dus–an old testament scholar–for demonstrating how interesting it is to consider history analyses earlier dating and dedicate this report to his 90th birthday. We are grateful to Alina Žárská for **Figures 2, 3**, and Mark Sabatini and Jade Hatton for language corrections. We would also like to thank for valuable and insightful comments to the revision of this report to Andreas Holzinger, Henrik Buschmann, Kazuhiko Nishitani, and our reviewers.

REFERENCES

Agić, H., Moczydłowska, M., and Yin, L. (2017). Diversity of organic-walled microfossils from the early Mesoproterozoic Ruyang Group, North China Craton - A window into the early eukaryote evolution. *Precambrian Res.* 297, 101–130. doi: 10.1016/j.precamres.2017.04.042

Anesio, A. N., and Laybourn-Parry, J. (2012). Glaciers and ice sheets as a biome. *Trends Ecol. Evol.* 27, 219–225. doi: 10.1016/j.tree.2011.09.012

Bai, H., Kuang, H., Liu, Y., Peng, N., Chen, X., and Yuchong Wang, Y. (2020). Marinoan-aged red beds at Shennongjia, South China: evidence against global-scale glaciation during the Cryogenian. *Palaeogeogr. Palaeoclimatol. Palaeoecol.* 559:109967. doi: 10.1016/j.palaeo.2020.109967

Barkat, R., Chakraborty, P. P., Saha, S., and Das, K. (2020). Alluvial architecture, paleohydrology and provenance tracking from the Neoproterozoic Banganapalle formation, Kurnool Group, India: an example of continental sedimentation before land plants. *Precambrian Res.* 350:105930. doi: 10.1016/j.precamres.2020.105930

Becker, B. (2013). Snow ball earth and the split of Streptophyta and Chlorophyta. *Trends Plant Sci.* 18, 180–183. doi: 10.1016/j.tplants.2012.09.010

Becker, B., Feng, X., Yin, Y., and Holzinger, A. (2020). Desiccation tolerance in streptophyte algae and the algae to land plant transition: evolution of LEA and MIP protein families within the Viridiplantae. *J. Exp. Bot.* 71, 3270–3278. doi: 10.1093/jxb/eraa105

Belkina, O. A., and Vilnet, A. A. (2015). Some aspects of the moss population development on the Svalbard glaciers. *Czech. Polar Rep.* 5, 160–175. doi: 10.5817/CPR2015-2-14

Benn, D. I., and Evans, D. J. A. (2010). *Glaciers And Glaciation*, Second Edn. London: Hodder Education.

Bianchetti, R., De Luca, B., de Haro, L. A., Rosado, D., Demarco, D., Conte, M., et al. (2020). Phytochrome-dependent temperature perception modulates isoprenoid metabolism. *Plant Physiol.* 183, 869–882. doi: 10.1104/pp.20.00019

Bose, P. K., Eriksson, P. G., Sarkar, S., Wright, D. T., Samanta, P., Mukhopadhyay, S., et al. (2012). Sedimentation patterns during the Precambrian: a unique record? *Mar. Pet. Geol.* 33, 34–68. doi: 10.1016/j.marpetgeo.2010.11.002

Bowles, A. M. C., Bechtold, U., and Paps, J. (2020). The origin of land plants is rooted in two bursts of genomic novelty. *Curr Biol.* 30, 530–536.e2. doi: 10.1016/j.cub.2019.11.090

Buschmann, H., and Zachgo, S. (2016). The evolution of cell division: from streptophyte algae to land plants. *Trends Plant Sci.* 21, 872–883. doi: 10.1016/j.tplants.2016.07.004

Caisová, L. (2020). *Draparnaldia*: a chlorophyte model for comparative analyses of plant terrestrialisation. *J. Exp. Bot.* 71, 3305–3313. doi: 10.1093/jxb/eraa102

Catalá, R., Medina, J., and Salinas, J. (2011). Integration of low temperature and light signaling during cold acclimation response in *Arabidopsis*. *Proc. Natl. Acad. Sci. U. S. A.* 27, 16475–16480. doi: 10.1073/pnas.1107161108

Chang, Y., Rochon, D., Sekimoto, S., Wang, Y., Chovatia, M., Sandor, L., et al. (2021). Genome-scale phylogenetic analyses confirm *Olpidium* as the closest living zoosporic fungus to the non-flagellated, terrestrial fungi. *Sci. Rep.* 11:3217. doi: 10.1038/s41598-021-82607-4

Chen, X., Ding, Y., Yang, Y., Song, C., Wang, B., Yang, S., et al. (2021). Protein kinases in plant responses to drought, salt, and cold stress. *J. Integr. Plant Biol.* 63, 53–78. doi: 10.1111/jipb.13061

Chen, R., Huangfu, L., Lu, Y., Fang, H., Xu, Y., Li, P., et al. (2021). Adaptive innovation of green plants by horizontal gene transfer. *Biotechnol Adv.* 46:107671. doi: 10.1016/j.biotechadv.2020.107671

Cheng, S., Xian, W., Fu, Y., Marin, B., Keller, J., Wu, T., et al. (2019). Genomes of subaerial Zygnematophyceae provide insights into land plant evolution. *Cell* 179, 1057–1067.e14. doi: 10.1016/j.cell.2019.10.019

Civáň, P., Foster, P. G., Embley, M. T., Seneca, A., and Cox, C. J. (2014). Analyses of Charophyte chloroplast genomes help characterise the ancestral chloroplast genome of land plants. *Genome Biol. Evol.* 6, 897–911. doi: 10.1093/gbe/evu061

Clarke, A., Morris, G. J., Fonseca, F., Murray, B. J., Acton, E., and Price, H. C. (2013). A low temperature limit for life on Earth. *PLoS One* 8:e66207. doi: 10.1371/journal.pone.0066207

Clarke, J. T., Warnock, R. C. M., and Donoghue, P. C. J. (2011). Establishing a time-scale for plant evolution. *New Phytol.* 192, 266–301. doi: 10.1111/j.1469-8137.2011.03794.x

Cock, J. M., Sterck, L., Rouzé, P., Scornet, D., Allen, A. E., Amoutzias, G., et al. (2010). The *Ectocarpus* genome and the independent evolution of multicellularity in brown algae. *Nature* 465, 617–621. doi: 10.1038/nature09016

Cole, D. B., Mills, D. B., Erwin, D. H., Sperling, E. A., Porter, S. M., Reinhard, C. T., et al. (2020). On the co-evolution of surface oxygen levels and animals. *Geobiology* 18, 260–281. doi: 10.1111/gbi.12382

Colina, F., Amaral, J., Carbó, M., Pinto, G., Soares, A., Cañal, M. J., et al. (2019). Genome-wide identification and characterisation of CKIN/SnRK gene family in *Chlamydomonas reinhardtii*. *Sci. Rep.* 9:350. doi: 10.1038/s41598-018-35625-8

Cox, C. J., Li, B., Foster, P. G., Embley, T. M., and Civáò, P. (2014). Conflicting phylogenies for early land plants are caused by composition biases among synonymous substitutions. *Syst. Biol.* 63, 272–279. doi: 10.1093/sysbio/syt109

de Carpentier, F., Lemaire, S. D., and Danon, A. (2019). When unity is strength: the strategies used by *Chlamydomonas* to survive environmental stresses. *Cells* 11:1307. doi: 10.3390/cells8111307

de Clerck, O., Kao, S. M., Bogaert, K. A., Blomme, J., Foflonker, F., Kwantes, M., et al. (2018). Insights into the evolution of multicellularity from the sea lettuce genome. *Curr. Biol.* 28, 2921–2933.e5. doi: 10.1016/j.cub.2018.08.015

de Vries, J., and Archibald, J. M. (2018). Plant evolution: landmarks on the path to terrestrial life. *New Phytol.* 217, 1428–1434. doi: 10.1111/nph.14975

de Vries, J., Curtis, B. A., Gould, S. B., and Archibald, J. M. (2018). Embryophyte stress signaling evolved in the algal progenitors of land plants. *Proc. Natl. Acad. Sci. U. S. A.* 115, 3471–3480. doi: 10.1073/pnas.1719230115

de Vries, J., de Vries, S., Slamovits, C. H., Rose, L. E., and Archibald, J. M. (2017). How embryophytic is the biosynthesis of phenylpropanoids and their derivatives in streptophyte Algae? *Plant Cell Physiol.* 58, 934–945. doi: 10.1093/pcp/pcx037

de Vries, J., Stanton, A., Archibald, J. M., and Gould, S. B. (2016). Streptophyte terrestrialisation in light of plastid evolution. *Trends Plant Sci.* 21, 467–476. doi: 10.1016/j.tplants.2016.01.021

de Vries, S., Stukenbrock, E. H., and Rose, L. E. (2020). Rapid evolution in plant-microbe interactions - an evolutionary genomics perspective. *New Phytol.* 226, 1256–1262. doi: 10.1111/nph.16458

de Vries, J., de Vries, S., Curtis, B. A., Zhou, H., Penny, S., Feussner, K., et al. (2020). Heat stress response in the closest algal relatives of land plants reveals conserved stress signaling circuits. *Plant J.* 103, 1025–1048. doi: 10.1111/tpj.14782

Delwiche, C. F., Karol, K. G., Cimino, M. T., and Sytsma, K. J. (2002). Phylogeny of the genus *Coleochaete* (Coleochaetales, Charophyta) and related taxa inferred by analysis of the chloroplast gene rbcL. *J. Phycol.* 38, 394–403. doi: 10.1046/j.1529-8817.2002.01174.x

Ding, Y., Jia, Y., Shi, Y., Zhang, X., Song, C., Gong, Z., et al. (2018). OST1-mediated BTF3L phosphorylation positively regulates CBFs during plant cold responses. *EMBO J.* 37:e98228. doi: 10.15252/embj.201798228

Ding, Y., Li, H., Zhang, X., Xie, Q., Gong, Z., and Yang, S. (2015). OST1 kinase modulates freezing tolerance by enhancing ICE1 stability in *Arabidopsis*. *Dev. Cell* 32, 278–289. doi: 10.1016/j.devcel.2014.12.023

Edwards, D., Morris, J. L., Richardson, J. B., and Kenrick, P. (2014). Cryptospores and cryptophytes reveal hidden diversity in early land floras. *New Phytol.* 202, 50–78. doi: 10.1111/nph.12645

Emiliani, G., Fondi, M., Fani, R., and Gribaldo, S. (2009). A horizontal gene transfer at the origin of phenylpropanoid metabolism: a key adaptation of plants to land. *Biol. Direct.* 4:7. doi: 10.1186/1745-6150-4-7

Eyles, N. (2008). Glacio-epochs and the supercontinent cycle after ∼3.0 Ga: tectonic boundary conditions for glaciation. *Palaeogeogr. Palaeoclimatol. Palaeoecol.* 258, 89–129. doi: 10.1016/j.palaeo.2007.09.021

Fayek, M., Harrison, T. M., Grove, M., Mckeegan, K. D., Coath, C. D., and Boles, J. R. (2001). *In situ* stable isotopic evidence for protracted and complex carbonate cementation in a petroleum reservoir, North Coles Levee, San Joaquin basin, California, U.S.A. *J. Sediment. Res.* 71, 444–458. doi: 10.1306/2DC40954-0E47-11D7-8643000102C1865D

Fujii, Y., Tanaka, H., Konno, N., Ogasawara, Y., Hamashima, N., Tamura, S., et al. (2017). Phototropin perceives temperature based on the lifetime of its photoactivated state. *Proc. Natl. Acad. Sci. U. S. A.* 114, 9206–9211. doi: 10.1073/pnas.1704462114

Fürst-Jansen, J. M. R., de Vries, S., and de Vries, J. (2020). Evo-physio: on stress responses and the earliest land plants. *J. Exp. Bot.* 71, 3254–3269. doi: 10.1093/jxb/eraa007

Gong, Z., and Han, G. Z. (2021). Flourishing in water: the early evolution and diversification of plant receptor-like kinases. *Plant J.* 106, 174–184. doi: 10.1111/tpj.15157

Gontcharov, A. A., and Melkonian, M. (2004). Unusual position of the genus *Spirotaenia* (Zygnematophyceae) among streptophytes revealed by SSU rDNA and rbcL sequence comparisons. *Phycologia* 43, 105–113. doi: 10.2216/i0031-8884-43-1-105.1

Guiry, M. D. (2013). Taxonomy and nomenclature of the Conjugatophyceae (= Zygnematophyceae). *Algae* 28, 1–29. doi: 10.4490/algae.2013.28.1.001

Han, X., Chang, X., Zhang, Z., Chen, H., He, H., Zhong, B., et al. (2019). Origin and evolution of core components responsible for monitoring light environment changes during plant terrestrialization. *Mol. Plant* 12, 847–862. doi: 10.1016/j.molp.2019.04.006

Harholt, J., Moestrup, Ø, and Ulvskov, P. (2016). Why plants were terrestrial from the beginning. *Trends Plant Sci.* 21, 96–101. doi: 10.1016/j.tplants.2015.11.010

Hedges, S. B., Tao, Q., Walker, M., and Kumar, S. (2018). Accurate timetrees require accurate calibrations. *Proc. Natl. Acad. Sci. U. S. A.* 115, 9510–9511. doi: 10.1073/pnas.1812558115

Heusser, C. J. (1972). Polsters of the moss *Drepanocladus berggrenii* on gilkey glacier, alaska. *Bull. Torrey Bot. Club* 99, 34–36. doi: 10.2307/2484240

Hodson, A., Anesio, A. M., Tranter, M., Fountain, A., Osborn, M., Priscu, J., et al. (2008). Glacial ecosystems. *Ecol. Monogr.* 78, 41–67. doi: 10.1890/07-0187.1

Hoffman, P. F. (2016). Cryoconite pans on Snowball Earth: supraglacial oases for Cryogenian eukaryotes? *Geobiology* 14, 531–542. doi: 10.1111/gbi.12191

Hoffman, P. F., Abbot, D. S., Ashkenazy, Y., Benn, D. I., Brocks, J. J., Cohen, P. A., et al. (2017). Snowball Earth climate dynamics and Cryogenian geology-geobiology. *Sci. Adv.* 3:e1600983. doi: 10.1126/sciadv.1600983

Hoffman, P. F., Halverson, G. P., Domack, E. W., Maloof, A. C., Swanson-Hysell, N. L., and Cox, G. M. (2012). Cryogenian glaciations on the southern tropical paleomargin of Laurentia (NE Svalbard and East Greenland), and a primary origin for the upper Russøya (Islay) carbon isotope excursion. *Precambrian Res.* 206-207, 137–158. doi: 10.1016/j.precamres.2012.02.018

Hoffman, P. F., and Schrag, D. P. (2002). The snowball Earth hypothesis: testing the limits of global change. *Terra Nova.* 14, 129–155. doi: 10.1046/j.1365-3121.2002.00408.x

Holzinger, A., Kaplan, F., Blaas, K., Zechmann, B., Komsic-Buchmann, K., and Becker, B. (2014). Transcriptomics of desiccation tolerance in the Streptophyte

green alga *Klebsormidium* reveal a land plant-like defense reaction. *PLoS One* 9:e110630. doi: 10.1371/journal.pone.0110630

Hoshino, Y., Poshibaeva, A., Meredith, W., Snape, C., Poshibaev, V., Versteegh, G. J. M., et al. (2017). Cryogenian evolution of stigmasteroid biosynthesis. *Sci. Adv.* 3:e1700887. doi: 10.1126/sciadv.1700887

Hotaling, S., Bartholomaus, T. C., and Gilbert, S. L. (2020). Rolling stones gather moss: movement and longevity of moss balls on an Alaskan glacier. *Polar Biol.* 43, 735–744. doi: 10.1007/s00300-020-02675-6

Huntley, J. W., Xiao, S., and Kowalewski, M. (2006). "On the morphological history of proterozoic and cambrian acritarchs," in *Neoproterozoic Geobiology and Paleobiology. Topics in Geobiology*, eds S. Xiao, and A. J. Kaufman (New York: Springer), 23–56. doi: 10.1007/1-4020-5202-2_2

Jensen, J. K., Busse-Wicher, M., Poulsen, C. P., Fangel, J. U., Smith, P. J., Yang, J. Y., et al. (2018). Identification of an algal xylan synthase indicates that there is functional orthology between algal and plant cell wall biosynthesis. *New Phytol.* 218, 1049–1060. doi: 10.1111/nph.15050

Jiao, C., Sørensen, I., Sun, X., Sun, H., Behar, H., Alseekh, S., et al. (2020). The *Penium margaritaceum* genome: hallmarks of the origins of land plants. *Cell* 181, 1097–1111.e12. doi: 10.1016/j.cell.2020.04.019

Karol, K. G., McCourt, R. M., Cimino, M. T., and Delwiche, C. F. (2001). The closest living relatives of land plants. *Science* 294, 2351–2353. doi: 10.1126/science.1065156

Kilian, J., Whitehead, D., Horak, J., Wanke, D., Weinl, S., Batistic, O., et al. (2007). The AtGenExpress global stress expression data set: protocols, evaluation and model data analysis of UV-B light, drought and cold stress responses. *Plant J.* 50, 347–363. doi: 10.1111/j.1365-313X.2007.03052.x

Knauth, L. P., and Kennedy, M. J. (2009). The late precambrian greening of the earth. *Nature* 460, 728–732. doi: 10.1038/nature08213

Komatsu, K., Takezawa, D., and Sakata, Y. (2020). Decoding ABA and osmostress signalling in plants from an evolutionary point of view. *Plant Cell Environ.* 43, 2894–2911. doi: 10.1111/pce.13869

Lamers, J., van der Meer, T., and Testerink, C. (2020). How plants sense and respond to stressful environments. *Plant Physiol.* 182, 1624–1635. doi: 10.1104/pp.19.01464

Lauterborn, R. (1894). Ueber die winterfauna einiger gewässer der oberrheinebene. mit beschreibungen neuer protozoën. *Biol. Zentralblatt* 14, 390–398.

Leebens-Mack, J. H., Barker, M. S., Carpenter, E. J., Deyholos, M. K., Gitzendanner, M. A., Graham, S. W., et al. (2019). One thousand plant transcriptomes and the phylogenomics of green plants. *Nature* 574, 679–685. doi: 10.1038/s41586-019-1693-2

Lemieux, C., Otis, C., and Turmel, M. (2007). A clade uniting the green algae *Mesostigma viride* and *Chlorokybus atmophyticus* represents the deepest branch of the Streptophyta in chloroplast genome-based phylogenies. *BMC Biol.* 5:2. doi: 10.1186/1741-7007-5-2

Li, F. W., Rothfels, C. J., Melkonian, M., Villarreal, J. C., Stevenson, D. W., Graham, S. W., et al. (2015). The origin and evolution of phototropins. *Front. Plant Sci.* 12:637. doi: 10.3389/fpls.2015.00637

Li, L. Z., Wang, S., Sahu, S. K., Marin, B., Li, H. Y., and Xu, Y. (2020). The genome of *Prasinoderma coloniale* unveils the existence of a third phylum within green plants. *Nat. Ecol. Evol.* 4, 1220–1231. doi: 10.1038/s41559-020-1221-7

Li, Z.-X., Evans, D. A., and Halverson, G. P. (2013). Neoproterozoic glaciations in a revised global palaeogeography from the breakup of Rodinia to the assembly of Gondwanaland. *Sediment. Geol.* 294, 219–232. doi: 10.1016/j.sedgeo.2013.05.016

Liu, Y. J., Hodson, M. C., and Hall, B. D. (2006). Loss of the flagellum happened only once in the fungal lineage: phylogenetic structure of Kingdom Fungi inferred from RNA polymerase II subunit genes. *BMC Evol. Biol.* 6:74. doi: 10.1186/1471-2148-6-74

Lutz, S., McCutcheon, J., McQuaid, J. B., and Benning, L. G. (2018). The diversity of ice algal communities on the Greenland Ice Sheet as revealed by oligotyping. *Microb. Genomics.* 4:e000159. doi: 10.1099/mgen.0.000159

Lutzoni, F., Nowak, M. D., Alfaro, M. E., Reeb, V., Miadlikowska, J., Krug, M., et al. (2018). Contemporaneous radiations of fungi and plants linked to symbiosis. *Nat. Commun.* 9:5451. doi: 10.1038/s41467-018-07849-9

Moczydłowska, M. (2008). The Ediacaran microbiota and the survival of Snowball Earth conditions. *Precambrian Res.* 167, 1–15. doi: 10.1016/j.precamres.2008.06.008

Moczydłowska, M., and Liu, P. (2021). Ediacaran algal cysts from the Doushantuo formation, South China. *Geol. Mag.* 158, 1–21. doi: 10.1017/S0016756820001405

Moczydłowska, M., Schopf, J. W., and Willman, S. (2010). Micro- and nano-scale ultrastructure of cell walls in Cryogenian microfossils: revealing their biological affinity. *Lethaia* 43, 129–136. doi: 10.1111/j.1502-3931.2009.00175.x

Moody, L. A. (2020). Three-dimensional growth: a developmental innovation that facilitated plant terrestrialisation. *J. Plant Res.* 133, 283–290. doi: 10.1007/s10265-020-01173-4

Morris, J. L., Puttick, M. N., Clark, J. W., Edwards, D., Kenrick, P., Pressel, S., et al. (2018b). The timescale of early land plant evolution. *Proc. Natl. Acad. Sci. U. S. A.* 115, E2274–E2283. doi: 10.1073/pnas.1719588115

Morris, J. L., Puttick, M. N., Clark, J. W., Edwards, D., Kenrick, P., Pressel, S., et al. (2018a). Reply to Hedges et al.: accurate timetrees do indeed require accurate calibrations. *Proc. Natl. Acad. Sci. U. S. A.* 115, E9512–E9513. doi: 10.1073/pnas.1812816115

Mustilli, A. C., Merlot, S., Vavasseur, A., Fenzi, F., and Giraudat, J. (2002). *Arabidopsis* OST1 protein kinase mediates the regulation of stomatal aperture by abscisic acid and acts upstream of reactive oxygen species production. *Plant Cell* 14, 3089–3099. doi: 10.1105/tpc.007906

Naranjo-Ortiz, M. A., and Gabaldón, T. (2019b). Fungal evolution: major ecological adaptations and evolutionary transitions. *Biol. Rev. Camb. Philos. Soc.* 94, 1443–1476. doi: 10.1111/brv.12510

Naranjo-Ortiz, M. A., and Gabaldón, T. (2019a). Fungal evolution: diversity, taxonomy and phylogeny of the Fungi. *Biol. Rev.* 94, 2101–2137. doi: 10.1111/brv.12550

Nick, P. (2013). Microtubules, signalling and abiotic stress. *Plant J.* 75, 309–323. doi: 10.1111/tpj.12102

Nie, Y., Foster, C. S. P., Zhu, T., Yao, R., Duchêne, D. A., Ho, S. Y. W., et al. (2020). Accounting for uncertainty in the evolutionary timescale of green plants through clock-partitioning and fossil calibration strategies. *Syst. Biol.* 69, 1–16. doi: 10.1093/sysbio/syz032

Nishiyama, T., Wolf, P. G., Kugita, M., Sinclair, R. B., Sugita, M., Sugiura, C., et al. (2004). Chloroplast phylogeny indicates that bryophytes are monophyletic. *Mol. Biol. Evol.* 21, 1813–1819. doi: 10.1093/molbev/msh203

Permann, C., Herburger, K., Felhofer, M., Gierlinger, N., Lewis, L. A., and Holzinger, A. (2021a). Induction of conjugation and cygospore cell wall characteristics in the Alpine *Spirogyra mirabilis* (Zygnematophyceae, Charophyta): advantage under climate change scenarios? *Plants* 10:1740. doi: 10.3390/plants10081740

Permann, C., Herburger, K., Niedermeier, M., Felhofer, M., Gierlinger, N., and Holzinger, A. (2021b). Cell wall characteristics during sexual reproduction of *Mougeotia* sp. (Zygnematophyceae) revealed by electron microscopy, glycan microarrays and RAMAN spectroscopy. *Protoplasma* 258, 1261–1275. doi: 10.1007/s00709-021-01659-5

Porter, P. R., Evans, A. J., Hodson, A. J., Lowe, A. T., and Crabtree, M. D. (2008). Sediment-moss interactions on a temperate glacier: falljökull, Iceland. *Ann. Glaciol.* 48, 25–31. doi: 10.3189/172756408784700734

Procházková, L., Řezanka, T., Nedbalová, L., and Remias, D. (2021). Unicellular versus filamentous: the glacial alga *Ancylonema alaskana* comb. et stat. nov. and its ecophysiological relatedness to *Ancylonema nordenskioeldii* (Zygnematophyceae, Streptophyta). *Microorganisms* 9:1103. doi: 10.3390/microorganisms9051103

Pšenička, J., Bek, J., Frýda, J., Žárský, V., Uhlířová, M., and Štorch, P. (2021). Dynamics of Silurian plants as response to climate changes. *Life (Basel)* 11:906. doi: 10.3390/life11090906

Puttick, M. N., Morris, J. L., Williams, T. A., Cox, C. J., Edwards, D., Kenrick, P., et al. (2018). The interrelationships of land plants and the nature of the ancestral Embryophyte. *Curr. Biol.* 28, 210–213. doi: 10.1016/j.cub.2018.01.063

Rabenhorst, G. L. (1870). *Kryptogamen-Flora von Sachsen, der Ober-Lausitz, Thüringen und Nordböhmen, mit Berücksichtigung der benachbarten Länder*. Leipzig: E. Kummer, doi: 10.24355/dbbs.084-200909111218-0

Rasmussen, S., Barah, P., Suarez-Rodriguez, M. C., Bressendorff, S., Friis, P., Costantino, P., et al. (2013). Transcriptome responses to combinations of stresses in *Arabidopsis*. *Plant Physiol.* 161, 1783–1794. doi: 10.1104/pp.112.210773

Remias, D., Schwaiger, S., Aigner, S., Leya, T., Stuppner, H., and Lütz, C. (2012). Characterisation of an UV- and VIS-absorbing, purpurogallin-derived secondary pigment new to algae and highly abundant in *Mesotaenium berggrenii* (Zygnematophyceae, Chlorophyta), an extremophyte living on glaciers. *FEMS Microbiol. Ecol.* 79, 638–648. doi: 10.1111/j.1574-6941.2011.01245.x

Rensing, S. A. (2020). How plants conquered land. *Cell* 181, 964–966. doi: 10.1016/j.cell.2020.05.011

Retallack, G. J. (2011). Neoproterozoic loess and limits to snowball Earth. *J. Geol. Soc.* 168, 289–308. doi: 10.1144/0016-76492010-051

Retallack, G. J. (2013). Ediacaran life on land. *Nature* 493, 89–92. doi: 10.1038/nature11777

Retallack, G. J., Gose, B. N., and Osterhout, J. T. (2015). Periglacial paleosols and Cryogenian paleoclimate near Adelaide, South Australia. *Precambrian Res.* 263, 1–18. doi: 10.1016/j.precamres.2015.03.002

Rubinstein, C. V., and Vajda, V. (2019). Baltica cradle of early land plants? Oldest record of trilete spores and diverse cryptospore assemblages; evidence from Ordovician successions of Sweden. *GFF* 141, 181–190. doi: 10.1080/11035897.2019.1636860

Saigo, T., Wang, T., Watanabe, M., and Tohge, T. (2020). Diversity of anthocyanin and proanthocyanin biosynthesis in land plants. *Curr. Opin. Plant Biol.* 55, 93–99. doi: 10.1016/j.pbi.2020.04.001

Salamon, M. A., Gerrienne, P., Steemans, P., Gorzelak, P., Filipiak, P., Le Hérissé, A., et al. (2018). Putative late ordovician land plants. *New Phytol.* 218, 1305–1309. doi: 10.1111/nph.15091

Sánchez-Baracaldo, P., Raven, J. A., Pisani, D., and Knoll, A. H. (2017). Early photosynthetic eukaryotes inhabited low-salinity habitats. *Proc. Natl. Acad. Sci. U. S. A.* 114, E7737–E7745. doi: 10.1073/pnas.1620089114

Servais, T., Cascales-Miñana, B., Cleal, C. J., Gerrienne, P., Harper, D. A. T., and Neumann, M. (2019). Revisiting the great Ordovician diversification of land plants: recent data and perspectives. *Palaeogeogr. Palaeoclimatol. Palaeoecol.* 534:109280. doi: 10.1016/j.palaeo.2019.109280

Shi, Y., Ding, Y., and Yang, S. (2018). Molecular regulation of CBF signaling in cold acclimation. *Trends Plant Sci.* 23, 623–637. doi: 10.1016/j.tplants.2018.04.002

Shields-Zhou, G. A., Porter, S., and Halverson, G. P. (2015). A new rock-based definition for the Cryogenian Period (circa 720 - 635 Ma). *Episodes* 39, 3–8. doi: 10.18814/epiiugs/2016/v39i1/89231

Shinde, S., Nurul Islam, M., and Ng, C. K. (2012). Dehydration stress-induced oscillations in LEA protein transcripts involves abscisic acid in the moss, *Physcomitrella patens*. *New Phytol.* 195, 321–328. doi: 10.1111/j.1469-8137.2012.04193.x

Shinohara, N., and Nishitani, K. (2021). Cryogenian origin and subsequent diversification of the plant cell-wall enzyme XTH family. *Plant Cell Physiol.* doi: 10.1093/pcp/pcab093 [Epub Online ahead of print].

Shinozawa, A., Otake, R., Takezawa, D., Umezawa, T., Komatsu, K., Tanaka, K., et al. (2019). SnRK2 protein kinases represent an ancient system in plants for adaptation to a terrestrial environment. *Commun. Biol.* 2:30. doi: 10.1038/s42003-019-0281-1

Stebbins, G. L., and Hill, G. J. C. (1980). Did multicellular plants invade the land? *Am. Nat.* 115, 342–353. doi: 10.1086/283565

Steemans, P., Hérissé, A. L., Melvin, J., Miller, M. A., Paris, F., Verniers, J., et al. (2009). Origin and radiation of the earliest vascular land plants. *Science* 324, 353–353. doi: 10.1126/science.1169659

Stewart, K. D., and Mattox, K. R. (1975). Comparative cytology, evolution and classification of the green algae with some consideration of the origin of other organisms with chlorophylls A and B. *Bot. Rev.* 41, 104–135. doi: 10.1007/BF02860837

Stibal, M., Šabacká, M., and Žárský, J. (2012). Biological processes on glacier and ice sheet surfaces. *Nat. Geosci.* 5, 771–774. doi: 10.1038/ngeo1611

Strassert, J. F. H., Irisarri, I., Williams, T. A., and Burki, F. (2021). A molecular timescale for eukaryote evolution with implications for the origin of red algal-derived plastids. *Nat Commun.* 12:1879. doi: 10.1038/s41467-021-22044-z

Strother, P. K., Battison, L., Brasier, M. D., and Wellman, C. H. (2011). Earth's earliest non-marine eukaryotes. *Nature* 473, 505–509. doi: 10.1038/nature09943

Su, D., Yang, L., Shi, X., Ma, X., Zhou, X., Hedges, B. S., et al. (2021). Large-scale phylogenomic analyses reveal the monophyly of bryophytes and Neoproterozoic origin of land plants. *Mol. Biol. Evol.* 38, 3332–3344. doi: 10.1093/molbev/msab106

Taylor, J. W., and Berbee, M. L. (2006). Dating divergences in the fungal tree of life: review and new analyses. *Mycologia* 98, 838–849. doi: 10.1080/15572536.2006.11832614

Valledor, L., Furuhashi, T., Hanak, A. M., and Weckwerth, W. (2013). Systemic cold stress adaptation of *Chlamydomonas reinhardtii*. *Mol. Cell Proteomics* 12, 2032–2047. doi: 10.1074/mcp.M112.026765

Wallin, M., and Strömberg, E. (1995). Cold-stable and cold-adapted microtubules. *Int. Rev. Cytol.* 157, 1–31. doi: 10.1016/S0074-7696(08)62155-5

Wang, S., Li, L., Li, H., Sahu, S. K., Wang, H., Xu, Y., et al. (2020). Genomes of early-diverging streptophyte algae shed light on plant terrestrialisation. *Nat. Plants* 6, 95–106. doi: 10.1038/s41477-019-0560-3

Wang, T.-G., Li, M., Wang, C., Wang, G., Zhang, W., Shi, Q., et al. (2008). Organic molecular evidence in the late neoproterozoic tillites for a palaeo-oceanic environment during the snowball earth era in the yangtze region, southern China. *Precambrian Res.* 162, 317–326. doi: 10.1016/j.precamres.2007.09.009

Wickett, N. J., Mirarab, S., Nguyen, N., Warnow, T., Carpenter, E., Matasci, N., et al. (2014). Phylotranscriptomic analysis of the origin and early diversification of land plants. *Proc. Natl. Acad. Sci. U. S. A.* 111, E4859–E4868. doi: 10.1073/pnas.1323926111

Williams, G. E., Gostin, V. A., McKirdy, D. M., and Preiss, W. V. (2008). The Elatina glaciation, late Cryogenian (Marinoan Epoch), South Australia: sedimentary facies and palaeoenvironments. *Precambrian Res.* 163, 307–331. doi: 10.1016/j.precamres.2007.12.001

Williamson, C. J., Cameron, K. A., Cook, J. M., Zarsky, J. D., Stibal, M., and Edwards, A. (2019). Glacier algae: a dark past and a darker future. *Front. Microbiol.* 10:524. doi: 10.3389/fmicb.2019.00524

Wodniok, S., Brinkmann, H., Glöckner, G., Heidel, A. J., Philippe, H., Melkonian, M., et al. (2011). Origin of land plants: do conjugating green algae hold the key? *BMC Evol. Biol.* 11:104. doi: 10.1186/1471-2148-11-104

Yallop, M. L., Anesio, A. M., Perkins, R. G., Cook, J., Telling, J., Fagan, D., et al. (2012). Photophysiology and albedo-changing potential of the ice algal community on the surface of the Greenland ice sheet. *ISME J.* 6, 2302–2313. doi: 10.1038/ismej.2012.107

Zawierucha, K., Kolicka, M., Takeuchi, N., and Kaczmarek, Ł (2015). What animals can live in cryoconite holes? A faunal review: cryoconite holes fauna. *J. Zool.* 295, 159–169. doi: 10.1111/jzo.12195

Zawierucha, K., Porazinska, D. L., Ficetola, G. F., Ambrosini, R., Baccolo, G., Buda, J., et al. (2021). A hole in the nematosphere: tardigrades and rotifers dominate the cryoconite hole environment, whereas nematodes are missing. *J. Zool.* 313, 18–36. doi: 10.1111/jzo.12832

Zhang, S., Su, J., Ma, S., Wang, H., Wang, X., He, K., et al. (2021). Eukaryotic red and green algae populated the tropical ocean 1400 million years ago. *Precambrian Res.* 357:106166. doi: 10.1016/j.precamres.2021.106166

Zhu, J. K. (2016). Abiotic stress signaling and responses in plants. *Cell* 167, 313–324. doi: 10.1016/j.cell.2016.08.029

Conflict of Interest: The authors declare that the research was conducted in the absence of any commercial or financial relationships that could be construed as a potential conflict of interest.

Advantages of publishing in Frontiers

OPEN ACCESS
Articles are free to read for greatest visibility and readership

FAST PUBLICATION
Around 90 days from submission to decision

HIGH QUALITY PEER-REVIEW
Rigorous, collaborative, and constructive peer-review

TRANSPARENT PEER-REVIEW
Editors and reviewers acknowledged by name on published articles

Frontiers
Avenue du Tribunal-Fédéral 34
1005 Lausanne | Switzerland

Visit us: www.frontiersin.org
Contact us: frontiersin.org/about/contact

REPRODUCIBILITY OF RESEARCH
Support open data and methods to enhance research reproducibility

DIGITAL PUBLISHING
Articles designed for optimal readership across devices

FOLLOW US
@frontiersin

IMPACT METRICS
Advanced article metrics track visibility across digital media

EXTENSIVE PROMOTION
Marketing and promotion of impactful research

LOOP RESEARCH NETWORK
Our network increases your article's readership